NEMEA-3
Neutron Measurements, Evaluations and Applications

Proceedings of the enlargement workshop
25-28 October 2006
Borovets, Bulgaria

Edited by A.J.M. Plompen

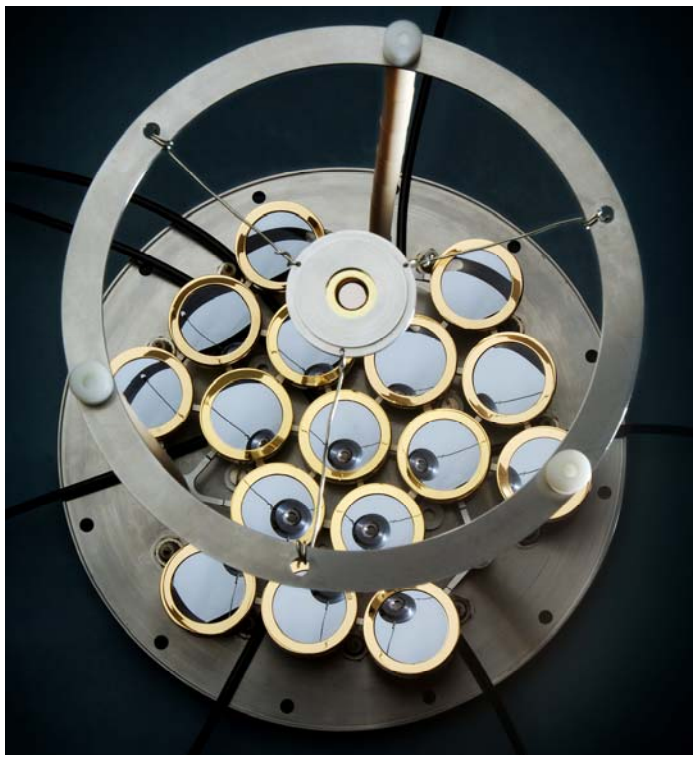

EUR 22794 EN

2007

EUROPEAN COMMISSION
DIRECTORATE-GENERAL
Joint Research Centre

Institute for Reference Materials and Measurements

The mission of IRMM is to promote a common and reliable European measurement system in support of EU policies.

European Commission
Directorate-General Joint Research Centre
Institute for Reference Materials and Measurements

Contact information
A.J.M. Plompen
European Commission
Directorate-General Joint Research Centre
Institute for Reference Materials and Measurements
Retieseweg 111
B-2440 Geel • Belgium

Email: Arjan.Plompen@ec.europa.eu

Tel.: +32 (0)14 571 381
Fax: +32 (0)14 584 273

http://www.irmm.jrc.be
http://www.jrc.ec.europa.eu

EUR Report 22794 EN
ISBN 978-92-79-06158-5
ISSN 1018-5593
Luxembourg: Office for Official Publications of the European Communities

Printed in Belgium

NEMEA-3
Neutron Measurements, Evaluations and Applications

Proceedings of the enlargement workshop
25-28 October 2006
Borovets, Bulgaria

Edited by A.J.M. Plompen

Foreword

October 25-28, 2006, the Enlargement workshop on Neutron Measurements, Evaluations and Applications, NEMEA-3 was held in Samokov Hotel, Borovets, Bulgaria. The workshop was organised by the Neutron Physics Unit of JRC-IRMM, in close collaboration with the local organiser, Prof. Natalia Janeva from the Insitute for Nuclear Research and Nuclear Energy in Sofia. The organisers were supported by a Program Advisory Committee consisting of Dr. E. Bauge, Commissariat à l'Énergie Atomique, Bruyères-le-Châtel, France, Dr. J. Blomgren, Uppsala University, Uppsala, Sweden, Dr. A.J. Koning, Nuclear Reactor Consultancy group, Petten, The Netherlands, Dr. Nichols, International Atomic Energy Agency (IAEA), Nuclear Data Section (NDS), and Prof. S.M. Qaim Forschungszentrum Jülich and University Köln, Germany. The purpose of the workshop was to stimulate exchange of knowledge on recent activities in the field of neutron measurements, evaluations and applications between researchers from new member states, candidate countries, and Western Balkan states with researchers from EU member states and elsewhere.

The workshop was opened with a session devoted to nuclear research and nuclear energy in Bulgaria. Prof. J.N. Stamenov presented an overview of the activities and responsibilities of the Institute for Nuclear Research and Nuclear Energy (INRNE) which is situated in Sofia, Bulgaria. Activities span the fields of elementary particle physics, nuclear and astrophysics, nuclear instrumentation, radiochemistry, dosimetry and radiation safety, neutron and reactor physics, nuclear energy and safety, radioactive waste management and monitoring and managing of the environment. INRNE is responsible for operation of the IRT-2000 research reactor, the radioactive waste repository in Novi Han, scientific support to the Kozloduy Nuclear Power Plant, analysis of nuclear materials from illicit trafficking and the management of radiation hazards. Dr. Kostov of the Nuclear Regulatory Agency (NRA) presented the acts and measures in place and under development that accompany the major nuclear programs in Bulgaria. For the Kozloduy site this includes the shutdown and decommissioning of the reactors 1 and 2 in 2002, the shutdown of reactors 3 and 4 upon entry of Bulgaria in the European Union in January 2006, the upgrade of the safety measures for the continuing reactors 5 and 6 and the on-site dry spent-fuel storage facility. The NRA is intimately involved in the planning of the Belene Nuclear Power Plant destined to replace the capacity for electricity generation in Bulgaria. Dr. Kostov noted that the Kozloduy power plant also supplies the surrounding countries (Romania, Macedonia, Serbia) and that the shutdown of reactors has cross-border implications. Finally, the NRA monitors the refurbishment of the INRNE's nuclear research reactor IRT-200 (previously IRT-2000). Prof. N.B. Janeva summarised INRNE's activities in neutron and nuclear energy research. Currently INRNE is refurbishing its research reactor with the aim of re-establishing the training facility for reactor operators and for opening new possibilities for research and applications. IRT-200 will be a 200 kW pool-type reactor with low-enriched uranium as fuel and seven horizontal and six vertical beam guides. One beam-guide will be devoted to Boron Neutron Capture Therapy (BNCT). Prof. Janeva's group is involved in nuclear data research and environmental radioactivity studies. Prof. C. Stoyanov presented an overview of the Laboratories of Nuclear and Theoretical Nuclear Physics. He highlighted a large number of international collaborations on issues of fundamental physics with involvement in experimental and theoretical efforts associated with international experimental facilities such as those of Dubna, CERN, GSI, and GANIL. An excursion was organised to INRNE on Saturday afternoon with emphasis on the progress of the IRT-200 project.

The workshop was organised in sessions on "Nuclear medicine", "Trends, models and theory", "Data needs evaluations and libraries", "Measurement facilities". "Inspection and characterisation", and "Experiments and measurements". Well-known invited speakers set the stage. Prof. Qaim presented an overview of the developments that have taken place in the production and use of diagnostic and therapeutic radioisotopes during the course of his career at Forschungszentrum Jülich and the Universität zu Köln. Recent conferences organised by him and his co-workers highlight the continuing interest and new developments in this field. Dr. Blomgren presented recent developments in the understanding of biomedical aspects of high-energy neutrons. Together with his co-workers he studies the cross sections

governing the interaction of high-energy neutrons with biologically relevant materials to improve the understanding of the delivered dose and its impact. His work has implications for the dose to aircraft personnel and for fast-neutron cancer therapy. Dr. Bauge presented an overview of trends in nuclear theory and nuclear modeling in a summary talk that covered the workshop on "Perspectives for nuclear data for the next decade", Bruyères-le-Châtel, 2005. Dr. Capote of the IAEA-NDS highlighted recent advances in modeling of neutron-induced reactions. He emphasised the progress that was made for the deformed optical model including the dispersive correction in the coupled-channels formalism. Illustrations were presented for the mass region around tungsten and for the actinides. Dr. Forrest presented the status and needs of nuclear data in the interest of the development of fusion power plants. He sketched the status of the ITER project that will develop an experimental fusion reactor at Cadarache, the interntational fusion materials irradiation facility (IFMIF) and the demonstration power plant (DEMO). The status of important nuclear data libraries were presented by Dr. Koning of NRG who presented the Joint European Fusion and Fission (JEFF) library project, and Dr. Trkov of the Jožef Stefan Institute, Ljubljana, Slovenia. The JEFF project recently established version 3.1 of the library after extensive benchmarking of the results. Quality assurance measures have led the French industry to initiate a program to adopt JEFF3.1 as the data library of choice for their reactor applications. Dr. Trkov presented the very successful evaluations by the Co-ordinated Research Project for the Th/U fuel cycle of the IAEA Nuclear Data Section. Significantly improved evaluations have led to the adoption of the files for this fuel cycle in the December 2006 release of the United States evaluated nuclear data file (ENDF/B-VII.0).

I conclude by acknowledging that the success of a workshop can only be made by all the people that support it. The approximately sixty participants contributed to the success of this workshop with fifty-four oral presentations and eighteen posters as well as a lively exchange of ideas during and after sessions. The social events, the reception, the conference dinner and the visit to Rila Monastery, further contributed to a good workshop spirit. I would here like to compliment Prof. Janeva and her staff on the excellent arrangements. The workshop organisation and participants owe many thanks to an excellent workshop secretary, Mrs. Carmen Cabanillas, to Mrs. S. Lehto who took care of the website, the poster and the announcement, and to Mr. I. Celen, Mrs. E. dalle Molle and their staff for support in administrative matters.

Arjan Plompen
June 2007

Hotel Samokov

Group photo in front of the hotel

Contents

Invited contributions

Oral contributions

Poster contributions

Perspectives on nuclear data for the next decade

E. Bauge

Commissariat à l'Énergie Atomique, DAM Ile-de-France, Service de Physique Nucléaire, BP 12, 91680 Bruyères-le-Châtel, France
eric.bauge@cea.fr

Abstract: On September 26-28 2006, an international workshop entitled "Perspective on Nuclear Data for the Next Decade" took place in Bruyères-le-Châtel, France. This workshop gathered around 60 participants from all over the world and was devoted to the difficult task of foreseeing the near future of nuclear data production. The importance of identifying the "hot topics" early on cannot be overstressed in an environment where the demand for more accurate nuclear data is increasing while the resources devoted to nuclear data production are stagnating at best. Both experimental and theoretical aspects of nuclear data were treated in 36 presentations covering a wide range of new advances that can be envisioned to be used for nuclear data production in the near future.

Introduction

The workshop entitled "Perspectives on Nuclear Data for the Next Decade" (P(ND)^2) was held in Bruyères-le-Châtel, France, on September 26th-28th 2005, organized under the auspices of the Organization for Economic Cooperation and Development (OECD)'s Nuclear Energy Agency (NEA), and hosted by the Commissariat à l'Énergie Atomique (CEA) in its DAM Ile-de-France (DIF) research center. This workshop is the direct descendant of the highly successful series of specialist meetings on optical model potentials (Paris 1985, Bruyères-le-Châtel 1996), and although its scope has widened beyond optical models only, it has been organized in the same spirit as its predecessors, as a specialist meeting dedicated to exploring the future of nuclear data evaluation.
With fewer and fewer evaluators in the world and more and more demand for high quality nuclear data, there is a risk that evaluators concentrate on producing new nuclear data to the detriment of working on the means of evaluating nuclear data (new models, new measurements…). Since the human resources for fundamental works on evaluation are diminishing, it becomes essential to clearly identify what physics is going to be important for the evaluation processes of the future. Moreover, demand for new types of data associated with emerging nuclear data uses could warrant new evaluation techniques that are presently only used in the context of fundamental research and not for nuclear data production.
The goal of the P(ND)^2 meeting was to identify the key points that are being worked on today in the laboratories and that are likely to be used in the evaluation process in the next 10-15 years. This meeting was focused on works that are not presently used in the evaluation process but that can be foreseen to become useful for evaluation in the next decade. Both theoretical modelling and experimental aspects of nuclear data evaluation were discussed.
The proceedings of this workshop [1] are published by OECD's Nuclear Energy Agency.

Experimental nuclear data

Since experiments are expensive, it is important to design them in such a way that the return on investment is maximized. This is achieved by careful planning and coupling closely with the experimental nuclear data users: the evaluators and theoreticians who turn experimental nuclear data into evaluations or refined models.

Facilities

Experimental nuclear data cannot be obtained without facilities, and besides existing ones there are few future or planned projects worth mentioning. One of them are the SPIRAL-2 facility in GANIL France where reaction on fission fragments far from the stability line will be measured, and where a high intensity neutron source will possibly be built [2]. The second important project in the nuclear data field is the high-energy neutron source at CERN that is a by-product of their high intensity neutrino source, which uses the decay of β–unstable nuclei in a storage ring to produce neutrinos. If these of β–unstable nuclei are carefully chosen to be

also delayed neutron emitters, there is a possibility of a high intensity high energy (100-600 MeV) neutron source that will mostly already be paid for by neutrino studies, and whose applications we can only start to imagine (see paper by J. Blomgren in [1]).

Detection systems and experimental techniques

For existing facilities like LANSCE (Los Alamos), GELINA (Geel), nTOF(CERN)… the challenge resides in performing experiments that are both relevant to the nuclear data needs, and feasible. This is becoming increasingly difficult since most the experiments that were both "easy" and useful have already been performed. Moreover, the evolution of nuclear data needs towards unstable, difficult to handle targets, necessitates innovative experimental techniques. For example, for very small (10 ng), hard to produce, or extremely radioactive targets, the technique of the Lead Slowing Down Spectrometer (see paper by R. Haight in [1]) allows to optimally use all the available neutrons by "recycling" the neutrons that do not react with the target until they interact with it.

Another way to measure reactions on hard to obtain or hard to handle targets is the use of transfer or ''surrogate" reactions. That technique relies on the assumption that the compound nucleus state populated by the transfer reaction is the same as that that would be obtained by an incident neutron. For example, by measuring ^{243}Am(^{3}He,t), the created ^{243}Cm compound nucleus is assumed to be the same as the one coming from the n+^{243}Cm. This method has already been successfully used to measure (n,f) and (n,γ) cross section on various Pa, Am and Cm isotopes (see paper by M. Aiche in [1]), by it is somewhat model-dependent, and the validity of the hypotheses underlying these measurements must be carefully assessed (see paper by J Escher in [1]),

Models are also needed in order to extract the (n,n') and (n,2n) from the measured (n,n'γ) and (n,2nγ) measured at GELINA or with GEANIE on LANCSE (see papers by A. Plompen and R. Haight in [1]). That model-dependence implies that theoretical support to experimentalists must follow in order to extract the full potential from these measurements.

Very nice fission fragment yields were measured at GSI using inverse kinematics proton induced fission for a wide range of fissionable projectiles and energies. The fission fragments were then sorted in a high-resolution magnetic spectrometer, and then detected (see paper by K.H. Schmidt in [1]). Accounting for these measurements constitutes a challenge to theoretical fission models.

Delayed neutrons time distributions from gamma-induced fission are measured using a free electron laser (ELSA) bremstrahlung light source (see paper by D. Ridikas in [1]). These measurements significantly improve on the previously known delayed neutron parameters for ^{238}U, and are invaluable for applications related to detection of illicit nuclear materials.

Finally, in order to differentiate between models, "new" types of observables must be measured. For example, light ions (Li-O) single and doubly differential spectra are rarely measured, yet they challenge the model predictions to a much larger extent than the usual n, p, d, t, and α projectiles. Measurements of light ion spectra using a Bragg Curve Spectrometer were discussed (see Baba paper in [1]), and the modelling of such reaction using the Iwamoto-Harada-Sato coalescence model was discussed (Y. Watanabe in [1]). This illustrates the importance of the interplay between experiment and modelling.

Evaluation

Masses

One of the most basic type of data to be evaluated is atomic masses, which are used as input for many other nuclear data evaluation, therefore it is of the utmost importance. Mass data evaluation is performed by compilation, inter-comparisons of experimental absolute and relative mass measurements in a network linking nuclides of which masses are to be evaluated (see paper by G. Audi in [1]). The advent of Penning traps has made mass measurements both easier and more precise, and models can be used to extrapolate the experimental information away from the stability line (Lunney in [1]). Improvement in the predictive power of mean-field mass calculations are linked to refinements of the effective interactions to be used mean-field and beyond the mean-field calculations, Such improvement of the Gogny D1S interaction has been shown to significantly reduce the A-dependent spread of the calculation vs experiment mass difference (F. Chappert in [1]).

Self contained models

In the case of very light systems (A < 5), it is possible to exactly solve the many body Schrödinger equation exactly knowing only the nucleon-nucleon interaction. The Fadeev-Yakubovski has been used to produce an *ab initio* evaluation of the neutron incident on deuteron system (R. Lazauskas in [1]).

A very promising approach for heavier systems (i.e. n+C) is the MCAS (Multi Channel Algebraic Scattering) model (K. Amos in [1]). It is a complete treatment coupling all the channels where nuclear structure and reactions are tightly coupled with exact treatment of the Pauli blocking. The resulting predicted total cross sections exhibit resonant structures that match the experimental ones, without resorting to resonance parameter adjustments as in R-matrix calculations.

Nuclear reaction models

Most of the time, several models must be used to calculate the complete range of nuclear reaction observables of interest for nuclear data. In this case models have to be closely coupled in a nuclear reaction code like TALYS (A.J. Koning in [1]), EMPIRE, STAPRE, MEND… These codes have in common the fact that they integrate the three basic nuclear reaction models for the calculation of nuclear reaction above the resonance range (optical model, pre-equilibrium, and, statistical model). They of course implement slightly different versions of these models (some being more refined than others), but they share the need for a lot of ingredients (model input parameters) that need to be obtained form adjustment, systematics or other model calculations. Obtaining these input parameters for all nuclei is the goal of the RIPL-3 effort, led by the IAEA (R. Capote in [1]). This third version of the RIPL effort is emphasizing the use of microscopic models to obtain these parameters rather than phenomenological adjustments.

The optical model potential (OMP) is one of the main ingredients needed for calculating nuclear reactions. The phenomenological dispersive optical model approach is able to reduce the number of adjusted OMP parameters, and at the same time improve the description of the energy dependence of the potential, producing model prediction that match the experimental data very closely (R. Capote in [1]).

Another ingredient that is important for statistical model calculations is the description of the level density, which measures the amount of phase space available in the exit channels. Traditionally, variants of the Fermi gas model are used to describe the level densities, however these have a lot of parameters that need to be finely adjusted to match experimental nuclear reaction data. Another approach is the calculation of the level density from nuclear structure models (shell model or mean field) that predict single particle orbitals that are subsequently form which the combinatorial of the particle-hole configurations is computed, producing *ab initio* predictions of the level density (see papers by C. Johnson and S, Goriely in [1]). Moreover, this combinatorial approach to the level densities allows for précis description of the spin- and parity-dependent components of level densities, which are only roughly described in Fermi gas model variants.

The gamma strength function $\Gamma\gamma$ used to calculate the relative weight of γ emission compared to other compound nucleus de-excitation channels. It is traditionally calculated by assuming a Lorenzian distribution for the dipole resonance strength. This hypothesis seems to be valid for stable nuclei, but nuclear structure models (QRPA) predict that far from stability, the dipole resonance strength differ significantly form the assumed Lorenzian shape. However it is possible to calculate $\Gamma\gamma$ directly from the results of QRPA calculations (S. Goriely in [1]), and those $\Gamma\gamma$ have been shown to be as good as the Lorentzian one in the valley of stability and can be expected to perform much better for exotic nuclei.

The modelling of pre-equilibrium is generally thought of as the weakest link in the nuclear reaction model chain used to evaluate nuclear data. However, recent show that the statistical model which lies “downstream” from the pre-equilibrium process in the reaction model chain, is very sensitive to the spin and parity distribution in which the pre-equilibrium “leaves” the compound nucleus studies (T. Kawano in [1]). The pre-equilibrium model used in this study is a more complete quantum formulation of the pre-equilibrium process (Feshbach-Kerman-Koonin or FKK model). However, even the hypotheses underlying this model can be criticized, and a more exact formulation of the pre-equilibrium process using ingredients that are individually validated (DWBA-style collision matrix elements), and doing away with the traditional assumptions of FKK, has been shown to produce significantly different continuum

multi-step scattering observables, with the added advantage of treating direct and pre-equilibrium emission on equal footing (M. Dupuis in [1]). There is however a major drawback to this new approach: it is extremely computation intensive, In order to “shoehorn” such a complicated modelling into the existing nuclear reaction codes, it is nevertheless possible to use the inversion approach (R. Mackintosh in [1]) since it can produce a simple, easy to handle local potential equivalent to the more delicate ones like the one used in the above study.
Another model that is not modelled in its full complexity in nuclear reaction codes is the direct semi-direct capture model. Yet, more careful treatment (G. Arbanas in [1]) of this process has been shown to alleviate calculations vs. experiment discrepancies.
Coupling to continuum channel (direct break-up) is rarely included in evaluations, however there is strong demand for evaluated data involving loosely bound participants like deuterons, light neutron rich nuclei (for fusion technology), and very far off stability nuclei (in astrophysics). The CDCC (Continuum Discretized Coupled Channels) approach explicitly treats the coupling to the continuum for deuterons (P. Chau in [1]) or light nuclei (N. Keeley in [1]).
Fission parameters (fission barrier height and curvature, transition states and class II and III states) can so far only be obtained reliably by adjustment to experimental fission cross sections, since no model is presently able to predict these parameters with the needed accuracy. However, a major step has been made in predicting fission fragment yields from nuclear structure calculations (H. Goutte in [1]). By solving the time dependent Schrödinger equation for a collective wave function of the fissioning nucleus in a two dimensional potential energy surface obtained from Hartree-Fock-Bogoliubov constrained on the elongation and asymmetry collective coordinates, the flux of the provability density crossing the scission line is calculated and the fission yields are derived from it. Although comparisons with experiment exhibit some differences, the agreement is very good considering that no adjustment was performed and that the only input for this calculation is the Gogny D1S nucleon-nucleon effective interaction.
Besides fissions cross sections and fission fragment yields, the fission neutron and gamma multiplicity and spectra are very important, especially for criticality studies. Descendants of the Los Alamos model for fission fragment decay are still used to this day for evaluating the mean neutron multiplicity. This approach besides having poor predictivity (parameters must be tuned) can only be used to calculate the mean neutron multiplicity and not the more detailed multiplicity distribution. A new study using a Monte-Carlo description of the statistical fission fragment decay was presented (P. Talou in [1]), This method can not only calculate the neutron multiplicity distribution but also all the correlation between neutron and gamma spectra. However, a strong sensitivity to initial conditions for fragment decay (yields and TKE) is seen, prompting further studies both experimental and theoretical.

Covariances
In order to assess the uncertainties associated with complex simulation calculations stemming from nuclear data, the covariance matrix of the evaluated data must be known. To determine this covariance matrix several approaches are shown. The Monte-Carlo sampling of model parameter space (A.J. Koning in [1]) can produce such a matrix with minimal specific treatment. On the other hand the Bayesian updating of prior information by new experimental evidence necessitates a more specific treatment: determination of the prior by maximizing the entropy of the model response to model parameter changes (H. Leeb in [1]), but it is potentially more accurate and less dependent on various hypotheses.

Final treatments

The processing of the evaluated nuclear data, i.e. turning the ENDF exchange file format into information that is usable by application codes, must be performed with care so that the information that is fed to application code is not degraded during processing (G. Chiba in [1])
After being produced, the performance of evaluated nuclear data must be assessed in various systems that mimic the whole range of potential applications. If the simulated restitution of the experimental system is consistent with the associated measurements, the evaluated data is satisfactory; otherwise a new evaluation is needed. A more precise analysis of the sensitivity of such integral experiment to the various cross sections in different energy groups, can guide the evaluators on the track of improving the evaluated data.

Finally, once evaluated data is deemed satisfactory and validated, it can go into an evaluated data library and is ready to be distributed to the final users. OECD Nuclear Energy Agency (NEA) is responsible for the nuclear data dissemination for OECD countries (see paper by Y. Rugama in [1]). It runs the NEA Data Bank Service [3], and also provides support to JEFF European evaluated nuclear data library project.

Summary

During the P(ND)^2 workshop, a lot of promising ways of improving the nuclear data have been shown. Some of them are already used to produce nuclear data like indirect measurement of hard to handle/obtain target through transfer reactions. Some of them will be implemented in the short term like the microscopic description of the level densities and gamma strength functions, which will be present in the next version of TALYS to be released at the ND2007 conference. Finally, some of the developments shown in P(ND)^2 are not mature enough to be of practical use for short term nuclear data application, but they show great promise for longer term uses. Two examples of such very promising developments are the fully microscopic fission yield calculation and the fully microscopic treatment of the pre-equilibrium process, which both show that significant progress has been recently achieved in the modelling of these processes.
Finally, all the participants to the P(ND)^2 workshop must be thanked for their great contributions that allows us to draw a clearer picture of the future of nuclear data production methods n the short to intermediate (up to 10 years) term.

References

[1] Proceedings of the “Perspectives on Nuclear Data for the Next Decade” Workshop, edited by E. Bauge and C. Nordborg, NEA/OECD, Paris, 2006.
[2] X. Ledoux, et al. in present proceedings.
[3] NEA Data Bank Service, http://www.nea.fr.
[4] ND2007, Nuclear Data for Science and Technology 2007, Nice April 22-27, www,nd2007.org.

Biomedical aspects of high-energy neutrons

J. Blomgren

Department of Neutron Research, Uppsala University, Box 525, S – 751 20 Uppsala, Sweden.
Jan.Blomgren@tsl.uu.se

Abstract: Presently, many new applications of fast neutrons are emerging or under development, like dose effects due to cosmic-ray neutrons for airplane crew, fast-neutron cancer therapy, studies of electronics failures induced by cosmic-ray neutrons, and accelerator-driven incineration of nuclear waste and energy production technologies. All these areas would benefit from improved neutron dosimetry. In this paper, the presently rapid progress on measurements of double-differential neutron-induced nuclear reaction data is described. With such data at hand, the full response of in principle any system, including human tissue, can be calculated in detail. This could potentially revolutionize our understanding of biological effects in tissue due to fast neutrons.

Introduction

Recently, a large number of biomedical applications involving high-energy (>20 MeV) neutrons have become important. It has been established during the last years that airflight personnel receive among the largest radiation doses in civil work, due to cosmic-ray neutrons [1]. Cancer treatment with fast neutrons is performed routinely at several facilities around the world, and today it represents one of the largest therapy modalities besides the conventional treatments with photons and electrons [2].

When a body is irradiated with charged particles, like electrons, the dose, i.e., the energy released per volume, is deposited directly. When uncharged particles are used, like photons or neutrons, an additional step is needed, i.e., the conversion of kinetic energy of the incident uncharged particle to charged particles within the volume. It is well known that the effect of a certain dose, i.e., a given deposited energy, can be very different for different particles in a biologic system. As an example, the cell survival rate for 1 Gy of 5 MeV electrons or 1 Gy of 5 MeV alpha particles differs by an order of magnitude. Thereby, the same dose given in, e.g., electron and neutron therapy can result in rather different biologic effects.

When comparing various therapy modalities, there are some striking features. Charged particles all deposit dose directly, but with different biologic results. Uncharged particles, i.e., photons and neutrons, first have to interact with tissue, resulting in charged particles being released. After having been released, these secondary charged particles deposit energy resulting in tissue damage.

When comparing photons and neutrons as primary particles, there is one striking difference. Photon interactions result almost exclusively in release of electrons, while neutrons induce emission of many different charged particles. This means that a fundamental understanding of the effects in tissue due to neutrons require knowledge of two stages. First, the probability for neutrons to create charged particles must be known, and this information has to be detailed, i.e., the particle type, its energy and direction has to be known. Second, the biologic effect of this secondary particle at its energy must be known.

Today, the biologic effects of the various charged particles released after neutron interaction in the most common atomic nuclei in tissue are relatively well known. Thus, the second stage above is under reasonable control. What is not equally well known is the first stage, i.e., the microscopic cross sections for creation of those charged particles.

In this paper, the presently rapid progress on measurements of double-differential neutron-induced nuclear reaction data is described. With such data at hand, the full response of in principle any system, including human tissue, can be calculated in detail. This could allow a fully reductionistic approach to the entire problem of understanding the biologic effects due to neutron radiation, as being outlined below.

Because cross sections for neutron-induced reactions are in general poorly known, the existing dosimetry methods and treatment techniques are to a large extent based on experience, rather than on knowledge of fundamental physics. Due to the recent development of neutron beams with good intensity and energy resolution, it is today possible to study all

the fundamental processes involved in detail, and thus dramatically improve both the dose determination in neutron fields and the radiation quality planning in connection with tumour therapy.
In the relevant energy range (up to about 70 MeV for therapy and even higher for aviation doses), it is unfortunately difficult to describe nuclear processes theoretically in a simple way. Compound nuclear processes, direct processes and intermediate or pre-compound processes are all important and nuclear reaction models must take into account all these processes and, where appropriate, the competition between them. As a result, predictions based on theory are sometimes uncertain to 30 % or more. Such uncertainties are far larger than acceptable in, e.g., a treatment situation.
This situation is different in photon and electron interaction with tissue, which is governed by the well-known electromagnetic interaction, in which theory predictions of cross sections can be made with an accuracy of far better than 1 %, i.e., other uncertainties dominate. If cross sections cannot be computed, they have to be measured, but the data base for neutrons is meagre in this energy region.
High-energy neutron data are also of primary importance in other applications, like single-event effects in electronics [3] and accelerator-driven systems for incineration of nuclear waste [4]. All the areas above are of interest from dosimetry point of view. For the applications involving tissue, it is evident that techniques for dose determinations are of great importance. Concerning electronics effects onboard aircraft, there is a need for light and inexpensive neutron intensity monitors, similar to the dosimeters used for estimation of health effects.

Links between fundamental physics and tissue effects

Like X-rays and gamma-rays, neutrons exert their biological effect through secondary charged particles, but whereas photons interact with atomic electrons, neutrons interact with nuclei and the secondary particles are nuclear particles such as protons, deuterons, alpha-particles and heavier nuclear recoils. Evidently, a neutron transfers its energy to tissue in two stages. The first stage involves the interaction of a neutron with a nucleus, which can result in a wide range of secondary charged particles. The second stage involves the transfer of energy from secondary charged particles to tissue through excitation and ionization. The quantity kerma, an acronym for Kinetic Energy Released in MAtter, is used to describe the initial interaction, i.e., the first stage. It corresponds to the kinetic energy released by the primary neutrons per unit mass in the form of secondary charged particles [5].
Absorbed dose is defined as energy absorbed per unit mass from the secondary charged particles, i.e., the second stage. Thus, the concepts of kerma and absorbed dose are not identical, because the secondary particles have a certain range and deposit their energy predominantly downstream their point of origin. The secondary charged particles are preferentially emitted in the forward direction, which means that the absorbed dose is low at the surface and rises with depth towards the range of the charged particles. Kerma, on the other hand, does not rise but falls slowly with depth as the incident beam is attenuated [6]. In photon dosimetry, kerma is a more directly useful quantity than for neutrons [7], since the difference between kerma and dose is smaller in this case.
It is important to emphasize that in neutron dosimetry, the kerma coefficient is only a measure of how much energy per unit fluence is given to light charged particles and residual nuclei in a certain volume, regardless of the nature of and energy spectrum of the secondary particles. Since the biological response varies dramatically with ionization capability, i.e., the particle type and energy, the same kerma or dose does not necessarily correspond to the same damage (see below).
There are two ways kerma coefficients are determined; from direct calorimetric measurement of kerma, and from calculation of kerma coefficients from basic nuclear cross sections. Direct measurement of kerma coefficients can be difficult and values are available only for a few elements and neutron energies. Moreover, such measurements require total particle equilibrium in the studied volume. This is not always the case in practice, which necessitates significant corrections. Calculation of kerma from basic nuclear data requires information on all significant reaction channels, including angular and/or energy distributions of secondary reaction particles, which have to be explicitly represented. Such information is taken from nuclear data libraries, which normally are obtained by evaluation of experimental microscopic cross sections and nuclear model predictions.

Radiation quality

Different types of ionizing radiation cause different tissue damage, in spite of the same energy being deposited. This is primarily due to the fact that the cell damage proceeds via two mechanisms, namely creation of free radicals and DNA strand breaks.

In the first mechanism, molecules in the cell are being ionized and become chemically much more reactive, which affects the cell chemistry and metabolism. This requires very little energy transfer, of the order of a few eV, and whether the creation of these reactive chemical elements is well localized or more diffuse does not make a very large difference. Instead, the total number of created reactive elements is most important, and thus the total deposited energy per unit mass gives a reasonable estimation of the cell damage. Thus, which type of particle causes the ionization is not very crucial.

In the second mechanism, the ionizing radiation breaks the DNA molecule and thereby disturbs the cell reproduction. This damage is much more efficient if both strands are struck close to each other. If just one strand is broken, the remaining one can often be used in the repair process. Thus, this mechanism is more efficient for radiation with large ionization per unit length, i.e., well localized radiation. This argument points towards relatively heavy ions, like alpha particles, which have a much larger ionization per unit length than, e.g., electrons.

Ionization per unit length is often expressed in terms of Linear Energy Transfer (LET). The "biological effectiveness" is related to LET, but not linearly. The lowest LET radiation is due to photons and electrons. The biological effect increases with increasing LET, until a maximum is reached at about 200 keV/μm. Going to even higher LET makes the effectiveness go down again, simply because a cell cannot be killed more than once, no matter how much localized dose is given.

Since high-energy neutrons produce a multitude of secondary particles, from high-energy protons, with relatively low LET, to low-energy alpha particles and heavier recoils, which have very high LET, the damage caused by neutrons is a complicated function of the delivered energy, or kerma.

Beyond KERMA

As mentioned above, the kerma coefficient is the average energy transferred from neutrons to charged particles (including recoils) per unit mass of material per unit neutron fluence. It is widely used for dosimetry in neutron therapy and radiation protection. Where applicable, mostly in the low-energy region, kerma coefficients can be directly measured. This is the reason why the kerma concept is being used; it allows a determination of the dose even if microscopic cross sections are unavailable. Alternatively, one can calculate kerma coefficients from microscopic nuclear data. A comparison of the calculated and the measured kerma coefficients provide a valuable integral test of the microscopic cross section data.

However, what is of more interest, especially in treatment planning, is the absorbed dose in the treatment volume, including all aspects playing a role, like, e.g., ionization density and oxygen abundance. Although kerma coefficients could be used for a rough estimate of the biologic effect, there is no simple relation between kerma and cell damage. In addition, such a calculation is not performed from first principles. The whole kerma concept could actually be omitted by calculating the biologic effect in a specific volume directly by a Monte Carlo radiation transport code.

It should be pointed out that double-differential cross sections contain much more information than kerma. Kerma can be obtained by integrating double-differential cross sections over all ejectile energies and angles, but in this process, valuable information is lost. For instance, it is possible that two reactions give the same kerma, but significantly different tissue damage, because the different particles are released, or energy or angular distributions can be different. On the other hand, knowledge of kerma does not allow double-differential cross sections to be determined. With the rapid development of computing power and numeric methods, full Monte Carlo modelling of radiation effects can be expected to become the standard tool within a relatively short future, and estimations based on kerma might gradually become less important.

Which data are important?

About half the dose in human tissue due to neutrons of several tens of MeV comes from proton recoils in neutron-proton (*np*) scattering, 10-15 % from nuclear recoils due to elastic neutron scattering and the remaining 35-40 % from neutron-induced emission of light ions,

i.e., protons, deuterons, tritons, ^{3}He- and α-particles. With double-differential cross sections for all these reactions in tissue-relevant nuclei, i.e., carbon, nitrogen, oxygen and calcium at hand, the dose distribution could be calculated in detail.
If it is clear which data are of most importance when determining the dose in human tissue, it is less obvious which cross sections to determine for improving dosimetry. Many different nuclear reactions are employed in dosemeters. This also involves reactions not taking place in tissue. An example is fission in bismuth, which has some nice features for dosimetry of high-energy neutrons. The cross section is very small all the way up to about 50 MeV, so it is very useful for dosimetry of high-energy neutrons in a low-energy neutron background. Fission is a good nuclear reaction for simple and portable equipment, because it releases extremely large energy per reaction, making the detection of it relatively unambiguous. With the presently rapidly increasing interest in dose effects in human tissue due to high-energy neutrons, a coordinated research programme spanning over the border between dosimetry and nuclear physics is well motivated, to establish a priority list concerning which nuclear cross sections to measure for development of fast-neutron dosimetry.

The nuclear data situation above 20 MeV

As was mentioned above, the relevant nuclear data for assessing the dose due to fast neutrons are *np* scattering, elastic scattering from nuclei, and light-ion production reactions. An extensive list of references to all experimental data obtained before 2003 is found in ref. [8], and only more recent data are explicitly refereed below.
Of these, the *np* scattering data are of the highest quality. The global data base comprises several thousand data points from thermal energies and up to about 1 GeV, and typically the experimental uncertainties are in the 5 % range. Recently, there has been an intense debate about the *np* scattering cross section at backward angles, where different data sets deviate by 10 % or even more (see ref. [9] for a review). These discrepancies, however, affect only a rather limited angular range, and for the present applications, this is of little importance, because the solid angle subtended is small, which results in very small contributions to the total uncertainty in dose determinations.
The data situation on elastic scattering from nuclei is rather satisfactory up to about 30 MeV. Above this energy, there are published measurements from UC Davis on a few nuclei, including carbon, at 65 MeV. A project on elastic scattering at 100 MeV is in progress at TSL in Uppsala. Up to now, data on hydrogen, deuterium, carbon, oxygen and lead have been published [10,11], and data on nitrogen, silicon, calcium, iron and yttrium are under analysis. The most important finding from a biomedical point of view is that the present nuclear models generally underestimate the cross sections for inelastic scattering on carbon and oxygen in the most important angular range, resulting in a kerma about 30 % too low.
Studies of light-ion production above 20 MeV have been undertaken at UC Davis, UCL Louvain-la-Neuve and Tohoku University. The UC Davis setup was used to measure all light ions emitted from carbon, nitrogen and oxygen at 27, 40 and 61 MeV. In the case of carbon, data are extensive in the forward direction, but more scarce at backward angles, whilst the nitrogen and oxygen data extend only out to 65°. At UCL Louvain-la-Neuve, measurements of the same light ions have been performed between 25 and 75 MeV for carbon and oxygen. The UC Davis and UCL Louvain-la-Neuve data display considerable discrepancies, especially for oxygen in the low-energy domain. Proton and deuteron data from Tohoku have been published for carbon at 65 and 75 MeV. These data, however, have a very high low-energy limit because the experiment was carried out in air.
Recently, similar data have been measured at 96 MeV at TSL Uppsala, covering the entire 20-160° range for all light ions. Full data on oxygen [12] and silicon [13] have been published, and data on carbon are under analysis [14]. It is found that the proton spectra on both carbon and oxygen have a higher cross section in the mid- to high-energy range at forward angles compared to recent state-of-the-art evaluations (see figure 1).

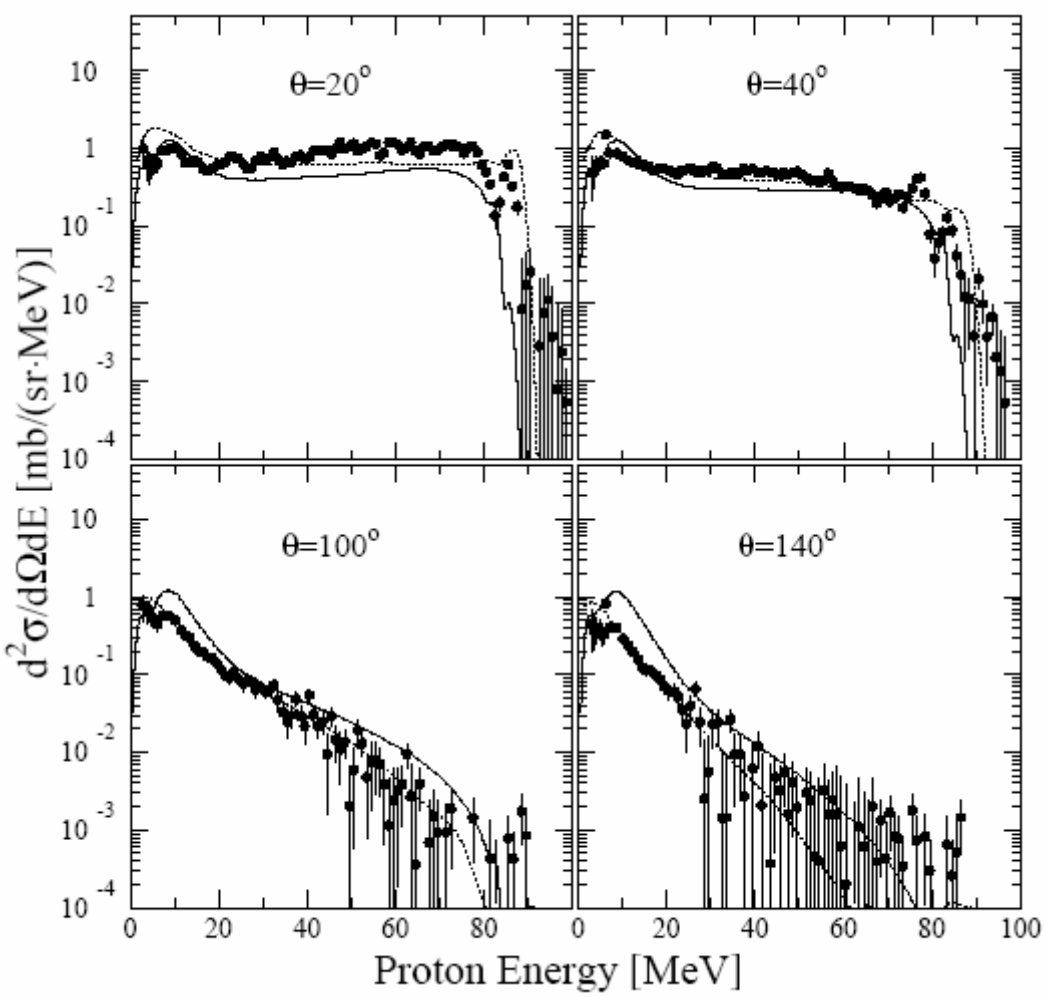

Figure 1. *Neutron-induced production of protons on oxygen at 96 MeV [12]. The curves refer to recent theory predictions. See the paper for details.*

This feature is probably caused by a stronger component of direct reaction mechanisms, e.g., quasi-elastic scattering, and leads, because of the energy weighting, to a partial kerma coefficient that is 35 % higher. Since protons give a large contribution to the total kerma, the obtained value for carbon is about 25 % higher than that given in the evaluations. It is notable that the new data at 96 MeV support a trend observed for similar data up to 73 MeV, both concerning cross sections and kerma coefficients. It is also striking that the kerma coefficients based on microscopic cross sections seem to be systematically higher than those determined using other techniques.

New data at an even higher energy is of high priority to better understand the evolution of various reaction mechanisms with neutron energy, and ultimately to resolve the problems of increasing discrepancy between data and theory with increasing energy. Such a measurement program at 180 MeV is in progress at TSL.

Proton, deuteron and triton production on carbon has been measured in the 300-580 MeV range at angles from 51° to 165° using the white neutron source at PSI. At these high energies, the cross sections can be reasonably well described by relatively simple scaling relations. This is an interesting observation, and it makes sense from basic nuclear physics arguments. At energies above 200 MeV or so, the reaction mechanisms are relatively simple, because only a few nucleons are involved. This means that information from free scattering can be used for reasonably precise predictions, while at lower energies, the effects of the nuclear medium are large, making the theory much more complicated.

Although these energies are higher than common treatment energies, they are of interest for dose delivery due to cosmic-ray neutrons. In addition, they can be of use to guide theory, also for lower energies. Effects clearly visible at 300 MeV might have their onset at much lower energy without being apparent.

To summarize, it seems as the biologic effects of high-energy neutrons have been underestimated. Recently, a re-evaluation of the effects of the Hiroshima and Nagasaki nuclear weapons have indicated that the biologic effect of neutrons might have been underestimated also at low energies (0-5 MeV) [15]. If this result is corroborated, it might affect future recommendations for radiation protection concerning neutrons.

Summary and conclusions

Many new applications of fast neutrons require improved understanding of the fundamental processes involved for their further development. With the presently rapid progress in high-quality measurements of neutron-induced nuclear cross sections, as well as in numeric computation and modelling, it is possible that Monte Carlo methods might become a standard tool within a foreseeable future for detailed calculations of the full response of in principle any system, including human tissue or detector media.
This could allow a fully microscopic approach to assessment of biologic effects in tissue due to neutrons, and this could potentially revolutionize our understanding of these effects. A prerequisite for this development is, however, a continuing rapid growth of the experimental data base on double-differential cross sections for light-ion production in relevant nuclei.

Acknowledgements
This work was supported by the European Union Council, the Swedish Natural Science Research Council, the Swedish Nuclear Fuel and Waste Management Company, the Swedish Nuclear Power Inspectorate, Ringhals AB, the Swedish Defence Research Agency, the Swedish International Development Authority, the Thai Ministry of University Affairs and the International Program in the Physical Sciences at Uppsala University.

References

[1] Bartlett, D.T. et al. , Radiat. Res. Congress Proceedings 2, 719-723 (2000). See also the Proceedings of the International Conference on Cosmic Radiation and Aircrew Exposure, Radiat. Prot. Dosim. 86(4) (1999).
[2] Tubiana, M., Dutreix, J. and Wambersie, A., Introduction to Radiobiology, Taylor & Francis (1990).
[3] J. Blomgren, EU enlargement workshop on Neutron Measurements and Evaluations for Applications, Budapest, Hungary, November 5-8, 2003. EUR Report 21100 EN, Luxembourg, ISBN 92-894-6041-5, European Communities, 2004, p. 130.
[4] J. Blomgren, EU enlargement workshop on Neutron Measurements, Evaluations and Applications, Bucharest, Romania, October 20-23, 2004. EUR Report 22136 EN, Luxembourg, ISBN 92-894-8618-X, European Communities, 2006, p. 1.
[5] A definition can be found in ICRU Reports 60 (1998) and 63 (1999).
[6] Bewley, D. K., The Physics and Radiobiology of Fast Neutron Beams (Medical Science Series), Adam Hilger Ltd., Bristol and New York, p. 18 (1989).
[7] Elford, J. H. and Cunningham, J. R. The Physics of Radiology (American Lectures series; Publication no 1054), 4th edition, Charles C. Thomas Publisher, Illinois, p. 218 (1983).
[8] J. Blomgren and N. Olsson, Radiat. Prot. Dosim. 103(4) (2003) 293.
[9] Critical Issues in the Determination of the Pion-Nucleon Coupling Constant, ed. J. Blomgren, Phys. Scr. T87 (2000).
[10] J. Klug et al., Phys. Rev. C 68 (2003) 064605.
[11] P. Mermod et al., 95 MeV neutron scattering on hydrogen, deuterium, carbon and oxygen, submitted to Phys. Rev. C.
[12] U. Tippawan et al., Phys. Rev. C 73 (2006) 034611.
[13] U. Tippawan et al., Phys. Rev. C 69 (2004) 064609.
[14] U. Tippawan et al., Light charged-particle production in 96 MeV neutron-induced reactions on carbon and oxygen, in Proceedings of Tenth International Symposium on Neutron Dosimetry (NEUDOS10), Uppsala, Sweden, June 12-16, 2006, eds. J. Blomgren and L. Lindborg, to appear in Radiat. Prot. Dosim.
[15] W. Rühm, The role of neutrons in Hiroshima and Nagasaki on cancer risk estimates from the a-bomb survivors, in Proceedings of Tenth International Symposium on Neutron Dosimetry (NEUDOS10), Uppsala, Sweden, June 12-16, 2006, eds. J. Blomgren and L. Lindborg, to appear in Radiat. Prot. Dosim.

Modelling of nuclear data in the fast neutron region

R. Capote[1], M. Sin[2] and A. Trkov[3]

1) International Atomic Energy Agency, NAPC-Nuclear Data Section, Vienna, Austria
2) University of Bucharest, Romania
3) Jozef Stefan Institute, Ljubljana, Slovenia
r.capotenoy@iaea.org

Abstract: With recent developments of nuclear reaction models and the current generation of reaction code systems, nuclear reaction theory is believed to be close to meeting the requirements for various practical applications. A brief overview of the methodology for nuclear data calculations in the fast neutron energy range is presented. Emphasis is put on the consistent and accurate description of all available experimental information as well as on the use of the validated set of input parameters taken from the IAEA/NDS Reference Input Parameter Library database. Theoretical nuclear reaction models that describe the main reaction mechanisms in the relevant energy range are reviewed with special attention paid to the dispersive optical model for nucleon scattering on deformed nuclei. Examples of nuclear data calculations associated with two recent IAEA Coordinated Research Projects (CRP) are presented, including neutron-induced fission cross-section calculations up to 60 MeV for thorium and protoactinium nuclei and neutron production cross-section in proton induced reaction on ^{186}W for the production of therapeutic radionuclide ^{186}Re.

Introduction

Past developments in nuclear technology for energy production were mainly based on uranium-plutonium thermal and fast reactors in order to improve the utilization of the resources of natural uranium. New nuclear data are required in order to address the needs of other emerging nuclear-based technologies for energy applications [1], such as accelerator driven waste incineration, thorium fuel cycle and advanced Gen-IV reactors, Unfortunately, due to the previous lack of interest in many of these new technologies, the quality of nuclear data for the relevant materials is significantly lower than for comparable materials in the traditional uranium and mixed-oxide fuel cycles [2]; moreover the characteristic maximum incident neutron energy of 20 MeV was commonly used, while an extension of the energy range up to 200 MeV is highly desirable There is also a renewed interest in non-energy applications [1] such as radioisotope production for diagnostics and therapy, charged-particle beam therapy, materials analysis and, especially, in nuclear astrophysics, which is constrained to relying upon theoretical calculations of nuclear reaction cross sections when modelling the distribution of isotopes throughout the universe.
Important experimental measurements of the cross sections of materials relevant to the new technologies have been reported recently – these data require new evaluation efforts. With recent developments of nuclear reaction models and the current generation of reaction code systems, nuclear reaction theory is believed to be close to meeting the requirements for theory based evaluation. An overview of theoretical nuclear reaction models that describe the main reaction mechanisms in the fast neutron energy range is presented in Section I. The current status of the Reference Input Parameter Library for nuclear model calculations is reviewed in Section 2. Examples of nuclear data calculations associated with two recent IAEA CRPs are presented in Section 3. Finally, the conclusions are given.

Nuclear data calculations in the fast neutron range

An important trend in the evaluation of neutron and charged-particle nuclear data is the increased use of nuclear reaction theory to compute cross sections, spectra and angular distributions for a variety of applications. This use of model codes offers many advantages such as the preservation of the energy balance and coherence of partial cross sections with total and/or reaction cross sections. Such theoretical approaches also allow the prediction of nuclear data for unstable nuclei and fill gaps in the existing experimental data. The nuclear data calculations presented here are based primarily on a theoretical analysis with the nuclear modular system EMPIRE 2.19 [3] In the evaluation process, the EMPIRE code accounts for

all nuclear reaction models needed to evaluate nuclear reactions in the whole energy range of interest. This range starts just above the resonance region, in the case of a neutron projectile, and can extend up to intermediate energies of 150-200 MeV. On the basis of a large suite of implemented nuclear reaction models, the EMPIRE system is able to produce a nuclear data file comprising a complete set of cross sections. The obtained file conforms to ENDF-6 format rules, satisfies internal consistency constraints and represents well the basic experimental data on which the evaluation is based.
The calculations described in this paper are based on a theoretical analysis that utilizes the optical and direct reaction models, pre-equilibrium exciton model and the full featured Hauser-Feshbach model. The coupled-channel ECIS03 code [4] incorporated into the EMPIRE-2.19 system was used for optical model calculations which are described in the next subsection. Pre-equilibrium emission was taken into account by module PCROSS, featuring one-component exciton model with gamma, nucleon and cluster emissions. Hauser-Feshbach (HF) [5] and Hoffmann-Richert-Tepel-Weidenmüller (HRTW) [6] versions of the statistical model were used for the compound nucleus cross section calculations. Both approaches include decay probabilities deduced in the optical model for fission [7] (if needed) and account for the multiple-particle emission, and the full gamma-cascade. We now focus on the description of the phenomenological dispersive coupled-channel optical model (DCCOM) potential for nucleon scattering up to 200 MeV.

Dispersive optical model for deformed nuclei

The optical model is one of the fundamental theoretical tools which provides the basis of nuclear reaction data analysis and evaluations. Koning and Delaroche [8] stressed the importance of deriving optical model potentials (OMP) *"based on a smooth, unique functional form for the energy dependence of the potential depths, and on physically constrained geometry parameters… this enables one to predict basic scattering observables over a broad mass range and over an energy range that covers several orders of magnitude in MeV. Thereby, the necessity of using different OMPs in different energy regions has been removed".* We want to stress once again on the utmost importance of the above statement for a successful nuclear data evaluation. Using the optical model, one can calculate not only total, elastic and reaction cross sections, but also transmission coefficients needed in the statistical and pre-equilibrium model calculations. Thus, the unique set of OMP parameters that can reproduce well nucleon scattering data over a wide energy range are essential to make reliable nuclear data prediction.
The EMPIRE default neutron and proton optical model calculations are based on the Koning and Delaroche [8] OMP for spherical nuclei. However, nuclei studied in this work are characterized by a stable ground-state deformation; therefore the coupled-channel calculation is needed. A dispersive coupled channel OMP has been derived recently for nucleon scattering on ^{232}Th nucleus [9] and a regional parameterization for actinide nuclei has been proposed [10,11]. A similar methodology has been applied to derive an OMP for nucleon scattering on tungsten isotopes. These two OMPs are used in nuclear data calculations presented in Section 3.
The derived DCC OM potential parameters for tungsten isotopes[†], assuming that the rigid-rotor axial symmetry holds, are listed in Table 1. The calculated total neutron cross section data were used to obtain the ratio $[\sigma(^{186}W)-\sigma(^{182}W)] / \{[\sigma(^{186}W) + \sigma(^{182}W)]/2\}$ for the DCC OM potential. Calculated results were compared with measured data in the Figure 1. Guenther experimental data were shifted down by -0.008, while DCC OMP calculations were shifted up by +0.006, well within the estimated uncertainty of the vertical scale (around 0.02) [13], arising from uncertainties in the areal densities of the tungsten targets. The measurements are very well reproduced by the axial rigid-rotor DCC OM potential calculations with the present optical potential parameters from Table 1. Similar agreement was obtained for the ratio of other tungsten isotopes.

[†] Presented at International Workshop on Nuclear Reaction Mechanisms, Varenna, Italy, June 2006,

Table 1. *Dispersive coupled-channel OMP parameters for nucleon induced reactions on W isotopes (DCC OMP parameters' definition follows Ref. [**Error! Bookmark not defined.**]). Geometry parameters that depend on the mass number are marked in bold. Parameters in bold correspond to ^{182}W, ^{184}W and ^{186}W respectively.*

	VOLUME	*SURFACE*	*SPIN-ORBIT*
Real depth [MeV]	V_0 = 48.3; λ_{HF} = 0.00933 C_{viso} = 10.0	dispersive	V_{SO} = 6.04 λ_{SO} = 0.005
Imaginary depth [MeV]	A_V = 10.75; B_V = 83.75 E_a = 130.	W_0 = 21.2; B_S = 14.69; C_S = 0.00968 C_{wiso} = 23.5	W_{SO} = -3.1 B_{SO} = 160.
Geometry [fm]	$\rho_{H\Phi}$ = 1:2377; 1:2342; 1:2307 $\alpha_{H\Phi}$ = 0:6290; 0:6280; 0:6270 ρ_{ς} = 1:0746 α_{ς} = 0:6790; 0:6870; 0:6950	ρ_{Σ} = 1:24 α_{Σ} = 0:510; 0:513; 0:516	$\rho_{\Sigma O}$ = 1:1293 $\alpha_{\Sigma O}$ = 0:59
Deformation	β_2 = 0.229, β_4 = -0.064, β_6 = +0.008 for ^{182}W β_2 = 0.242; β_4 = -0.073, β_6 = +0.017 for ^{184}W β_2 = 0.197; β_4 = -0.092; β_6 = -0.0011 for ^{186}W		
Coulomb param.	C_{Coul} = 2.00, r_C = 1.0619 and a_C = 0.640		

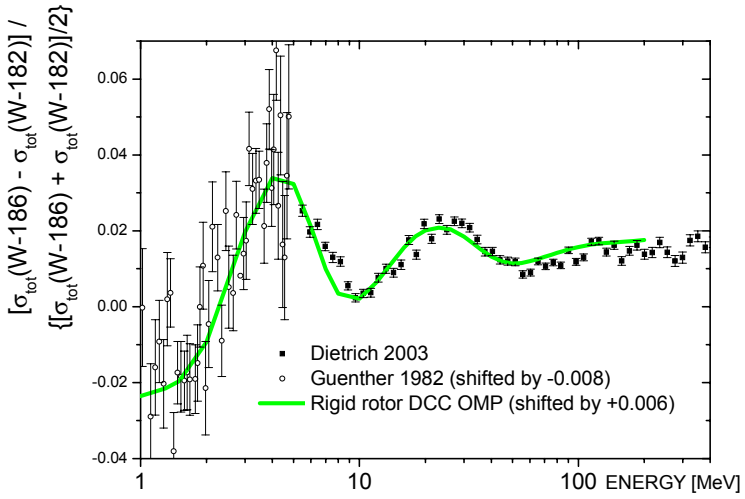

Figure 1. *Energy dependence of the measured ratio [$\sigma(^{186}W)$-$\sigma(^{182}W)$] / {[$\sigma(^{186}W)$ + $\sigma(^{182}W)$]/2} data by Guenther et al [12] and Dietrich et al [13] versus DCC OMP calculations*.

Recommended Input Parameters Library (RIPL-2 and RIPL-3)

The major sources of uncertainty in any model based evaluation are the input parameters required to undertake the theoretical calculations. The practical use of nuclear model codes requires considerable numerical input data that describe the properties of the nuclei under consideration and the interactions involved. Therefore, the IAEA has organized extensive coordinated efforts to develop and assemble a library of evaluated and tested input parameters for nuclear-model calculations. An electronic Starter File was developed and made available to users worldwide in 1998 as RIPL-1 [14]. Subsequent studies resulted in the revision and extension of the starter file to produce a consistent library containing recommended input parameters, large amounts of theoretical data suitable for nuclear reaction calculations, and a number of computer codes for parameter retrieval, determination and other uses. A new *Handbook for Calculations of Nuclear Reaction Data, RIPL-2 [15]* has been published recently and is also available on-line (http://www-nds.iaea.org/RIPL-2/). While RIPL-2 constitutes a consistent set of nuclear reaction input parameters, the database is limited to neutron-induced reactions up to 20 MeV (i.e., typical for conventional power

reactors) and a selected set of charged-particle induced reactions. Extensions to the RIPL-2 database are required in order to address the needs of other emerging nuclear-based technologies as those covered in the current work. Therefore, a third and final phase of the IAEA RIPL project is on-going to address *"Parameters for the calculation of nuclear reactions of relevance to non-energy nuclear applications"*.
Examples of recent nuclear data calculations, relying on RIPL parameters, associated with two recent IAEA Coordinated Research Projects are discussed in the next Section.

Recent theoretical nuclear data calculations within IAEA CRPs

Neutron induced fission reaction on ^{232}Th and ^{231}Pa in the fast neutron range

The highlights of the coordinated research project of the International Atomic Energy Agency (IAEA) on the evaluated nuclear data of nuclides for the thorium-uranium fuel cycle are presented in a complementary paper at the same venue [16]. We show here results of the theoretical calculation of neutron induced fission reactions on ^{232}Th and ^{231}Pa up to 60 MeV. Full evaluation will be published elsewhere. Near-threshold behaviour has been extensively discussed in Ref. [7]. The initial set of the nuclear model parameters employed in present calculations was based on the IAEA RIPL-2 database [15] as updated within the RIPL-3 CRP [17]. However, the adjustable nuclear model parameters need to be varied to reproduce the selected set of experimental data for the nucleus under study. An example of the measured and evaluated neutron-induced fission cross-section data for ^{232}Th and ^{231}Pa are shown in Figures 2 and 3. Considerable effort has been expended on the description of the important and complex fission threshold resonance region of both nuclei.

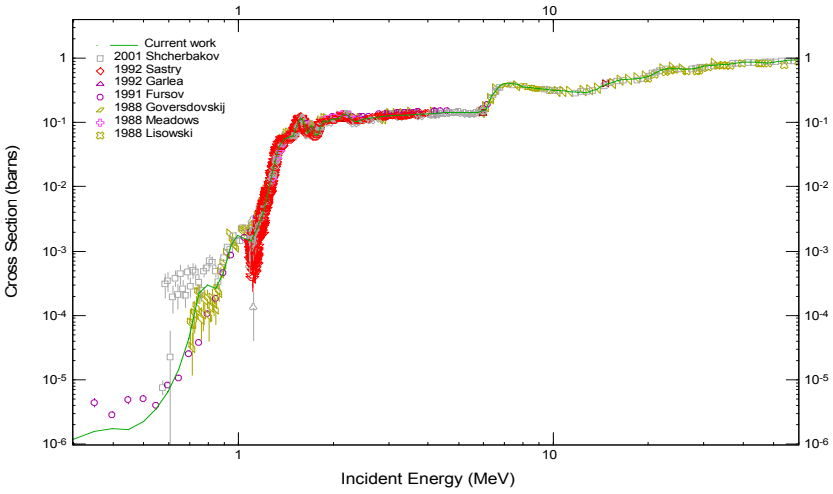

Figure 2. *Measured and evaluated cross-section data for ^{232}Th(n,f).*

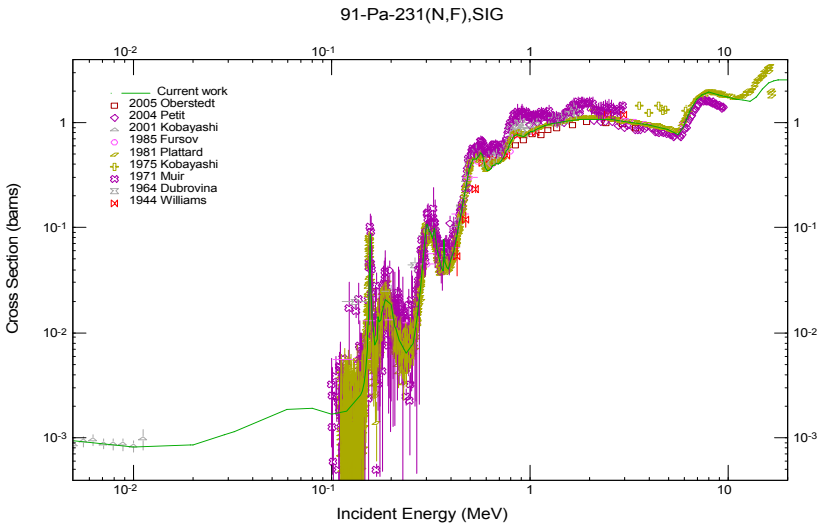

Figure 3. *Measured and evaluated cross-section data for ^{231}Pa(n,f).*

Cross sections for the production of therapeutic radionuclides

Radiopharmaceuticals play an important role in modern medicine in terms of both diagnostic investigations and therapeutic treatment. The role of nuclear data is mainly with respect to ensuring the quality assurance of the radioactive materials and methods adopted in such work [18,19]. Generally, the radionuclides used in nuclear medicine possess particular decay characteristics – low-energy α, β^- and Auger electron emitters. While effective in diagnostic and therapeutic treatments, these somewhat elusive decay characteristics can create difficulties when using such properties to determine their production cross sections to ensure a pure radionuclidic product; therefore knowledge of their production reaction cross sections is often poorly defined.

An IAEA Coordinated Research Project (CRP) has been successfully organized with the primary aim of improving the production cross-section data for therapeutic radionuclides. The work is close to completion [20]. Experimental data compilations and data selection, theoretical calculations and the final evaluations for each of the reactions producing therapeutic radionuclides will become available within a few months. As an example, one of the reactions under study for the production of beta-emitting ^{186}Re radioisotope by a proton induced reaction on ^{186}W is shown in Figure 4. EMPIRE and ALICE theoretical calculations are shown together with the selected experimental data and the CRP recommendation (Pade spline fit of experimental data. Dispersive coupled-channel optical model parameters for proton incident on ^{186}W (see Table 1) were employed in the EMPIRE calculations.

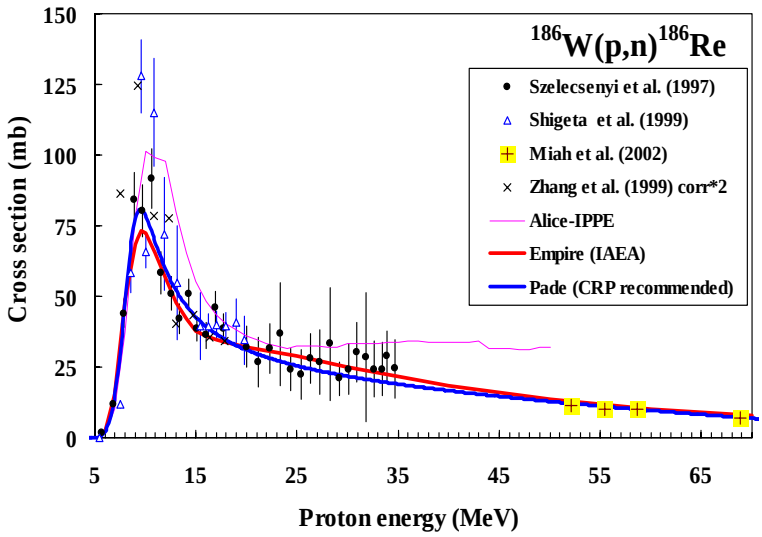

Figure 4. *Measurements and calculations of the ^{186}W(p,n)^{186}Re cross-section*

Conclusions

A brief overview of the methodology for nuclear data calculations in the fast neutron energy range has been presented emphasizing the consistent and accurate description of all available experimental information and the use of the validated set of input parameters taken from the IAEA/NDS Reference Input Parameter Library database. EMPIRE neutron induced fission cross-section calculations on thorium and protoactinium up to 60 MeV, and EMPIRE calculated therapeutic radionuclide ^{186}Re production by proton induced reaction on ^{186}W are being shown to be in good agreement with available experimental data. Nuclear reaction theory is shown to be in good shape to meeting the requirements for various practical applications.

Acknowledgements

Authors would like to thank all of the participants associated with the various IAEA/NDS CRPs for their contributions identified with the resulting recommended data. RC would like to thank E. Soukhovitskii, J.M. Quesada and S. Chiba for their significant contribution to the development of the dispersive coupled-channel optical model potentials; Special thanks to A. Nichols for his constant encouragement and support.

References

[1] D. W. Muir and M. Herman (Eds), Long Term Needs for Nuclear Data Development, Summary Report of an Advisory Group Meeting, 28 November – 1 December 2000, INDC(NDS)-423, May 2001, IAEA, Vienna, Austria.

[2] V. G. Pronyaev, Assessment of Nuclear Data Needs for Thorium and Other Advanced Cycles in Summary Report of an IAEA Consultants' Meeting, 26 – 28 April 1999, INDC(NDS)-408, IAEA, Vienna, 1999.

[3] M. Herman, P. Oblozhinský, R. Capote et al, Recent developments of the nuclear reaction model code EMPIRE, AIP Conf. Proc. 769 (2005) 1184-1187.

[4] J. Raynal. Optical model and coupled-channels calculations in nuclear physics in Computing as a language of physics, ICTP International Seminar Course, Trieste, Italy, Aug.2-10, 1971 (IAEA, Vienna, 1972), p.281.

[5] W. Hauser and H. Feshbach, Phys. Rev. 87 (1952) 366.

[6] H.M. Hoffmann, J. Richert, J.W. Tepel and H.A. Weidenmuller, Ann. Phys. (N.Y.) 90 (1975) 403.

[7] M. Sin, R. Capote, A. Ventura, M. Herman, and P. Oblozhinský, Fission of light actinides: 232Th(n,f) and 231Pa(n,f) reactions, Phys. Rev. C74 (2006) 014608.

[8] A. Koning and J. P. Delaroche, Local and global nucleon optical models from 1 keV to 200 MeV, Nucl. Phys. A713 (2003) 231-310.

[9] E. Sh. Soukhovitskii, R. Capote, J. M. Quesada, and S. Chiba, Dispersive coupled-channel analysis of nucleon scattering from 232Th up to 200 MeV, Phys. Rev. C72 (2005) 024604.

[10] R. Capote, E. Sh. Soukhovitskii, J. M. Quesada, and S. Chiba, Is a global coupled-channel dispersive optical model potential for actinides feasible? Phys. Rev. C72 (2005) 064610.

[11] R. Capote, E. Sh. Soukhovitskii, J. M. Quesada, S. Chiba and E. Bauge, Isospin dependent dispersive coupled channel optical model potential for actinides, submitted to Phys. Rev.

[12] P. T. Guenther, A. B. Smith, and J. F. Whalen, Fast-neutron total and scattering cross sections of 182W, 184W, and 186W, Phys. Rev. C26 (1982) 2433 – 2446.

[13] F. S. Dietrich, J. D. Anderson, R. W. Bauer, S. M. Grimes, R. W. Finlay, W. P. Abfalterer, F. B. Bateman, R. C. Haight, G. L. Morgan, E. Bauge, J. P. Delaroche and P. Romain. Importance of isovector effects in reproducing total cross section differences, Phys. Rev. C67 (2003) 044606.

[14] O. Bersillon, E. Běták, R. Capote, M. B. Chadwick, T. Fukahari, A. V. Ignatyuk, S. Kailas, J. Kopecky, V. M. Maslov, G. L. Molnár, P. Obložinský, G. Reffo, Z. Su, M. Uhl and P. G. Young, Handbook for Calculations of Nuclear Reaction Data, Reference Input Parameter Library, IAEA-TECDOC-1034, August 1998, IAEA, Vienna, Austria.

[15] T. Belgya, O. Bersillon, R. Capote, T. Fukahori, Ge Zhigang, S. Goriely, M. Herman, A. V. Ignatyuk, S. Kailas, A. J. Koning, P. Obložinský, V. Plujko and P. G. Young, Handbook for Calculations of Nuclear Reaction Data, RIPL-2, IAEA-TECDOC-1506, August 2006, IAEA, Vienna, Austria.

[16] A. Trkov, Highlights from the Coordinated Research Project on the Thorium-Uranium Fuel Cycle, Third Workshop on Neutron Measurements, Evaluations and Applications (NEMEA-3), 25 – 28 October 2006, Borovets, Bulgaria.

[17] S. Goriely and R. Capote Noy (Eds), Parameters for Calculation of Nuclear Reactions of Relevance to Non-Energy Nuclear Application (Reference Input Parameter Library: Phase III) in Summary Report of the Second Research Coordination Meeting, 28 November – 2 December 2005, INDC(NDS)-0492, March 2006, IAEA, Vienna, Austria.

[18] S. M. Qaim, Nuclear Data Relevant to the Production and Application of Diagnostic Radionuclides, Radiochim. Acta, 89 (2001) 233-232.

[19] S. M. Qaim, Therapeutic Radionuclides and Nuclear Data, Radiochim. Acta, 89 (2001) 297-302.

[20] J.-Ch. Sublet and R. Capote Noy (Eds), Nuclear Data for the Production of Therapeutic Radionuclides, Summary Report of the Third Research Coordination Meeting, 29 May – 2 June 2006, INDC(NDS)-0501, August 2006, IAEA, Vienna, Austria.

ITER, IFMIF and the role of nuclear data

R. A. Forrest

Euratom/UKAEA Fusion Association, Culham Science Centre, Abingdon, Oxon, OX14 3DB, UK
robin.forrest@ukaea.org.uk

Abstract: The aim of fusion research is to achieve as soon as possible the commercial generation of electricity. Fusion is making the transition from an emphasis on plasma physics towards technology and the construction of power plant size facilities for which ITER and IFMIF are crucial. ITER is a fusion device with similar dimensions to a power plant, to be constructed in France. IFMIF is a materials test facility that will generate intense fluxes of neutrons to investigate the damage to materials needed in the prototype power plant.
Designs for such devices require neutron and photon transport calculations to generate the spectra required to provide the nuclear responses. Such calculations require cross section data for all the elements present, typically at energies (14 MeV) larger than those required for fission. The design of IFMIF means that neutrons with energies up to 55 MeV are of importance, increasing further the amount of nuclear data required. General purpose files contain data for a limited number of target nuclides (<400) but in considerable detail, whilst activation libraries cover many more targets (~800), including radioactive ones, and many more reaction types but in less detail.

Introduction

Fusion research worldwide is focused on developing the ability to generate electricity. The ITER project is the next step in this effort; the device will be constructed at Cadarache in France. This is a major international project funded by seven international partners who together represent more than half the world's total population. ITER is designed [1] to generate 500 MW of fusion power, up to ten times more than the energy supplied. In the Fast track concept [2] emphasised by the European Union, ITER is the final experimental fusion device; it will be followed by DEMO which will generate electricity and act as a prototype for future commercial designs. ITER is designed to demonstrate all the technologies required for DEMO except one; the relatively low fluences mean that the materials will not experience the levels of damage envisaged in DEMO. This high fluence testing demands a materials testing facility, IFMIF [3], which will be developed further as part of the European/Japanese Broader Approach agreement.
The design and licensing of devices such as ITER and IFMIF rely to a large extent on data provided by neutronics design calculations. These require qualified computational tools and validated nuclear data for the modelling of neutron transport and the calculation of relevant nuclear responses.
This paper provides an outline of the long-term strategy for fusion technology and gives an overview of the role played by the various types of nuclear data. The current status of the data and the development needs are discussed. The focus will be on the work carried out in Europe, with mention of the work in Japan and the USA.

Fusion Technology Strategy

The roadmap [4] leading to commercial fusion generation of electricity somewhere between 2030 and 2050 emphasises the central nature of ITER supported by IFMIF and other subsidiary machines. According to this strategy the areas of most importance for nuclear data work are the Test Blanket Modules (TBM) in ITER and in the design of IFMIF, especially the target and test cell regions [5]. TBMs will provide the capability to test the various blanket concepts. These are very complex components with issues of thermal hydraulics and diagnostics as well as tritium breeding. IFMIF will use beams of high energy deuterons and therefore the interaction of these with materials emphasises other areas of nuclear data. In addition to the nuclear data it is necessary to develop and qualify computational tools, especially in the area of sensitivity analysis and uncertainty and to carry out integral experiments to test the nuclear data and tools.

Nuclear data for fusion

The range of the nuclear data required for fusion has increased dramatically because of IFMIF. Whereas for ITER only data for neutron and photon transport calculations were needed, for IFMIF the upper energy limit has increased from 20 to 60 MeV and the incident particles now include protons and deuterons as well as neutrons. Inelastic neutron reactions are particularly important since double-differential cross section data are required to properly describe the energy-angle distributions of the emitted secondary neutrons. Secondary photons, produced in the neutron-induced reactions make significant contributions to nuclear responses such as heating and it is therefore necessary that they are included.
Activation calculations require cross sections for a larger number of target nuclides since both stable and radioactive target must be considered. The reason is that in high neutron fluxes long-lived radioactive nuclides are present long enough to react, leading to multi-step pathway production of activity. However, although about twice as many targets and many more reaction types are needed than in a transport file, only cross sections as a function of energy data need to be included. Another type of nuclear data that must be considered, especially for activation calculations, is decay data including half-lives, energy releases and decay modes. In order to carry out experiments it is necessary to be able to describe the neutron spectrum in detail. This is typically achieved using a series of activation foils and an unfolding code. However, as measurements move to energies above 20 MeV the necessary dosimetry data are lacking, this area is one being addressed by the IAEA.

Data needs for ITER
The range of materials in the ITER design is very large. The various components include the first wall components, the TBMs, shield modules, the vacuum vessel, superconducting magnets and the bio-shield. Wall materials are Be, W, C and CuCrZr. The TBMs will contain Be, Li_4SiO_4, Li_2TiO_3, Pb-Li, Eurofer and coolant. The steels used in the shield and vacuum vessel (SS-316L and SS 30467), the magnets and the bio-shield contain the elements: H, He, B, C, N, O, Na, Mg, Al, Si, P, S, K, Ca, Ti, V, Cr, Mn, Fe, Ni, Cu, Nb, Mo, Sn, Ta and W.
For all these materials it is necessary to have general purpose libraries up to 20 MeV with covariance data that have been well validated by benchmarking. Activation data are required for not only these materials but for all other elements as the contribution from impurities is very important.

Data needs for IFMIF
The IFMIF neutron source consists of two accelerators producing a deuteron beam of energy 40 MeV and current 250 mA. This impinges on a flowing lithium target and produces a high intensity neutron field behind the target. The neutron spectrum is fusion relevant, but also has a high-energy tail that extends up to 55 MeV. This energy is significantly larger than the neutron energies relevant for D-T plasmas (14 MeV) and means that the existing data libraries need extension. The reactions between d and Li need careful evaluation so that a realistic neutron spectrum can be calculated. In addition to the neutron-induced data, the interactions of deuterons with materials must also be studied. This is because there will be beam losses in the accelerator and also because the lithium target will contain a range of impurities. The main data need is for activation calculations and will cover all elements as in the case of neutron-induced reactions. It is anticipated that during the initial testing phase the accelerator will use H_2^+ or H^+ rather than D^+ as it is anticipated that this will give less activation of the accelerator. In order to confirm this it is also necessary to have a proton-induced library covering the same wide range of targets.
The materials that will be subjected to the high energy neutron field, apart from the IFMIF device itself are the reduced activity ferritic-martensitic steel (Eurofer), divertor materials such as W and more advanced materials such as SiC and vanadium alloys. The highest priority is assigned to the main constituents of Eurofer: Fe, Cr, W, V, Mn, C and Ta.

Status of fusion nuclear data

Within Europe there has been work on a dedicated fusion nuclear data library that culminated in the European Fusion File (EFF-2.4) [6]. Since that was produced EFF data have been integrated into the general purpose data library JEFF, the most recent version of which is JEFF-3.1 [7]. In Japan there is the JENDL-FF, while in Russia and the US fusion relevant data are included in BROND and ENDF/B-VI respectively, note that the latest release of the US evaluations, ENDF/B-VII, is expected at the end of the year. Nuclear data for fusion was a

major extension of the data for fission and IAEA initiated an international effort to generate a data library that could be used in the ITER project. The first library, FENDL-1 was released in 1994 and has been extensively benchmarked. This was followed by FENDL-2 in 1997 and FENDL-2.1 in 2004 [8].
Activation library development has been most extensive in Europe leading to various versions of the European Activation File (EAF). The current version is EAF-2005.1 [9] released in 2006. EAF-97 was a major contributor to the FENDL-2 activation file, while for the FENDL-2.1 activation file users were recommended to use EAF-2003 which is also the JEFF-3.1 activation file. Some details of the JEFF-3.1 and EAF-2005.1 libraries are given below.

JEFF-3.1
The latest version of the JEFF library, JEFF-3.1, was released in May 2005. The neutron general purpose library contains incident neutron data for 381 materials. The activation library contains data for 774 targets. The decay data library contains data for 3,852 isotopes. The proton special purpose library contains incident proton data for 26 materials. The thermal scattering law library covers 9 materials, and the fission yield library covers 19 isotopes of neutron induced fission yield and 3 isotopes with spontaneous fission yields.
Although the main motivation in moving form JEFF-3.0 to JEFF-3.1 was to resolve various issues relevant to fission such as the underestimated reactivity of small low-enriched Uranium systems when using JEFF-3.0 data, it also enabled recent evaluation work to be included. The evaluations from EFF, particularly relevant to fusion included in JEFF-3.1 are: ^{9}Be, ^{28}Si, ^{46,47,48,49,50}Ti, V, ^{52}Cr, ^{56}Fe and ^{58,60}Ni. Note that the EFF evaluations for W isotopes were completed too late for inclusion in JEFF-3.1, but will be available along with current evaluations for ^{181}Ta and ^{55}Mn for JEFF-3.2. Further details on JEFF can be found in reference [10].

EAF-2005.1
The maintenance release, EAF-2005.1 was produced because of errors in 250 reactions introduced in the n-induced library following the five-fold increase in reaction numbers moving from EAF-2003 to EAF-2005, but also so that the d-induced library [11] could be distributed. Cross section data are given for 62,637 n-induced reactions and for 60,688 d-induced reactions. Decay data are available for 2,192 nuclides; the EASY-2005 overview [12] gives further details and references. The next version, EAF-2007 available at the beginning of 2007, will include a proton-induced library as well as significant improvements to the d- and n-induced libraries.

The role of nuclear data

The role of nuclear data for the two projects considered here, ITER and IFMIF are rather different as is the emphasis that needs to be placed on the two main types of nuclear data, transport and activation. Transport data are required for the main elements in the device under study; they must be comprehensive and should include covariance information. By contrast, for activation impurities, whilst unimportant for transport, often dominate the response in terms of activity or gamma dose rate. This means that once data libraries have been assembled it is necessary to determine which radionuclides are important and the reactions that are responsible for their production.
Deficiencies need to be addressed by new measurements and it is especially important that these cover as wide an energy range as possible. However many of the reactions identified are unlikely to be measured in the near future because either the target nuclide is radioactive or the daughter nuclide is stable or very long-lived. In such cases it is necessary to rely on model calculations and this area has had major advances recently, not as regards new physical models but rather in the ease of use of the various models, and the combination of them so that complete nuclear data files can be produced relatively quickly. This enables starter files to be generated that can be supplemented by well measured quantities or even to act as a final file where none existed before. These model codes are starting to address the area of covariances and uncertainty and promise the ability to produce data which are currently missing and much needed.
An example of an area of work important to ITER is the breeding blanket benchmark experiment [13]. This is designed to test the code and data capabilities that will be required to design a TBM and also to develop the various diagnostics, measurements and analysis capabilities that will be required when the TBM is operational. One of the most important

areas is the production of tritium. The mock up consists of a stainless steel box about 31x31x29 cm filled with metallic beryllium and steel cassettes filled with Li_2CO_3 arranged in a layered structure to approximate the HCPB TBM design. Eight stacks of twelve Li_2CO_3 pellets were used to measure the amount of tritium produced. Following irradiation at the Frascati Neutron Generator (FNG) the pellets were analysed by ENEA, TUD and a Japanese group. An MCNP model was constructed and calculations made using EFF and FENDL data. The C/E results were on average between 0.90 and 0.97 showing that the tritium breeding calculations were conservative. This is an extremely important result as it means that the tritium economy assumptions made for power plants are justified. The level of uncertainty on the results is about 2% due to uncertainties in the ^{7}Li and ^{9}Be cross sections while the total uncertainty of about 6.5% is dominated by the experimental uncertainties. Tritium production is most sensitive to the ^{9}Be(n,2n) cross section. The reason for the under-prediction of tritium production is currently under investigation.

As an example of the determination of the important radionuclides and reactions consider an importance diagram for chromium. Figure 1 shows the diagram for heat output. A series of inventory calculations are carried out using mono-energetic neutrons and the nuclides that dominate, i.e. produce more than 50% of the heat at various decay times are identified. These results are then shown in the diagram by regions labelled by the nuclide. Thus at decay times up to ~ 1000 s at energies < 20 eV and > 3 MeV there are two regions where ^{52}V dominates. The reactions that produce this nuclide are different at the two energies: at high energies the ^{52}Cr(n,p)^{52}V reaction is responsible while at low energies the pathway is ^{50}Cr(n,γ)^{51}Cr(β^{+})^{51}V(n,γ)^{52}V which contains two reactions and a decay. The FISPACT inventory code gives these pathways as part of the output and so enables all the important reactions to be found. Figure 1 is taken from the 'Activation Handbook' [14] a large compilation which contains the activation properties of all the elements and includes data for irradiations in four fusion relevant spectra as well as the importance diagrams covering the energy range from 0.05 eV to 20 MeV, calculated by using EASY-2003. From an analysis of these results it is possible to show that, while 1,917 nuclides are present in the EAF library, 754 are sufficient to describe the activation properties of all elements for irradiations below 20 MeV and decay times up to 10^{6} years. Similarly 1,341 reactions out of the total of 12,617 present in EAF-2003 suffice to produce all the dominant nuclides. This is a very significant reduction and means that effort can be focussed on improving reactions that are most important for applications such as ITER. This focussing is developed further in references [15] and [16] which discuss the data needs for both decay data and cross sections. Reference [15] lists 100 reactions that need to be further considered by the measurement community, and listing 339 reactions which are important but very difficult to measure and so require more detailed model calculations to improve them.

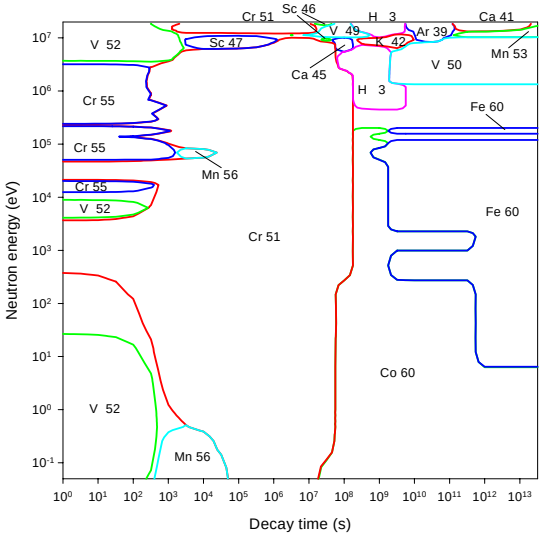

Figure 1. *Activity importance diagram for Cr.*

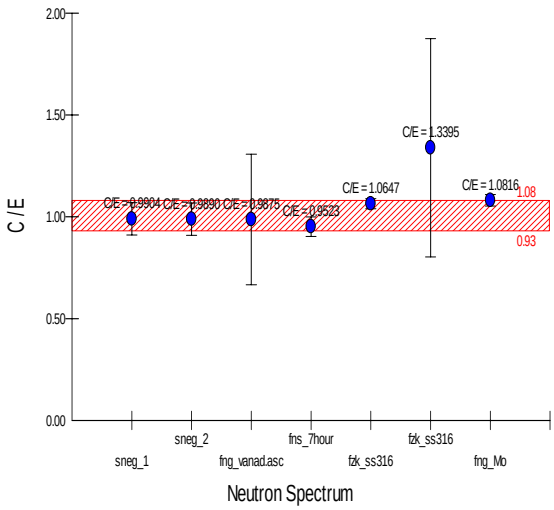

Figure 2. *Integral data for ^{100}Mo(n,2n)^{99}Mo.*

Validation of activation libraries

The validation of the EAF libraries has been done by comparing measurements of the activity of a range of materials in fusion relevant neutron spectra (integral data) and comparing these with calculations with EASY. A new approach which associates C/E not with the radionuclide

but with the reaction producing it has several advantages. In the latest validation report [17], 453 reactions were considered and the report shows C/E plots for each as well as graphs of the differential data. Figure 2 shows results for ^{100}Mo(n,2n)^{99}Mo, in this case there is overlap between the band representing the EAF library uncertainty and the error bars of the individual measurements and so the reaction is judged to be validated. This example shows results for several neutron spectra, unfortunately for most of the reactions there are only one or two C/E values indicating the need for more measurements. When the reactions that have either differential or integral data are counted it is found that there are only about 1,700. This raises the question as to how the majority of reactions in a library such as EAF-2005 can be checked.

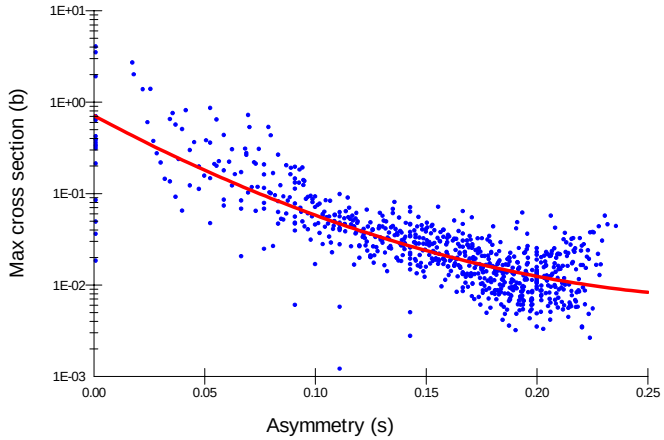

Figure 3. *σ_{max} for (n,p) data in EAF-2005.1 plotted as a function of asymmetry.*

A new approach has recently been developed [18] which involves plotting various quantities such as the maximum cross section (σ_{max}) of a reaction as a function of *A* or *s* (asymmetry). Such a plot is shown in Figure 3 for (n,p) reactions and it can be seen that there is a clear trend which makes it easy to identify reactions that are very discrepant. This has been found to be a very efficient method of spotting reactions with gross errors and will be used in the production of new libraries such as EAF-2007.

Development needs

The long-term fusion programme dictates the future development of fusion nuclear data. Thus the most urgent need is to continue the improvement of data evaluations required for the neutronics analyses of TBMs such as Li, Be, Pb and O, particularly to provide the covariance data. This requires revisiting older evaluations without any uncertainty information in the data files. Covariance data can be obtained either from analyses of experimental data or by theoretical methods. In general, for IFMIF there is a need to extend the data libraries above 20 MeV. This has already been done for the W isotopes, ^{181}Ta and is in progress for ^{55}Mn. While some new evaluation effort is possible many of the deficiencies will need to be addressed by using data from other evaluations. It is especially important that covariance data be added to all these files especially at energies > 20 MeV.

Activation libraries already exist up to 60 MeV for n-,d- and p-incident particles. Of these only the n-induced one has been extensively validated and compared with differential data, much work remains to be done on general improvements of the charged particle libraries. The n-induced library contains uncertainty data for each reaction, but only in a simplified form. There is a need to extend these to more energy groups using existing evaluations, experimental data and model calculations. At this stage it is not feasible to include covariances, but these may also need to be considered in the long-term. Uncertainty libraries are required for both of the charged particle libraries.

Only a very small part of the EAF cross section library is supported by experimental data. This needs to be expanded. Especially valuable are data around or above 20 MeV since they can be very important in deciding between different model calculations. Integral data especially with neutron spectra that extend above 20 MeV are also very important in validating data libraries. A survey of the d-induced reactions most important for IFMIF needs to be done. As a result of this measurements on d-induced reactions may be required.

Conclusions

ITER and IFMIF are important drivers of the extension of nuclear data. ITER, especially for the design of TBMs, requires well qualified transport files extending to 20 MeV containing photon production and a complete treatment of angle-energy distributions of emitted particles.

Covariance data covering correlations between energies of a reaction and between reactions for a target are necessary, but care must be taken to ensure that these are in a format usable by applications. Modern model codes must be used to ensure that files and libraries are complete before focussing on quality improvements. Neutron-induced activation files have reached a high standard, and it is known which reactions are of high priority for improvement. The need for new differential data, particularly around 20 MeV are crucial in supporting model calculations.
IFMIF is responsible for the major extension of data needs, as all data files need to be extended at least up to 60 MeV. The range of materials is similar to that required for ITER, but at higher energies the need for covariance data is more acute. For activation it has been necessary to consider reactions of both deuterons and protons with materials, and unlike the neutron-induced library the experimental support is limited – there are no integral measurements and even the most important reactions are not yet identified. Uncertainty data (not yet covariances) need extending for the n library and including for the d and p ones. The development work on new tools and the benchmarking and validation of new files is essential, and will expand as the data needs become focussed on the higher accuracies that will become essential to support the final design and operation of the ITER and IFMIF devices.

Acknowledgements
This work, supported by the European Communities under the contract of Association between EURATOM/UKAEA, was carried out within the framework of EFDA. The views and opinions expressed herein do not necessarily reflect those of the European Commission.

References
[1] N. Holtkamp, An Overview of the ITER Project, 24th Symposium on Fusion Technology, Sept. 2006, Warsaw, Poland. To be published in Fus. Eng. Design.
[2] I. Cook, N. Taylor, D. Ward, L. Baker and T. Hender, Accelerated development of fusion power, UKAEA FUS 521, 2005.
[3] IFMIF International Team, IFMIF Comprehensive Design Report, 2004.
[4] K. Lackner, R. Andreani et al., Long-term fusion strategy in Europe, J. Nucl. Mat. 307-311, 10-20 (2002).
[5] P. Batistoni, U. Fischer and R.A. Forrest, Requirements for nuclear data development and neutronic analysis efforts in the EU Fusion Technology Program 2007-2013 (FP7), EFF-DOC 959 (2006).
[6] M.A. Kellett, R.A. Forrest and P. Batistoni, A brief overview of the European Fusion File (EFF) Project, Nucl Fusion, 44, 555-559 (2004).
[7] A. Koning, R.A. Forrest, M. Kellett, R. Mills, H. Henriksson and Y. Rugama, The JEFF-3.1 Nuclear data library, JEFF Report 21, to be published.
[8] D. Lopez Aldama and A. Trkov, FENDL-2.1, Update of an evaluated nuclear data library for fusion applications, INDC(NDS)-467 (2004).
[9] R. A. Forrest, J. Kopecky and J-Ch. Sublet, The European Activation File: EAF-2005 cross section library, UKAEA FUS 515 (2005).
[10] A.J. Koning, The current status and new directions of the JEFF project, this Workshop.
[11] R.A. Forrest and I. Cook, Deuteron-induced activation data in EAF for IFMIF calculations, 24th Symposium on Fusion Technology, Sept. 2006, Warsaw, Poland. To be published in Fus. Eng. Design.
[12] R. A. Forrest, The European Activation System: EASY-2005 overview, UKAEA FUS 515 (2005).
[13] P. Batistoni at al., Neutronics experiment on a HCPB breeder blanket mock-up, 24th Symposium on Fusion Technology, Sept. 2006, Warsaw, Poland. To be published in Fus. Eng. Design.
[14] M.R. Gilbert and R.A. Forrest, Comprehensive handbook of activation data calculated using EASY-2003, Fus. Eng. Design, 81, 1511-1516 (2006).
[15] R.A. Forrest, Data requirements for neutron activation Part I: Cross sections, Fus. Eng. Design, 81, 2143-2156 (2006).
[16] R.A. Forrest, Data requirements for neutron activation Part II: Decay data, Fus. Eng. Design, 81, 2157-2174 (2006).
[17] R.A Forrest et al., Validation of EASY-2005 using integral measurements, UKAEA FUS 526 (2006).
[18] R.A. Forrest and J. Kopecky, Statistical analysis of cross sections – A new tool for data validation, to be published in Fus. Eng. Design.

The current status and new directions of the JEFF project

A.J. Koning

Nuclear Research and Consultancy Group NRG, 3 Westerduinweg, 1755 ZG Petten, The Netherlands
koning@nrg-nl.com

Abstract: The Joint Evaluated Fission and Fusion (JEFF) project is a collaborative effort among the member countries of the NEA Data Bank to develop a reference nuclear data library. The JEFF library contains sets of evaluated nuclear data, mainly for fission and fusion applications; it contains a number of different data types, including neutron and proton interaction data, radioactive decay data, fission yield data, thermal scattering law data and photo-atomic interaction data. The latest version of the JEFF library, JEFF-3.1, was released by the NEA in May 2005. JEFF-3.1 combines the efforts of the JEFF and EFF/EAF (European Fusion File / European Activation File) working groups who have contributed to this combined fission and fusion library. The neutron general purpose library contains incident neutron data for 381 materials from ^{1}H to ^{255}Fm. The activation library (based on the European Activation File, EAF-2003) contains 774 different targets from ^{1}H to ^{257}Fm. The radioactive decay data library contains data for 3852 isotopes, of which 226 are stable. The proton special purpose library contains incident proton data for 26 materials from ^{40}Ca to ^{209}Bi. The thermal scattering law library covers 9 materials, and the fission yield library covers 19 isotopes of neutron induced fission yields from ^{232}Th to ^{245}Cm and 3 isotopes with spontaneous fission yields (^{242}Cm, ^{244}Cm and ^{252}Cf). To address new nuclear data needs, for the next release of JEFF, we foresee more required effort on experimental, theoretical and validation work. The needed upgrade of the JEFF library concerns among others efforts on fission product evaluations, minor actinide evaluations, and inclusion of more covariance data in the files.

Introduction

The objective of the OECD Nuclear Energy Agency (NEA) coordinated Joint Evaluated Fission and Fusion (JEFF) data project is to develop and promote the use of high quality evaluated nuclear data sets in standard formats for a wide range of scientific and technical applications. The JEFF project assesses the needs for nuclear data improvements and brings together experts in different areas such as experiments, data evaluations, verification and compilation of the data under strict quality assurance procedures, file processing and benchmarking.

JEFF is a collaborative effort between NEA Data Bank member countries. The project maintains close links with other similar international efforts and projects aimed at producing evaluated nuclear data, for example through active participation in the NEA Working Party on International Nuclear Data Evaluation Co-operation (WPEC). While the objective of the JEF-2.2 library (1992) was to achieve improved performance for existing reactors and fuel cycles, its successor, the JEFF-3 project, aims at providing users with a more extensive set of data for a wider range of applications. While existing reactors and fuel cycles remain the essential application areas of the nuclear data library, innovative reactor concepts (Gen-IV systems), transmutation of radioactive waste, fusion, medical applications, and various non-energy related industrial applications are now also envisaged as scientific application areas that will make use of the JEFF data. The European Fusion File (EFF) also contributes to the JEFF project through evaluations and data validation.

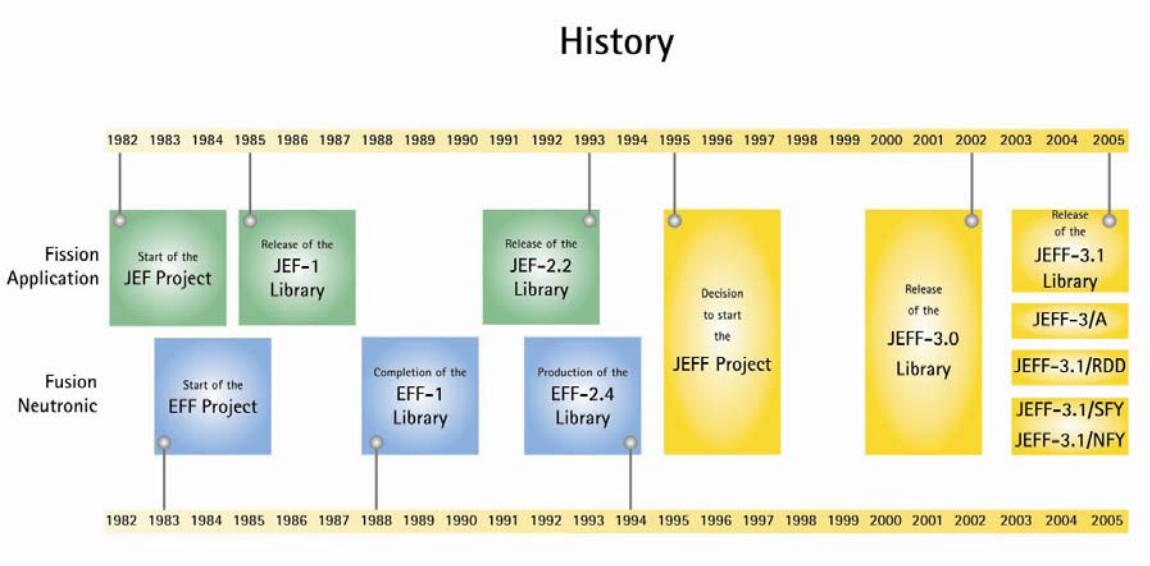

Figure 1. *The evolution of the JEFF project.*

Figures 1 illustrates the evolution of the JEFF project, including the latest release of JEFF-3.2. The JEFF-3.1 release consists of the following libraries:

- Neutron general purpose library
- Neutron activation library
- Thermal scattering library
- Decay data library
- Fission yield data library
- Proton special purpose library

General and special purpose libraries

Following the release of the JEFF-3.0 library in April 2002, various benchmark tests have confirmed the expected performance improvements of this neutron general purpose library over JEF-2.2. However, they have also shown that the reactivity of small low-enriched Uranium systems, relevant to LWR analyses, is underestimated by about 500 pcm when using JEFF-3.0 data. The ^{238}U inelastic, scattering and capture cross sections have been identified as the possible reasons for this underestimation. A new ^{238}U evaluation has been assembled, resulting in appreciably improved k_{eff} values. Subgroup 22 of WPEC has contributed significantly to these improvements. Very extensive automated benchmark tests have been conducted, probing the current quality of the new data library. These benchmark tests include for example criticality calculations performed with MCNP, TRIPOLI and APOLLO for an unprecedented set of benchmark cases. The current-day computer power enables future revisions of the JEFF library to be quickly tested with such benchmarking schemes.
Revised thermal scattering data have been produced for all important moderator and structural materials and this was included in JEFF-3.1.
It was decided to adopt an 8 time group representation for delayed neutron data, as suggested by subgroup 6 of WPEC. It is considered that this representation has two advantages - the longest lived, dominant precursors are explicitly represented and there is the calculation convenience of having the same set of time constants for all fissioning isotopes.
Another reason to develop the JEFF-3.1 neutron general purpose library is that a significant number of isotopes have undergone a major revision in the last few years. This holds both for the general purpose and the special purpose libraries. New evaluations are included for the Ti isotopes (IRK Vienna), the Ca, Sc, Fe, Ge, Pb and Bi isotopes (NRG Petten), ^{103}Rh, ^{127}I, ^{129}I, the Hf-isotopes, $^{236\text{-}238}$U, and ^{241}Am (CEA). For other isotopes, more recent evaluations from other libraries were adopted.
Various experimental nuclear data activities have taken place during the development of JEFF-3.1. The programme at the N-TOF facility at CERN comprised capture and fission cross-section measurements including isotopes of relevance to the Thorium fuel cycle and several transuranic isotopes. The measurement programme at IRMM Geel covered mainly

neutron data related to waste transmutation and other innovative concepts, as well as basic nuclear physics and standards data.
A final justification for releasing JEFF-3.1 is that there was a desire from the nuclear industry (in particular in France) to start validating the new JEFF library in the fall of 2005.
Extensive benchmarking of the JEFF-3.1 data library is now underway, both for the general purpose and for the special purpose sub-libraries. The benchmarking currently concentrates mainly on criticality, effective delayed neutron parameters, and shielding using a Monte Carlo approach (MCNP). At a later stage, a wider validation of benchmark results, using different methods (deterministic and Monte Carlo), codes and for various integral quantities, can be expected.
A quality assurance procedure has been developed at NEA for the assembly, basic testing and loading of the JEFF-3.1 library into a database. Verifications performed at the loading stage include format checks (CHECKR), physics checks (FIZCON and PSYCHE), processing using different versions of NJOY and graphical comparisons with other data libraries. Specific tools were developed within this framework (e.g. the JANIS data display program and database loading programs) and existing programs (e.g. FIZCON, INTER) were extended to enable more stringent consistency checks.
For the next release, JEFF-3.2, we foresee more efforts on fission product evaluations, minor actinide evaluations, and inclusion of more covariance data in the files.

Activation library, JEFF-3.1/A

The Activation Data Library in ENDF-6 format, JEFF-3.1/A, is based on the European Activation File (EAF-2003). The JEFF-3.1/A library contains 12 617 excitation functions involving 774 different targets from ^{1}H to ^{257}Fm, atomic numbers Z=1 to Z=100, in the energy range 10^{-5} eV to 20 MeV. Uniquely, a uncertainty file is also provided that quantifies the degree of confidence placed in the data for each reaction channel.
Calculations of the activation of materials, arising from the operation of fusion devices producing large fluxes of neutrons from the D-T reaction, play an important role in fusion technology studies. In order to have confidence in the results of such calculations, it is necessary that the inventory code and the data libraries are thoroughly validated. This is done by comparing the predictions of the code system with activation measurements made on materials relevant to fusion technology in well-characterised neutron fields.
The European Activation File (EAF) project has been an ongoing process performed through European and world-wide co-operation, leading to the creation of successive EAF versions. The EAF-2003 release has benefited from the generation and maintenance of comprehensive activation files and the development of the new processing code SAFEPAQ-II . Therefore, the JEFF project has adopted this version of the activation files for the JEFF-3.1/A library.
The EAF nuclear data library has been developed as part of the EFDA (European Fusion Development Agreement) Fusion Technology Programme. A series of measurements on fusion relevant materials in several complementary neutron fields have been carried out over the last few years. In addition, analyses of measurements, carried out outside Europe and outside the fusion programme, have been undertaken.
Cross section validation exercises, against both experimental data and systematics, enable a comprehensive assessment of the data. The SAFEPAQ-II software is used to apply a series of modifications to the original source data. A very important set of modifications concerns renormalization and branching using experimental or systematic data. A total of 3,225 reactions (26% of all the reactions) have thus been changed. This is a challenging task as the source contains non-threshold reactions with an energy dependent branching ratio.
Validation using integral data has been performed by means of direct comparison with measurements of sample materials under fusion-relevant neutron spectra. Irradiations have been carried out at ENEA FNG, FZK Isochron-cyclotron, Sergiev Posad SNEG-13 and JAERI FNS and integral C/E comparisons made (C/E is the ratio of the library value to the experimental value). The results of these benchmark exercises, in concurrence with differential data, have indicated where modifications to the data should be applied.
It should be noted that most of the measurements were carried out with fusion relevant materials, resulting in small uncertainties for activities produced in major nuclides, but larger uncertainties for activities produced in minor nuclides or impurities.

Thermal scattering law library

The thermal scattering law library contains the following 9 evaluations: hydrogen bound in water, zirconium, polyethylene (CH_2) and CaH_2, deuterium bound on D_2O, ^{9}Be, Graphite, ^{24}Mg and finally calcium bound in CaH_2. All files are new evaluations, except ^{9}Be and hydrogen in polyethylene, which are from the JEFF-3.0 library. Many of the evaluations are the result of an IAEA coordinated project on thermal neutron scattering. Calculations for a variety of temperatures were made with the LEAPR module of NJOY to obtain thermal scattering data that are accurate over a wider range of energy and momentum transfer. To validate these files on a microscopic level, detailed comparisons with a significant number of measurements of differential and integral neutron cross sections and other relevant data have been performed. The current models used for these files are able to describe the experimental data reasonably well. The generating and processing chain for the thermal neutron scattering files with NJOY was carefully investigated.

Radioactive decay data library, JEFF-3.1/RDD

Radioactive decay data forms an integral part of the nuclear data requirements for nuclear applications. The JEFF-3.1 decay data library contains 3 852 nuclides from the neutron to ^{272}Rg. The Decay Data sub-group of the JEFF Project decided that a completely new start should be made in the construction of this library compared to the previous versions. Below follows some background of the evolution of the project.

The basis for the selection of isotopes were taken from the NUBASE-2003 file, which contains basic nuclear properties, hence all known isomers were identified from here. Three evaluated libraries, from within Europe, were used to replace individual NUBASE files, for almost 600 nuclei in all, Two libraries originated from the UK (UKPADD-6.4 and UKHEDD-2.4) and the third from the Decay Data Evaluation Project (DDEP) conducted by the Laboratoire National Henri Bequerel (LNHB) at Saclay, France.

Files were also selected from the ENSDF library - these files contain decay data derived from basic nuclear structure data. Approximately 900 nuclei, containing sufficient data to allow calculation of their energy balance to a consistency of better than 1%, were selected from ENSDF.

The JEFF-3.1 library stores all data in the internationally accepted ENDF-6 format. Recent enhancements, allowing the storage of basic nuclear properties for stable nuclei (i.e. spin and parity), have been adopted in this library. The isotopic abundances for all appropriate nuclei (taken from NUBASE-2003) have been added as the last line in the comments section (MF=1, MT=451) whilst an un-used field in the format is investigated.

Throughout the compilation process the library has followed the NEA QA procedures and been checked with the standard ENDF Utility Codes STANEF, CHECKR and FIZCON. Significant enhancements to the FIZCON code have been added for the verification of decay data and also minor corrections to the latest versions (7.00/7.01) have been implemented following problems noted in checking this JEFF library, most notably the checking of the symbol field for meta-stable states and the inclusion of stable nuclei. Users should be warned that earlier versions of the checking codes, e.g. version 6.11, should not be used in testing this library.

Fission yield libraries, JEFF-3.1/NFY&SFY

The fission product yield libraries include independent and cumulative yields for the neutron-induced fission of ^{232}Th, $^{233,234,235,236,238}U$, $^{237,238}Np$, $^{238,239,240,241,242}Pu$, ^{241,242m,} ^{243}Am, $^{243,244,245}Cm$ and the spontaneous fission of $^{242,244}Cm$ and ^{252}Cf. The principle changes from earlier libraries includes; an extended experimental database, calculation of the cumulative yields using the JEFF-3.1 decay data, improved calculation of uncertainties in the yields, improved adjustment to the physical constraints and the inclusion of new ternary yield data for ^{3}H and ^{4}He.

Proton special purpose library

The proton special purpose library consists of 26 evaluated isotopes. The data are based primarily on a theoretical analysis with the nuclear model code TALYS. The nuclear model parameters of TALYS have been adjusted to reproduce the existing experimental data. For several materials that are of key importance to transmutation programs (ADS), valuable

experimental data was provided by the EU FP5 HINDAS project. Together, this results in data files that provide a complete representation of nuclear data needed for transport, damage, heating, radioactivity, and shielding applications over the incident proton energy range from 1 to 200 MeV.

Plans for JEFF-3.2

There is no exact target date for JEFF-3.2 yet. An indication is 2008-2009. General items that will be worked on are:

- Corrections to JEFF-3.1 deficiencies
- An extensive benchmarking report for JEFF-3.1
- Inclusion of more covariance data
- Revising and testing of fission products
- More emphasis on minor actinides
- New photonuclear, proton and deuteron library.
- Adoption of EAF-2005(7) as activation library.
- Update and further tests of the decay data and fission yield libraries
- Thermal scattering data
- Gamma production data
- TALYS-1.0
- NJOY extensions

Specific neutron evaluations that will be renewed and/or updated:

- Revision and validation of U-235,238.
- New evaluation for Pu-239 to improve analysis of MOX.
- New evaluation for Cr, Mn, Ta and W isotopes (EFF).
- Revised evaluation for Pb, Bi and Am using Geel measurements and TALYS.
- New evaluation for Th-232,Pa-233 using n-TOF/IRMM measurements (IAEA CRP).
- New evaluation for H-2, Sm-151, Np-237, Zr and Hf-isotopes.

For validation and benchmarking we foresee activities on:

- Criticality (ICSBEP) with Monte Carlo: MCNP and TRIPOL (basically done for JEFF-3.1)
- Integral experiments with deterministic codes :ERANOS, SCALE, etc.
- Fuel inventory, reactivity variation, FP integral experiments (open or confidential)
- 14 MeV shielding and activation benchmarks.
- Decay heat benchmarks
- IRPHE cases, if available.

The JEFF team

The following scientists and institutes have contributed to the successful release of the JEFF-3.1 nuclear data libraries.

Chairs:

O. Bersillon (Decay data), R.A. Forrest (EFF) and A.J. Koning (JEFF)

Evaluation:

O. Bouland (CEA), A. Courcelle (CEA), M.C. Duijvestijn (NRG), E. Dupont (CEA), J. Kopecky (JUKO), D. Leichtle (FZK), F. Marie (CEA), M. Mattes (Stutt), E. Menapace (ENEA), B. Morillon (CEA), C. Mounier (CEA), G. Noguerre (CEA), P. Pereslavtsev (FZK), P. Romain (CEA), O. Serot (CEA), S. Simakov (FZK), S. Tagesen (IIK), H. Vonach (IIK)

Experimental nuclear data:

P. Batistoni (ENEA), P. Bem (Rez), F. Gunsing (CEA), M. Pillon (ENEA), A. Plompen (IRMM), P. Rullhusen (IRMM), K. Seidel (TUD)

Nuclear modelling and theory:

M. Avrigeanu (NIP), V, Avrigeanu (NIP), E. Bauge (CEA), H. Leeb (TUW), M.J. Lopez Jimenez (CEA)

Processing, benchmarking and validation:

D. Bernard (CEA), A. Bidaud (CEN), R. Dagan (FZK), C. Dean (Serco),
P. Dos- Santos Uzarralde (CEA), U. Fischer (FZK), A. Hogenbirk (NRG),
R. Jacqmin (CEA), C. Jouanne (CEA), I. Kodeli (IAEA), J. Leppanen (VTT),
S.C. van der Marck (NRG), R. Perel (RIP), R. Perry (Serco), M. Pescarini (ENEA),
A. Santamarina (CEA), J.C. Sublet (CEA), A. Trkov (IAEA)

Decay data and fission yields:

M.M. Be (CEA),T.D. Huynh (CEA), M.A. Kellett (IAEA), R. Mills (Nexia), A. Nichols (IAEA)

NEA Data Bank:

H. Henriksson, C. Nordborg, A. Nouri, Y. Rugama, E. Sartori

Participating institutions:

Technische Universitaet Wien (TUW), Vienna, Austria
Institut fuer Isotopenforschung und Kernphysik (IIK), Vienna, Austria
Nuclear Physics Institute Rez (Rez), Czech Republic
VTT Processes (VTT), Finland
Commisariat à l'Energie Atomique (CEA) Bruyères-le-Chatel, France
Commisariat à l'Energie Atomique (CEA) Cadarache, France
Commisariat à l'Energie Atomique (CEA) Saclay, France
CEN de Bordeaux (CEN), France
Forschungszentrum Karlsruhe (FZK), Germany
Stuttgart University (Stutt), Germany
Technische Universitaet Dresden (TUD), Germany
Racah Institute of Physics (RIP), Jerusalem, Israel
National Agency for New Technology, Energy and the Environment (ENEA), Italy
Nuclear Research and Consultancy Group (NRG), Petten, the Netherlands
JUKO Research (JUKO), Alkmaar, the Netherlands
National Institute of Physics and Nuclear Engineering (NIP), Bucharest, Romania
UK Atomic Energy Authority Fusion (UKAEA), Abingdon, United Kingdom
Nexia Solutions Ltd., Seascale (Nexia), United Kingdom
Serco Assurance (Serco), Winfrith, United Kingdom

International organizations:

Institute for Reference Materials and Measurements (JRC/IRMM)
International Atomic Energy Agency (IAEA)
Nuclear Energy Agency (OECD/NEA) Data Bank

Acknowledgments
We acknowledge the support and dedication of many colleagues in the nuclear data community in Europe, Japan and the USA without whom this work would not have been possible, in particular: C. Chabert, J-P Delaroche, H. Derrien, H. Duarte, B. Duchemin, I. Duhamel, A. Filatenkov, E. Fort, F. Froehner, J. Galy, C-S. Gil, W. Haeck, F-J Hambsch, M. Herman, S. Hilaire, M. Honusek, T. Ivanova, D-H. Kim, N. Larson, P. de Leege, R. MacFarlane, A. Mengoni, L. Mercatali, L.C. Mihailescu, W. Mannhart, M.C. Moxon, S. Pelloni, P. Ribon, D. Ridikas, G. Rimpault, J.L. Rowlands, E Simeckova, J. Tommasi, B. Zefran, M. Zmitko, and Harm Gruppelaar, who left us too soon to experience the impact of his work.

Neutron data measurements at IRMM

A.J.M. Plompen

EC-JRC-IRMM, Retieseweg 111, 2440 Geel, BE
arjan.plompen@ec.europa.eu

Abstract: An overview is presented of recent neutron data measurements and equipment developments at IRMM. Neutron data activities are organised in two main activities, the first is centered on nuclear waste minimisation and, more generally, nuclear safety, while the second concentrates on neutron standards and basic science.
Neutron data measurements at IRMM use two neutron-production facilities, the white pulsed neutron source GELINA for very high resolution neutron time-of-flight measurements from thermal to 20 MeV and the Van de Graaff quasi mono-energetic neutron source which covers the range from 0.1 to 20 MeV.
At GELINA current campaigns concentrate on (n,xnγ) cross section measurements for isotopes of lead and for bismuth, on capture and total cross section measurements for criticality safety in a collaboration with US-DOE, and on fission of ^{236}U and on the ^{10}B(n,α) standard.
At the Van de Graaff laboratory current work concerns the fission process – fission isomers, the fission neutron spectrum, neutron multiplicity and fission fragment distributions –, the study of light charged particle emission in neutron-induced reactions on lithium, carbon and oxygen, and the study of activation cross sections on Cr, Ni, Cu, Zr, Ta and W.
Various technical developments are underway to allow new and/or improved studies of cross sections in the coming years. These include, an array of eight high purity germanium detectors for the study of (n,xnγ) cross sections on structural materials and fission products, an array of 10 C_6D_6 detectors in close-packed geometry for capture studies, the VERDI fission fragment spectrometer and the NEPTUNE facility

Introduction

The current overview concerns recent work performed at the IRMM GELINA and Van de Graaff facilities, excluding the work already shown elsewhere in these proceedings [1-5].

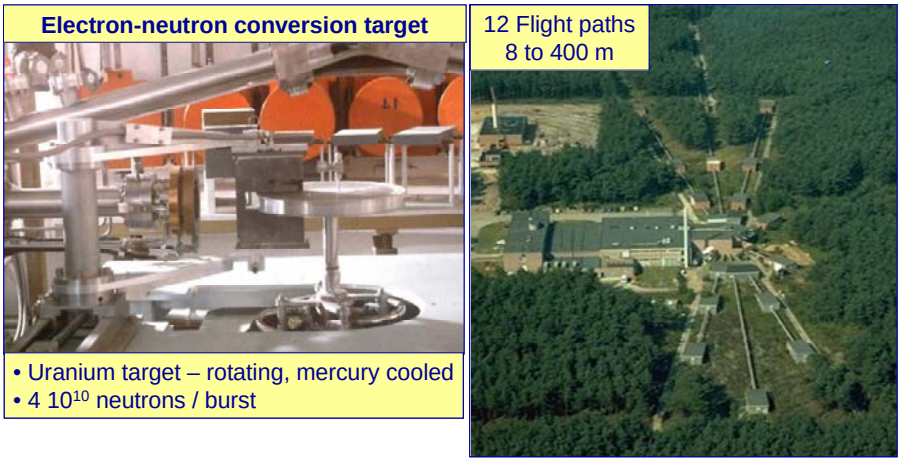

Figure 1. *Neutron producing rotary target with water moderators (left) and the flight path area (right) of the GELINA facility.*

The GELINA facility

The GELINA facility consists of a pulsed electron linear accelerator that produces a white neutron spectrum after impact on a large rotating depleted uranium target as a result of bremsstrahlung and ^{238}U(γ,xn) and ^{238}U(γ,F) reactions. The useful direct neutron spectrum

ranges from several keV to 20 MeV, while a Be-canned water moderator extends the spectrum down to several meV. Typical operating conditions are 800 pulses per second of 70-140 MeV electrons and a pulse width of 0.7 ns [6]. Long time-base measurements to reach below 1 eV may be made at 50 pulses per second. High resolution neutron time-of-flight measurements can be performed at a range of flight paths with lengths varying from 8 to 400 m (Fig. 1).

The study of (n,xnγ) cross sections

At Flight Path 3, 200 m, high purity germanium detectors (HPGe) are used to study neutron-induced inelastic scattering and (n,2n) reactions by measuring the production cross sections of the associated gamma-rays. The experimental lay-out used so far is presented in Fig. 2. Recently measurements were completed for ^{206,207,208}Pb on enriched isotopes and on ^{209}Bi using natural materials. Results contribute to the Integrated Project on EUROpean TRANSmutation (EUROTRANS) in the domain on NUclear DAta for TRAnsmutation (NUDATRA [7]). Inelastic scattering is of interest to accelerator driven systems and lead-cooled fast reactors and a lack of accuracy of current day libaries has been highlighted elsewhere [8]. Excellent results have been obtained for lead and bismuth with high resolution and high accuracy data for the main transitions in inelastic scattering. The inelastic cross section and level cross sections were deduced. Following the first demonstration of the possibility to measure cross sections for the (n,2n) process of ^{207}Pb at GELINA [9], it was shown that for all nuclei studied so far such cross sections can be measured [10-12]. Table 1 presents an overview of the results obtained for lead and bismuth. For further details see references [11,12].

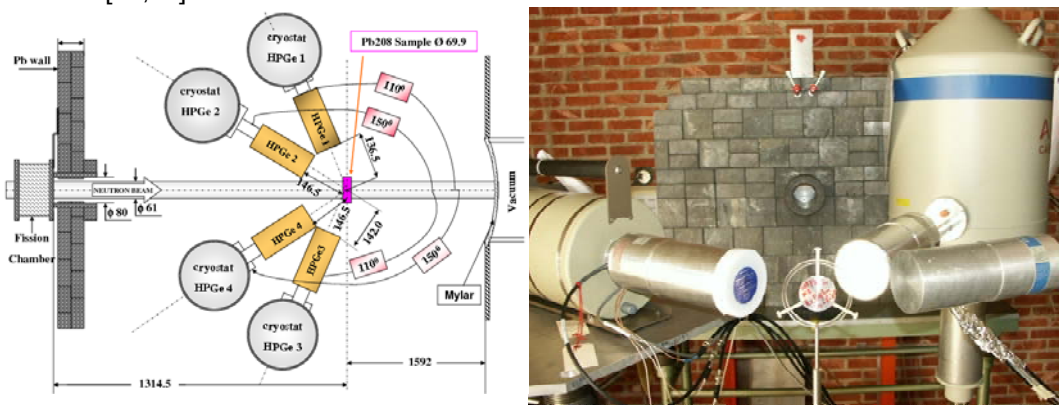

Figure 2. *Schematic overview (left) and picture (right) of an actual setup used for the (n,xng) measurements*

Table 1. *Overview of the measurements performed for lead and bismuth inelastic scattering and (n,xnγ) measurements.*

Nucleus	Reaction	Nr. meas. γ-rays	E_{max} (MeV)
^{206}Pb	(n,n'γ)	23	3.56
	(n,2nγ)	2	0.70
^{207}Pb	(n,n'γ)	15	4.32
	(n,2nγ)	4	1.70
^{208}Pb	(n,n'γ)	29	5.56
	(n,2nγ)	5	3.22
	(n,3nγ)	1	0.80
^{209}Bi	(n,n'γ)	39	3.80
	(n,2nγ)	8	1.09

The study of the isomer ratio of neutron capture by bismuth

The ^{209}Bi(n,γ)^{210}Bi reaction leads to the population of a ground state with a half life of 5 days and an isomer with a half life of 3 million years. The former beta decays to the well known short-lived alpha-emitter ^{210}Po (138 days), while the latter is itself an alpha-emitter. ^{210}Po, for obvious reasons, is a health hazard for handling of irradiated lead-bismuth eutectic, while the long-lived isomer ^{210m}Bi contributes to the nuclear waste. The isomer ratio IR=σ_g/σ_m measures the production of the ground state versus that of the metastable state (isomer). For thermal neutrons this ratio was determined to be 1.27(5) by Borella et al. [13]. This results differs considerably from available estimates (Fig. 3), which furthermore suggest an energy dependence of this ratio.

At GELINA a measurement campaign was undertaken to verify if this energy dependence is born by experiment as suggested by Saito et al [14]. Three HPGe detectors are placed at a short flight path as shown in figure 4, with the aim to identify gamma-rays populating the ground state or the isomer following neutron capture by bismuth. Measurements are complicated as a result of the low capture cross section and the neutron sensitivity of germanium detectors. Nevertheless, several resonances from 0.8 to 15 keV can be studied. Clear signatures for a resonance-dependent isomer ratio were observed [15]. Measurements have been completed and the analysis is ongoing.

To support an improved resonance evaluation for bismuth, in parallel, transmission and capture measurements are ongoing to improve the knowledge of the resonance parameters [16].

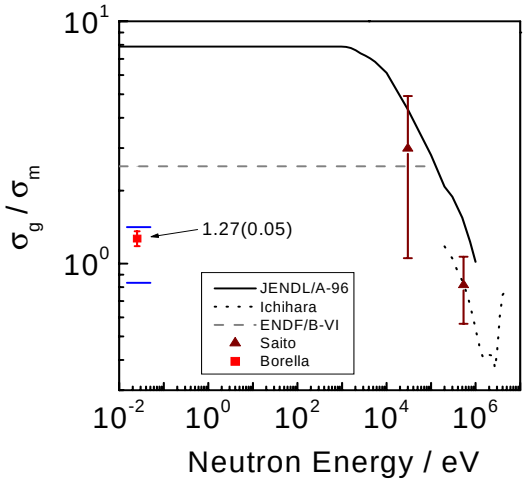

Figure 3. *Measurements and evaluations of the isomer ratio for the ^{209}Bi(n,γ)^{210m,g}Bi reaction.*

Figure 4. *Measurement setup consisting of HPGe detectors and shielding.*

Fission studies

Fission studies include the investigations of ternary fission of Cm isotopes (^{244,246,248}Cm) and the fission cross section of ^{236}U in the resolved resonance region. Both works concern an intensive involvement of the U. Gent. For ternary fission a comparison is made of thermal neutron induced ternary particle yields (in particular alphas and tritons) and spontaneous fission for the same fissioning system. Thus, two data points are obtained for each nucleus, one for zero excitation energy and the other corresponding to the neutron binding energy. Thermal neutron measurements are performed at the ILL. The fraction of so-called long-range alpha-particles per binary fission event shows a clear excitation energy dependence while for tritons this number is practically independent of excitation energy [17].

For the ^{236}U(n,f) reaction data are obtained from 1 eV to a few 10s of keV. The data have been taken and the analysis will be finalised for the ND2007 conference. Preliminary results show that many resonances in ^{236}U have falsely assigned fission widths [18].

The Van de Graaff facility

The 7 MV Van de Graaff accelerator is a single-ended machine dedicated to the production of quasi mono-energetic neutron fields in the range from 0.1 to 21 MeV using the well known ^{7}Li(p,n)^{7}Be, ^{3}H(p,n)^{3}He, ^{2}H(d,n)^{3}He and ^{3}H(d,n)^{4}He binary reactions. Currently, ongoing work includes fission studies, measurements of activation cross sections, studies of charged particle emission cross sections and dosimeter development and characterisation.

Measurements of the fission neutron spectrum of ^{235}U

A long-standing issue of significant importance to nuclear power reactors concerns the shape of the spectrum of fission neutrons from neutron-induced fision on ^{235}U. Important questions concern its incident neutron energy dependence and the possible mechanisms that determine the spectrum for the emitted neutrons. A detailed model of this spectrum was developed at Los Alamos by Madland and Nix [19].

At the Van de Graaff new measurements were made for incident neutrons of 0.5 MeV and for emitted neutrons of 0.8 to 10 MeV. The measured spectra are almost perfectly Maxwellian below 6 MeV in shape and agree with six earlier data sets. Moreover, the results suggest a clear angle dependence of the spectral shape. Both these features are not consistent with the model of Madland and Nix [19]. Measurements use the time-of-flight technique with liquid scintillators allowing for pulse shape analysis. The efficiency is characterised by a second time-of-flight measurement using a ^{252}Cf fission chamber. Further work is ongoing.

Study of the ^{16}O(n,α) reaction with a time projection chamber

The ^{16}O(n,α)^{13}C reaction recently received considerable attention through a subgroup on the criticality under prediction of light-water reactors at the Working Party for Evaluation Co-operation of the OECD Nuclear Energy Agency. The detailed understanding of the criticality of light-water reactors has important economic impact and the neutron removal through this reaction is one of the less well understood smaller contributions to the criticality estimate. For this reaction several earlier direct measurements exist, which are complemented with data inferred from the inverse reaction. In principle, direct and inverse reactions can be combined in an R-matrix analysis, however, due to the considerable spread in the data from 0.5 to 6 MeV incident neutron energy, no reliable result can be expected.

At IRMM, new measurements are underway using a one dimensional Time-Projection-Chamber (TPC, Fig. 5) that was developed in the context of the study of the ^{10}B(n,α)^{7}Li reaction [20,21]. For this work the technique is further developed in going from the study of a thin layer target to a gaseous (CO_2) target. A large number of preliminary data are available from 1.5 to 5.5 MeV incident neutron energy. These data are clearly different from earlier measurements and concur better with evaluated results (JEF2.2 and JENDL3.3). Further improved measurements and data analysis accounting better for spurious neutrons and other neutron source and detector characteristics are underway to prepare a new and accurate data set for improved evaluations.

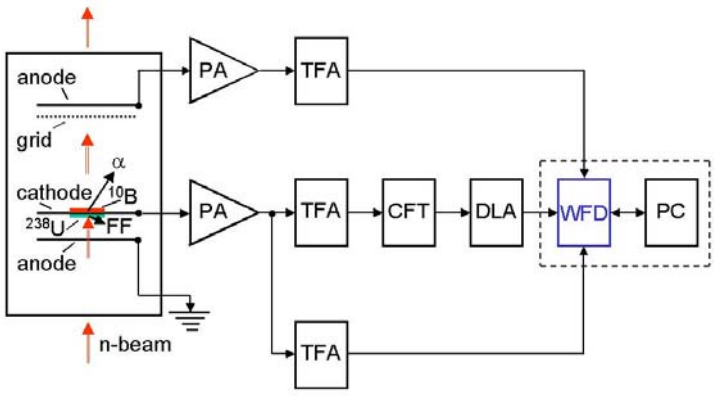

PA=Preamplifier, TFA=Timing Filter Amplifier, CFT=Constant Fraction Timing,
DLA=Delay Line Amplifier, WFD=Waveform Digitizer, PC=Personal Computer

Figure 5. *Schematic of the one dimensional TPC and its electronics/data-acquisition diagram as used for the measurements of the cross section of the ^{16}O(n,α)^{13}C reaction.*

Transnational access

Several experiments have been carried out at IRMM which are supported by the Transnational Access facility NUclear DAta MEasurements NUDAME of the European Commission. NUDAME supports proposals for measurements of parties external to IRMM. In 2006 support was given to the measurement of the ^{243}Am(n,f) cross section, the search for a fission isomer in ^{235}U [1], the measurement of a cross section for the 125 μs isomer in ^{206}Pb [1] and for the characterisation of various dosemeters. All these measurements took place at the VdG. At GELINA capture and transmission cross sections were determined for Cd and Hf. NUDAME will operate for one more year to complete by 31 March 2009.

Acknowledgements
The author acknowledges the contributions made by IRMM permanent and temporary staff and its external collaborators. The work for lead and bismuth inelastic scattering and (n,xnγ) cross sections, as well as for the study of the isomer ratio in neutron-capture by bismuth is supported by the EUROTRANS Integrated Project of the European Commission. NUDAME is a transnational access scheme funded by the European Commission.

References

[1] S. Oberstedt, “NEPTUNE – the new isomer spectrometer at IRMM”, p.89.
[2] V. Semkova, R. Jaime Tornin, A. Moens, A.J.M. Plompen, “Neutron-induced activation cross sections of different isotopes of Zr, W and Ta from the threshold to 20 MeV”, p.113.
[3] I.Z. Ivanov, P. Siegler, S. Kopecky, A. Trkov, M. Moxon, “Cadmium transmission measurements at GELINA”, p.77.
[4] L.C. Mihailescu, A. Borella, R. Capote, K.H. Guber, I. Ivanov, S. Kopecky, L.C. Leal, P. Schillebeeckx, P. Siegler, I. Sirakov, R. Wynants, “Neutron cross-section measurements on ^{103}Rh and ^{133}Cs for improved nuclear criticality safety”, p.149.
[5] A. Negret, C. Borcea, A.J.M. Plompen, “Upgrade of the setup for neutron inelastic scattering measurements at GELINA”, p.153.
[6] D. Tronc, J.M. Salomé, K. Böckhoff, “A new pulse compression system for intense relativistic electron beams”, Nucl. Instrum. Meth. A 228, 217 (1985); and references therein.
[7] NUDATRA website: http://fachp1.ciemat.es/nudatra/ (nudatra, pbmahe).
[8] G. Aliberti, G. Palmiotti, M. Salvatores, C.G. Stenberg, “Impact of nuclear data uncertainties on transmutation of actinides in accelerator-driven assemblies”, Nucl. Sci. Engin. 146, 13 (2004).
[9] A. Pavlik, P. Baumann, C. Borcea, E. Jericha, S. Jokic, M. Kerveno, S. Lukic, J.P. Meulders, L.C. Mihailescu, R. Nolte, A.J.M. Plompen, I. Raskynite, G. Rudolf and the n_TOF collaboration, “Cross-section measurements for (n,xn) reactions by in-beam gamma-ray spectroscopy”, Proc. Int. Conf. on Nuclear Data for Science and Technology – ND2004, Sep. 26 – Oct. 1, 2004, Santa Fe, USA, AIP conf. proceedings 769, 876 (2005).
[10] L.C. Mihailescu, C. Borcea, A.J. Koning, A.J.M. Plompen, “High resolution measurement of neutron inelastic scattering and (n,2n) cross-sections for ^{52}Cr”, Nucl. Phys. A 786, 1 (2007).
[11] A.J.M. Plompen, P. Baumann, C. Borcea, E. Jericha, S. Jokic, M. Kerveno, S. Lukic, L.C. Mihailescu, A. Pavlik, G. Rudolf, “Gamma production cross sections from neutron inelastic scattering and (n,2n) reactions; the cases of 209Bi, 206,207,208Pb”, XVI Int. School on Nucl. Phys., Neutron Phys. And Nucl. Energy, Sep. 19-26, 2005, Varna, Bulgaria, BgNS Transactions 10, 85 (2005).
[12] L.C. Mihailescu, “Neutron (n,xnγ) cross-section measurements for ^{52}Cr, ^{209}Bi, ^{206,207,208}Pb from threshold up to 20 MeV”, Report EUR 22343 EN, ISBN 92-79-02885-5, ISSN 1018-5593, European Communities (2006).
[13] A. Borella, A. Moens, P. Schillebeeckx, R. Van Bijlen, G.L. Molnár, T. Belgya, Z. Révay, L. Szentmiklósi, “The ^{209}Bi(n_{th},γ)^{210}Bi and ^{209}Bi(n_{th},γ)^{210m,g}Bi cross sections determined at the Budapest Neutron Centre”, Proc. Int. Conf. on Nuclear Data for Science and Technology – ND2004, Sep. 26 – Oct. 1, 2004, Santa Fe, USA, AIP conf. proceedings 769, 648 (2005).

[14] K. Saito, M. Igashira, T. Ohsaki, T. Obara, H. Sekimoto, “Measurement of the cross sections of the ^{210}Po production and ^{209}Bi(n,γ) by keV neutron capture of ^{209}Bi”, (EXFOR entry 22836, www.nea.fr/html/dbdata/x4), Report JAERI-C-03-006,133 (2002).
[15] A. Borella, T. Belgya, E. Berthoumieux, N. Colonna, C. Domingo-Pardo, F. Gunsing, S. Marrone, T. Martinez, C. Massimi, P.M. Mastinu, P.M. Milazzo, P. Schillebeeckx, G. Tagliente, J. Tain, R. Terlizzi, R. Wynants, “Determination of the branching ratio for the ^{209}Bi(n,γ)^{210}Bi reaction from 500 eV to 20 keV”, Proc. of PHYSOR-2006, ANS Topical meeting on Reactor Physics, contribution B042 (2006).
[16] A. Borella, F. Gunsing, S. Kopecky, P. Mutti, P. Schillebeeckx, P. Siegler, R. Wynants, “Determination of the neutron resonance parameters for ^{209}Bi from new capture and transmission measurements at GELINA”, Proc. of PHYSOR-2006, ANS Topical meeting on Reactor Physics, contribution B043 (2006).
[17] S. Vermote, C. Wagemans, O. Serot, J. Heyse, T. Soldner, P. Geltenbort, “Int. Conf. Dynamical Aspects of Nuclear Fission”, 2-6 Oct. 2006, Smolenice, Slovak Republic (2006).
[18] C. Wagemans et al. in Nuclear Data for Science and Technology – ND2007, abstract 113.
[19] D.G. Madland, J.R. Nix, Nucl. Sci. Eng. 81, 213 (1982).
[20] G. Giorginis and V. Khryatchkov, “The cross-section of the ^{10}B(n,α)^{7}Li reaction measured in the MeV energy range”, Nucl. Instrum. Meth. A 562, 737 (2006).
[21] G. Giorginis and V. Khryatchkov, “The effect of particle leaking and its implications for measurements of the (n,α) reaction on light elements by using ionisation chambers”, Nucl. Instrum. Meth. A 538, 550 (2005).

Production of diagnostic and therapeutic radionuclides

S. M. Qaim

Institut für Nuklearchemie, Forschungszentrum Jülich, D-52425 Jülich, Germany
s.m.qaim@fz-juelich.de

Abstract: The radionuclides used in diagnostic and therapeutic nuclear medicine are briefly considered. Some basic aspects of their production, namely reaction cross section data, target development for irradiations, chemical processing and quality control, are elaborated. The production methods of commonly used photon and positron emitters for diagnosis and of β^-, α- or Auger electron emitters for internal radiotherapy are discussed. Whereas the photon emitters and therapeutic radionuclides are produced using both reactors and cyclotrons, the positron emitters can only be produced at a cyclotron. Some new strategies and trends in the production of both diagnostic and therapeutic radionuclides are considered.

Introduction

In medicine, radioactive isotopes find application both in diagnosis and therapy [1]. The underlying principle of a diagnostic application is that the radiation dose to the patient should be as low as possible. This calls upon the use of very special type of radionuclides which can be detected efficiently from outside the body. In general, short-lived γ-ray emitters (with a single or at least a dominant γ-ray of energy between 70 and 250 keV) and positron emitters are commonly used, the former finding application in Single Photon Emission Computed Tomography (SPECT) and the latter in Positron Emission Tomography (PET). The organ specificity of the radionuclide is achieved by binding it to a suitable chemical compound (i.e. preparing a labelled compound). The field of diagnostic nuclear medicine (i.e. diagnostic studies using radioactive tracers) is flourishing [1].
In contrast to diagnostic studies, radiation therapy is performed either using external radiation sources or by introducing a radionuclide in an organ. The latter is often done mechanically, and is known as *brachytherapy*. In recent years, however, considerable progress has been achieved in bringing the radionuclide to the desired organ via a biochemical pathway, i.e. by attaching it to a molecule which acts as a vehicle for transport to the organ (this is denoted as *endoradiotherapy*). The radionuclides used for this type of therapy must emit corpuscular radiation (α- or β^- particles, conversion or Auger electrons). This is a fast developing field. It should be mentioned that the level of radioactivity encountered in therapy is much higher than in a diagnostic application, and consequently the radiation dose to the patient is much higher.
This communication deals with the production of both diagnostic and therapeutic radionuclides. Some of them are obtained using nuclear reactors while the others are preferentially generated at cyclotrons. In general, nuclear reactors and cyclotrons should be regarded as complementary facilities. Many of the production techniques involved are similar.

Some basic aspects of radionuclide production

The production of a medically important radionuclide with the required purity demands an accurate knowledge of the reaction cross section data, the application of suitable irradiation technology and the development of a chemical separation procedure. The recovery of the enriched material, if used as target, as well as the quality control of the radiochemically separated product are also important parts of the production process. Often several nuclear processes lead to the formation of the same radionuclide. The choice of the method then depends on the achievable yield and purity of the product as well as on the availability of the irradiation facility (reactor or cyclotron). Some of those aspects are discussed below in detail.

Nuclear reaction cross section data: These are needed in radionuclide development programmes mainly for optimisation of production routes. Since radionuclides are produced in reactors as well as at cyclotrons, both neutron and charged particle induced reaction cross section data are required. The energy ranges involved are rather broad. In case of neutrons, mostly thermal energies and the fission neutron spectrum are important, but with charged particles, energy ranges extending from a few MeV up to several hundred MeV are encountered.

In reactor production of radionuclides, the most commonly used nuclear routes include (n,γ), (n,fission) and (n,p) processes [2, 3]. The (n,γ) reaction has generally a high cross section so that the yield of the product is rather high. The excitation function of a typical neutron capture reaction [4] is shown in Fig. 1. The major interest is in the thermal energy region where both the cross section and the neutron flux are high. In the epithermal region the cross section has a resonance character and the integrated cross section (resonance integral) has a high value but, since the neutron flux is relatively low, the contribution of this region to the formation of the radionuclide is rather small. The high energy component of the neutron spectrum contributes only negligibly to the formation of the (n,γ) product since both the reaction cross section and the neutron flux have low values. It should also be mentioned that in high neutron flux reactors the two neutron capture process may also occur, e.g. $^{186}W(n,\gamma)^{187}W(n,\gamma)^{188}W$.

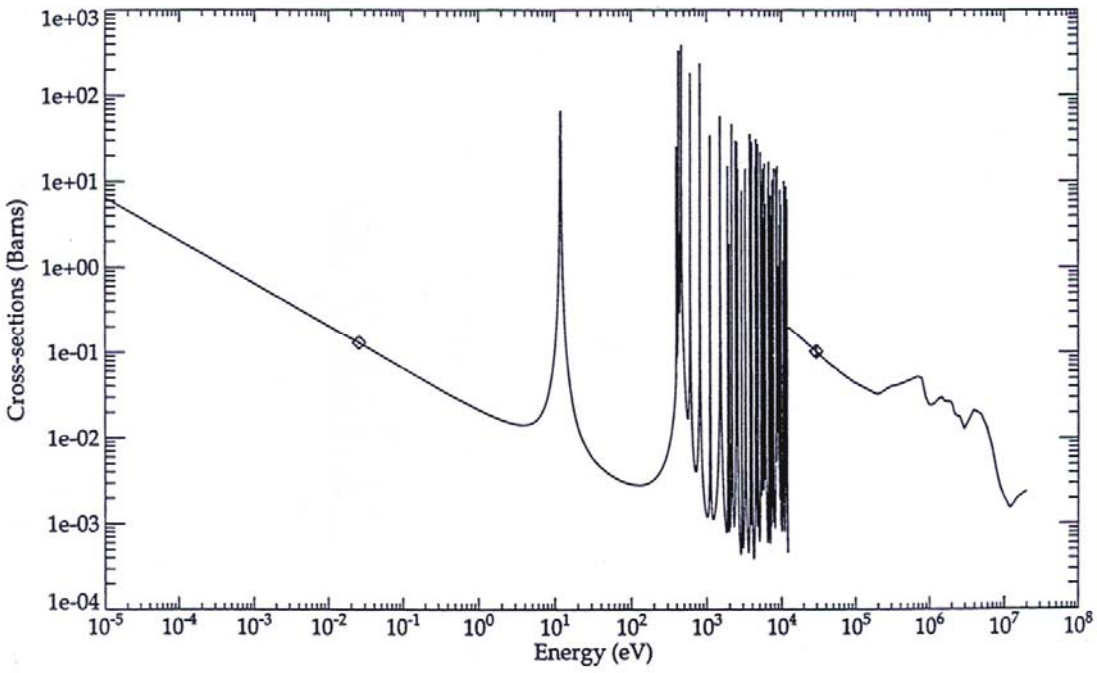

Figure 1. *Excitation function of the $^{98}Mo(n,\gamma)^{99}Mo$ reaction (taken from Ref. [4]).*

The specific radioactivity (defined as radioactivity per unit mass) achieved in an (n,γ) reaction is rather low. Therefore, often an alternative route of production is looked for. This may include the use of the fission process or an (n,p) reaction. The fission process is a very suitable method but the chemical processing involved, is rather extensive. Two very important radionuclides, namely ^{99}Mo (^{99m}Tc) and ^{131}I, are produced via the fission process. The (n,p) reaction cross section is generally low. This reaction is therefore only occasionally used to produce a radionuclide. The most important cases studied are: $^{32}S(n,p)^{32}P$, $^{33}S(n,p)^{33}P$, $^{67}Zn(n,p)^{67}Cu$ and $^{89}Y(n,p)^{89}Sr$ reactions. Some of those reactions are discussed in more detail in these Proceedings [5].

In production of radionuclides using charged particles from an accelerator or a cyclotron, the reaction cross section data play a very important role. Due to rapid degradation of the projectile energy in the target material, the energy range covered within the target is relatively broad and, since the reaction cross section varies rather rapidly with energy, it is not appropriate to adopt an average cross section over the whole energy range. One needs rather the full excitation function of the nuclear process to be able to calculate the yield with a reasonable accuracy. Production of radionuclides may be carried out using protons, deuterons, ^{3}He- or α-particles. At small-sized cyclotrons, low energy reactions like (p,n), (p,α), (d,n), (d,α), etc. are used. At higher energies, on the other hand, (p,xn) reactions are commonly utilized. In special cases the (p,spall) process is applied. Beams of ^{3}He- and α-particles are only occasionally used.

The optimisation of production route of a radionuclide involves a selection of the projectile energy range that will maximize the yield of the desired product and minimize that of the radioactive impurities. Whereas the non-isotopic impurities produced can be removed by

chemical separations, the level of isotopic impurities can be suppressed only by using enriched isotopes as target materials and/or by a careful selection of the projectile energy range effective in the target. The production of ^{123}I ($T_{½}$ = 13.2 h), an important SPECT-radionuclide, and of ^{124}I ($T_{½}$ = 4.18 d), an emerging PET-radionuclide, via the proton induced reactions on highly enriched ^{124}Te provide two very good examples of the role of nuclear data in obtaining a product of high radionuclidic purity. The excitation functions of the (p,n) and (p,2n) reactions [6] are shown in Figure 2. If the incident proton energy and the ^{124}Te target thickness are chosen such that the effective proton energy in the target corresponds to E_p = 25 → 18 MeV, then ^{123}I of good purity is obtained (the total ^{124}I impurity being < 1.0 %).

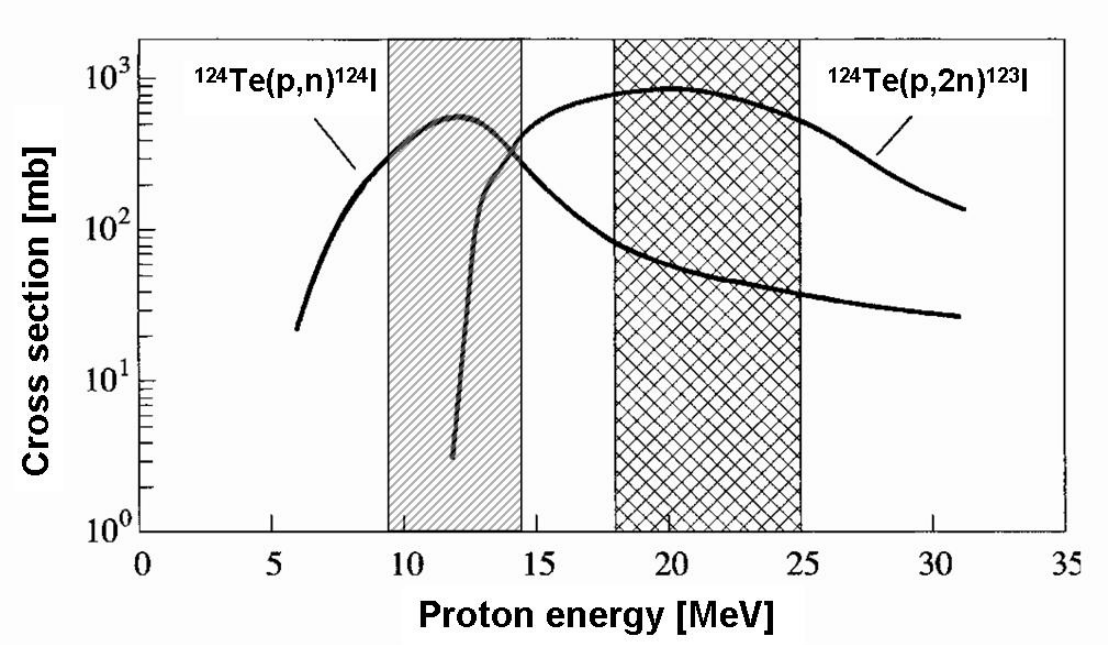

Figure 2. *Excitation functions of ^{124}Te(p,n)^{124}I and ^{124}Te(p,2n)^{123}I reactions. The suitable energy ranges for production of ^{124}I and ^{123}I are shown by shaded areas (adapted from Refs. [5] and [6]).*

If, on the other hand, the proton energy and the target thickness correspond to E_p = 14.0 → 9.0 MeV, then ^{124}I of very high purity is obtained. Thus the role of nuclear reaction cross section data in quality assurance of the desired product cannot be overemphasized.

Target development for irradiations:The irradiation of samples in a nuclear reactor is generally well developed. In most cases the material is sealed in a quartz ampoule which is then placed in an Al capsule and irradiated. Special techniques for irradiating pressurised gases have also been worked out.

The development of ***targetry*** for irradiation at a cyclotron constitutes one of the major efforts in production of neutron deficient radionuclides in sufficient quantities [7, 8]. Due to the use of high beam currents the power density effective at a target is rather high (up to a few kWcm^{-2}); an efficient heat transfer is thus one of the prime requirements in target construction. Metals, alloys, oxides, liquids and gases can all be used as target materials provided they can withstand high beam currents, do not lead to radiation induced strong chemical changes, give rise to a high yield of the radionuclide, and allow its easy chemical separation.

Irradiation of solids can be done within the vacuum system of a cyclotron or using extracted beams. In the latter case there is more versatility in the shape of the beam. Through controlled defocussing and wobbling it is possible to decrease the power density effective at a target. Nonetheless, due to high beam currents used, there is a severe strain on the window foil separating the cyclotron vacuum from the target. The target body has thus to be a good heat conductor. The chemical nature of the radioactive product and the method of chemical separation are often deciding factors in the choice of the material for construction. The back of the target is generally cooled by a stream of water and the front by a stream of He gas. The poor thermal-conducting target material is occasionally transformed into a suitable alloy. Another concept involves the use of slanting beams. This method of target construction and irradiation has now become standard technology for large scale production of commercial

radionuclides like ^{67}Ga, ^{111}In, ^{103}Pd and ^{201}Tl. In all those cases beam intensities of up to 1 mA delivered by a robust cyclotron are fully utilized.
Irradiation of liquids and gases is often done for production of short-lived positron emitters (^{11}C, ^{13}N, ^{15}O and ^{18}F). Efficient and remotely controlled (and mostly automated) systems are now commercially available [1, 9]. Production of ^{13}N and ^{18}F via the ^{16}O(p,α)^{13}N and ^{18}O(p,n)^{18}F reactions, respectively, the former using natural water and the latter using ^{18}O-enriched water, provide excellent examples of liquid targets. A nitrogen gas target is often used for production of ^{11}C and ^{15}O via ^{14}N(p, α)^{11}C and ^{14}N(d,n)^{15}O reactions, respectively.

Chemical processing and quality control: The radiochemical separation procedure applied in the production of a radionuclide depends on the irradiated sample. In case of gaseous targets, the product activity is generally removed from the target by simple expansion. On the other hand, if the radioactive product is adsorbed on the inner walls of the gas target, its removal is often done by rinsing the walls. In the case of a liquid target, the irradiated water is passed through an ion-exchange column whereby the product ^{13}N or ^{18}F is adsorbed on the column.
As regards solid targets, both dry and wet chemical separation methods are used. The dry method generally involves distillation. The best example is furnished by separation of radioiodine from irradiated TeO_2 at 755°C. Optimisation experiments revealed that above the melting point of TeO_2 the removal of radioiodine is fast and almost quantitative, and the loss of the target material is negligible [10]. Furthermore, the target is regenerated for the next production run. In many production processes a wet chemical procedure may be absolutely necessary. In general, solvent extraction and ion-exchange techniques are commonly used but occasionally methods like co-precipitation, adsorption, wet distillation, electrodeposition, etc. are preferred.
The separation of ^{99}Mo from the fission products provides a good example of the combination of several radiochemical methods. A $^{235}UAl_3$ pellet, irradiated in a nuclear reactor, is treated with NaOH and, after filtration the solution is acidified with HNO_3 and passed through an alumina column. ^{99}Mo is adsorbed on the column and subsequently eluted with 1 N NH_4OH. It is again adsorbed on an anion-exchanger and then eluted with HNO_3. The eluted volume is reduced by evaporation to dryness and then taken up in 1 N NaOH. In this state ^{99}Mo is fixed on an alumina column to build a radionuclide generator. The product nuclide ^{99m}Tc ($T_{½}$ = 6.0 h) is milked off periodically with saline solution. It exists as $Na^{99m}TcO_4$. A flow sheet of the separation procedure is given in Fig. 3. The European Pharmacopoeia demands that the level of the α-emitting actinides in ^{99m}Tc is < 10^{-10}. The method of separation is very well developed and TBq amounts of ^{99}Mo are now commonly produced.

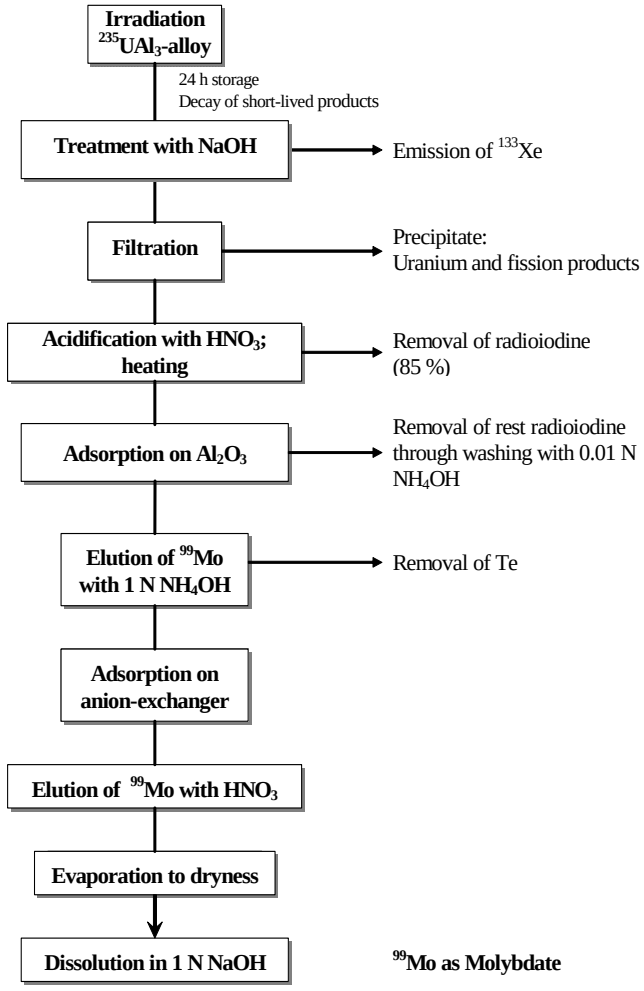

Figure 3. *Flow sheet of separation of ^{99}Mo from fission products after irradiation of $^{235}UAl_3$-alloy in a nuclear reactor.*

The final step in a chain of operations for the production of a medical radionuclide consists of quality assurance of the product. In general, four aspects must be given due consideration.

These are radionuclidic purity, radiochemical purity, chemical purity and specific activity. In short very clean and efficient working methods are mandatory.

Production of SPECT radionuclides

The photon emitters most commonly used in SPECT studies are ^{99m}Tc ($T_{½}$ = 6.0 h), ^{123}I ($T_{½}$ = 13.2 h) and ^{201}Tl ($T_{½}$ = 3.06 d). To some extent ^{67}Ga ($T_{½}$ = 3.26 d) and ^{111}In ($T_{½}$ = 2.8 d) are also used. The former is produced using a nuclear reactor whereas the latter four are generally obtained using a medium-sized cyclotron ($E_p \leq 30$ MeV).

Due to its easy availability via the ^{99}Mo → ^{99m}Tc generator system as well as due to the versatility of technetium chemistry, the radionuclide ^{99m}Tc has become by far the most important diagnostic radionuclide. It is freely available and is routinely applied in all parts of the world. The parent nuclide ($T_{½}$ = 2.75 d) can be generated via two routes.

- ^{98}Mo(n,γ)^{99}Mo and
- ^{235}U(n,fission)^{99}Mo

As discussed above, in the (n,γ) process the specific activity achieved is low. This difficulty is not encountered while using the fission process. Today ^{99}Mo is produced and separated only at a few nuclear reactors in the world. It is, however, distributed to several regional centres, where generators are prepared and supplied to nuclear medical centres in their respective areas.

The radionuclide ^{123}I is produced at a small-sized cyclotron using the low-energy ^{123}Te(p,n)-reaction or at a medium-sized cyclotron via the ^{124}Xe(p,x)-process. The latter route involves sophisticated gas targetry since the highly enriched ^{124}Xe target gas is very expensive. The production of the radionuclide ^{201}Tl, on the other hand, is carried out using a two step process. In the first step the precursor ^{201}Pb ($T_{½}$ = 9.4 h) is generated via the ^{203}Tl(p,3n)-reaction and is separated from the thallium target. In the second step, after a growing-in time of about 32 h, no-carrier-added ^{201}Tl is isolated. Both ^{123}I and ^{201}Tl are easily available but, due to their higher cost, are much les commonly used than ^{99m}Tc and its various compounds.

Production of PET radionuclides

For PET studies presently three short-lived radionuclides, namely ^{11}C ($T_{½}$ = 20.4 min), ^{15}O ($T_{½}$ = 2.03 min) and ^{18}F ($T_{½}$ = 109.6 min), are intensively used. Occasionally ^{13}N ($T_{½}$ = 10.0 min) is also utilised. All the four radionuclides are produced at a small cyclotron. Two other commonly used positron emitters are ^{68}Ga ($T_{½}$ = 67.6 min) and ^{82}Rb ($T_{½}$ = 1.3 min). They are obtained via generator systems. The parent activities ^{68}Ge ($T_{½}$ =270.8 d) and ^{82}Sr ($T_{½}$ =25.0 d) are produced either via intermediate energy (p,xn) reactions or via the high energy spallation process.

The most common routes used for the production of the organic short-lived positron emitters are given in Table 1. A cyclotron with $E_p \leq 20$ MeV and $E_d \leq 10$ MeV is adequate for production purposes. Today robust cyclotrons and fully automated production units are becoming commercially available.

The increasing significance of positron emission tomography demands development of new positron emitters. Considerable amount of research work is underway in this direction. Of all radionuclides considered so far, five positron emitters, namely ^{64}Cu ($T_{½}$ = 12.7 h), ^{73}Se ($T_{½}$ = 7.1 h), ^{76}Br ($T_{½}$ = 16.0 h), ^{86}Y ($T_{½}$ = 14.7 h) and ^{124}I ($T_{½}$ = 4.18 d), are finding increasing applications. They are produced via various charged particle reactions.

Table 1. *Production methods of commonly used positron emitters*

Radionuclide	$T_{½}$ (min)	Production process	Energy range (MeV)	Yield* (MBq/μAh)
^{11}C	20.3	^{14}N(p,α)	13 → 3	3820
^{13}N	10.0	^{16}O(p,α)	16 → 7	1665
^{15}O	2.03	^{14}N(d,n)	8 → 0	2368
		^{15}N(p,n)	10 → 0	2220
^{18}F	109.6	^{18}O(p,n)	16 → 3	3893
		^{20}Ne(d,α)	14 → 0	1110

* calculated from known excitation function for the given energy range [11].

Production of therapeutic radionuclides

Some of the radionuclides used in internal radiotherapy are listed in Table 2. Their production methods are also given [12]. Most of the radionuclides are β^- emitters. However, the demand for α- and Auger electron emitters is increasing. Evidently, both reactors and cyclotrons are useful for production purposes, though some of the radionuclides are now increasingly produced using a medium-sized cyclotron. The new trend in internal radiotherapy is tilted to the use of highly-ionising short-range radiation. Thus α-particle and Auger electron emitters are gaining more significance.

Table 2. *Production methods of some therapeutic radionuclides*

Radionuclide	$T_{½}$	E_{max} of emitted particle (MeV)	Production process	Energy range (MeV)
^{32}P	14.3 d	1.7 (β^-)	$^{32}S(n,p)$	FS
^{89}Sr	50.5 d	1.5 (β^-)	$^{89}Y(n,p)$	FS
^{90}Y	2.7 d	2.3 (β^-)	$^{90}Sr \rightarrow {}^{90}Y$ (generator)	
^{131}I	8.0 d	0.6 (β^-)	$^{130}Te(n,\gamma)^{131}Te \rightarrow {}^{131}I$	Thermal
			$^{235}U(n,f)$	Thermal
^{211}At	7.2 h	5.9 (α)	$^{209}Bi(\alpha,2n)$	28 → 20
^{225}Ac	10.0 d	5.8 (α)	$^{229}Th \rightarrow {}^{225}Ra \rightarrow {}^{225}Ac$ (decay chain)	25 → 15
			$^{226}Ra(p,2n)$	
^{103}Pd	17.0 d	Auger electrons	$^{103}Rh(p,n)$	13 → 7
^{125}I	59.4 d	Auger electrons	$^{124}Xe(n,\gamma)^{125}Xe \rightarrow {}^{125}I$	Thermal

Conclusion

The radionuclide production technology is well established and both nuclear reactors and cyclotrons are commonly used. The development of a new medical radionuclide involves considerable fundamental work. The new trends in medical radionuclide research involve production of long-lived positron emitters for investigating slow metabolic processes and of highly-ionising short-range α-particle and Auger electron emitters for internal radiotherapy.

References

[1] G. Stöcklin, S.M. Qaim and F. Rösch, Radiochim. Acta 70/71, 249 (1995).
[2] S. M. Qaim (Editor), Nuclear Data for Medical Applications, Radiochim. Acta 89, 189-337 (2001) Special Issue.
[3] Manual for reactor produced radioisotopes, IAEA-TECDOC-1340, International Atomic Energy Agency, Vienna, Austria (2003).
[4] J. Kopecky (Compiler), Atlas of Neutron Capture Cross Sections, Report INDC(NDS) 362, International Atomic Energy Agency, Vienna, Austria (1997).
[5] I. Spahn, M. Al-Abyad, S. Sudár, S. M. Qaim, H. H. Coenen, these Proceedings.
[6] B. Scholten, Z. Kovács, F. Tárkányi, S. M. Qaim, Appl. Radiat. Isot. 46, 255 (1995).
[7] S. M. Qaim, Nucl. Instr. Meth. A282, 283 (1989).
[8] Proceedings of the International Workshops on Targetry and Target Chemistry (Bienniel, 1985 – 2006).
[9] G. Stöcklin, V. W. Pike (Editors), Radiopharmaceuticals for Positron Emission Tomography, Kluwer Academic Publisher, Dordrecht, The Netherlands (1993).
[10] S. M. Qaim, A. Hohn, Th. Bastian, K. M. El-Azoney, G. Blessing, S. Spellerberg. B. Scholten, H. H. Coenen, Appl. Radiat. Isot. 58, 69 (2003).
[11] S. M. Qaim, Radiochim. Acta 89, 223 (2001).
[12] S. M. Qaim, Radiochim. Acta 89, 297 (2001).

Highlights from the coordinated research project on the thorium-uranium fuel cycle

A. Trkov[*1)], *R. Capote*[2)]

1) "Jožef Stefan" Institute, Jamova 39, SI-1000 Ljubljana, Slovenia
2) International Atomic Energy Agency, Wagramerstrasse 5, A-1400, Vienna, Austria
Andrej.Trkov@ijs.si

Abstract: The highlights of the coordinated research project of the International Atomic Energy Agency (IAEA) on the evaluated nuclear data of nuclides for the thorium-uranium fuel cycle are presented. The objectives of the project and the deliverables are defined. The basic principles of project organisation are presented, with examples of results from individual tasks. An important aspect of the project is broad international collaboration with contributions from big research laboratories that have a long tradition in data evaluation, as well as small research groups making small but important state-of-the-art contributions to the project. The pivot point is the coordination role of the IAEA of collecting contributions and assembling them in a consistent way into the final output. The data files resulting from the project are available on the IAEA web site; the documentation is still in preparation. The evaluated data files for ^{232}Th and ^{231,233}Pa were adopted for the ENDF/B-VII library in the USA.

Introduction

Past developments in nuclear technology have been streamlined towards the utilisation of uranium in thermal reactors and in fast breeder reactors so as to improve the utilisation of natural uranium resources. After the accident at Three Mile Island and Chernobyl, opposition to nuclear technology became very strong: restructuring of the industry to reduce energy consumption was progressively implemented, and new reserves of natural gas and oil were discovered. Thus, the continued development of nuclear technology almost stopped, apart from safety-related issues. The lack of an increase in demand for nuclear fuel removed the urgency to develop fast breeder reactors. Furthermore, when considering economic and safety aspects, such reactors had little or no advantages compared to conventional thermal reactors. Therefore, development of this technology stopped in a significant number of countries including France, which was the most advanced in the field and had a full-scale fast breeder reactor in operation for some time.
With increasing awareness of the global changes to the environment, nuclear power is slowly re-gaining its position as an appropriate option for energy supply with negligible emission of greenhouse gases. This position is subject to the condition of increased inherent safety, reduction of the risk of fissile material proliferation and a viable solution to the problems of long-term radioactive waste disposal. New concepts of nuclear technology for power production are being investigated to satisfy these needs. Thorium-based nuclear fuel cycle offers many advantages:

- Neutron capture in ^{232}Th yields ^{233}U, which is a highly efficient nuclear fuel. A thermal breeder (or near-breeder) reactor concept based on thorium fuel is feasible.
- The build-up of long-lived higher actinides, which are the main source of long-term residual radioactivity in the waste, is much smaller in thorium fuel. This fact can be used with advantage in the design of critical as well as subcritical accelerator-driven systems.
- Thorium fuel is more proliferation-resistant due to highly radioactive constituents, which can not be separated out by chemical means. Handling of such material in improvised clandestine laboratories is practically impossible.
- World reserves of thorium are much larger than reserves of uranium.

Due to the above advantages there is rising interest in innovative fuel cycle concepts based on thorium fuel. Unfortunately, due to the previous lack of interest in thorium fuel cycle, the quality of nuclear data for the relevant materials is lower than for the comparable materials in

[*] IAEA staff member and responsible project officer until April 2006.

the uranium or mixed oxide (plutonium) fuel cycle. In some cases the uncertainties in the nuclear data are a factor of three larger than the target accuracies set by the designers [1].
Numerous activities are in progress in many countries that anticipate the use of thorium-based fuel for accelerator-driven systems (ADS) applicable to power production and radioactive waste transmutation [2]. Active design effort is taking place on an advanced heavy reactor concept in India that uses thorium fuel [3]. Important new experimental measurements of cross sections of materials relevant to the Th-U fuel cycle have been reported or are in progress [4,5]. These data have to be evaluated, verified and validated on integral benchmarks to ensure valid design calculations. There is a definite need for improved evaluated nuclear data and the International Nuclear Data Committee (INDC) endorsed the project Nuclear Data for Th-U Fuel Cycle with high priority at 22nd meeting on 11-14 May 1999. Therefore, the International Atomic Energy Agency (IAEA) took the initiative and started a co-ordinated research project (CRP) to produce new evaluated nuclear data files for nuclides of relevance for the Th/U fuel cycle.

Objectives

The overall objective of the IAEA CRP on evaluated nuclear data for thorium-uranium fuel cycle is:

- Incorporate newly available experimental information into evaluated nuclear data files, which can be processed and used by designers of nuclear plants.
- Activate available human resources and to facilitate interaction and sharing of work to complete the task defined in the previous item in a timely and professional manner.
- Produce improved evaluated nuclear data files that will allow more accurate design calculations of innovative fuel cycle concepts involving the thorium-uranium fuel cycle.

The nuclides of primary interest for evaluation are: ^{232}Th, ^{231,232}Pa and ^{232,233,234,236}U.

Project organisation

Historically, production of complete evaluated data files for important nuclides was primarily the domain of laboratories with long tradition in nuclear data evaluation. Usually, the evaluation effort was part of national projects in countries with strong nuclear power programmes; the user was charged with the task as to which of the competing evaluations to trust. The IAEA project was organised to produce more than just evaluation of existing evaluations with minor improvements by taking advantage of the possibility to team-up the best specialists in individual fields from anywhere in the world and combining their partial results in a consistent manner.
Activities within the CRP included:

- Critical assessment of the available experimental information with emphasis on new data and renormalization to modern standard cross-sections (if necessary).
- Derivation (or adjustment) of resonance parameters for the resolved and the unresolved resonance range, including resonance covariance data.
- Derivation of nuclear model input parameters consistent with the state-of-the-art theoretical models and reproducing the experimentally measured cross sections as much as possible.
- Construction of the cross section covariance matrix prior by the Monte Carlo technique from nuclear model calculations through random variation of nuclear model input parameters.
- Adjustment of the covariance matrix by the introduction of experimentally measured cross sections
- Formatting of the evaluated data in ENDF-6 format.
- Verification of the formatted data to ensure that they are formally correct, internally consistent and that they truly represent the experimental data, from which they were derived.
- Processing of the data into application libraries for validation purposes. Preliminary validation of processed data on existing externally provided benchmark test cases (if available).

At the time of project implementation an activity was in progress at the Los Alamos National Laboratory to review and improve the evaluated nuclear data for the uranium isotopes. It was decided to accept these files as a US contribution to the project, with minor modifications, mainly taken from the MINSK library [7]. The evaluations extend up to 30 MeV.
The evaluated nuclear data files for ^{232}Th and ^{231,233}Pa are completely new evaluations in the energy range up to 60 MeV.

Assessment of experimental information
The main source of the experimental data was the EXFOR database [6]. Care was taken that the most up-to-date database was used. A convenient tool for comparing experimental data with the contents of evaluated data files was the Endver package [7], developed and available from the IAEA. An example of an intercomparison plot is shown in Figure 1.

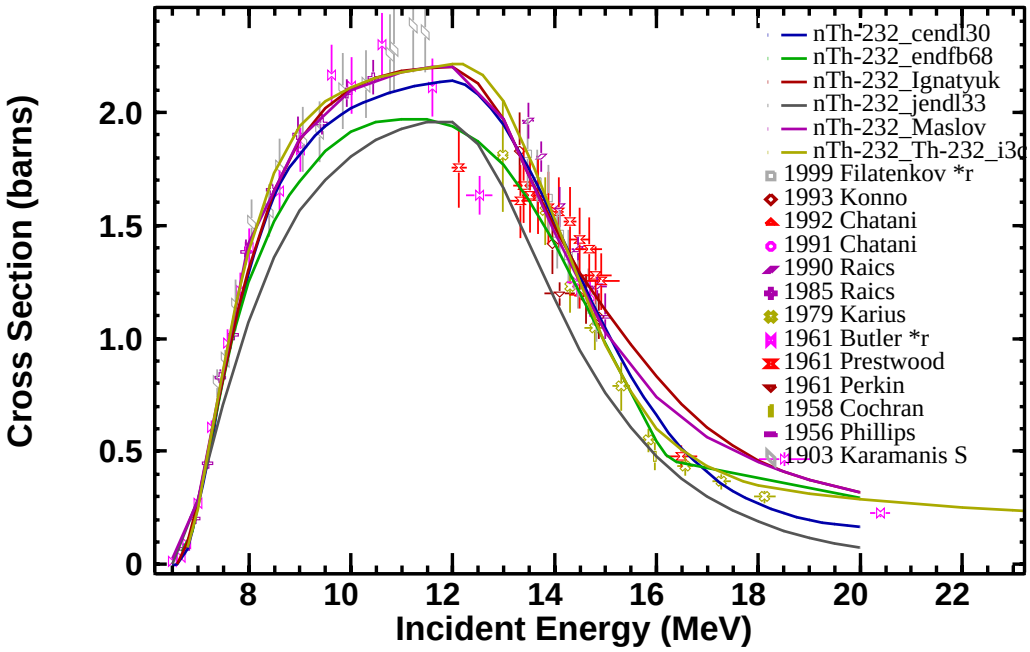

Figure 1. *Example of intercomparison of the (n,2n) cross section of ^{232}Th from various sources with experimental data from the EXFOR database. The data from the IAEA CRP are labelled Th-232_i3c.*

Resonance parameters
In addition to old measurements in the EXFOR database, several new measurements became available from the n-TOF project at CERN and the measurements on the Gelina facility at the Institute for Reference Materials and Measurements (IRMM). Resonance data were analysed mainly with the SAMMY code at the Oak Ridge National Laboratory, at IRMM and by members of the n-TOF project (where applicable). The resonance parameters of ^{232}Th were analysed with great care and there is broad consensus that the data set resulting from the project is “the best” that can be derived from the presently available experimental data. The resonance parameters for other nuclides involve minor adjustments of the available data and the production of covariance information by the so-called retro-active method.

Nuclear model input parameters
The starting point were the parameters from the RIPL-2 database [7], which is the result of a complementary project of the IAEA. Additional information was provided from the JENDL project from Japan, the CENDL project from China, the BROND project from Russia and from the evaluations activities in Minsk, Byelorussia. Original new work was done on the models of fission with the triple-humped fission barrier. For illustration the calculated fission cross section is compared with measurements in Figure 2. The final set of input model parameters is a major improvement over all previously existing work in this field. The details are described in a complementary paper at the same venue. All calculations were done with the EMPIRE-II code, which is available from the IAEA [7].

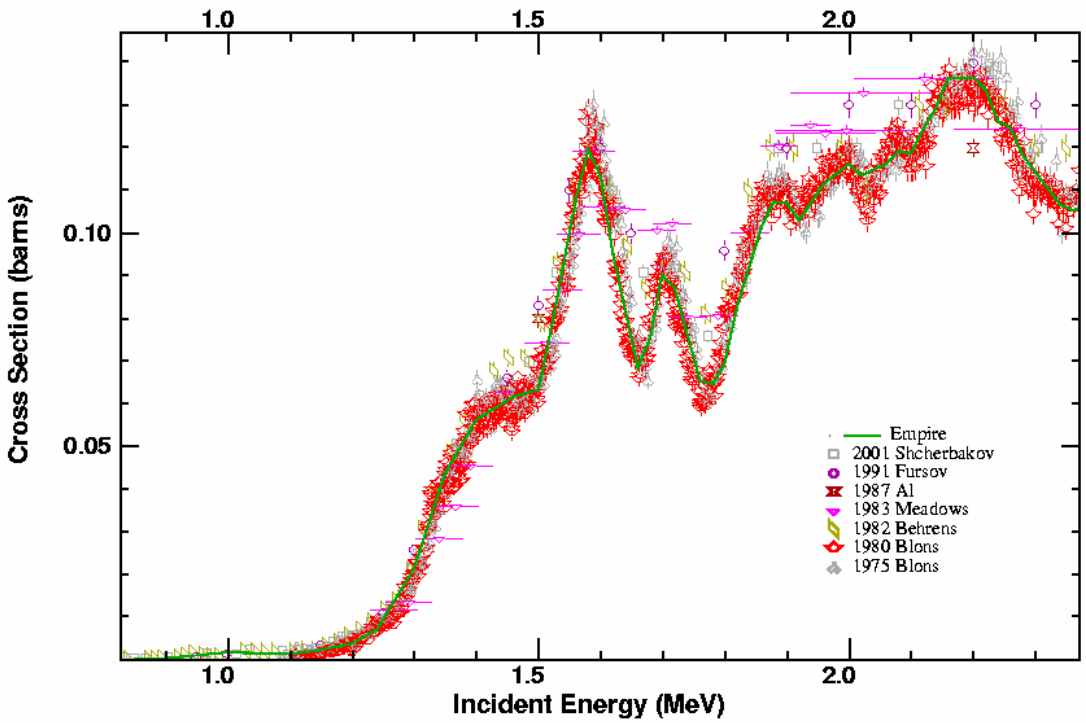

Figure 2. *Fit of the fission cross section data of ^{232}Th with the triple-humped fission barrier model.*

Cross section covariance matrices

Covariance data of the resonance parameters were obtained as a by-product of the resonance analysis. In this section the covariances of the cross sections above the resonance region are addressed. One of the common problems with generalised least squares technique in cross section data evaluation is the difficulty of imposing physical constraints on the variations of cross sections, such as physical bounds and other physical consistency conditions, which are naturally included in nuclear model calculations. To take "the best of the two worlds", the covariance matrix prior was generated by running EMPIRE-II with the option to randomly vary selected input parameters. Several hundred runs were processed into ENDF-6 formatted files and a global covariance matrix was generated, defining variances and correlations between all cross sections. The range of variations of parameters was chosen by "best judgement" from physical considerations. The approach is valid because the model parameters used in the calculations are actually *regional parameters*, applicable to light Actinides. The covariance matrix produced in this way was used as a prior to the GANDR system [8]. Experimentally measured cross section data were then fed into GANDR to impose additional constraints in order to reduce the uncertainties. The covariance matrix of the radiative capture cross section is shown in Figure 3.

Data formatting

Conversion of the output of the EMPIRE-II system into ENDF-6 format is done with the EMPEND code, which is part of the EMPIRE-II distribution. Additional utility codes were used to merge the resonance data and the covariance data consistently into the file. Some manual editing of the comments was necessary, before the file verification and validation procedures were implemented.

Data verification and validation

Data verification ensures that the data in an evaluated data file conform to ENDF-6 format rules, satisfy internal consistency constraints and represent well the basic experimental data on which the evaluation is based. The ENDF Utility Codes and ENDF Pre-Processing codes were used to perform format and consistency checks. The ENDVER package was used to compare the cross sections with experimental data. The results are available on the project web page "http://www-nds.iaea.org/Th-U/".

The main source of suitable benchmarks for data validation was found in the International Handbook of Evaluated Criticality Safety Benchmark Experiments (ICSBEP), which refers to reactor lattices [9]. They include a thorium-reflected plutonium sphere, six measurements

simulating infinite medium multiplication factor and eight thermal lattices. In all of the above cases the multiplication factor was the primary observable. The ICSBEP handbook also contains RBMK lattice cases with thorium absorbers and other lattices with thorium impurities, but these were not considered because of their low sensitivity to thorium data. To fulfil the needs of accelerator-driven systems and hybrid systems, a benchmark was included in which the leakage spectrum from a thorium sphere with a 14 MeV source in the centre was measured. The benchmark is to be included in the new release of the SINBAD benchmark collection of the NEA Data Bank [10]. The full analysis of the benchmarks was presented at the NENE-2006 conference in Portorož [11]. For illustration the results are presented in Figure 4 for the SB series of benchmarks with enriched ^{235}U (cases SB-1, 5) or ^{233}U (all other cases) fuel in zirconium matrix and light water moderator.

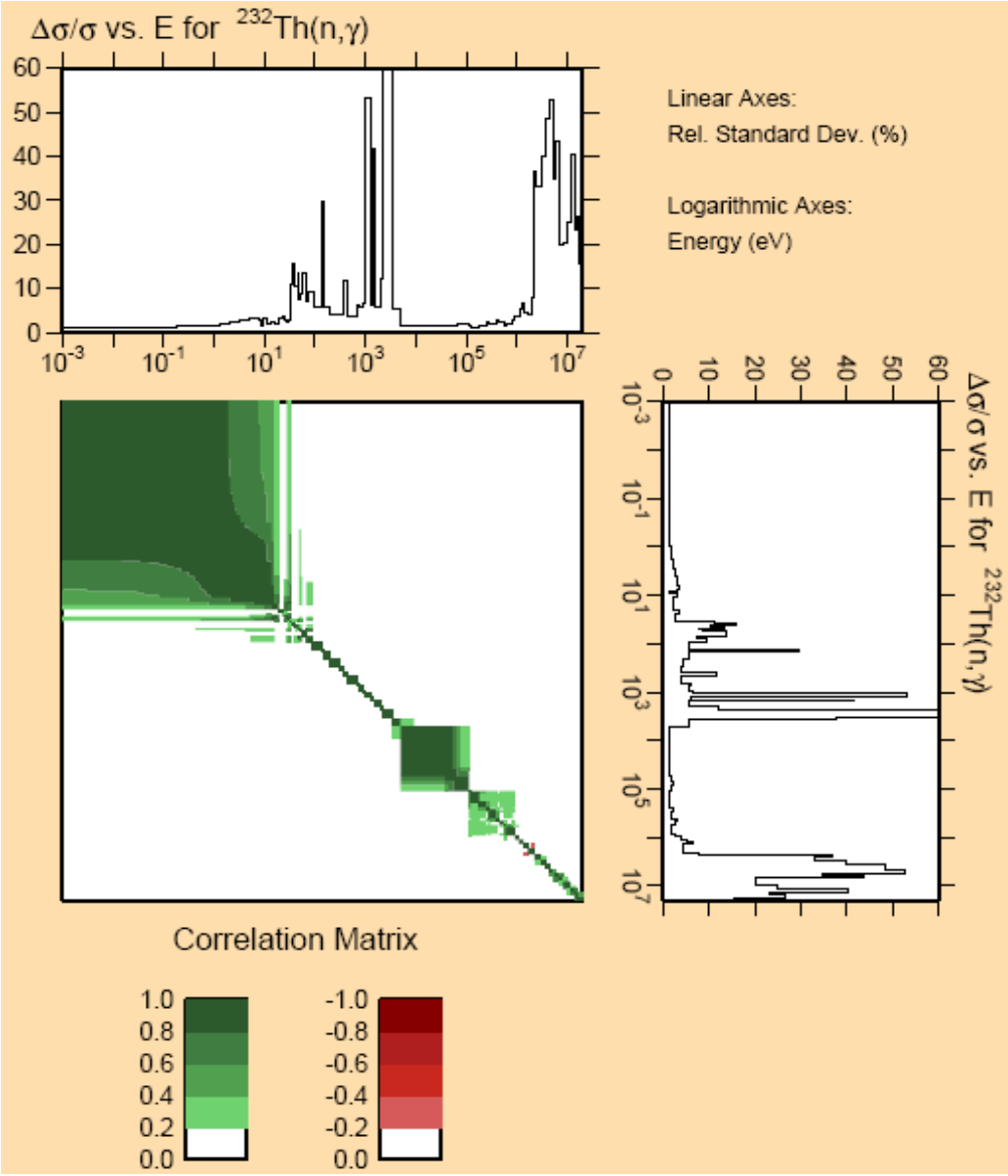

Figure 3. *Example of a covariance matrix of the radiative capture cross section of ^{232}Th.*

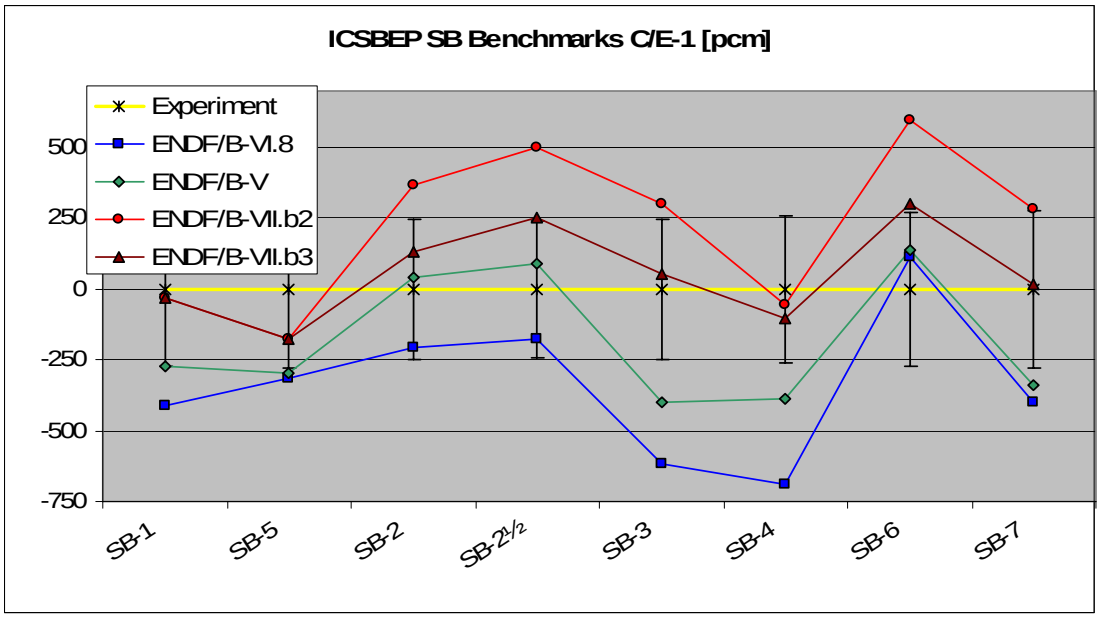

Figure 4: *Example of benchmark results with the MCNP Monte Carlo code and different data libraries for the SB-series of benchmarks. The final results with the data from the project are labelled ENDF/B-VII.b3.*

Conclusions

Completely new evaluated nuclear data files were produced for ^{232}Th, ^{231,232}Pa and were adopted for the ENDF/B-VII project in the USA. Improvements were made to the evaluated data files for ^{232,233,234,236}U, mainly based on Los Alamos and Minsk evaluations.
The coordinated research project on the thorium-uranium fuel cycle utilised heavily the synergy with other projects and activities of the IAEA, a number of International Projects and local activities in a number of research centres around the world. The project sets an example of how to optimise the internationally available resources to produce evaluated data files with a broad consensus on quality and validated performance on practical benchmark test cases.

References

[1] Consultants' Meeting on Assessment of Nuclear Data Needs for Thorium and Other Advanced Cycles, Vienna, 26-28 April 1999, INDC(NDS)-408, August 1999.
[2] Proceedings of IAEA TC Meeting, Feasibility and Motivation for Hybrid Concepts for Nuclear Energy Generation and Transmutation, Madrid, 17-19 Sept.1997, IAEA-TC-9033, 1998.
[3] AGM, Long-Term Needs for Nuclear Data Development, Vienna, 28 Nov.- 1 Dec. 2000, INDC(NDS)-428, Aug.2001.
[4] International Conference on Nuclear Data for Science and Technology, Tsukuba, 7-12 Oct. 2001, proceedings.
[5] International Conference on Nuclear Data For Science and Technology, Santa Fe, 26 Sept – 1 Oct 2004, proceedings.
[6] Nuclear Reaction Data Center Network, Experimental Nuclear Reaction Data (EXFOR), http://www-nds.iaea.org/
[7] International Atomic Energy Agency, Nuclear Data Services, "http://www-nds.iaea.org/".
[8] D.W. Muir: GANDR - Global Assessment of Nuclear Data Requirements, Project of the International Atomic Energy Agency, Vienna (mailto:A.Mengoni@iaea.org).
[9] Organization for Economic Cooperation and Development - Nuclear Energy Agency (OECD-NEA): The International Criticality Safety Benchmark Evaluation Project, http://icsbep.inel.gov/
[10] OECD/NEA: SINBAD FUSION, Neutronics Benchmark Experiments, Package ID NEA-1553, NEA Data Bank, Paris, http://www.nea.fr/abs/html/nea-1553.html
[11] A. Trkov, R. Capote: Validation of ^{232}Th Evaluated Nuclear Data Through Benchmark Experiments, International Conference Nuclear Energy for New Europe 2006, Portorož, Slovenia, September 18-21, 2006 (conference proceedings to be published).

Isotope production by (n,γ) reactions and the nucleon radiative capture to discrete states

E. Bétak[1,2)]

1) Institute of Physics SAS, Dúbravská cesta 9, 84511 Bratislava, Slovakia
2) Faculty of Philosophy and Sciences, Silesian University, 74601 Opava, Czech Republic
betak@savba.sk

Abstract: The reactions of the neutron radiative capture (and similarly for those of protons) represent a great interest for possible new ways of production of therapeutic and diagnostic isotopes and also for their deep insight into the details of nuclear reaction process itself. The latter can be studied in more detail by reactions leading to discrete and/or semi-discrete states; more frequently those induced by protons are studied (due to the energy resolution). The high-energy gammas originating from the reactions of nucleon radiative capture at incident energies close to or above 10 MeV can be described by either the semi-direct-direct model or within the pre-equilibrium approach.

Introduction

The reactions of the neutron radiative capture are of great interest for possible new ways of production of medical isotopes [1,2]. The (n,γ) reactions may serve as the means of production of some radiopharmaceuticals either directly (^{89}Sr, ^{103}Pd, ^{153}Sm and others) or via suitable generators (e.g. ^{125}Xe serves as a generator for ^{125}I). In accord with the Research Coordination Meetings [2,3], we estimate the cross sections of the corresponding (n,γ) reactions from above the resonance region up to about 20 MeV. This energy region is --- in fact --- not much interesting for practical applications, and, correspondingly, the data are rather rare here.
The reactions of nucleon radiative capture are also a suitable tool for their deep insight into the details of nuclear reaction process itself. The latter can be studied in more detail by reactions leading to discrete and/or semi-discrete stattes; more frequently those induced by protons are studied (due to the energy resolution).

The Model and the Computer Codes

We used the computer codes EMPIRE-II v. 2.19 [4] and TALYS [5]. At excitation energies above 10 MeV, they both are based on the pre-equilibrium single-particle radiative mechanism [6,7], which has been elaborated proved to be very successful at the incident energies below about 30 MeV in previous codes (see, e.g. Refs. [8,9]). On the other hand, it gives also a good and reliable description at energies as low as about 5 MeV [10,11]. The γ emission rates can be expressed as [6,7]

$$\lambda_\gamma\left(n,E,\varepsilon_\gamma\right)=\frac{\varepsilon_\gamma^2\sigma_{GDR}(\varepsilon_\gamma)}{\pi^2\hbar^3c^2}\frac{\sum_{m=n,n-2}b(m,\varepsilon_\gamma)\omega(m,E-\varepsilon_\gamma)}{\omega(n,E)}, \qquad (1)$$

with *b*'s the corresponding branching ratios (see [6,7]). With the inclusion of spin, however, they become much more complicated, but --- fortunately - - they factorize [12], and the energy-dependent parts are identical to those of the spin-independent ones. The photoabsorption cross section σ_{GDR} is usually taken in the form of the giant dipole resonance approximated by the corresponding Lorentzian (or a double-humped Lorentzian in the case of deformed nuclei).
The main differences between TALYS and EMPIRE important for the pre-equilibrium stage of the reaction may be summarized as follows: *i)* The basic approach is the two-component one (i.e. distinguishing between the neutrons and the protons) in TALYS, whereas one-component formulation with a charge factor is used in EMPIRE; *ii)* One-particle radiation mechanism for the γ emission is used in EMPIRE, but TALYS adds the quasideuteron (two-particle), what may cause some differences (however, very small ones) at excitation energies above about 30 MeV; *iii)* Though the level densities (using the default option) are the same in both codes

(with parameters taken from RIPL [13]), different (semi-)microscopic approaches are available for the advanced user; *iv)* Classical optical model with allowance for the deformed potential is used to calculate the particle transmission coefficients T_l in EMPIRE with parameters from libraries, and the local and global (spherical) parametrization of Koning and Delaroche [14] is employed in TALYS. (This influences the γ emission only via the competition with that of the particles.) Previous calculations done using other codes demonstrated sensitivity of the calculations to the details of the level density parameters, than one order of magnitude, and also the influence of the temperature-dependent width of the GDR, which is rather surprising at excitation energies well below 50 MeV [10]; the detailed form of the GDR and the differences among different level density models are only of marginal influence and practically may be neglected [2,3]. Thus, the calculations are relatively reliable far off the closed shells and (simultaneously) close to the beta-stability line, and rather unsure near closed (or even doubly closed) one(s), where one has to pay the utmost care to the parameters (see, e.g., [10]). Generally, there is no straightforward solution for nuclei close to the drip lines, and calculations performed with different model assumptions and/or codes may serve as a rough estimate how reliable the evaluation may be.

Medical Isotopes --- Excitation Functions

The need to produce isotopes for diagnostic and therapeutic purposes stimulated also calls for further measurements and evaluations of the (n,γ) reactions at energies below 20 MeV. Generally, there are not many data on such (n,γ) reactions [15] in the continuum region. We present the data together with the calculations of TALYS [5] and EMPIRE-II v. 2.19 [4]) in Figs. 1-2. The ^{191}Ir(n,γ) reaction (Fig. 1) is more simple case, whereas we have calculated separately the cross sections both to the ground and to the metastable states in ^{165}Ho(n,γ) (Fig. 2).

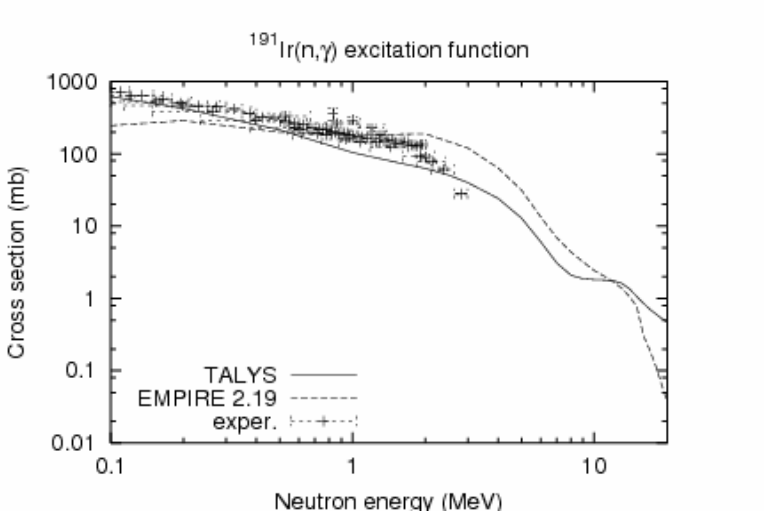

Figure 1. *The excitation function of the ^{191}Ir(n,γ) reaction between 100 keV and 20 MeV, as calculated by EMPIRE-II v. 2.19 and by TALYS, and compared to the EXFOR experimental data.*

Essentially, we kept the default parameters in EMPIRE, just with allowance for full inclusion of pre-equilibrium emission and γ cascades. Details of the form of the Giant Dipole Resonance (which enters the calculations of the γ emission via the detailed balance principle) and of other parameters did not show much influence on the resulting excitation functions calculated using EMPIRE-II v. 2.18 [3], and we therefore applied this approach also to version 2.19 and to TALYS[1].

[1] It is *essential* to include the γ cascades at all stages of the process, but the details of the GDR form are only of marginal influence at our energies [2,3].

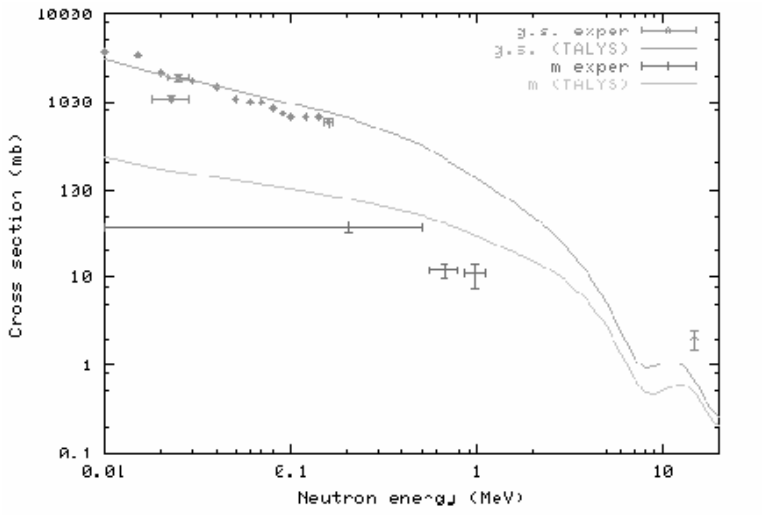

Figure 2. *The excitation function of the 165Ho(n,γ) reaction between 100 keV and 20 MeV, as calculated by TALYS, compared to the EXFOR experimental data [15] (only the data published since 1975 are included). The upper set of points and the curve refers to the ground state, whereas the lower one to the isomer.*

Transitions to Discrete States Populated in proton Radiative Capture

Here again, separate states have been considered. We have calculated transitions to the discrete states in ^{208}Pb(p,γ), measured recently by Lipoglav\v sek et al. [16,17]. In addition to the pre-equilibrium statistical calculations, also those within the direct-semi-direct (DSD) model, performed by the Ljubljana group ([16,17,18]) are presented here. As an example, we give here the γ energy spectrum obtained at 15.7 MeV in coincidence with the 896 keV transition ($f_{7/2}^-$ ---> g.s.) is presented in Fig. 3 [2] .The overall agreement of the three calculations and the data is reasonable, however, some differences still can be marked.

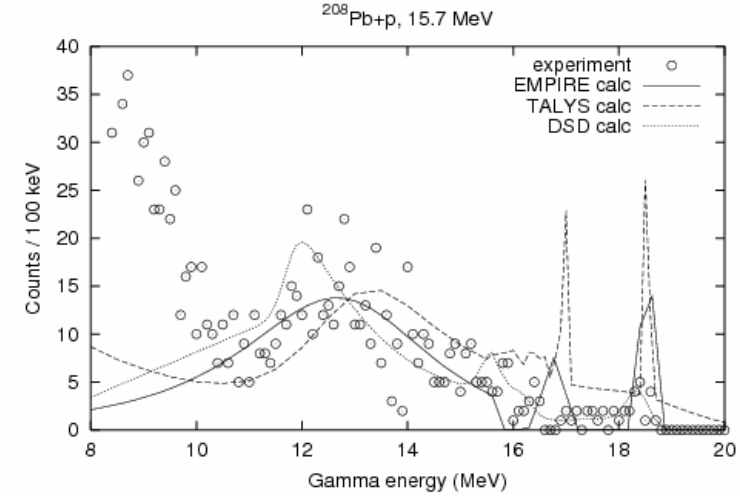

Figure 3. *The γ spectrum measured in coincidence with the f7/2 (896 keV) transition in 208Pb+p at 15.7 MeV.*

[2] A preliminary calculations of the pre-equilibrium γ spectra from this reaction has been published in Ref. [18]. The EMPIRE calculation is given without accounting for γ's after nucleon emission, for better comparison to the DSD calculations. The visible gap in the EMPIRE sprectrum near 18 MeV is just an artefact of insufficient dimension of the output table listing.

Conclusions

We have presented the ability of pre-equilibrium approach to describe the excitation curves of the (n,γ) reactions between 0.1 MeV and 20 MeV, and to predict their behaviour in cases where there is a lack of the experimental data, both for the total cross sections, and also individually for those to the ground and the isomer states. The pre-equilibrium approach was tested against data and the DSD calculations for the ^{208}Pb(p,γ) reactions from few MeV to about 20 MeV. Therein, the statistical way of pre-equilibrium description does not work so nicely --- it is explained by specific non-statistical behaviour in the vicinity of doubly-magic ^{208}Pb. Two codes, EMPIRE and TALYS, used for the pre-equilibrium calculations give results of similar quality, and there is no clear dominance of one of them over the other.

Acknowledgments
The author thanks A. Likar and T. Vidmar for many discussions on the DSD approach, and R. Capote-Noy, M. Herman and A. Koning for discussions on EMPIRE and TALYS codes. He is also grateful to JRC IRMM for supporting participance at the NEMEA-3 workshop. This work has been supported in part by the IAEA Contract No. 12425, VEGA Grant No. 2/4102 and the APVV project No. SK-SI-2006.

References

[1] S.M. Qaim, This Workshop (2006) and Report SMR-1148-38, ICTP Trieste, 1999.
[2] Nuclear Data for the Production of Therapeutic Radionuclides. Summary Report of First Research Coordination Meeting. Prepared by J.-Ch. Sublet and R. Paviotti-Curcuera. Report INDC(NDS)-444, IAEA Vienna 2003.
[3] Nuclear Data for the Production of Therapeutic Radionuclides. Summary Report of Second Research Coordination Meeting. Prepared by J.-Ch. Sublet and R. Capote Noy. Report INDC(NDS)-465, IAEA Vienna 2004.
[4] M. Herman et al Report NNDC-BNL, Upton, USA 2005.
[5] A. Koning, S. Hilaire, M. Duijvestijn, Report 21297/04.62741/P FAI/AK/AK, NRG Petten 2004.
[6] E. Běták, J. Dobeš, J., Phys. Lett. 84B, 368 (1979).
[7] J.M. Akkermans, H. Gruppelaar, Phys. Lett. 157B, 95 (1985).
[8] E. Běták, Report INDC(CSR)-016/LJ, IAEA Vienna 1989.
[9] Běták, P. Obložinský, Report INDC(SLK)-001, IAEA Vienna 1993.
[10] E. Běták, F. Cvelbar, J. Kopecky, J., Phys. Rev. C46, 945 (1992).
[11] F. Cvelbar, E. Běták, A. Likar, J. Phys. G21, 377 (1995).
[12] P. Obložinský, Phys. Rev. C35, 407 (1987).
[13] RIPL-2, http://www-nds.iaea.or.at/ripl-2/. IAEA Vienna 2002.
[14] A. Koning, J. Delaroche, Nucl. Phys. A, 713, 231 (2003).
[15] EXFOR-CINDA for applications, version 1.63i (CD-ROM), http://www-nds.iaea.or.at/exfor/, IAEA Vienna 2004 and 2006.
[16] M. Lipoglavšek et al.,Phys. Lett. B, 593, 61 (2004).
[17] A. Likar et al., Phys. Rev. C, 73, 044609 (2006).
[18] E. Béták et al.,in 11th Internat. Conf. Nucl. Reacts. Mechanisms, Varenna, June 2006 (submitted).

Delayed gammas detection technique for nuclear waste characterization

S. Boyer[1)], E. Berthoumieux[1)], D. Doré[1)], D. Ridikas[1)], X. Ledoux[2)], F. Carrel[3)], M. Gmar[3)], B. Poumarède[3)]

1) CEA/DSM Saclay, DAPNIA/SPhN, 91191 Gif-sur-Yvette, France
2) CEA/DAM Ile-de-France, DPTA/SPN, 91680 Bruyères-le-Châtel, France
3) CEA/DRT Saclay, LIST/DETECS, 91191 Gif-sur-Yvette, France
eric.berthoumieux@cea.fr

Abstract: Photons can be used to detect small amounts of nuclear material inside massive nuclear waste storage barrels or large cargo containers. The method consists of the irradiation of the waste barrels by photons in order to create photofission reactions on actinides. By detecting the decay gammas associated with fission, it is possible to determine the presence of the actinides and their mass contained in the waste barrel.
The experimental data on delayed gamma emission following photofission is very scarce and insufficient for the above purposes. Therefore, within the INPHO project (**In**terrogation by **Pho**tons) the measurements of delayed gamma spectra have been performed at CEA. The gamma detection device was composed of the BGO detector. ^{238}U and ^{232}Th targets were irradiated separately to determine fundamental parameters (decay gamma energy and time spectra). Preliminary data analysis of this experiment will be presented, including model calculations based on systematic from neutron induced fission.

Introduction

Recently, non-destructive characterization of waste containers and detection of nuclear materials, both based on photofission process, has attracted particular attention. This technique employs intense beam of Bremsstrahlung photons with energy above 6 MeV in order to induce photofission on actinides. Simplicity and attractive costs of low energy electron accelerators, associated with prompt neutron (PN), delayed neutron (DN) and delayed-decay photon (DP) detection devices, make possible to detect small amounts of fissile material present in massive nuclear waste storage barrels. In principle, the same technique could be applied in nuclear material control on the borders [1].
The measurement of DNs and DPs emitted by fission products brings specific information on localization and quantification of the nuclear material. A simultaneous measurement of both of these delayed signals can overcome some important limitations due to matrix effects like heavy shielding and/or the presence of light elements as hydrogen [1, 2].
To determine the total number of DP events, one needs a detector which allows counting of high energy photons in an environment, where photons and neutrons are both present. We have chosen the BGO crystal scintillator the properties of which (efficiency, neutron transparency, etc.) are well suited for this purpose.
The investigated gamma energy range was above 2-3 MeV to maximize the counting of delayed gamma from photofission compared to the active background. Similarly as in the delayed neutron experiments [3], different irradiation-decay cycles were employed to optimize the extraction of “unique” decay parameters of delayed gammas.
This paper presents our first experimental results and preliminary data analysis on photofission induced DP energy and time spectra. Determination of the fundamental parameters at different gamma energy cuts has been performed for ^{238}U, while for ^{232}Th the analysis is still in progress. Comparison with model calculations based on systematic from neutron induced fission will also be discussed.

Description of the experiment

The experiment was performed using the ELSA electron accelerator of CEA/DAM Ile-de-France at Bruyères-le-Châtel [4]. A 15 MeV-electron beam with an energy resolution lower than 100 keV and an average intensity of ~1 μA was employed. All irradiations were done with a frequency of 1 Hz and with the 70 μs pulse duration. The electrons were converted into Bremsstrahlung photons using a 2 mm-thick tantalum target. The distance from the target to

the actinide samples was ~150 cm along the beam axis. The ^{238}U and ^{232}Th samples were ~400 g and ~300 g metallic cylinders respectively. A massive lead collimator narrowed the photon beam to reduce the background.
Each measurement consisted of a repetitive cycles of irradiation and counting once the beam is switched off. The irradiation and counting time were adjusted in order to maximize the contribution of different groups with their characteristic decay periods, namely 70μs (single pulse) – 30 s (142 cycles), 10 s – 50 s (60 cycles), 60 s – 300 s (21 cycles), and 300 s – 300 s (15 cycles).
Each gamma event was recorded with two parameters, its energy and the elapsed time since the end of the irradiation. For each irradiation time, a run without any sample was also performed in order to estimate the active gamma background.
A 5"– diameter $\times$ 3"– height BGO scintillator (127S76/5 BGO + preamplifier AS16, SAINT GOBAIN) was used to detect high-energy gammas. The BGO was placed at the angle of 90° with respect to the beam axis and embedded in a $30 \times 30 \times 40$ cm polyethylene block as shown in Fig. 1. The distance from the uranium sample to the detector was ~100 cm.

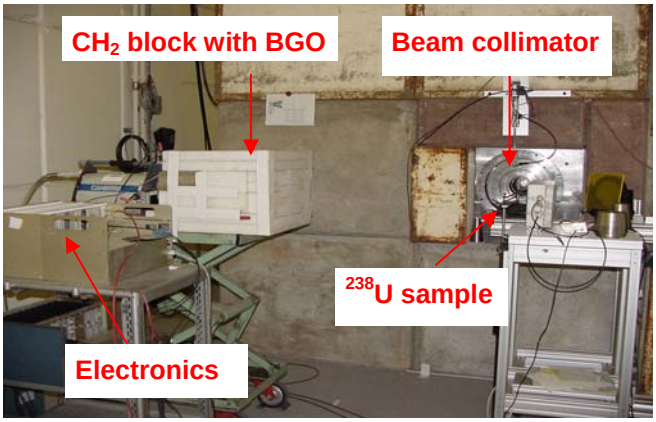

Figure 1. *Experimental set up for DP measurements at the ELSA electron accelerator*

Both the time and energy spectra were recorded event by event. In order to determine with a good accuracy the "start" of the gamma decay, the last 2 s of the beam were recorded for each cycle. The dead time of the whole system was estimated to be about 20 %.

Preliminary results of data analysis

Fig. 2 presents both energy and time spectra of DPs obtained in this experiment. By choosing the DP energies higher than 2 MeV we analyzed the raw DP time spectra as a sum of exponentials in the case of ^{238}U, namely

$$F(t) = \sum_i A_i \exp(-\lambda_i t) \times (1 - \exp(-\lambda_i T_{irr})) + C \,. \qquad \text{(Eq. 1)}$$

As in the approach well known in the case of delayed neutrons, we wanted to extract "unique parameters" $\{A_i; \lambda_i\}$, which could be used to predict the DP activity for variable irradiation (T_{irr}) and decay (t) times. Note that the above equation is rather good approximation once T_{irr} is much shorter than t or both of them are "infinitely" long. The constant *C* was added in order to take into account the active background, which was assessed at 10 % of the raw signal. The same approach can be applied for ^{232}Th but by choosing the DP energies higher than 3 MeV due to the "naturally" present the 2.614 MeV gamma line of ^{208}Tl (see Fig. 2).
The following fitting procedure was employed: starting from the 300 s / 300 s (irradiation / counting) cycles, the specific values for group 1 were determined. Then in the 60 s / 300 s irradiation the first group parameters were fixed to determine the other group parameters, and so on until the single pulse irradiation. The measured average decay half-lives for ^{238}U are shown in Table 1.

Table 1. *Experimental results on DP averaged half-lives $T^i_{1/2}$ for ^{238}U.*

DP group	i = 1	i = 2	i = 3
$T^i_{1/2}$ **(s)**	158 ± 8	26 ± 1	1.89 ± 0.13

At the 2nd stage, these values were fixed and tested by fitting all the time spectra once again. The results are shown in Figure 3 for the representation of the "unique global fit" in the case of 4 different irradiation periods. One can clearly see that all spectra are well reproduced. Finally, using these "unique" time constants, relative group contributions A_i will be extracted for each irradiation time. This work is still in progress.

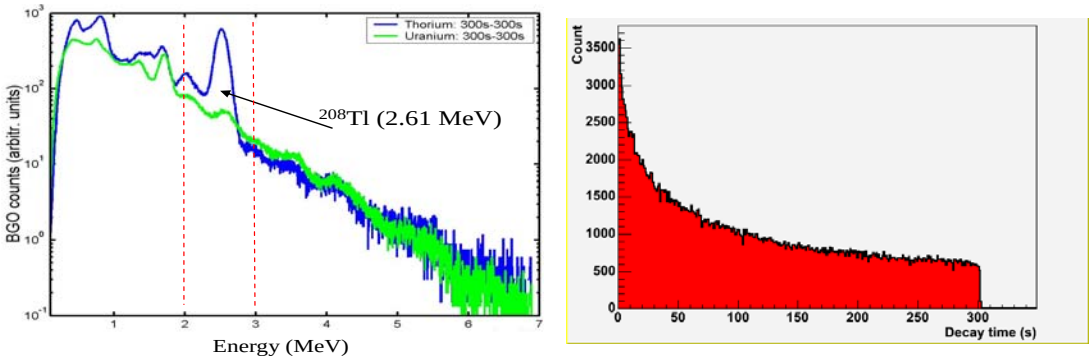

Figure 2. *On the left – DP energy spectra from photofission of ^{238}U (in green) and ^{232}Th (in blue); on the right – DP time spectra for ^{238}U ($E\gamma$> 2MeV and 300s-300s irradiation-decay).*

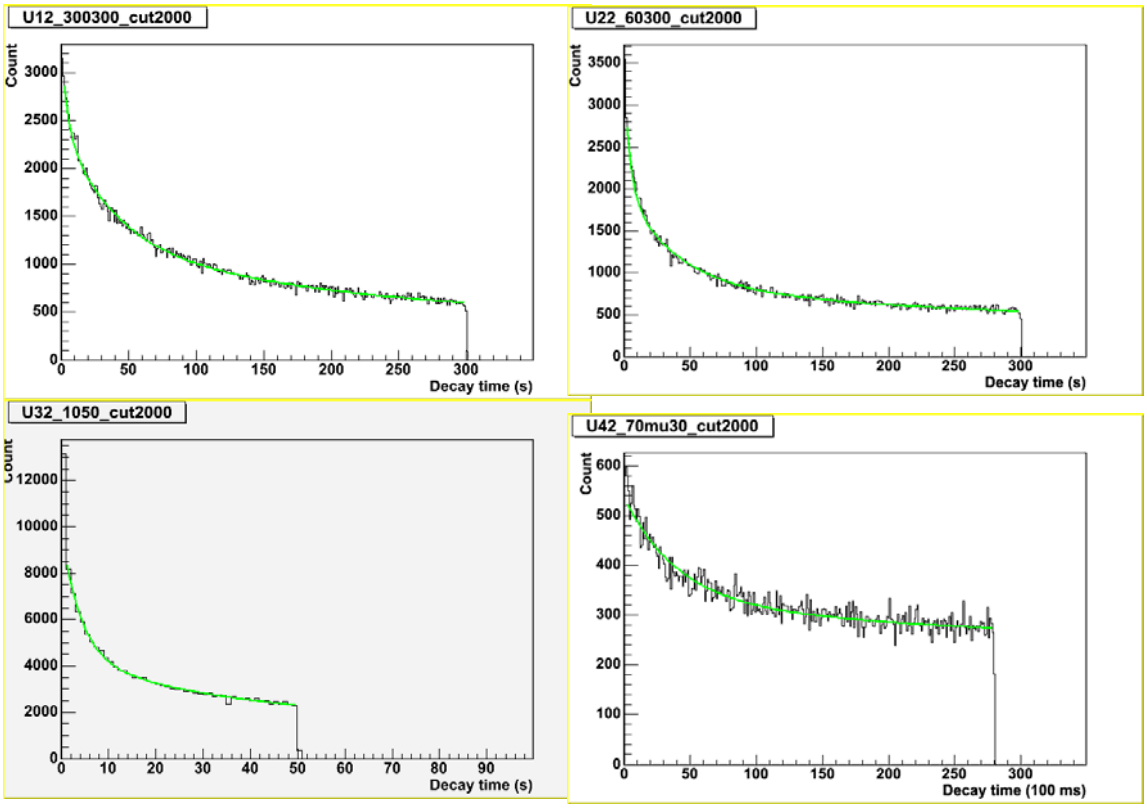

Figure 3. *^{238}U relevant unique fit with time constants fixed according to Table 1 and a 2 MeV gamma energy cut. See the legend for irradiation-decay periods.*

Total number of DP per photofission

Theoretically, an infinite time irradiation allows to determine the total number of delayed gammas emitted per fission. Let us assume that the 300 s / 300 s cycles correspond to this particular case, i.e. the major DP contributors have reached their production equilibrium. The total number of high energy DPs per fission at a given time can be obtained by:

$$\nu_{DP} = \frac{N_\gamma(t)}{N_{fiss}} = \frac{N_{BGO}(t)}{N_{fiss}\varepsilon_{BGO}}, \qquad \text{(Eq. 2)}$$

where N_{BGO} is the number of DP detected per second at time t (see Fig. 3), N_{fiss} - the number of fissions per second, ε_{BGO} - the total BGO efficiency, which includes the intrinsic detector efficiency, solid angle and attenuation both in uranium target and in shielding.
The number of fission events and the BGO efficiency were evaluated using the MCNPX code [5] calculations taking into account in detail the experimental set-up geometry and the information related to the primary electron beam intensity. The calculated value for the number of fissions was $N_{fiss} = 1.75 \times 10^6$ fissions.s^{-1}.μA^{-1} for ^{238}U. By taking into account the theoretical energy spectra of DP from neutron induced fission [6] and using MCNPX we estimated that $\varepsilon_{BGO} = 2.46 \times 10^{-4}$ events per incident DP with $E_\gamma > 2$MeV.
In order to check these simulations the absolute efficiency calibration measurements were done with low energy gamma sources such as ^{137}Cs ($E\gamma$ = 661 keV) and ^{60}Co ($E\gamma$ = 1333 keV/1173 keV) and identical experimental geometry. The experimental and simulated efficiencies agreed within 13 %.
The total DP emission of ^{238}U was also estimated using the CINDER code [6], based on neutron induced fission process. The experimental irradiation conditions were taken into account in these simulations. If one assumes that both n-fission and γ-fission of ^{238}U result in similar fission products, the predicted DP value is in a good agreement with our experimental result as shown in Table 2. More detailed analysis on these comparisons is in progress.

Table 2. *Results on υ_{DP} for the ^{238}U target with with $E_\gamma > 2$ MeV.*

Decay time t = 1s	Exp. $^{238}U(\gamma,fiss)$	Eval. $^{237}U(n,fiss)$	Eval. $^{238}U(n,fiss)$
υ_{DP} (γ/fission)	0.462 ± 0.070	0.555	0.607

Conclusions

The DP emission following photofission was measured in the case of ^{238}U and ^{232}Th targets. 15 MeV end-point Bremssthralung photons were employed to induce photofission and BGO was used to detect high energy gammas.
The DP decay curves were studied with different energy cuts from 2 MeV to 3.5 MeV. The decay time parameters for ^{238}U were determined for variable irradiation times and photon energies higher than 2 MeV, while data analysis for ^{232}Th is still in progress. It seems that all irradiations can be reproduced with only 3 averaged half lives, namely ~158 s, ~26 s and ~2 s. The obtained time constants are compatible with known major photofission products (high energy gamma emitters) determined by gamma off line spectroscopy at CEA [7]. The experimental total high energy (above 2 MeV) DP emission per photofission for ^{238}U is ~0.46, what is very close to the value of ~0.61 known from neutron induced fission on the same nucleus. Further investigations have to be undertaken including the extraction of relative group contributions in particular.
The future experiments will be done using ^{235}U, ^{237}Np and ^{239}Pu targets.

References

[1] M. Gmar et al., “Detection of nuclear material by photon activation inside cargo containers”, Non-intrusive detection technologies, Proceedings of SPIE Defence and Security Symposium, 17–21 April 2006, Orlando, Florida, USA.
[2] D. Ridikas et al., “Nuclear Material Interrogation via High-energy β-delayed Gamma Rays from Photo-fission”, Proc. of the International Workshop on Neutron Measurements, Evaluations and Applications (NEMEA-2), 20-23 October 2004, Bucharest, Romania.
[3] D. Doré et al., “Delayed neutron yields and spectra from photofission of actinides with Bremsstrahlung photons below 20 MeV”, EPS Journal of Physics: Conference Series 41 (2006) 241.
[4] J-L. Lemaire, “Gamma rays and X rays production for experiments at ELSA facility”, Proceedings of LINAC 2004, Lübeck, Germany.
[5] J. Hendricks et al., “MCNPX extension : version 2.5.0 “, LA-UR-05-2675, LANL, USA, April 2005.
[6] W.B. Wilson et al., “Status of CINDER90 codes and data”, LA-UR-99-361 LANL, USA 1999.
[7] F. Carrel et al., “Etude et développement d’une technique de dosage des actinides dans les colis de déchets”, DETECS/SSTM/RAP/05-21 – 2005 (in French).

The EURITRACK project: experimental tests of a Tagged Neutron Inspection System for cargo containers

C. Carasco[1)], B. Perot[1)], S. Bernard[1)], A. Mariani[1)], J.-L. Szabo[2)], G. Sannie[2)], G. Viesti[3)], G. Nebbia[3)], S. Pesente[3)], M. Lunardon[3)], C. Bottosso[3)], S. Moretto[3)], D. Fabris[3)], A. Zenoni[4)], G. Bonomi[4)], A. Donzella[4)], A. Fontana[5)], E. Giroletti[5)], V. Valkovic[6)], D. Sudac[6)], M. Moszynski[7)], T. Batsch[7)], M. Gierlik[7)], D. Wolski[7)], W. Klamra[8)], P. Le Tourneur[9)], M. Lhuissier[9)], A. Colonna[10)], C. Tintori[10)], P. Peerani[11)], V. Sequeira[11)], M. Salvato[11)]

1) Commissariat à l'Energie Atomique, 13108 St Paul-lez-Durance Cedex, France
2) Commissariat à l'Energie Atomique, 91191 Gif-Sur-Yvette Cedex, France
3) INFN and Università di Padova, Via Marzolo 8, I-35131 Padova, Italy
4) INFN and Università di Brescia, 38 Via Branze, 25123 Brescia, Italy
5) INFN and Università di Pavia, 6 Via Bassi, 27100 Pavia, Italy
6) Institute Ruder Boskovic, 54 Bijenicka c. 10000 Zagreb, Croatia
7) Soltan Institute for Nuclear Studies, PL 05-400 Otwock-Swierk, Poland
8) Department of Physics, Royal Institute of Technology,10691 Stockholm, Sweden
9) EADS-SODERN, 20 Av. Descartes 94451 Limeil-Brévannes Cedex, France
10) CAEN S.p.A., 11 Via Vetraia, 55049 Viareggio (LU), Italy
11) European Commission, JRC IPSC–CCR, I-21020 Ispra (VA), Italy
bertrand.perot@cea.fr

Abstract: The EURopean Illicit TRAfficking Countermeasures Kit project is part of the 6th EU Framework program and aims at developing a neutron inspection system for detecting threat materials in cargo containers. Neutron interactions in the container produce specific gamma-rays used to determine the chemical composition of the inspected material. The use of D-T tagged neutrons allows the inspection of a suspect voxel identified by previous X-ray scan. The Tagged Neutron Inspection System (TNIS) consists of a transportable neutron generator including a position-sensitive alpha detector, large volume neutron and gamma-ray detectors, front-end electronics to process alpha-gamma coincidence time and gamma-ray energy, and a data read-out and analysis software. The system has been integrated at the Neutron Laboratory of the Institute Ruder Boskovic (Zagreb, Croatia). Detection tests have been carried out with various targets hidden in a section of container filled with various materials simulating the transported goods. Results demonstrate the capability of the TNIS to inspect well-defined voxels and identify the hidden materials. For instance, a target simulating 100-kg of explosives was detected in a 10-minutes measurement inside a container completely filled with metallic boxes of 0.2-g/cm^3 average density. The TNIS is presented and the main results obtained at the Zagreb test site are reported.

Introduction

The use of cargo containers by terrorists to hide explosive devices has now become a serious threat. Explosives have to be distinguished from benign materials by an elemental analysis of the transported goods. Such discrimination is often not possible with widely used X-ray or gamma-ray imaging systems. On the other hand, inspections based on neutron systems [1] provide information on the chemical composition of the controlled objects. Indeed, inelastic scattering between the neutron and a given nucleus produces specific gamma-rays indicating that the element is inside the container. In this way, a measurement of the ratio between carbon, oxygen and nitrogen is feasible and allows the identification of explosives. Within the EURITRACK project [2], efforts have been dedicated to build a Tagged Neutron Inspection System (TNIS) [3] with a compact sealed neutron generator which produces 14-MeV neutrons from the ^{3}H(^{2}H,n)^{4}He fusion reaction. The beam is tagged by detecting the alpha particle with a pixel detector made of 8×8 YAP:Ce crystals. The matrix is coupled to a multi-anode photomultiplier and inserted inside the neutron generator. Since the alpha and the neutron are emitted nearly back to back, the measurement of the alpha particle position gives the neutron emission angle. The gamma rays produced by the interaction of the neutron with nuclei inside

the container are detected by a set of NaI(Tl) detectors surrounding the cargo container. The elemental composition of a precise volume element identified as suspect in previous X-ray radiography is studied by using the time-of-flight information to select the voxel. A prototype of the EURITRACK system has been mounted at the Ruder Boskovic Institute (IRB) of Zagreb, Croatia. It consists of a cargo container section, a transportable neutron emitting module in which the position sensitive alpha detector is embedded, fast neutron and gamma-ray detectors, front-end electronics and a data acquisition and processing software. A group of sixteen 5"×5"×10" NaI(Tl) detectors is placed on top of the container, two 5"×5"×10" NaI(Tl) are positioned on the opposite side of the neutron generator and two cylindrical 5"×5" detectors are near the neutron generator. Tests of the TNIS have been performed with samples hidden in metallic, organic and heterogeneous matrices.

Metallic matrix

A test has been carried out with a liquid nitrogen, water and graphite target simulating a 100-Kg TNT target hidden in the centre of the container filled with a 0.2-g/cm^3 average density iron matrix, made of iron boxes filled with iron wire balls. Fig.1 shows the setup and the associated alpha-gamma coincidence time, for a 10-minutes acquisition with a total isotropic neutron emission of $3{\cdot}10^7$ n/s. Note that the tagged emission is about 1% of the total one. The main features of the setup can be identified on the time spectrum, where the samples are clearly revealed by bump structures. Note that with a real 100-kg TNT block, nitrogen, carbon and oxygen would appear in a single peak. The bump around 60 ns comes from iron and lead blocks located after the second container wall. The flat signal at negative time is due to the time-uncorrelated events and is used to subtract the random background from energy spectra related to positive coincidence time areas. The energy spectrum for a coincidence time between 22 ns and 45 ns, corrected from random background, is shown in fig. 2 for 13-hour and 10-minute acquisitions, both with a total neutron emission of $3{\cdot}10^7$ n/s. On the long run, the specific energy peaks of nitrogen (2.3- 3.7- 4.4- 5.1-, 7.0-MeV), carbon (4.4-MeV), oxygen (2.7- 3.7- 6.1-, 7.1-MeV) and associated escape peaks are visible. The peaks of aluminium (2.2- and 3.0-MeV), which mainly constitutes the liquid nitrogen flask, are discernible too. The 4.4-MeV and 2.3-MeV peaks are still visible on the short run. An unfolding algorithm [4] will be used to estimate the relative contributions of carbon, oxygen and nitrogen.

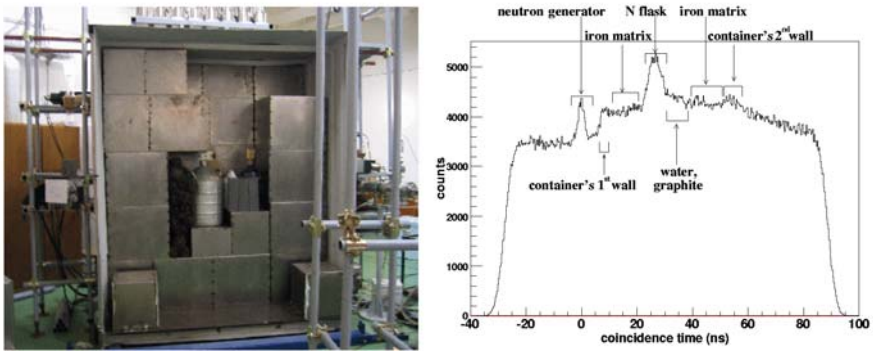

Figure 1. *Metallic matrix setup (left) and associated alpha-gamma coincidence time for the top detectors (left). On the photo, part of the iron matrix is removed to show the hidden target.*

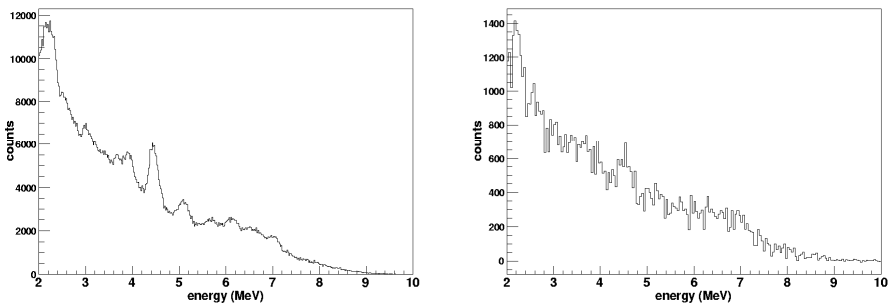

Figure 2. *Energy spectra corresponding to the target region, obtained after 13-hour (left) and 10-minute acquisitions (right).*

Organic matrix

Organic matrices are an important issue since the neutron beam is greatly attenuated, making difficult the container investigation. A performance test has been carried out with a graphite target hidden in the centre of a 0.5-g/cm^3 density wood matrix filling half of the container. The graphite block is screened from the neutron source and from the top detectors by 37.5 cm and 66 cm of wood, respectively. Fig. 3 shows the setup and the associated alpha-gamma coincidence time acquired after 10 minutes with a total neutron emission of $3{\cdot}10^7$ n/s. The coincidence time spectrum has been formed with the detectors located above the wood matrix. In such a configuration, the photons coming from the graphite target undergo the largest attenuation. The area between 8 ns and 14 ns refers to the wood matrix whereas the graphite target is identified by the peak between 14 ns and 21 ns. Fig. 4 shows the energy spectra related to the wood matrix and to the graphite target coincidence time regions. The 4.44- and 6.13-MeV peaks correspond respectively to carbon and oxygen. The graphite target is clearly indicated by an increase of the carbon-to-oxygen ratio. The presence of a residual oxygen contribution in the graphite region is due to the effect of neutron scattering inside the wood matrix, leading to an overlap of the signal of adjacent regions.

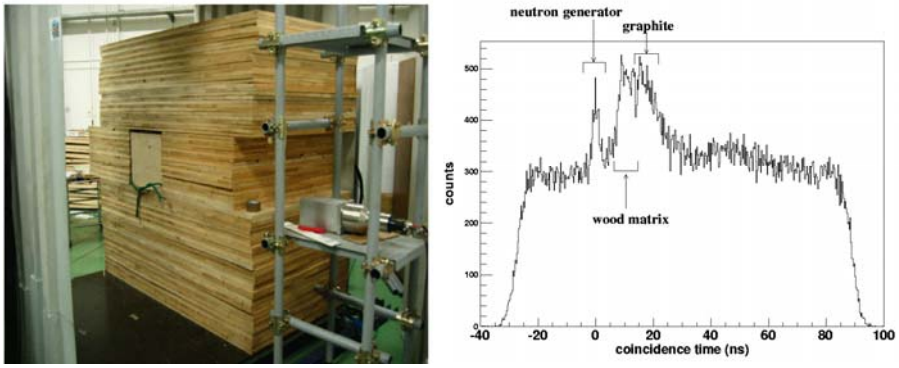

Figure 3. *Organic matrix setup (left) and the associated alpha-gamma coincidence time for the top detectors (left). In this picture, the graphite block is hidden inside the wood matrix.*

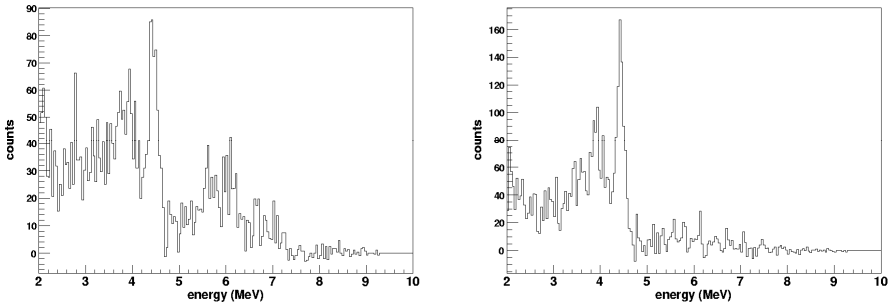

Figure 4. *Energy spectra corresponding to the wood filling of the container (left) and to the graphite target hidden in the middle of the wood matrix (right).*

Heterogeneous matrix

The container has been also loaded with miscellaneous goods in order to simulate an heterogeneous freight. An example is presented in fig. 5, with an alpha-gamma coincidence time spectrum related to a 10-minute acquisition with a total neutron emission of $3{\cdot}10^7$ n/s. A 19-liter water bottle has been inserted in the middle of the container. The time spectrum reveals several peaks corresponding to the various goods loaded in the container. Especially, the peak between 26 ns and 32 ns is due to the water target. Moreover, as shown in fig. 6, the energy spectrum related to this peak shows a large 6.13-MeV oxygen peak, which is not as large in other regions of the coincidence time spectrum. The unfolding algorithm [4] clearly indicates that the relative amount of oxygen is the largest in the area between 26 ns and 32 ns. Generally, the energy spectra will be different from one area of the time spectrum to the other, depending on the elements composing the inspected goods. These elements will be identified in the different areas of the time spectrum with the unfolding algorithm [4], making

possible the detection of potential threats within the different items inside the container.

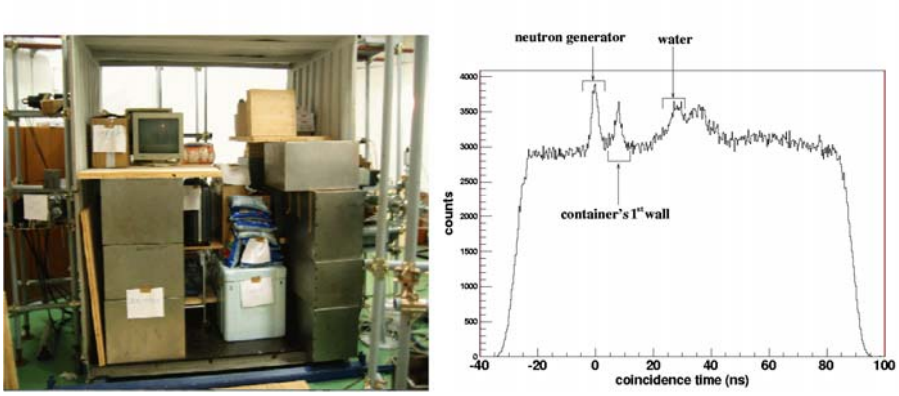

Figure 5. *Example of heterogeneous freight (left), including a water bottle not visible on the picture, and alpha-gamma coincidence time for the top detectors (right).*

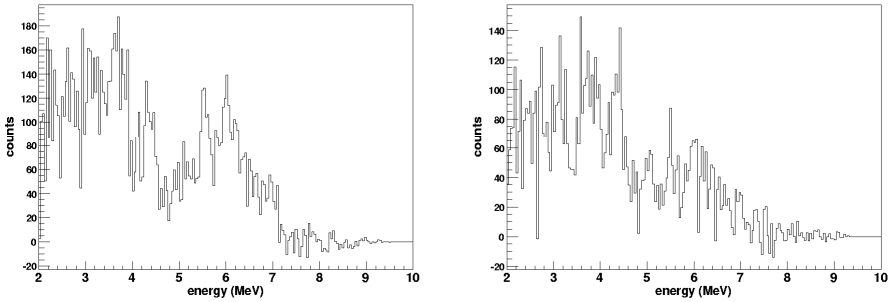

Figure 6. *Energy spectra obtained from the coincidence time shown in fig. 5, related to the water target zone between 32 ns and 36 ns (left) and to the neighbouring zone (right).*

Conclusion

The tests of the TNIS performed at IRB Zagreb in June 2006 demonstrate its ability to detect, in 10 minutes, a 100-kg TNT-equivalent target hidden in a container fully-filled with iron goods of 0.2-g/cm^3 mean density, which is the reference case of the EURITRACK project. The alpha-gamma coincidence time spectrum reveals a strong heterogeneity in the center of the container, where carbon, oxygen and nitrogen have been identified in the energy spectrum. The tests have shown that the system is also able to detect targets placed inside a dense homogeneous organic matrix or inside an heterogeneous matrix. An unfolding algorithm will determine the relative contributions of relevant elements (C, N, O, Fe…), with the purpose to identify threat materials hidden in heterogeneous or homogeneous container fillings.

Acknowledgements
This work is supported by the European Union through the EURITRACK project (FP6-2003-IST-2 Proposal/Contract 511471).

References

[1] T. Gozani, Nucl. Inst. Methods B213, 460 (2004) and reference therein.
[2] B. Perot et al., “The EURITRACK project: development of a tagged neutron inspection system for cargo containers”, in SPIE’s International Symposium on Defense and Security, Orlando (USA), 17-21 April, 2006.
[3] S. Pesente et al., Nucl. Inst. Methods B241, 743 (2005).
[4] P. Peerani et al., “The EURITRACK concept for cargo inspection with tagged neutrons”, this conference.

A comparison of measured and calculated neutron spectra modified by bismuth slabs

A. Fenyvesi[1)], L. Oláh[2)], J. Jordanova[3)], J. Csikai[1, 2)]

1) Institute of Nuclear Research of the Hungarian Academy of Sciences (HAS ATOMKI), Bem tér 18/c, P.O. Box 51, H-4001 Debrecen, Hungary
2) Institute of Experimental Physics, University of Debrecen (UD IEP), Bem tér 18/a, P.O. Box 105, H-4001 Debrecen 1, Hungary
3) Institute for Nuclear Research and Nuclear Energy, Bulgarian Academy of Sciences, Tzarigradsko chausse 72, 1784 Sofia, Bulgaria

fenyvesi@atomki.hu

Abstract: Transport experiments have been done with bismuth slabs using d+Be broad spectrum, as well as monoenergetic d+D neutrons. The d+Be neutrons were produced using E_d = 9.61 MeV deuteron bombarding energy at the low intensity neutron irradiation site of the MGC-20E cyclotron of ATOMKI. The d+D neutrons were produced via the $^2H(d,n)^3He$ (Q = 3.269 MeV) nuclear reaction at the neutron generator of UD IEP. Leakage spectra of neutrons behind bismuth slabs of different thicknesses have been measured in the energy range up to E_n = 14.7 MeV with a proton recoil spectrometer. The Pulse Height Response Spectrometry (PHRS) method was employed. The measured results have been compared with those predicted by the three dimensional Monte Carlo code MCNP-4C and pointwise cross sections from the ENDF/B-VI and FENDL-2.0 data libraries. Disagreements were observed between the results of the measurements and calculations in both cases using these evaluated data libraries. Also, differences have been observed comparing the results of calculations obtained by using ENDF/B-VI data and the results of calculations with FENDL-2.0 data. The discrepancies are beyond the uncertainties of the measurements and calculations below 3 MeV neutron energy and around 5 MeV and 8 MeV.

Introduction

The Pb-Bi eutectic alloy (44.5% Pb and 55.5% Bi) has important applications in advanced nuclear technologies where relatively hard neutron spectra are needed. It has has been used or considered as coolant of the blanket in some types of fission fast reactors, as high power target material at intense spallation neutron sources, as coolant of the fuel blanket of some accelerator driven systems such as accelerator-based nuclear waste transmutation systems, and as collant of blanket modules for burning transuranic actinides at future fusion reactors. All these applications need detailed knowledge of the neutron transport and precise and consistent relevant microscopic cross section data.

A few years ago we developed a 3-steps method [1] for integral testing of cross section data sets. The method employs the Pulse Height Response Spectrometry (PHRS) technique, and the steps are a) performing measurements of spectra modified by slabs of different thicknesses exposed by different neutron sources, b) Monte Carlo simulations with the MCNP-4C code [2] using differential cross section data taken from measurements and/or libraries of evaluated data, c) comparison of the obtained experimental data with results of the simulations.

This approach has been applied by us for bismuth in the 1 MeV $\leq E_n \leq$ 14.7 MeV neutron energy range. In this work we present our results obtained for the cross section data sets taken from the ENDF/B-VI and FENDL-2.0 evaluated data libraries.

Experimental

Broad spectrum d+Be neutrons were generated using E_d = 9.61 MeV deuteron bombarding beam at the low intensity neutron irradiation site at the MGC-20E cyclotron of HAS ATOMKI. Monoenergetic d+D neutrons were generated at the low intensity neutron generator at UD IEP using E_d = 180 keV deuterons. Blocks of slabs of 2 cm x 30 cm x 30 cm (up to 7 pcs) were put in between the neutron source and the detector. The details of the experimental arrangements are shown in Figures 1 and 2. The spectra of neutrons modified by the slabs

were measured by a Pulse Height Response Spectrometer (PHRS) based on a 5 cm diameter x 5 cm long cylindrical NE213 liquid scintillation detector. The derivative unfolding method was used to unfold the neutron spectra from the spectra of recoiled protons.

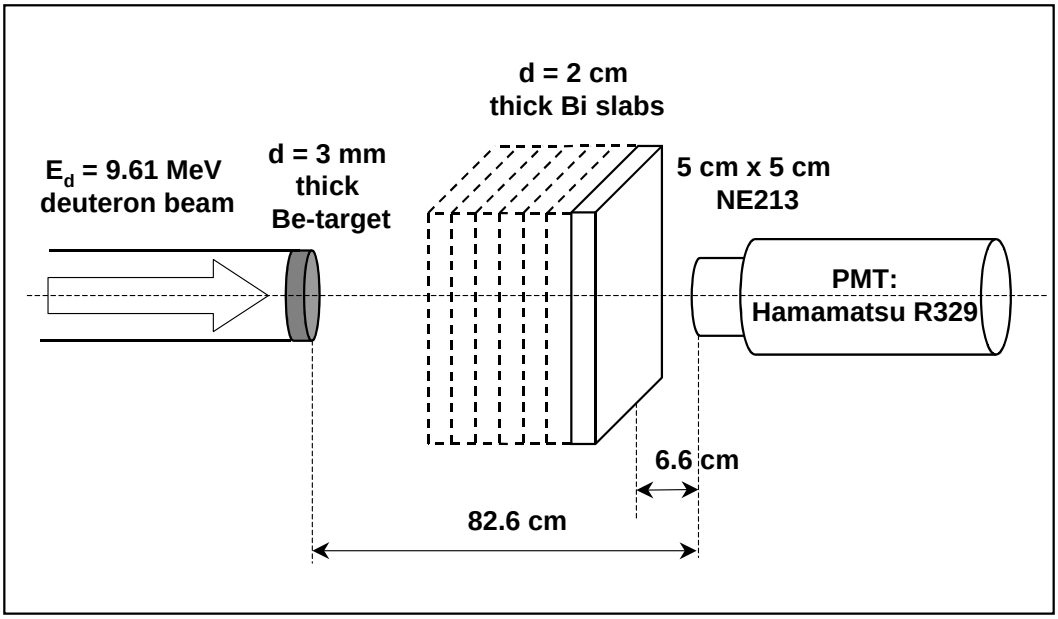

Figure 1. *The experimental arrangements of the measurements with d+Be neutrons.*

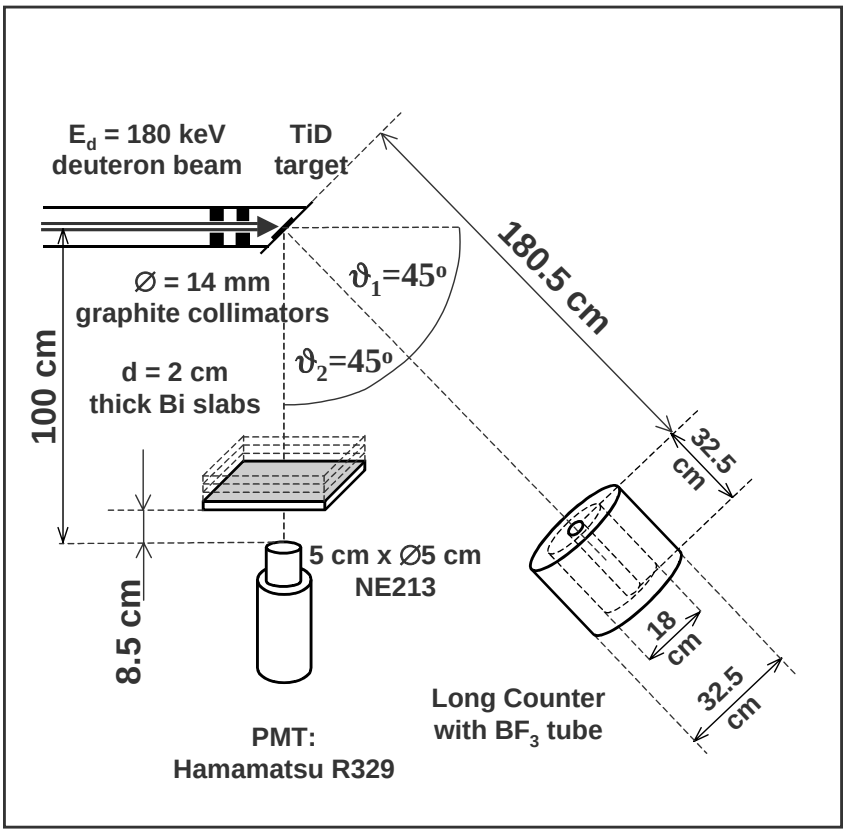

Figure 2. *The experimental arrangements of the measurements with d+D neutrons.*

Monte Carlo calculations

For transport simulations the MCNP-4C code and point-wise cross sections of the ENDF/B-VI and FENDL-2.0 data libraries were used. The neutron spectra measured without slabs were used a) to construct input spectra for the calculations and b) to normalize the calculated spectra to the total yields. Angular biasing was used to accelerate the computation. The biasing half cone angles were 29.5^{o} and 15.5^{o} for the measurements performed at the cyclotron and the neutron generator, respectively. The largest cell of nonzero importance was a sphere with radius of 50 cm and 55 cm for the measurements performed at the cyclotron and the neutron generator, respectively. A ring detector was specified on the source-detector axis to tally the neutrons that reached the NE213 scintillator. It was coaxial with the scintillator. The neutrons were scored until 1% statistical uncertainty was achieved, except for energy bins of low neutron fluxes, where 5% or less had to be reached.

Results

Figure 3 shows the neutron spectra measured with d+Be and d+D neutrons for d = 6cm slab thickness. The results of the MCNP calculations using ENDF/B-VI and FENDL 2.0 library data are also shown with the comparison of the results of the two calculations. Table 1 shows the integrated yields measured with d+Be neutrons and the corresponding ratios of the calculated and experimental values (C/E) for different slab thicknesses in different energy intervals.
There are disagreements between the measured and calculated neutron spectra both in the cases of d+Be and d+D neutrons. Also, the results of calculations obtained using ENDF/B-VI data differ from the results of calculations with FENDL-2.0 data. The differences below 3 MeV and around 5 MeV and 8 MeV are beyond the uncertainties of the measurements and calculations. These and the C/E values for the integrated yields suggest some discrepancies that are increasing with increasing slab thickness.

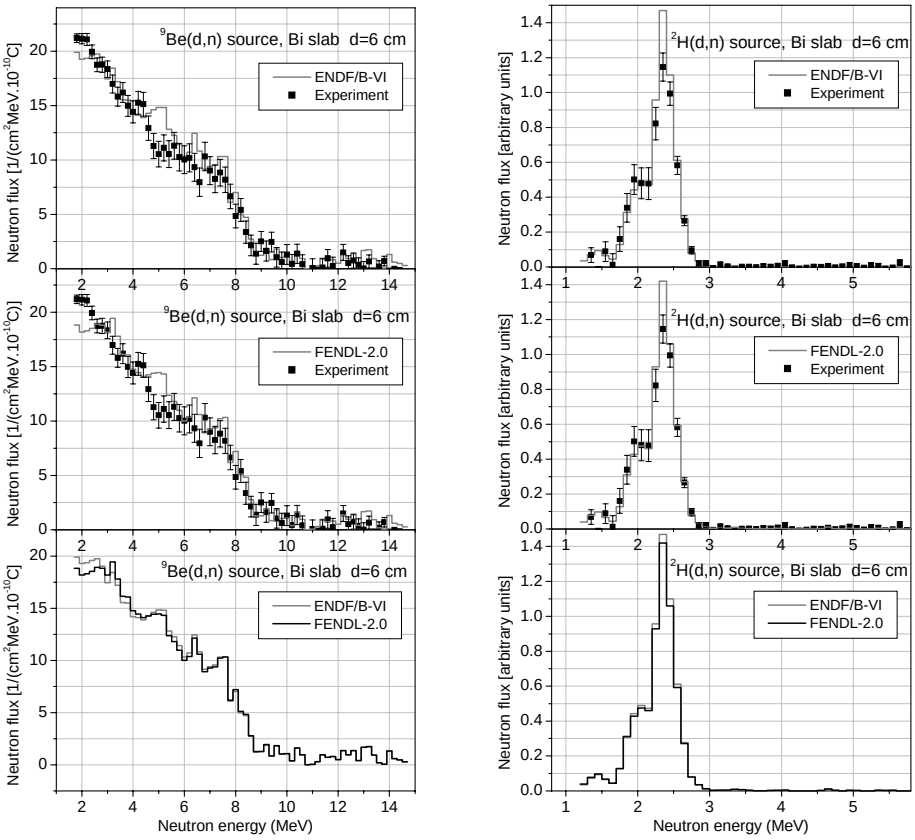

Figure 3. *The measured neutron spectra and the results of the MCNP calculations using ENDF/B-VI (up) and FENDL 2.0 library data (middle). The results of the two calculations are compared in the lowest chart. The thickness of the bismuth slab was d = 6cm.*

Table 1. *Integrated yields measured with d+Be neutrons and the corresponding ratios of the calculated and experimental values (C/E) for different slab thicknesses in different energy intervals.*

Slab thickness (cm)	**Measured value** ($cm^{-2}MeV^{-1}/10^{-10}A$)	**C/E**		**Measured value** ($cm^{-2}MeV^{-1}/10^{-10}A$)	**C/E**	
		ENDF B-VI	**FENDL 2.0**		**ENDF B-VI**	**FENDL 2.0**
	1.9 - 2.9 MeV			**2.9 - 5.9 MeV**		
4	22.16 ± 1.7 %	0.93	0.90	49.14 ± 2.2 %	1.05	1.05
8	18.07 ± 1.4 %	0.99	0.94	35.02 ± 2.0 %	1.08	1.10
14	11.48 ± 1.3 %	1.13	1.05	18.92 ± 2.2 %	1.20	1.25
	5.9 - 14.5 MeV			**1.9 - 14.5 MeV**		
4	27.92 ± 5.0 %	1.22	1.22	99.2 ± 1.8 %	1.07	1.07
8	20.88 ± 4.5 %	1.18	1.17	74.0 ± 1.6 %	1.08	1.08
14	12.06 ± 4.8 %	1.21	1.20	42.5 ± 1.7 %	1.19	1.18

The differences between the calculations and measurements suggest that cross sections for the elastic scattering and for the inelastic scattering to levels of the continuum might be discrepant in both libraries. Further measurements with monoenergetic and broad spectrum neutrons and detailed sensitivity analysis could reveal the sources of the discrepancies.

Conclusions

Transport experiments were done with bismuth slabs of different thicknesses using broad spectrum d+Be and monoenergetic d+D neutrons. The 1.3 MeV - 14.7 MeV neutron energy range was covered. A Pulse Height Response Spectrometer was employed for measuring neutron spectra. Simulations were also done with the MCNP-4C code using the ENDF/B-VI and FENDL-2.0 evaluated data files. The observed C/E values and the differences between the measured and calculated neutron spectra suggest discrepancies in the scattering cross section data of both libraries for Bismuth.

Further experiments should be done at different angles both with mono-energetic and broad spectrum neutrons and the extension of the energy range up to neutron energies above E_n = 14.7 MeV. Also, we suggest to perform detailed sensitivity analysis of the results of measurements and calculations to clarify the reason of the discrepancies. Similar experiments would be useful for Lead, too, since it is also a main component of the eutectic Pb-Bi alloy that has important nuclear energetics applications.

Acknowledgements

This work was supported in part by the Hungarian Research Fund (OTKA) under Contract No. T 025024 and the Bulgarian National Foundation under Contract No. F445. We thank the crew of the MGC-20E cyclotron of ATOMKI for performing the irradiations at the d+Be source. We thank Mr. J. Szegedi and Mr. I. László for their technical help in carrying out the experiments at the neutron generator and Mr. M. Orbán MSc student for his help in collecting the neutron spectra.

References

[1] Jordanova, J. et al., Nucl. Instr. and Meth. in Phys. Res. A 421 (1999) 522-530.

[2] Briesmeister, J. F., Editor, LA–13709–M, Los Alamos National Laboratory, New Mexico, USA, April 2000.

Photonuclear reaction cross section of ^{152}Sm

K.Y. Hara[1)], H. Harada[1)], F. Kitatani[1)], S. Goko[2)], S. Hohara[2,3)], T. Kaihori[2)], A. Makinaga[2)], H. Utsunomiya[2)], H. Toyokawa[3)], K. Yamada[3)], and Y. Watanabe[4)]

1) Japan Atomic Energy Agency (JAEA), 2-4 Shirane, Shirakata, Tokai-mura, Naka-gun, Ibaraki 319-1195, Japan
2) Konan University, Okamoto 8-9-1, Higashinada, Kobe 658-8501, Japan
3) National Institute of Advanced Industrial Science and Technology (AIST), 1-1-1 Umezono, Tsukuba, Ibaraki 305-8568, Japan
4) Kyushu University, Kasugakoen 6-1, Kasuga, Fukuoka 816-8580, Japan
hara.kaoru@jaea.go.jp

Abstract: The cross sections of the ^{152}Sm(γ,n) and ^{197}Au(γ,n) reactions were measured with the laser-Compton scattering γ beam at the energy from 8.3 MeV to 12.4 MeV. The present data for ^{197}Au measured as the standard were in good agreement with the previous data and the recent recommendation, while the present data for ^{152}Sm are smaller than the previous data near neutron threshold energy.

Introduction

Neutron capture cross sections of the unstable nuclei ^{151}Sm ($t_{1/2}$=90yr) are the fundamental data for nuclear transmutation and nuclear astrophysics. The ^{151}Sm is one of the important radioactive fission products in the nuclear waste [1]. On the other hand, the branching point nucleus ^{151}Sm is important for characterizing the *slow* neutron capture process (s-process) nucleosynthesis in the asymptotic giant branch stars. Very recently, the neutron capture cross sections for ^{151}Sm (ground-state) were measured by using a highly radioactive sample at CERN [2] and Karlsruhe [3]. Since the low-lying excited-state of ^{151}Sm can be populated under the stellar condition, the reliable model calculation of the capture cross section for the low-lying excited-state as well as the ground-state is desired to determine the (n,γ) reaction rate of ^{151}Sm in the stellar environment [4]. In this study, the cross sections of the inverse ^{152}Sm(γ,n)^{151}Sm reaction were measured at low energy in order to evaluate the capture cross section of ^{151}Sm. We present the photonuclear data for ^{152}Sm and the results of calculation with a nuclear reaction code TALYS [5]. In addition, the cross sections of ^{151}Sm(n,γ) reaction calculated by TALYS are compared with the recent data [2,3].

Experimental method

The cross sections of the inverse ^{152}Sm(γ,n)^{151}Sm reaction were measured with the laser-Compton scattering (LCS) γ rays at 8.3-12.4 MeV. The ^{197}Au(γ,n) reaction cross sections were also measured in the same energy region as a standard. The LCS γ rays were produced in head-on collisions of Nd:YVO_4 Q-switch laser photons (λ_{2nd}=532nm) with relativistic electrons in the storage ring TERAS [6]. Quasi-monochromatic beams of LCS photons which were collimated into a 2 mm spot in diameter with a Pb block were used to irradiate an enriched $^{152}Sm_2O_3$ sample or a metallic gold sample. The energy spectrum of the LCS γ beam was measured with a 120% Ge detector and analyzed with a Monte Carlo code EGS4 [7] to determine the energy distribution of the LCS beam. A large volume NaI(Tl) detector was used to monitor the flux of LCS beam. The neutrons emitted from the (γ,n) reaction were detected with a 4π-type neutron detector. The neutron detector consists of 20 ^{3}He proportional counters embedded in a polyethylene moderator.

Data analysis and the photonuclear cross sections for ^{152}Sm

In the data analysis, the (γ,n) cross sections were deduced with the iteration method [8]. The present data for ^{152}Sm and ^{197}Au were compared with the previous data compiled in the IAEA document [9]. Figure 1 shows the cross sections of the ^{197}Au(γ,n) reaction as a function of the

average energy of LCS rays E_{av}. The E_{av} was defined by $\int_{Sn}\{n_\gamma(E_\gamma)E_\gamma\}\,dE_\gamma / \int_{Sn}\{n_\gamma(E_\gamma)\}\,dE_\gamma$, where $n_\gamma(E_\gamma)$ is the energy distribution of LCS beam and S_n is the neutron threshold energy. The previous data [10-12] and the recent recommended cross section [13] are also shown in Fig. 1. The present data for ^{197}Au are in good agreement with the previous data by Veyssiere et al. [11] and the recent recommendation [13]. The cross sections of the ^{152}Sm(γ,n) reaction are shown in Fig. 2 by the similar manner in Fig. 1. The present data for ^{152}Sm at higher energies above 10.2 MeV are agreement with the previous data by Carlos et al. [14], but are smaller at low energy. In particular, the discrepancy is factor two at 8.3 MeV near neutron threshold energy (S_n=8.26 MeV). Although the iteration method made the assumption of the function form of cross section mandatory, the results of the photon difference method confirmed that the cross section for ^{152}Sm do not show the apparent structure of the cross section such as the previous data [14] near threshold. The photonuclear reaction cross sections for ^{152}Sm and ^{197}Au deduced from the photon difference method were consistent with the results of the iteration method. The details of the photon difference method for the LCS beam and the results were described in [15]. The uncertainties of the cross sections in the iteration method tend to be small compared with those in the photon difference method.

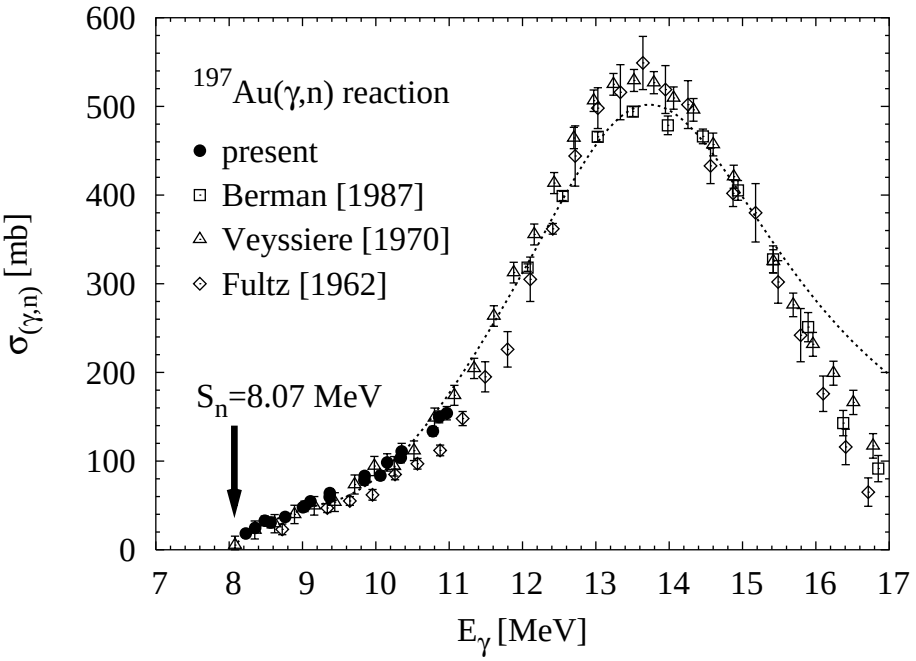

Figure 1. *Photonuclear reaction cross section of ^{197}Au deduced from the iteration method (solid circle). The previous data were measured with the positron annihilation source by Fultz et al. [10] (open squares) and by Berman et al. [11] (open triangles), and by Veyssiere et al. [12] (open diamonds). The photonuclear cross section for ^{197}Au was recently recommended by Vogt et al. [13] (dotted line) on the basis of the previous data and their data measured at low energy with the bremsstrahlung photon.*

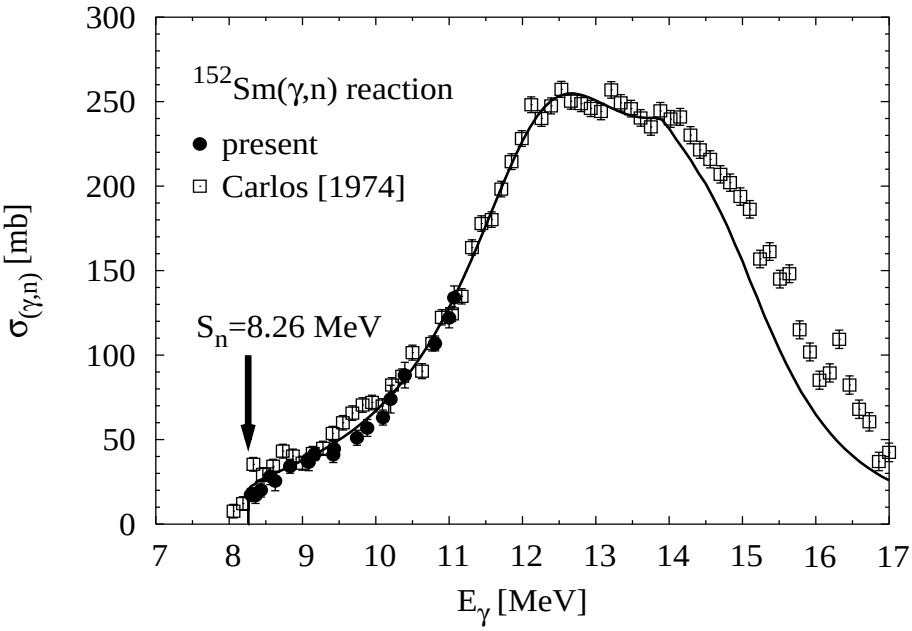

Figure 2. *Photonuclear reaction cross section of ^{152}Sm deduced from the iteration method (solid circle). The previous data were measured with the positron annihilation source by Carlos et al. [13] (open squares). The calculation with TALYS default parameters is shown by the solid line.*

TALYS default calculation: Neutron capture cross sections for ^{151}Sm

The neutron capture cross section for ^{151}Sm was calculated with TALYS default parameters. The calculated cross section in the energy range from 1 keV to 1 MeV is shown in Fig. 3 by the solid line. For comparison, the recent data are also shown in Fig. 3 by the open circles [2] and the solid triangles [3]. The TALYS calculation for the neutron capture cross section dose not agree with the recent data. In contrast, the photonuclear reaction cross section for ^{152}Sm calculated with TALYS default parameters is consistent with the present data, but tend to be larger than the present data at the low energy. The calculated cross section of the ^{152}Sm(γ,n) reaction is shown by the solid line in Fig. 2.

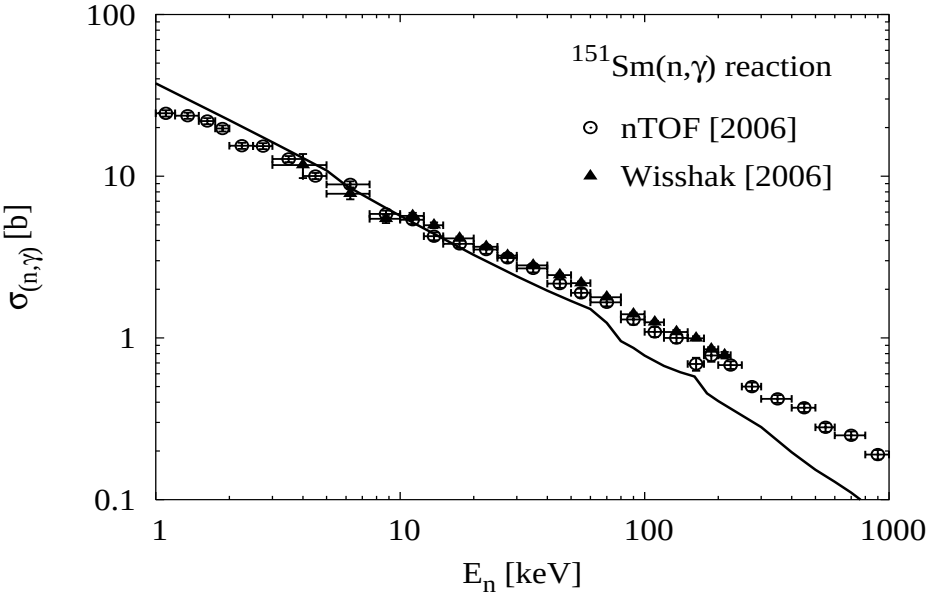

Figure 3. *Neutron capture cross section of ^{151}Sm calculated with TALYS default parameters. The neutron capture cross sections for ^{151}Sm were measured by using a highly radioactive sample at CERN [2] (open circles) and Karlsruhe [3] (solid triangles).*

Conclusions

The cross sections of the ^{152}Sm(γ,n) and ^{197}Au(γ,n) reactions were measured with the LCS γ beam at the energy from 8.3 MeV to 12.4 MeV. The present data for ^{197}Au measured as the standard were in good agreement with the previous data and the recent recommendation. On the other hand, the present data for ^{152}Sm are smaller than the previous data near neutron threshold energy. In the near future, the neutron capture cross sections for ^{151}Sm in the keV-MeV energy range will be evaluated with the present photonuclear data for ^{152}Sm as constraint in the statistical model calculations.

References

[1] OECD/NEA, Accelerator-driven System (ADS) and Fast Reactor (FR) in Advanced Nuclear Fuel Cycles, A Comparative Study (2002).
[2] U. Marrone et al., Phys. Rev. C 73, 034604 (2006).
[3] K. Wisshak et al., Phys. Rev. C 73, 015802 (2006).
[4] A. Mengoni, International Conference on Nuclear Data for Science and Technology, Santa Fe, USA, Sep. 26-Oct.1, 2004 (AIP, New York, 2005) p.1209.
[5] A.J. Koning, S. Hilaire, and M. Duijvestijn, TALYS-0.64 user manual, NRG Report 21297/04.62741/P FAI/AK/AK (2005).
[6] H. Ohgaki, H. Toyokawa, K. Kudo, et al., Nucl. Instr. and Meth. A 455, 54 (2000).
[7] W.R. Nelson, H. Hirayama, and W.O. Roger, the EGS4 Code Systems, SLAC-Report No. 265 (1985).
[8] H. Utsunomiya et al., Phys. Rev. C 74, 025806 (2006)
[9] IAEA, Handbook on photonuclear data for applications, Cross sections and Spectra, IAEA Report No.1178 (2000).
[10] S.C. Fultz et al., Phys. Rev. 127, 1273 (1962).
[11] A. Veyssiere et al., Nucl. Phys. A158, 561 (1970).
[12] B.L. Berman et al., Phys. Rev. C 36, 1286 (1987).
[13] K. Vogt et al., Nucl. Phys. A707, 241 (2002).
[14] P. Carlos et al., Nucl. Phys. A225, 171 (1974).
[15] K.Y. Hara et al., J. Nucl. Sci. Technol., to be submitted.

Evaluated data projects within the Nuclear Energy Agency

H. Henriksson[1)], Y. Rugama[1)]

1) OECD/Nuclear Energy Agency, 12 Blvd des Îles, 92130 Issy-les-Moulineaux
henriksson@nea.fr

Abstract: The Nuclear Energy Agency (NEA) is a specialised agency within the Organisation for Economic Co-operation and Development (OECD), an intergovernmental organisation of industrialised countries, based in Paris, France. The NEA Data Bank is also part of an international network of data centres in charge of the compilation and dissemination of basic nuclear data offering easy access to the main databases with bibliographical information, evaluated libraries, e.g. the Joint Evaluated Fission and Fusion (JEFF) library, as well as experimental data in the EXFOR database. A large number of benchmark experiments for data and code validation are also available from the NEA, such as ICSBEP (Criticality Safety), IFPE (Fuel Performance) SINBAD, (Shielding) and IRPhE (Reactor Physics). The NEA offers nuclear data services, such as collection of experimental and evaluated data, validation and distribution of the JEFF library, and development of data display programs. Meetings and workshops with working groups on international collaboration on evaluated data are also organised as well as international conferences on nuclear data.

Introduction

The Organisation for Economic Co-operation and Development (OECD) is an intergovernmental organisation of industrialised countries, based in Paris, France. The Nuclear Energy Agency (NEA) is a semi-autonomous agency within the OECD, specialised on the use of nuclear energy. As part of an international network of data centres in charge of the compilation and dissemination of basic nuclear data, the NEA collects experimental data from its member countries [1]. The NEA web site (www.nea.fr) offers easy access through web retrievals of the main nuclear databases with bibliographical information, evaluated libraries, e.g. the Joint Evaluated Fission and Fusion (JEFF) library [2-3] and experimental data.
This paper presents an overview of the NEA activities and the main emphasis will be given to evaluated data projects including the JEFF library progress. Examples of recent work are given as well as a discussion on the forth-coming evaluation efforts. The NEA offers a suite of services, from user's requests for a specific measurement to the production of application libraries. Examples are given below on some of the phases in this work.

NEA activities on evaluated data

The mission of the NEA is to assist its member countries in maintaining and further developing the scientific, technological and legal bases for safe, environmentally friendly and economical use of nuclear energy for peaceful purposes. The NEA works as a forum for international co-operation helping its member countries with technical expertise in, for example, nuclear safety and regulation, nuclear energy development, radiation protection and public health, nuclear science and the Data Bank activities. The primary role of the NEA Data Bank is to provide scientists in universities, governmental research institutes and industry with reliable nuclear data and computer programs for use in different nuclear applications. The Data Bank organises seminars, workshops and training courses a few times per year on computer programs that are considered to be of special interest to users.
The NEA Working Party on international nuclear data Evaluation Co-operation (WPEC) is established to promote the exchange of information on nuclear data evaluations, measurements, nuclear model calculations and validation. WPEC provides a framework for co-operative activities between the six major evaluation projects (BROND, CENDL, ENDF, FENDL, JEFF and JENDL). It assesses the needs for nuclear data improvements and addresses those needs by initiating joint efforts, such as the High Priority Request List (HPRL).

Evaluated data from request to application

The work on evaluated data can be seen as an up-going spiral, where the **request** for new or improved data serves as a starting point. The experimental results from these requests are collected in the experimental data base **EXFOR**, and later used in evaluating reactions for data libraries together with theoretical models implemented in **computer codes**. The **evaluations** are checked and validated by comparison with **integral experiments**. Finally, data are prepared for specific **applications** by computer codes. In general, needs for more data are requested at this point, why the work starts all over again, but from a better position as experimental data and theoretical models are upgraded during the process. Below follows some examples of the steps described above (in **bold** face).

The high priority request list (HPRL)
The HPRL is a collection of experimental data requests needed for new evaluations to be used in nuclear industry and for future nuclear applications (e.g. Generation-IV reactors or ITER) [4]. The HPRL provides therefore a guide for those planning new measurements, nuclear calculations and evaluation programmes.
Requests are reviewed by external referees coordinated by the NEA, and divided into high priority ones, where a quantitative justification is needed, and general requests where a more qualitative justification is sufficient. All requests need to be tied to a certain project. The HPRL project is organised through the WPEC and the request list is maintained by the Data Bank and is presented on the home page (www.nea.fr/html/dbdata/hprl). The requests are divided in high priority ones, where a quantitative justification is needed, and general requests where a more qualitative justification is sufficient. All requests need to be tied to a certain project including a project life span.

EXFOR
The NEA Data Bank is collecting, preparing and distributing experimental reaction data stored in a database called EXFOR, that was initiated already 1969 [1]. EXFOR is coordinated through an international network of four nuclear data centres, namely the NEA Data Bank, the National Nuclear Data Center at Brookhaven National Laboratory (USA), the Nuclear Data Section at IAEA and the Russian Nuclear Data Center at the Institute of Physics and Power Engineering in Russia.
In addition to storing the experimental data points and their bibliographic information, experimental information including source of uncertainties is also compiled. EXFOR comprises neutron- as well as charged-particle reaction data with incident particles of $A \leq 12$ and energies up to about 1 GeV. Selected photon-induced reaction data are also included. EXFOR contains at present 16,500 experiments from 1935, divided in 123,000 different reactions.
The bibliographic database CINDA is closely linked to EXFOR, and contains a complete bibliography of all neutron data published since 1932, as well as an index to corresponding EXFOR entries and evaluated data. Besides neutron data, CINDA also covers photo-neutron, photo-fission and spontaneous fission data. CINDA is available on web retrieval, through the JANIS program, and as a book that can be requested from the NEA.

Computer codes for data evaluation, validation and applications
The NEA computer program services distribute software packages and group cross-section data sets. The activity includes collection of programs, compilation and verification that the computer program package is complete and adequately documented. The computer program collection covers a wide range of nuclear energy and radiation physics applications, including codes for preparation of application data, such as NJOY for the processing of evaluated data into the ACE format used by MCNP.

Evaluated data and the Joint Evaluated Fission and Fusion (JEFF) project
The Joint Evaluated Fission and Fusion (JEFF) project comprises sets of evaluated nuclear data mainly for fission and fusion applications; it contains a number of different reactions, including neutron and proton interaction data, radioactive decay data, fission yield data, thermal scattering law data and an activation library. The JEFF project is managed by the Scientific Co-ordination Group (SCG) that meets biannually. The JEFF project also consists of the European Fusion File (EFF) and European Activation File (EAF) projects funded by the European Fusion Development Agreement (EFDA) monitored by a working group biannually in conjunction with the other JEFF working group meetings. The history of the JEFF project is

shown in Fig. 1, with the starting point in the early 1980s where the fission and fusion projects were two separate groups. The two communities joined their efforts in 1995 and that resulted in the JEFF-3.0 library [2], released in 2002.
The JEFF-3.1 Nuclear Data Library is the latest version [3] and it was released by the NEA in May 2005. It contains data evaluations collected and checked at the NEA Data Bank in co-operation with several laboratories in the Data Bank member countries. Within the framework of the JEFF project, the JEFF Working Group on Radioactive Data and Fission Yields decided to produce improved versions of the decay data and fission-yield libraries with a release in conjunction with the JEFF library. Activation data has also been included in the latest version, based on the EAF-2003 library. The neutron data library covers 381 isotopes, which is an increase from 340 in JEFF-3.0. There are 26 isotopes in the proton data library, and 9 materials are covered in the thermal scattering law file. A great achievement was to include covariance data for many isotopes in the neutron data library. The special purpose library on activation data contains 774 target nuclei with over 12,600 neutron induced reactions. Included is also radioactive decay data with about 3,852 isotopes and spontaneous and neutron induced fission yield data. Processed data for MCNP is available from the NEA and the full documentation of JEFF-3.1 will be published in the end of 2006 as JEFF Report 21.

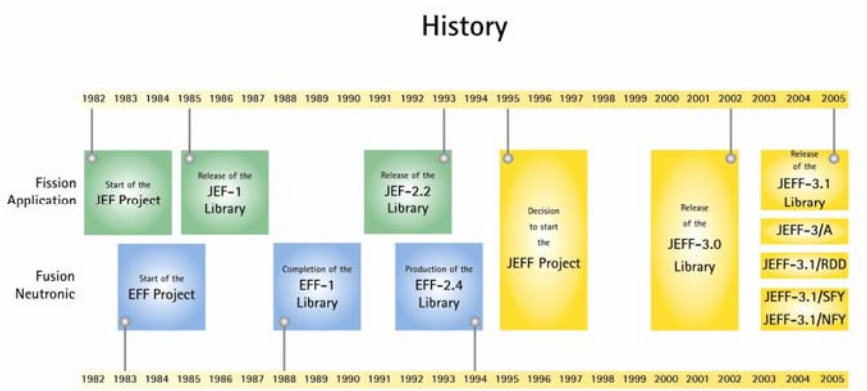

Figure 1. *JEFF time line from the beginning of the two separate fission (JEF) and fusion (EFF) projects in the early 1980s to the release of JEFF-3.1 in May 2005.*

Databases of Integral Experiments
The NEA Data Bank preserves data from integral experiments to assist users in having well documented information available for benchmark testing, especially in the context of the development of future nuclear energy systems. Integral experimental data with benchmark quality have been compiled, reviewed and published. The most relevant ones for nuclear data are the International Criticality Safety Benchmark Experiments (ICSBEP), International Reactor Physics Experiments Evaluations (IRPhE), and the Radiation Shielding and Dosimetry Benchmark Experiments (SINBAD).
The international database for radiation integral shielding experiments called SINBAD is an established set of radiation shielding and dosimetry data [5]. The, 78 experiments in SINBAD are relevant in reactor and accelerator shielding, as well as in fusion blanket neutronics. In addition to the experimental results together with uncertainties, the database includes characterization of the radiation source, description of the shielding materials and the relevant detectors used as well as the transport computer code inputs used for the interpretation of the experiment. Further extensions are planned for the near future.

Visualisation of nuclear data with JANIS
The program JANIS is designed to facilitate the visualisation and manipulation of nuclear data including remote access to the NEA databases [6]. The software is free of charge and can be requested on DVD or launched directly from the NEA web page: http://www.nea.fr/janis. JANIS comprises a range of functionalities such as the browser window showing a nuclide chart where isotopic data are displayed, such as decay modes. Ratios of cross sections can be calculated and displayed, e.g. from JEFF and ENDF/B. An example of an NEA web retrieval of evaluated data is presented in Fig 2a, and Fig 2b shows the JANIS display window when plotting the retrieved data together with experimental data from EXFOR.

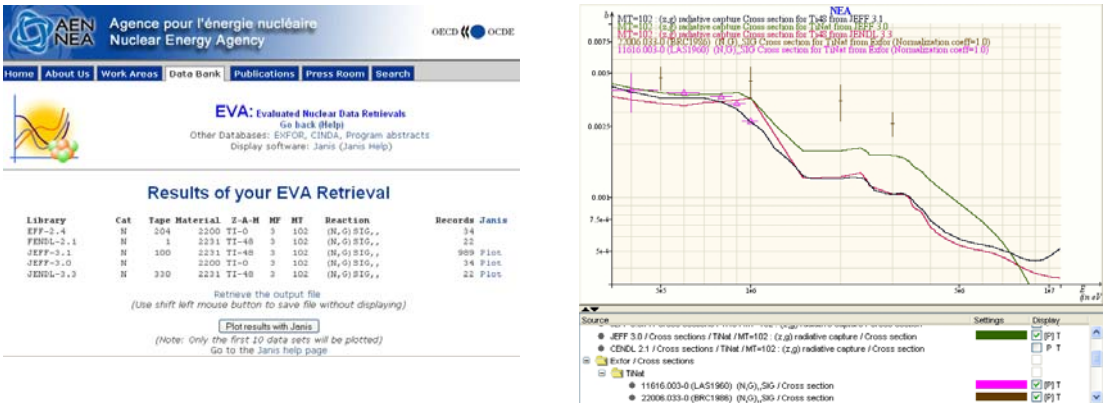

Figure 2 *Web retrieval of evaluated data (a, left) with corresponding plots (b, right) through the EVA web page at the NEA.*

Future evaluation work within JEFF and prospects for JEFF-3.2

The work on a new JEFF data library has focused on inclusion of more covariance data as well as photo fission evaluations. The main evaluations to be reviewed concern ^{55}Mn, ^{56}Fe, Pb isotopes, ^{209}Bi, ^{232}Th, ^{235}U, ^{237}Np, ^{239}Pu, ^{241}Am, ^{243}Am. Evaluations of delayed neutron data for photo-fission will be performed as well as covariance data for important nuclides within a collaboration in WPEC. A photonuclear data library is going to be prepared and gamma production data is envisaged. A revision of the decay data library will also be released.

Work is continuing on further evaluations for JEFF within the EFF group, including ^{55}Mn and ^{52}Cr up to 150 MeV. Separate calculations aimed for the EAF activation file will be carried out on Cu and Mn while the covariances of oxygen will be investigated theoretically. A new version of EAF, EAF-2007, is in preparation and it will contain deuteron- and proton-induced activation data as well as an enlarged neutron activation file thanks to calculations with the code TALYS. Other activities concern benchmarking efforts of recent EFF evaluations, such as Pb and V, as well as activity measurements on Cr, La, Sn and Re for EAF. The measurements on the HCPB mock up will be completed and these will be followed by similar experiments on the Helium Cooled Lithium-Lead blanket concept. These updates will be incorporated into the next JEFF library to be ready by 2009.

Acknowledgements
The authors acknowledge all contributions from NEA colleagues and all members of the JEFF project.

References

[1] O. Schwerer, V. McLane, H. Henriksson and S. Maev, Nuclear Reaction Data Centre Network: A Success Story, AIP Conf Proc. 769 (2005) 83, ND2004, Santa Fe, USA.
[2] NEA Data Bank, The JEFF-3.0 Nuclear Data Library, JEFF Report 19, (2005), ISBN 92-64-01046-7.
[3] A.J. Koning, et al., Status of the JEFF nuclear data library, AIP Conf Proc. 769 (2005) 177, ND2004, Santa Fe, USA, and NEA Data Bank, JEFF Report 21 (to be published).
[4] D. Smith, et al., The OECD Nuclear Energy Agency Request List for Nuclear Data, AIP Conf Proc. 769 (2005) 545, ND2004, Santa Fe, USA, and http://www.nea.fr/html/dbdata/hprl/
[5] I. Kodeli, E. Sartori and B. Kirk: SINBAD Shielding Benchmark Experiments Status and Planned Activities, ANS 14th Top. Meeting of Rad. Prot. and Shielding Division, Carlsbad, USA, 2006, and the SINBAD database: http://www.nea.fr/html/science/shielding/
[6] N. Soppera, H. Henriksson, A. Nouri, P. Nagel, E. Dupont, JANIS-2: An Improved Version of the NEA Java-based Nuclear Data Information System, AIP Conf Proc. 769 (2005) 557, ND2004, Santa Fe, USA.

Activation experiment on tantalum in the NPI p-^{7}Li neutron field

M. Honusek[1)], P. Bém[1)], V. Burjan[1)], U. Fischer[2)], M. Götz[1)], V. Kroha[1)], J. Novák[1)], S.P. Simakov[2)], E. Šimečková[1)]

1) Nuclear Physics Institute Řež, CS-25068 Řež, Czech Republic
2) Forschungszentrum Karlsruhe, D-76021 Karlsruhe, Germany
honusek@ujf.cas.cz

Abstract: The work aims to make the benchmark test of activation cross section data up to 38 MeV neutron energy. The standard ^{7}Li(p,n) reaction on thin lithium target induced by the variable-energy proton beam of NPI cyclotron was used for the production of quasi-monoenergetic neutron field. A carbon backing for the Li target was utilized. The stable operation of the source was achieved under cooling of the foil and the carbon backing separately. The system permits to produce neutron flux density of about 3 x10^{9} n/cm^{2}/s for the neutron energy of 30 MeV.
The tantalum samples of 15 mm in diameter and of 0.75 mm thickness were activated. All investigated Ta samples were stacked in packets containing the "reference" dosimetry foils of gold. The most important data obtained for 38 and 26 MeV proton beam are described. The analysis of resulting specific activities and reaction rates is carrying out in terms of C/E ratio (E – measured reaction rate, C - the predicted value of this observable calculated for the neutron spectrum). The neutron flux and spectra across the Ta samples are calculated using the double-differential cross section data of the ^{7}Li(p,n) reaction measured by other authors. Activation cross-sections data for selected reactions of neutrons on ^{181}Ta nuclide were taken from EAF-2005 library. We put the accent on neutron energies higher than 20 MeV. The preliminary results are discussed.

Introduction

The neutron cross-section data of reactions at incident energies E_n > 20 MeV are needed to improve the accuracy of neutronic calculations incorporated with various fusion technologies like IFMIF (International Fusion Material Irradiation Facility) and for the tests of nuclear reaction models as well.
The neutron activation of Tantalum - a constituent of low-activation Eurofer steel - is of importance for nuclear fusion applications. There are almost no experimental cross-sections data on Ta for neutron energies > 20 MeV and only limited data on experimental cross-sections exist for neutron energies < 20 MeV [1].
In the following sections we describe the quasi-monoenergetic p-^{7}Li neutron source, the activation experiment on Ta foils and the method of data evaluation. The resulting radioactive isotopes were studied by means of gamma spectroscopy methods. The preliminary analysis in terms of C/E results was carried out using the cross-section data from EAF 2005 library [1] and neutron spectra from Ref. [2].

Experimental equipment and neutron spectrum

The target station of quasi-monoenergetic neutron source based on ^{7}Li(p,n) reaction is shown in Fig. 1. Here (left part), the overall view of target chamber is shown together with the removable holder-transporter of Li foils (vertical part of the construction) On the right, the detail scheme of Li-foil holder cooled by the 5^{o} C alcohol stream is shown. The proton beam from isochronous cyclotron U120M strikes the Li foil at variable energies from 11 to 38 MeV. The carbon backing serves as a beam stopper. The irradiated foils could be placed at and above distance of 46 mm from the Li foil (not shown in the picture).
To evaluate the neutron spectral flux at sample positions the spectral yield of source reaction p+^{7}Li(C backing) were taken from the Ref. [2]. The spectra consist of quasi-monoenergetic part corresponding to the reactions to g.s. and 0.429 MeV states in ^{7}Be, and of the low-energy tail generated a) by reactions on ^{7}Li leading to further excited states in ^{7}Be and b) by reactions of protons on carbon stopper (see Fig.2).

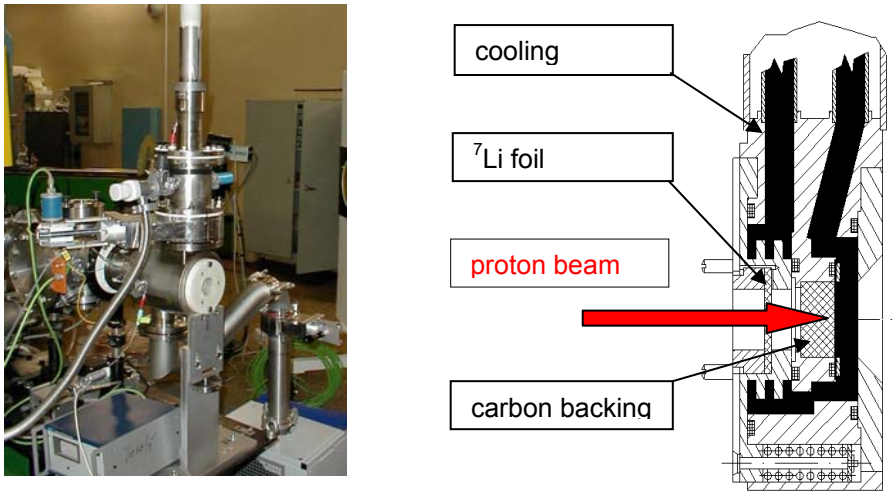

Figure 1. *The target station of NPI p-^{7}Li neutron source: left - owerall view, right - detail scheme of cooled Li-foil holder. Further details see in the text*

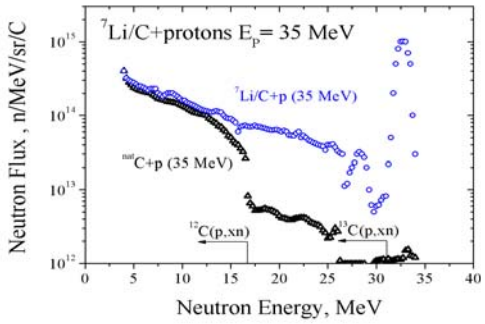

Figure 2*. The typical neutron spectra from the reaction p+(Li+C) and p+ C taken from the Ref.[2].*

Experimental procedure and results

The stack of irradiated foils (Ta and Au) was activated simultaneously at two distances (46 and 86 mm) from the Li foil to test the effect of the flux-density gradient in the vicinity of neutron source. The Au foil was used as a "reference monitor" [2]. The weights of foils (14 and 15 mm in diameter) were of 0.14 and 2.4 g for Au and Ta, respectively. The time profile of the neutron source strength during the irradiation was monitored by the proton beam current on the neutron-source target, recorded by a calibrated current-to-frequency converter on PC.
Foils were irradiated at two proton beam energies of the p-^{7}Li(C) source (37 and 26 MeV). The typical proton beam current was about 3 μA. The activation was carried separately with Li+C and C targets to investigate the contribution of neutrons from carbon stopper. The density of neutron flux at foil positions was approximately evaluated using the data of Ref. [2].
Irradiated samples were investigated by means of gamma-spectroscopy method. Two calibrated HPGe detectors of 23 and 50 % efficiency and FWHM of 1.8 keV at 1.3 MeV were used. Activated isotopes were identified on the basis of $T_{1/2}$, γ-ray energies and intensities. Cooling times of gamma measurement ranged from minutes to approx. 100 day. (Each foil was measured at approx. 5 cooling times). Resulting isotope activities related to unitary proton beam current were obtained. The lists of observed reactions on Au and Ta are shown in Table 1 and Table 2. Note, that there are two stable isotopes of Ta – ^{181}Ta (99.988 %) and ^{180m}Ta (0.012 %).
Typical experimental uncertainties are 4-6 % except ^{195}Au, ^{177}Lu and ^{177}Ta where such values are about 15 % and sometimes up to 40 %.

Table 1. *Isotopes observed from irradiations of Au foil.*

Isotope	*$T_{1/2}$*	*reaction*	*Threshold (MeV)*
Au194	38.02 h	(n,4n)	23.20273
Au195	186.09 d	(n,3n)	14.78950
Au196	6.183 d	(n,2n)	8.11245
Au196m	9.6 h	(n,2n)	8.70811
Au198	2.69517 d	(n,γ)	0

Table 2. *Isotopes observed from irradiations of Ta foil. Thresholds are given for reactions on ^{181}Ta, reactions on ^{180m}Ta are mentioned in italic.*

Isotope	T1/2	reaction	Threshold (MeV)	
Ta182	114.43 d	(n,γ)	0	
Ta180	8.152 h	(n,2n)	7.6	*((n,n) 0)*
Ta178m	2.36 h	(n,4n)	22.2 + x	*((n,3n)14.6+x)*
Ta177	56.56 h	(n,5n)	29.2	*((n,4n) 21.5)*
Hf181	42.39 d	(n,p)	0.25	
Hf180m	5.5 h	(n,d)	3.7 + 1.1	*((n,p) 0)*
Hf179m	25.05 d	(n,t)	4.9 + 1.1	*((n,d) 3.5+1.1)*
Lu177	6.734 d	(n, n α)	0	*((n, α) 0)*

Comparison of experimental results and calculated values

The comparison is based on the usual C/E ratio, where C and E correspond to the calculated and experimental activity, respectively. In the calculations, the cross section data were taken

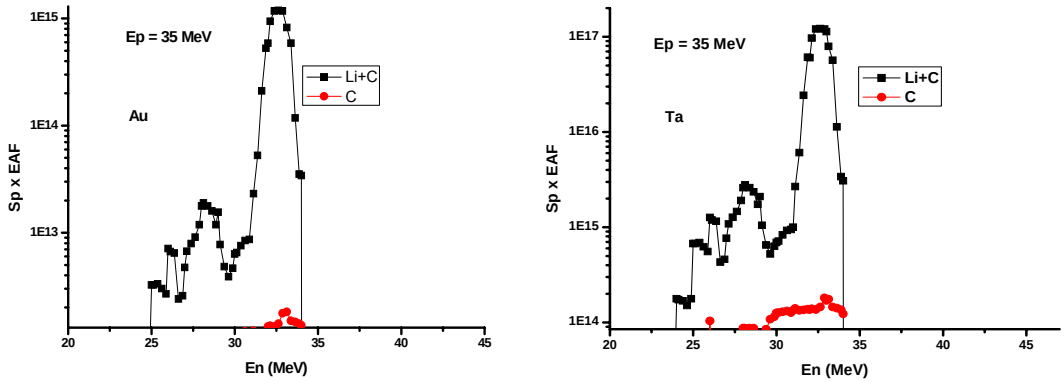

Figure 3. *Product of spectrum x cross-sections (C value) vs. neutron energy for reaction (n,4n). Left reaction on Au. Right – reaction on Ta*

from EAF-2005 [1], the neutron spectra were taken from Ref. [2]. The spectra reported for proton energies of 35 & 40 MeV and 25 MeV were used to compare present data measured with proton energy of 37.5 and 26 MeV, respectively. Similar approach was utilized also for data obtained with carbon stopper only. In present calculation, the possible difference between spectral yield (measured in the point-like-geometry, Ref. [2] and the form of spectra in the sample position (due to the integration over space and energy) was not taken into account. The MCNPX simulation and experimental testing of the integration effects is under progress.

As an example of the analysis, we present results of (n,4n) reactions on Au and Ta - see Fig.3. It is clearly seen that for this reaction the effect of quasi-monoenergetic peak dominates over low-energy tail of spectra (including neutrons produced in carbon stopper). The C/E ratios for (n,4n) reactions are given in Table 3 and 4.

Table 3. *C/E ratios (neutron spectra produced by different proton energies) for reaction (n,4n) on Au.*

Neutron source	Foil distance	Exp.Err. (%)	C/E 35 MeV	C/E 40 MeV
Li+C	46 mm	3	1.050	0.883
Li+C	86 mm	3	0.868	0.730

Table 4. *C/E ratios (spectra at different energies) for reaction (n,4n) on Ta.*

Neutron source	Foil distance	Exp.Err. (%)	C/E 35 MeV	C/E 40 MeV
Li+C	46 mm	4	0.243	0.157
Li+C	86 mm	3	0. 207	0.143

As a preliminary ('finger print'), the following C/E values are given for investigated reactions:
For the Au nuclide the observed C/E ratios are close to 1. For reactions on theTa nuclide the C/E ~ 1 for Ta181(n,p)Hf181 and (n,2n)Ta180, ~ 0.3 for Ta181(n, nα)Lu177, ~ 0.25 for Ta181 (n,4n)Ta178m, ~ 3 for Ta181 (n,d)Hf180n and ~ 30 for Ta181 (n,t)Hf179m. The further tests of EAF-2005 activation cross-section library are needed.
Note, that except the integral value, there are no experimental cross-section data for reactions on Ta. In present work, the cross-section value of 24 mb (uncertainty 12 %) for the reaction Ta181(n,5n)Ta177 at 35 MeV neutron energy (reaction threshold 29.2 MeV) could be determined under assumptions, that the effect comes from quasi-monoenergetic spectrum part only, the reaction (n,4n) on Ta180m is neglected and the cross-section is constant in the region of quasi-monoenergetic peak.

Conclusions

The isotope activities produced in Ta and Au foils by neutrons with energies of about 35 and 24 MeV were measured using the quasi-monoenergetic p-7Li neutron source (proton energies of 37.5 and 26 MeV, respectively) The spectral yield data for ^{7}Li(p,n) from Ref. [2] were used to the analysis of measured data.
The space-integration effects on the shape of spectrum at foil position will be investigated using the combination of measured data and the MCNPX calculations.

Acknowledgements
This work was performed with partial support of EFDA Technology Program, the Ministry of Education and the Ministry of Trade and Industry of CR.

References

[1] R. A. Forrest, J. Kopecky, M. Pillon, K. Seidel, S. P. Simakov, P. Bém, M. Honusek and E. Šimečková, UKAEA Report, UKAEA FUS 526, 2005.
[2] Y.Uwamino et al., NIM A389 (1997) 463.

Cadmium transmission measurements at GELINA

I.Z. Ivanov[1)], P. Siegler[1)], S. Kopecky[1)], A. Trkov[2)], M. Moxon[3)]

1) European Commission, Joint Research Centre, Institute for Reference Materials and Measurements, Retieseweg 111, 2440 Geel, Belgium
2) International Atomic Energy Agency, P.O. Box 100, Wagramer Strasse 5, A-1400, Vienna, Austria
3) 3 Hyde Copse, Marcham, United Kingdom

Ivaylo.IVANOV@ec.europa.eu

Abstract: The lack of good quality data for cadmium (Cd) may be a source for the long standing discrepancy between resonance integral measurements and the values calculated from the resolved resonance parameters. Therefore it was suggested that some new measurements should be carried out at IRMM Geel on natural Cd to try to resolve this problem. These measurements were performed in collaboration with the IAEA, Vienna in the framework of NUDAME. Measurements with thick natural Cd sample enriched to 99.99% in Cd were performed. The sample had a thickness of 25.8 mm corresponding to 0.120 at/b. The experiment was built up at flight path number 2 of GELINA. The neutron detector, a Li-glass scintillator, was placed at 26.45 m from the neutron producing target. The Li-glass had an effective diameter of 110 mm and was 12.7 mm thick. The data obtained in our measurements was compared to the existing one in ENDF/B-VI library. In this paper we report our first results from the analysis of the data obtained in these measurements. The resonance parameters were extracted from the transmission data by using the analysis code REFIT.

Introduction

Precise measurements of neutron cross-section substantially provide the quantitive nuclear data requisite to various applications of the nuclear engineering. Neutron resonance parameters are finding an increasingly important role in practical applications that are concerned with computations of reactor temperature coefficients, neutron reaction yields, self-protection effects, and related matters.

The total neutron cross-section of cadmium is crucial not only for the design and development of nuclear reactors but also for the basic study of neutron interaction with nuclei. Cadmium is one of the elements with a large total neutron cross-section in the thermal neutron energy region and it is a useful absorbing material for the control rods in thermal reactor. Sheets of Cd between 1 and 3 mm thick are often used as a neutron absorber in integral neutron experiments, such as integral benchmark and neutron activation measurements. The near-thermal resonance in ^{113}Cd at 0.178 eV removing the neutron flux below a nominal energy of 0.5 eV. Consequently, the neutron cross-section of ^{nat}Cd is very important for a correct interpretation and analysis of such experiments. Nonetheless, the neutron total, capture and scattering cross sections in cadmium have not been studied often. Most of the experiments focused on measurements of resonances for ^{113}Cd + n in support to parity violation studies [1, 2]. The last major experiment that could be used in non-fundamental applications was performed by Liou et al. in 1974 [3]. In the energy region above 3 keV there is a study by Musgrove et al [4] of the capture cross section. Experimental data, which can be used for an evaluation of the ^{nat}Cd (n,γ) and ^{nat}Cd (n,tot) reactions in the thermal and resolved resonance region, are rather scarce.

The lack of good quality data for cadmium may be a source of the long-standing discrepancy between resonance integral measurements and the values calculated from the resolved resonance parameters. Therefore, it was suggested that new measurements should be carried out at IRMM, Geel on natural cadmium to try to resolve this problem and contribute to further new evaluation for the resolved energy region. These measurements were performed in collaboration with the IAEA, Vienna in the framework of NUDAME. In this paper we report our preliminary results from the analysis of the data obtained in these measurements. The resonance parameters were extracted from the transmission data by using the analysis code REFIT [5].

Experimental set-up

To improve the experimental data-base for the determination of the resonance parameters for ^{nat}Cd, high resolution transmission and capture measurements were performed at the IRMM Time-Of-Flight facility GELINA [6]. The accelerator was operated at 400 Hz and 35-μA average electron current, providing electron pulses with 100-MeV average electron energy and a pulse width of 1 ns. Neutrons are produced by (γ,n) and (γ,f) reactions, induced via Bremsstrahlung from the electron beam hitting a mercury-cooled rotating uranium target. To produce a neutron spectrum in the low-energy region, two water-filled Be containers of 4 cm thickness are used as moderators.

We performed transmission measurements with a thick natural Cd sample enriched to 99.99% in Cd. The sample consisted of plates with a total mass of 441.6 g. The sample had a thickness of 25.8 mm corresponding to a thickness of 0.120 at/b.

The experiment was built up at a 26.45 m flight-path number 2 of GELINA. Here the angle between the flight path and the normal to the moderator is 9^{o}. The moderated neutron beam was collimated by different annular collimators within an evacuated beam pipe. The Cd sample was placed, at 9.1 m distance from the neutron producing target, in an automatic sample changer, operated by the data acquisition system. The sample changer was placed behind a 294 mm long collimator, made up of Li_2CO_3 plus resin and Cu. The 15 mm aperture of the last Cu collimator resulted in a neutron beam with a diameter of 15 mm at the sample position. During the measurements we kept the following filters permanently in the beam: a 0.004 at/b thick ^{nat}Cd overlap filter – to eliminate the slow neutrons from a previous accelerator cycle, an additional 5 mm thick Pb filter – to reduce the intense γ-ray flash and a fixed Na filter – to continuously monitor the background at 2.85 keV.

The neutrons were detected by a Li-glass scintillator (NE 905), enriched to 95 % in ^{6}Li, placed at 26.45 m from the neutron producing target. The Li-glass scintilator had an effective diameter of 110 mm and was 12.7 mm thick. It was mounted in a light tight aluminium box together with two EMI 9823 KQB PhotoMulTipliers (PMT), placed perpendicularly to the neutron beam axis. The anode pulses of both PMT's are transmitted to a constant fraction discriminator to create fast logic signals for a coincidence unit. Whenever two pulses are present within a 30 ns coincidence window, a coincidence pulse is sent to the Fast Time Coder (FTD). In this experiment we used a new FTD, which determines with a precision of 0.5 ns the Time Of Flight (TOF) of the detected neutron from the time difference between the start signal, given at each electron burst, and the stop signal from the coincidence unit. By selecting only coincident pulses a significant improvement of the signal-to-noise ratio in the TOF-spectrum is obtained. Together with these time spectra we also recorded the response of the neutron flux monitors - two BF_3 proportional counters, installed at different positions around the target hall to verify the stability of the accelerator and to normalise the sample-in and sample-out measurements to the same total neutron fluence. The temperature at the sample position was continuously monitored. The average temperature will be used in the resonance shape analysis program to calculate the Doppler broadening of the resonances.

During the first five days the experiment was done only with the Cd sample and the filters mentioned above. For determination of the background "black" resonance filters were additionally placed in the beam during the second 5 days – Au, Rh, Co, In. We performed an additional measurement for a precise determination of gamma flash position. The gamma flash of GELINA was used as a reference for measuring both the actual timing of the electron burst and the overall time resolution of the detection chain.

Results and discussion

In our transmission experiment the TOF spectra were measured alternating the sample in and out of the neutron beam, using a sample changer. To avoid systematic uncertainties due to possible slow variations of the beam profile or detector efficiency as a function of time, the alternating sequence of measurements was repeated many times in order to approach an identical incoming average neutron fluence for the "in" and "out" cycles. The transmission factor T was then obtained as the ratio of the time-integrated spectra C_{in} and C_{out}, corrected for their background contribution B_{in} and B_{out} respectively:

$$T(T_n) = N\frac{C_{in} - B_{in}}{C_{out} - B_{out}}$$

The normalisation factor N accounts for differences in integrated intensities of the incident neutron beam during the “in” and “out” cycles. For the normalisation to the same neutron fluence the information of the BF_3 neutron flux monitors was used.
We corrected our TOF spectra for losses due to the dead time in the detector and the electronics chain. The dead time was monitored continuously by a registration of the time-interval distribution between different events. From the time interval spectrum, we deduced a dead time τ_d = 94ns.
In our experiment the background was derived from the saturated resonance dips formed by the “black” resonances of Na, Co, Au, Rh and In filters, removing all neutrons at 2.85 keV, 132 eV, 4.9 eV, 1.25 eV and 1.457 eV, respectively. The background (C_{bg}) over the whole time range was parameterized by a hybrid function including a constant term:

$$C_{bg} = a_1 + a_2 T^{a_3} + a_4 e^{-a_5 T} + a_6 e^{-a_7 T}$$

where a_1, a_2,a_3, a_4, a_5, a_6 and a_7 are parameters adjusted to fit the observed minima of the “black” resonances and T - the time-of-flight of the detected event.
We used the data processing package AGS for dead time correction, background fitting and subtraction, normalization and TOF-to-energy conversion of our raw TOF spectra and last but not least for derivation of the transmission factor [7]. The package also includes a full propagation of uncertainties, starting from the uncorrelated uncertainties due to counting statistics.
Dead time corrected cadmium TOF spectra and the shape of the background for sample-in and sample–out measurements are presented in Figure 1.
Figure 2 presents a comparison between cadmium transmission data obtained in our measurements and the transmission calculated by the resonance parameters in the existing evaluations in the ENDF/B-VI.8, JEFF 3.1 and JENDL 3.3 Libraries. Cadmium evaluations in both libraries - ENDF/B-VI and JEFF are identical; they are using exactly the same resonance parameters. It is easy to see that there are significant differences between the obtained Cd transmission data and the ENDF/B-VI and JEFF evaluations in the low energy region. Therefore in our Resonance Shape Analysis (RSA), we decided to use as initial values in the low energy region the resonance parameters from the JENDL Library.
At the beginning of our analysis we determined the nuclear radii for the individual isotopes of Cd. The nuclear radius for individual isotopes was determined in the fits from the resonance-potential interference effects in the regions of the larger s-wave resonances. Figure 3 presents an example of such a fit.
Cadmium transmission data obtained in our measurements have been fitted and analyzed in the energy region from 20 eV up to 800 eV. In Figure 4 you can see part of the preliminary results.

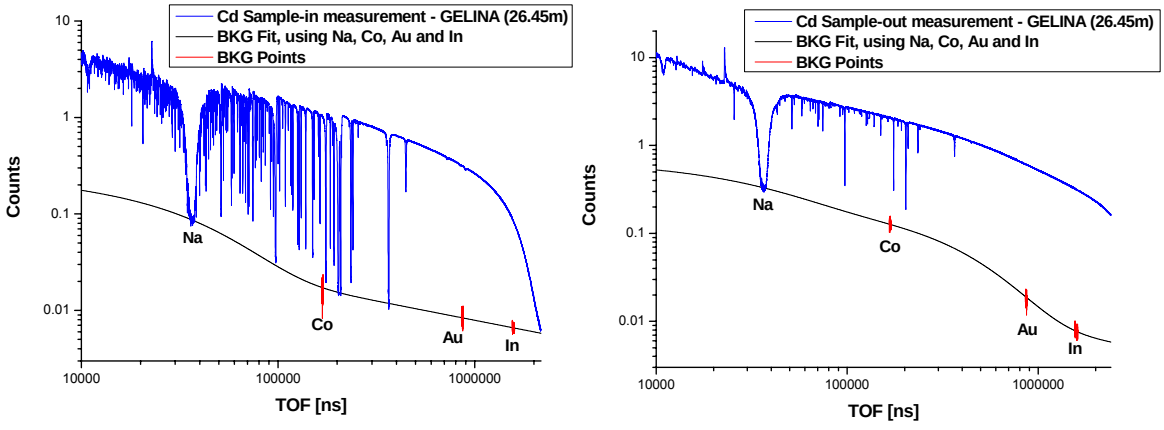

Figure 1. *Dead time corrected cadmium TOF spectra and the shape of the background for sample-in and sample–out measurements.*

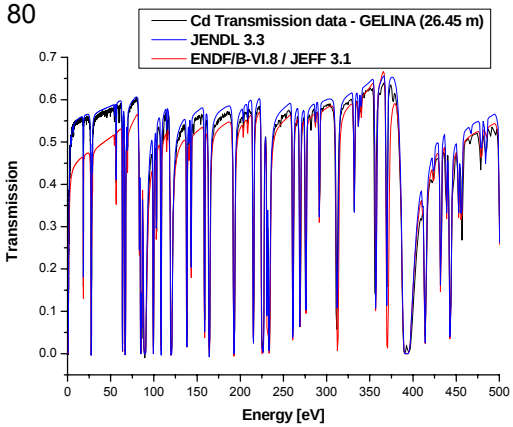

Figure 2. *Comparison between Cd experimental data and ENDF/B-VI and JENDL evaluations.*

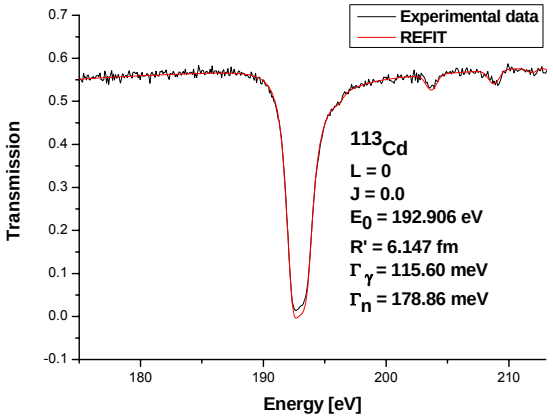

Figure 3. *Determination of the nuclear radius for ^{113}Cd.*

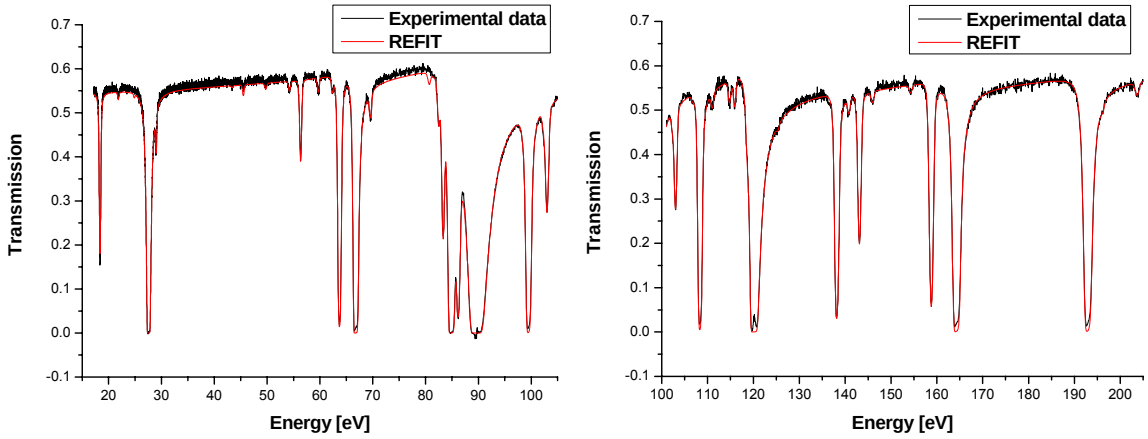

Figure 4. *Preliminary results in the energy region from 20 eV to 200 eV.*

Conclusions

Cadmium transmission data have been measured between thermal and 2.5 keV neutron energy. The obtained accuracy was improved compared to the existing data. It is easy to see that there are significant differences between the obtained Cd transmission data and the ENDF/B-VI evaluation in low energy region.

Cadmium transmission measurements at 40 Hz at GELINA, planned for January, 2007, will lead to improved resonance parameters in the thermal energy region and especially for the lowest well-known resonance at 0.178 eV of ^{113}Cd.

Finishing the analysis of this Cd transmission data, we are going to include in our analysis transmission and capture data obtained in measurements at the 50 m and 30 m flight paths of GELINA, performed with samples with various thicknesses in order to receive a complete dataset of resonance parameters for the cadmium cross-section.

References

[1] B. M. Frankle, C. D. Bowman, J. D. Bowman, S. J. Seestrom, E. I. Sharapov, Yu. P. Popov and N. R. Roberson, Phys. Rev. C 45(1992)2143.

[2] F Gunsing, K. Athanassopulos, F. Corvi, H. Postma, Yu. P. Popov and E. I. Sharapov, Phys. Rev. C 56(1997)1266.

[3] H. I. Liou, G. Hacken, F. Rahn, J. Rainwater, M. Slagowitz and W. Makofske, Phys. Rev. C 10(1974)709.

[4] A. R. de L. Musgrove, B. J. Allen and R. L. Macklin, Phys. G; Nuc. Phys. 4(1978)771.

[5] M. C. Moxon and J. B. Brisland, “REFIT, A least square fitting program for resonance analysis of neutron transmission and capture data”, AEA-In-Tec-0470 (United Kingdom Atomic Energy Authority, Harwell, 1991).

[6] J. M. Salome and R. Cools, Nucl. Instrum. Methods, 179 (1981) 13.

[7] C. Bastian, “AGS, a set of UNIX commands for neutron data reduction”, Proceedings of the International Conference on Neutron Research and Industry, Crete, Greece, 1996, Bellingham, WA, 1997, p. 611.

Quasi-absolute neutron-induced fission cross section of ^{243}Am

G. Kessedjian[1)], M. Aiche[1)], G. Barreau[1)], A. Bidaud[1)], S. Czajkowski[1)], D. Dassié[1)], B. Haas[1)], B. Jurado[1)], L. Mathieu[1)], L. Tassan-Got[2)], J. Wilson[2)], F.-J. Hambsch[3)], S. Oberstedt[3)], I. AlMahamid[4)], J. Floyd[5)], W. Lukens[5)], D. Shuh[5)]

1) CENBG, F-33175 Gradignan Cédex, France
2) IPN Orsay, F-91406 Orsay, France
3) EC-JRC-IRMM, B-2440 Geel, Belgium
4) Laboratory of Inorganic and Nuclear Chemistry, NY 12201, USA
5) LBNL, CA 94720, USA
kessedji@cenbg.in2p3.fr

Abstract: The existing evaluations of the ^{243}Am neutron-induced fission cross section have been questioned by recent studies performed at the GNEISS facility. In the neutron energy range from 1 to 6 MeV the GNEISS data present deviations of more than 15% with respect to the evaluations. In order to solve this problem, we have performed a first quasi-absolute measurement of this fission cross section from the fission threshold up to the onset of second-chance fission. To achieve this goal we have used the neutron-proton scattering cross section as reference reaction to reconstruct the incident neutron flux. This cross section is known with a precision better than 1 % for a wide range of neutron energies (1 meV to 20 MeV). This high precision explains why we can call our measurement “quasi-absolute”.

Introduction

^{243}Am is present in a rather important amount in the waste generated by current PWR nuclear reactors. Nowadays, ^{241}Am and ^{243}Am are the only isotopes that can be fully separated and extracted from spent fuel rods. Therefore, they represent the only nuclei for which fast neutron incineration could be seriously considered in a relatively near future. A reliable design of incineration reactors requires the precise knowledge (around 5% of accuracy) of the neutron-induced fission cross section of ^{243}Am in a fast neutron spectrum. However, in the 1 to 6 MeV neutron-energy range, the existing data indicate significant discrepancies and could be segregated into two distinct groups. The most recent data from Laptev et al. [1] lie in the higher-cross section group which is more than 15% above evaluations and older values by Knitter et al. [2]. Actually, this discrepancy seems to be related to a normalisation problem [3] due to the difficulty in determining precisely the neutron flux. In order to solve this controversy, we have performed for the first time a quasi-absolute measurement of the ^{243}Am neutron-induced fission cross section. Most of the fission data on ^{243}Am have been measured in reference to the ^{235}U neutron-induced fission cross section. In our case we have used the neutron-proton scattering cross section as a reference reaction to determine the incident neutron flux. While for the ^{235}U fission cross section the dispersion between available data is 5%, the neutron-proton scattering cross section is known with a precision better than 1% for a wide range of neutron energies (1 meV to 20 MeV [4]). This high precision explains why we can call our measurement “quasi-absolute”.

Experiment

The experiment was performed at the VdG-driven neutron source of the IRMM in Belgium. The T(p,n)^{3}He reaction was used to produce neutrons with energies ranging from 1 to 4 MeV and the D(d,n)^{3}He reaction to produce neutrons in the 4 to 8 MeV energy range. Two ^{243}Am targets each of about 550 µg/cm^2 thickness were placed back-to-back in between two sets of photovoltaic cells in a very compact geometry. The cells allowed detection of fission fragments with an efficiency of approximately 70%. A polypropylene foil was placed at 45 mm from the ^{243}Am targets. This foil served as a radiator to convert neutrons into protons. Its thickness varied from 10 to 50 µm depending on the neutron energy. Protons recoiling from the polypropylene foil were detected by means of a Si telescope located at 75 mm from the

foil. The ensemble polypropylene-telescope formed our neutron detector. The telescope also detected the charged particles originating from the interaction of neutrons with the Si of the telescope. This background was measured by stopping the protons in a tantalum screen placed behind the polypropylene foil. A neutron monitor assured the normalisation of the standard and background measurements.

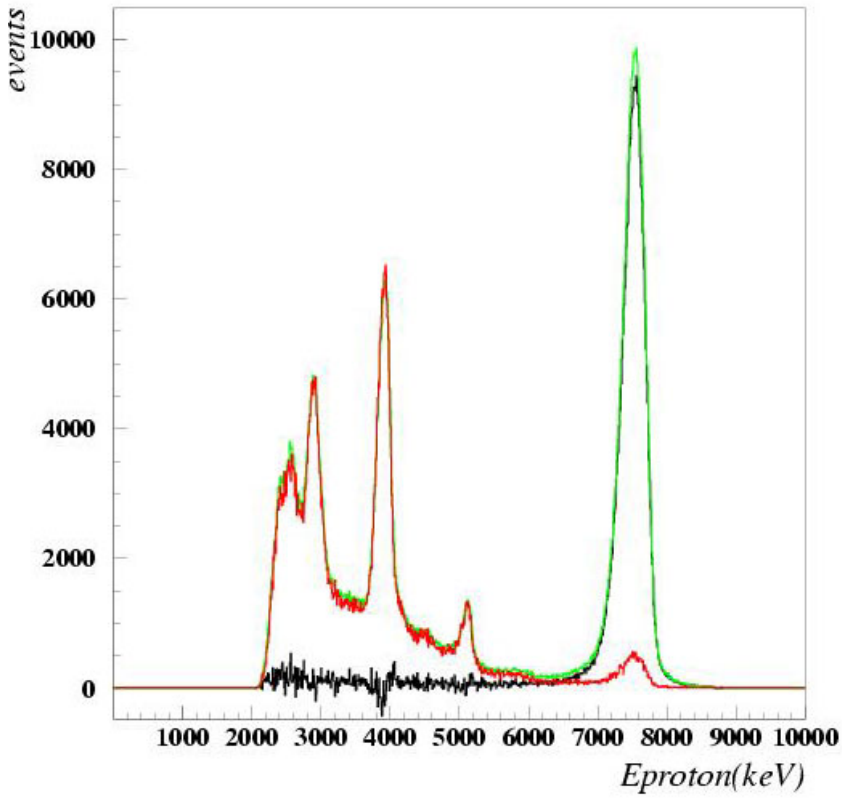

Figure 1. *Number of detected protons as a function of the total kinetic energy. The curve in green represents the standard measurement, the curve in red the background measurement, and the curve in black the result after background subtraction. The latter shows the proton peak associated to the incident neutron flux.*

As for the fission-fragment detection, the photovoltaic cells present the advantage of having an intrinsic efficiency of 100% and of being almost insensitive to the neutron beam and the alpha activity of the targets. In the following we will concentrate in the determination of the incident neutron flux from the protons scattered in the polypropylene foil. Figure 2 presents the number of detected protons as a function of the total kinetic energy before and after background subtraction. This background is mainly due to the reaction $^{29}Si(n, \alpha)^{26}Mg$ since the alpha particles have the same energy as the scattered protons. The spectrum that results from the background subtraction presents only one peak corresponding to the protons produced by the interaction of the quasi-monoenergetic incident neutron flux with the polypropylene foil.

The neutron energy spectrum is generated by a Monte-Carlo simulation. This simulation takes into account the angular distributions of the neutrons emerging from the neutron source and of the elastic scattered protons, the energy loss of the charged particles in the neutron source and in the polypropylene, the energy resolution effects of the incident beam and the energy straggling caused by the detectors. When the simulated proton spectrum is in agreement with the experimental result (upper part of figure 2.), we deduce the neutron spectrum (lower part of figure 2.), the mean value of the neutron-proton elastic scattering cross section and the efficiency of the proton detector.

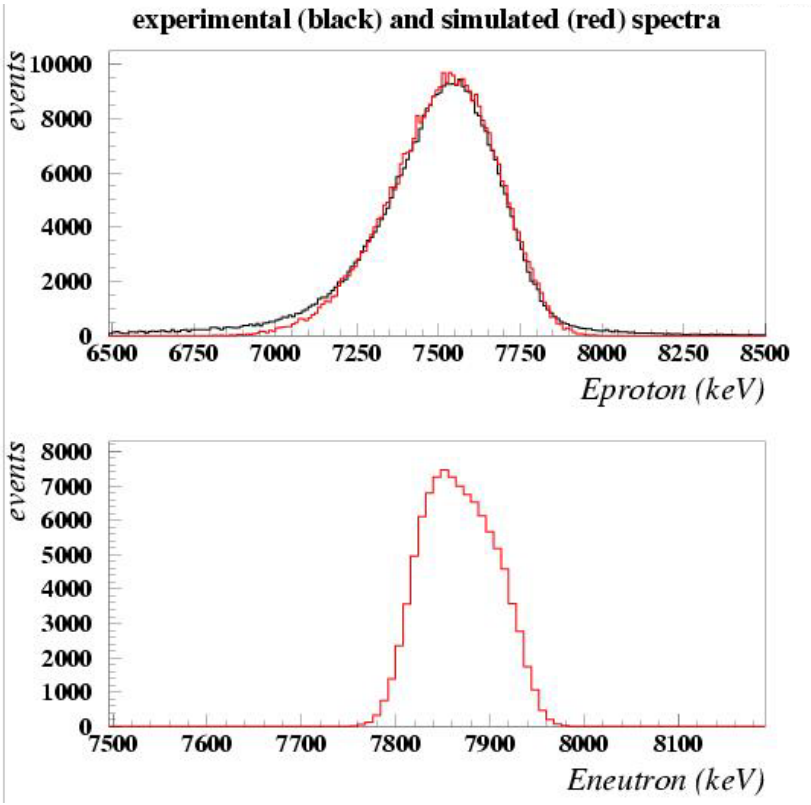

Figure 2. *Upper figure, experimental and simulated spectra of recoil protons as a function of total kinetic energy. Lower figure, simulated neutron spectrum as a function of kinetic energy.*

Preliminary results for the fission cross section determined in this experiment are displayed in figure 3. Our results are in agreement with the international evaluations and the data of Knitter et al. [2]. Consequently, our data indicate that the latest results of Laptev et al. [1] over predict this cross section. The overall precision of our data is of 4%. The statistical uncertainty represents only 1% of the total uncertainty. The systematic error includes the uncertainty in the determination of the geometrical efficiency and of the thicknesses of the ^{243}Am target and the polypropylene foil, as well as the uncertainty of the neutron-proton elastic scattering cross section.

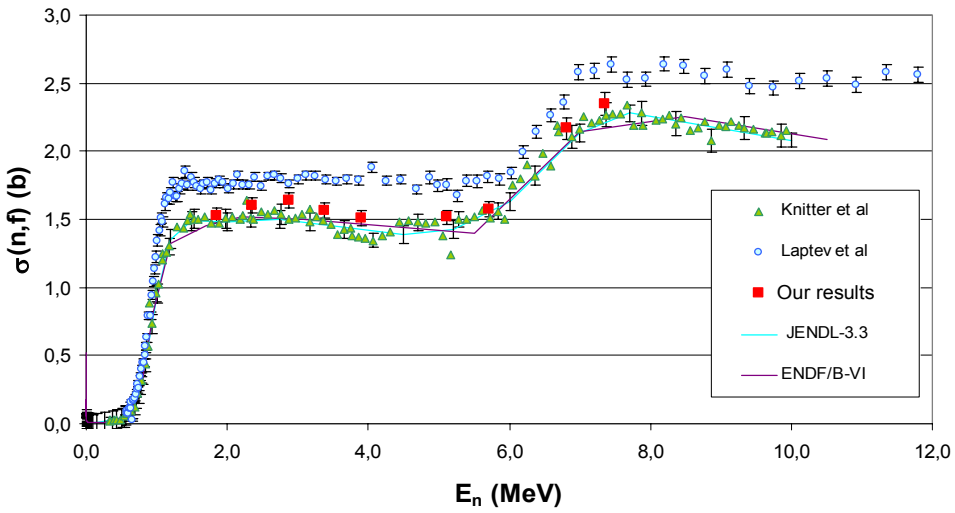

Figure 3. *Preliminary results for the fission cross section of ^{243}Am as a function of neutron energy in comparison with other experimental results and with the JENDL and ENDF evaluations.*

Conclusion and perspectives

We have presented the first measurement of the fission cross section of ^{243}Am in reference to the neutron-proton scattering cross section. This new measurement consolidates the validity of the existing evaluations. These results will be completed at the CENBG where we will perform measurements at the fission threshold and between 3.5 and 5 MeV. In addition, we will use the statistical code of the CENBG to perform our own evaluation of this cross section. In that way, fundamental fission parameters such as fission barrier heights and curvatures will be determined. These parameters can then be used to infer other neutron-induced cross sections that are much more difficult to measure like capture, inelastic and (n,2n) cross sections.

Acknowledgements
This work has been supported by the CNRS programme PACE/GEDEPEON and the EURATOM Transnational Access Programme NUDAME. We thank the IPN Orsay for building the high-quality ΔE detector of the Si telescope.

References
[1] A. B. Laptev et al., Nucl. Phys. A 734 (2004) E45.
[2] H. H. Knitter et al., Nucl. Sci. Eng. 99 (1988) 1.
[3] P. Talou, et al., Nucl. Sci. Eng. 155 (2007) 84.
[4] A. D. Carlson, Private Communication.

A neutron beam facility at SPIRAL-2

X. Ledoux[1)], M. Aïche[2)], G. Ban[3)], G. Barreau[2)], P. Baumann[4)], P. Bem[5)], V. Blideanu[6)], J. Blomgren[7)], S. Czajkowski[2)], P. Dessagne[4)], E. Dupont[6)], T. Ethvignot[1)], U. Fischer[8)], F. Gunsing[6)], B. Jacquot[9)], B. Jurado[2)], M. Kerveno[4)], F. R. Lecolley[3)], J. L. Lecouey[4)], F. Negoita[10)], S. Oberstedt[11)], M. Petrascu[10)], A. Plompen[11)], F. Rejmund[9)], D. Ridikas[6)], G. Rudolf[4)], O. Shcherbakov[12)], S.P. Simakov[8)], J. Taïeb[1)]

1) CEA/DIF, DPTA/ SPN, 91980 Bruyères-le-Châtel Cedex, France
2) Centre d'Etudes Nucléaires de Bordeaux-Gradignan, 33175 Gradignan, France
3) LPC, ISMRa et Université de Caen, CNRS/IN2P3, France
4) Institut Pluridisciplinaire Henri Curien, Strasbourg, France
5) Nuclear Physics Institute, 25068 Řež, Czech Republic
6) CEA Saclay, DSM/DAPNIA, 91191 Gif-sur-Yvette, France
7) Department of Neutron Research, Uppsala University, Uppsala, Sweden
8) Forschungszentrum Karlsruhe, Institute for Reactor Safety, Karlsruhe, Germany
9) GANIL, CEA/CNRS, Caen, France
10) NIPNE, Bucharest, Romania
11) European Commission, JRC/IRMM, Geel, Belgium
12) PNPI, Gatchina, Russia

xavier.ledoux@cea.fr

Abstract: The SPIRAL-2 facility, dedicated to the production of radioactive beams, is expected to be operational in 2011. The LINAG (linear accelerator of GANIL) of SPIRAL-2 [1] could be used to produce high energy neutrons. The use of the proton and deuteron beams on different converters like C, D_2, Li or Be will allow to produce high intensity neutron flux in the 100 keV- 40 MeV energy range. In this paper we will show how the primary ion beam characteristics (energy, time resolution and intensity) are adequate to create a neutron time-of-flight facility [2]. We will also discuss the potential of this new installation to investigate numerous topics both in fundamental and applied physics. In particular, cross section measurements could be performed for different purposes like nuclear data evaluation, fission and fusion technology, Accelerator Driven Systems, nuclear medicine, astrophysics, etc. [3].

Introduction

The future SPIRAL-2 facility, currently under construction at GANIL, Caen (France) will produce rare isotope beam (RIB) in the mass range from A=60 to A=140. These nuclei will be produced by the fission of ^{238}U induced by fast neutrons, which are generated by the break-up of deuteron on a carbon converter. A high-power, superconducting driver LINAC, delivering a high-intensity deuteron as well as proton and heavy ions beams, will be built. The characteristics of the LINAG (LINear Accelerator of Ganil) are particularly well suited to the construction of a neutron beam and irradiation facility, which is called Neutrons for Science (NFS). This facility will be a very powerful tool for physics with neutron beams from fundamental research to applications like the transmutation of nuclear waste, design of future fission and fusion reactors, nuclear medicine or the test and development of new detectors.

Time-of-flight facility

Two working modes of the future installation have been considered: a pulsed neutron beam facility for in-flight measurements and an irradiation facility for activation measurements. The facility will be composed of the primary proton/deuteron beam extension in a dedicated cave with a target converter (neutron production target). Behind the converter a thick concrete wall with a collimated channel define the neutron beam. Downstream of the collimator a neutron hall would allow performing experiments at desired distances between 5 and 30 m (see Fig. 1). A possibility of having a second channel at 30 degrees is also envisaged, what would allow performing simultaneously two independent measurements with quite different fluxes

both in energy spectra as well as in flux intensities. The clearing magnet placed between the converter and the collimator allows the deviation of an outgoing beam (in case of thin converter) to the beam dump and clean up of the neutron beam from the secondary charged particles created in the converter.

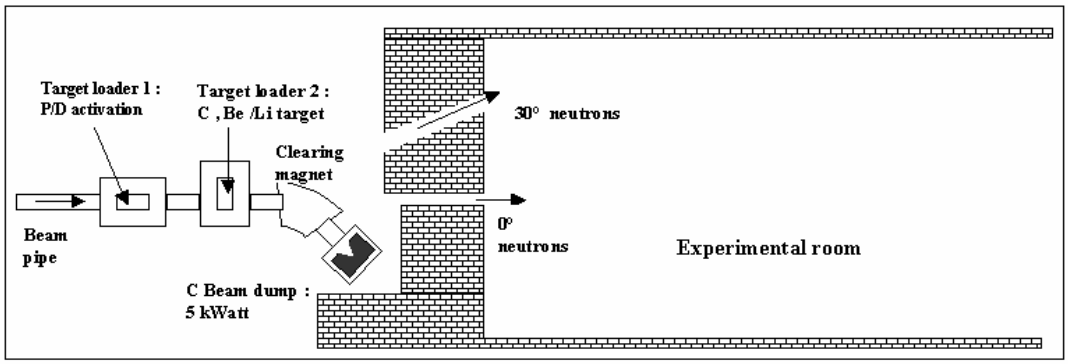

Figure 1. *Schematic view of the NFS facility.*

The LINAG is designed to accelerate deuterons up to 40 MeV and protons up to 33 MeV (40 MeV is by now optional). The frequency is 88 MHz, the burst duration is 200 ps and the nominal intensity is 5 mA. Two types of neutron sources will be available depending on the production reaction. A white spectrum is generated by the interaction of deuteron on a thick converter, while quasi-mono-energetic neutrons are produced by the $^{7}Li(p,n)^{7}Be$ reaction on a thin target (see Fig 2). The white spectrum has an average energy of 14 MeV and the use of beryllium instead of carbon converter increases the flux by a factor of 2. The 33 MeV protons can produce quasi-mono-energetic neutrons up to 31 MeV. The energy resolution and the low energy tail depend on the lithium target thickness. A pulsed beam is required to measure the neutron energy and to separate quasi-mono-energetic neutrons from tail.
Energy measurement by time-of-flight (TOF) technique requires a specific time structure to ensure a high resolution energy measurement and to prevent overlap from previous bursts. The resolution depends on the burst duration, the neutron energy and the flight path (L) while the overlap depends on the reaction threshold, the repetition frequency and L. The initial LINAG frequency (F_0=88 MHz) being too high should be divided by a certain factor N. This can be achieved by using a unique burst selector. The resulting maximum intensity on the converter is 5 mA/N. We can see in Fig. 3 that using a fast detector and L=30 m long flight-path allows to perform energy measurements with high resolution ($\Delta E/E < 1\%$) and even with slow detectors like HPGe ($\Delta t \approx 8$ ns) the energy resolution is not worse than 5%.

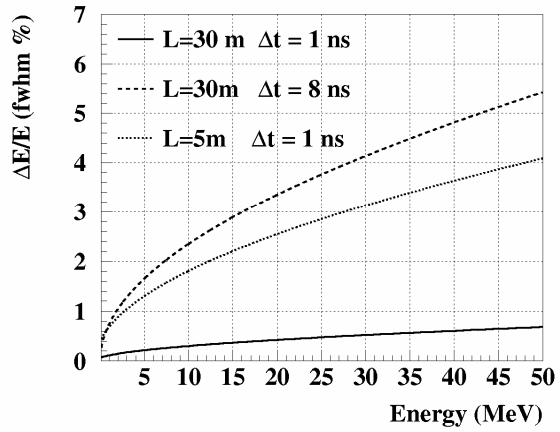

Figure 2. *Energy resolution for the NFS facility.*

The published neutron production data [4, 5], the assumptions on the beam division and flight path allow us to evaluate the available fluxes and compare it to other existing TOF facilities in Europe, namely GELINA at Geel and n_TOF at CERN. For short flight path and/or high energy threshold the flux is limited by the maximum intensity the converter can sustain. We

estimate that an intensity of 50 μA (2 kW) should not cause any particular difficulties. We see on Fig. 3 that NFS is complementary to the two other facilities. In the 1-40 MeV energy range the flux is greater than at n_TOF by a few orders of magnitude. Note that the high flux of NFS is due its high operational frequency.

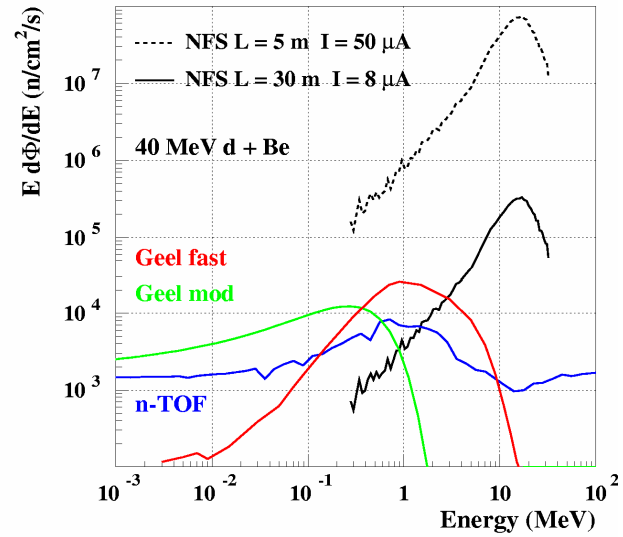

Figure 3. *Neutron flux at NFS and compared to GELINA (Geel) and n_TOF (CERN) facilities.*

Activation Measurements

A station dedicated to measurements by activation technique for neutron and deuteron induced reactions is also envisaged. The sample should be placed as close as possible to the converter in order to maximize available neutron/deuteron flux. The maximum ion beam intensity is estimated to be around 50 □A (see above). For the quasi-monokinetic neutron flux replacing the magnet by a beam stopper made of carbon seems to be a more adequate solution since in this case the sample could be positioned closer to the Li target. In Fig. 4 the neutron flux available close to the converter (5 cm) for a beam intensity of 50 □A is presented. Note that even at this reduced intensity the available neutron fluxes are higher than in the existing neutron facilities in Europe, where irradiations by high energy neutrons are performed.

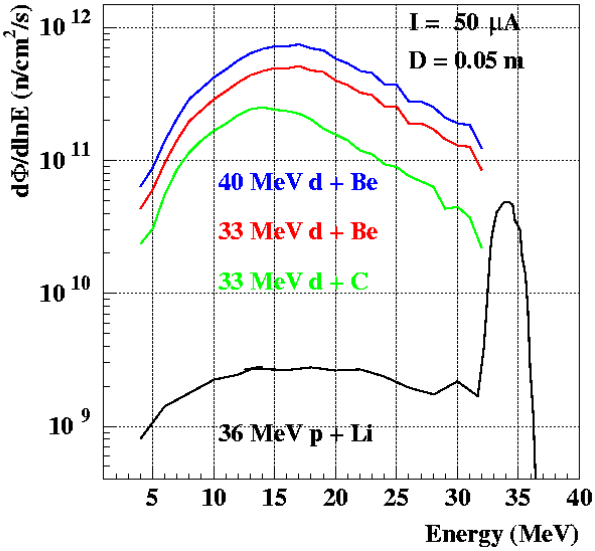

Figure 4. *Expected neutron flux for irradiations and activation measurements.*

The LINAG offers the possibility of delivering proton and deuteron beams with variable energy up to 33 and 40 MeV respectively. Thus a charged particle irradiation station can be created

without major difficulties, although it requires a specific set-up to place and remove the sample, and measure the beam current.

Physics case

The NFS facility could be used for cross-section measurements as well as for fundamental research [6, 7]. The 1-40 MeV energy range is particularly well suited for studies on the transmutation of nuclear waste in ADS or in the new generation fast reactors.
Required fission cross-sections are often unknown above 14 MeV (or known with big uncertainties). A high neutron flux is absolutely needed because for the actinides of interest being radioactive only small samples can be used. The study of the fission process for fundamental research could also be achieved. Coincidence experiments could be performed, where the fragment mass and charge distribution could be measured. The continuous beam allows studying the process at variable excitation energies during the same experiment.
The (n,X) reactions are also of first importance in numerous applications. We saw that measurements using germanium detector are possible with good energy resolution, so (n,n'γ) and (n,xn) can be studied. The impact of such reactions in large systems as nuclear reactors is very important on the energy distribution of the fast neutron spectrum. The NFS energy range allows one to access the opening of new reaction channels like (n,2n), (n,3n), (n,4n)…This is also the region where the pre-equilibrium process becomes important and measurements are needed to constrain strongly the existing models. The production of charged particles is of primary importance too because it leads to the generation of gases and defaults in the structural materials. If double differential measurements have been performed above 40 MeV, presently no data exist below this energy. It seems that the existing experimental apparatus could be used at NFS.
The fusion technology projects like IFMIF and ITER require activation cross-section measurements in fast neutron, proton and deuteron induced reactions [8, 9]. These data are absolutely needed to determine the nuclear safety issues such as γ-dose rate, heat generation, waste transportation and storage. Such measurements could be achieved by activation technique in the dedicated irradiation stations.

Conclusion

The LINAC of the future SPIRAL-2 facility offers the possibility to create a pulsed neutron beam facility including a neutron/deuteron/proton induced activation station. The NFS characteristics in terms of the neutron flux and energy resolution in the 1-40 MeV energy range would make it a very powerful tool for dedicated physics studies and at the same time complementary to other existing laboratories in Europe. A Letter of Intent (LoI) has been recently written and presented to the Scientific Advisory Committee of GANIL. Up to now 12 different laboratories representing 8 countries have joined this initiative.

References

[1] Report (white paper) "LINAG Phase I", June 2002, GANIL, Caen, France.
[2] X. Ledoux, D. Ridikas et al, "Neutrons for Science (NfS) at SPIRAL-2 (Part II : Time-of-flight)", Internal report DAPNIA 05-40, CEA Saclay, France (2005).
[3] D. Ridikas, X. Ledoux et al, "Neutrons for Science (NfS) at SPIRAL-2", Internal report DAPNIA 05-30, CEA Saclay, France (2005).
[4] Meulders et al., Phys. Med. Biol. (1975) vol 20 n°2, p235.
[5] Schumacher et al., NIMA421 (1999) p2843.
[6] International Workshop on Neutrons for Science (NFS) at SPIRAL-2, GANIL, Caen, France; 13-14 December 2004.
[7] A. Plompen, "Nuclear Data Needs for Nuclear Energy (fission) and Possible Contributions of SPIRAL2", 15th Colloque GANIL, Giens, France (2006).
[8] U. Fischer, "Nuclear data needs for fusion technology and possible contribution by SPIRAL2", 15th Colloque GANIL, Giens, France (2006).
[9] P. Bem et al., "Activation cross section benchmarks at NPI cyclotron", Workshop on Activation Data - EAF 2007, 02-04 October 2006, Prague, Czech Republic.

Effective interaction Hamiltonians in direct reactions

A. Likar[1,2], T. Vidmar[1]

1) Jožef Stefan Institute, Jamova 39, SI-1000 Ljubljana, Slovenia
2) University of Ljubljana, Faculty of Mathematics and Physics, Jadranska 19, SI-1000 Ljubljana, Slovenia
andrej.likar@ijs.si

Abstract: In direct reactions the use of optical model wave functions partly accounts for the influence of the continuum spectrum of the system under investigation on the transition amplitudes. Our aim is to show that effective non-Hermitian transition operators should be used in addition. The discussion here is limited to a simple model of the direct radiative capture process, which, however, clearly demonstrates the basic problems encountered when dealing with effective non-Hermitian Hamiltonians. The findings from the treatment of this model are then used to propose a general approach to the determination of the form of effective transition operators for direct reactions.

Introduction

Proper inclusion of the continuum part of the spectrum into reaction models is a long-standing and fascinating subject in nuclear physics. The treatment of damping of well defined states and a subsequent determination of the resonance widths is one of the central problems of quantum mechanics. Its development started with the Weisskopf-Wigner [1] theory of natural line widths, followed by the work of U. Fano [2] in atomic physics and the development of the Feshbach projection formalism [3]. Recently, the interest in nuclei far from stability revived the subject of the proper form and use of effective interactions in the shell model [4]. Perhaps the most interesting new feature of such an approach is the emergence of the nuclear analog of super-radiant states, well known in solid state physics and pioneered by R. Dicke. For a decaying nucleus V. Sokolov and V. Zelevinsky [5] have pointed to the existence of this new type of collective phenomena, common to other open systems.
Radiative capture of fast nucleons has been studied theoretically and experimentally for decades [6,7]. A particularly simple model traditionally used for these processes, known as the direct-semi-direct model, uses optical-model wave functions to describe the initial state of the reaction and single particle states for the final state. It has been shown that the influence of the continuum part of the spectrum on the transition amplitude is not properly accounted for by simply using the optical model wave function as the initial state of the system and the Fermi golden rule [8]. Effective transition operators should be used in addition in order to assure charge conservation, which is inherent in quantum electrodynamics. To illustrate the point, we propose a simple model for which the technical demands are reduced to a minimum, while the physical content remains intact.

The model

We consider here a simple model of a nucleus with only the ground state $|0\rangle$ and an excited state $|1\rangle$. This two level nucleus can be excited by a charged nucleon from a one-dimensional continuum. The Hamiltonian of this system can be written as

$$H = T + H + V, \qquad (1)$$

where T is the kinetic energy operator of the nucleon, H is the two-level Hamiltonian of the nucleus and V stand for the interaction Hamiltonian between the two. The interaction is given by

$$V = g\,\delta(x)\,(a^{+} + a), \qquad (2)$$

where $\delta(x)$ stands for the Dirac delta function and a^{+} and a are the creation and annihilation operators of the nucleus, respectively. The strength of the interaction coupling is denoted by g. The general form of the wave function $|\psi\rangle$ is then given by

$|\psi> = \alpha(x)|0> + \beta\ (x)|1>.$ (3)

From the equation for the stationary states of the system,

$H\ |\psi> = E\ |\psi>,$ (4)

we find the coupled equations for $\alpha(x)$ and $\beta(x)$:

$T\ \alpha(x) + g\ \delta(x)\ \beta(x) = E\ \alpha(x),$ (5a)

$T\ \beta(x) + \varepsilon\ \beta(x) + g\ \delta(x)\ \alpha(x) = E\ \beta(x).$ (5b)

Here, ε stands for the energy of the excited state of the nucleus. This system has the ground state solution with energy E_g, in which the nucleon is bound to the nucleus, and the continuum solution characterized by the energy E. The boundary condition for the solution in the continuum is, as usual, the requirement that the incoming part of the function $\alpha(x)$ represent a plane wave:

$\alpha(x) = \exp(ikx) + S \exp(-ikx),$ for $x < 0.$ (6)

Here, S denotes the scattering amplitude. The function $\alpha(x)$ is an optical model wave function. To show this we eliminate the function $\beta(x)$ from the system of Eqs.(5):

$(T+ \varepsilon - E)\ \beta(x) = -g\ \delta(x)\ \alpha(x),$ (7a)

$$\beta(x) = -(T+ \varepsilon - E)^{-1}\ g\ \delta(x)\ \alpha(x) = -\ g \int dx'\ G_\beta^{(+)}\ (x-x')\ \delta(x')\ \alpha(x')$$

$$= -g\ G_\beta^{(+)}\ (x)\ \alpha(0).$$ (7b)

Here, the Green's function $(T+ \varepsilon - E)^{-1}$ is denoted by $G_\beta^{(+)}(x-x')$. It is given by

$G_\beta^{(+)}(x-x') = 1/(2\ i\ k_\beta)\ \exp(-i\ k_\beta\ (x-x'))$, $x-x' > 0,$

$G_\beta^{(+)}(x-x') = 1/(2\ i\ k_\beta)\ \exp(i\ k_\beta\ (x-x'))$, $x-x' < 0.$ (7c)

We finally arrive at an equation for the function $\alpha(x)$ with an imaginary absorptive delta potential:

$T\ \alpha(x) - i\ (g^2\ /2k_\beta)\ \delta(x)\ \alpha(x) = E\ \alpha(x),\quad k_\beta^{\,2} = E - \varepsilon.$ (7d)

The potential $V_{opt} = -i\ (g^2\ /2k_\beta)\ \delta(x)$ is both imaginary and energy dependent. In our case it is also local, due to the use of the delta function potential.

The solution for the ground state can be obtained along the same lines. The boundary condition for the function $\alpha(x)$ is now that $\alpha(x)$ should be zero for large $|x|$. The function $\alpha(x)$ is in this case the solution of the equation:

$T\ \alpha(x) - (g^2\ /2\kappa_\beta)\ \delta(x)\ \alpha(x) = E_g\ \alpha(x),\quad \kappa_\beta^{\,2} = |E_g| + \varepsilon.$ (8)

The potential in this equation is an ordinary attractive potential with zero range. The energy of the ground state can easily be shown to be

$- E_g = \varepsilon/2\ (-1+(1+g^4/4\varepsilon^2)^{1/2}).$ (9)

Having obtained both the initial and the final state we can now study radiative transitions between them. To keep the discussion simple, we assume that only the nucleon is charged.

Radiative transition

The proper transition matrix element of the electromagnetic transition operator H_γ acting between the initial state $|\psi_E\rangle$ and the final ground state $|\psi_g\rangle$ of the system is simply

$$T_\gamma = \langle \psi_g | H_\gamma | \psi_E \rangle =$$

$$(\alpha^*_g(x)\langle 0| + \beta^*_g(x)\langle 1|) H_\gamma (x) (\alpha_E(x)|0\rangle + \beta_E(x)|1\rangle =$$

$$\int dx\, \alpha^*_g(x) H_\gamma (x) \alpha_E(x) + \int dx\, \beta^*_g(x) H_\gamma (x) \beta_E(x). \qquad (10)$$

The first term is traditionally taken as the full representative of the transition matrix element. This is, however, incorrect. Namely, the omitted second term in the equation above is by no means negligible and actually guarantees that, according to Siegert's theorem, one can replace the current density operator with the charge density operator to arrive to $H_\gamma(x)$ without affecting the matrix element T_γ. Neglecting the second term in (10) therefore violates the continuity equation and therefore charge conservation, which is of paramount importance in quantum electrodynamics.

The result for T_γ can be rewritten using only functions $\alpha_g(x)$ and $\alpha_E(x)$ and taking into account Eq. (5b). We have for $\beta_E(x)$

$$\beta_E(x) = -\int dx'\, G_\beta^{(+)}(x-x')\, g\delta(x')\, \alpha_E(x') = -g\, G_\beta^{(+)}(x)\, \alpha_E(0), \qquad (11)$$

and similarly for $\beta_g(x)$:

$$\beta_g(x) = -\int dx'\, G_\beta(x-x')\, g\delta(x')\, \alpha_g(x') = -g\, G_\beta(x)\, \alpha_g(0), \qquad (12)$$

with the Green's function for the for the bound state given by

$$G_\beta(x-x') = 1/(2\kappa_\beta) \exp(-\kappa_\beta (x-x')),\ x-x' > 0,$$

$$G_\beta(x-x') = 1/(2\kappa_\beta) \exp(\kappa_\beta (x-x')),\ x-x' < 0. \qquad (12b)$$

With these substitutions the transition matrix element acquires the form

$$T_\gamma = \langle \psi_g | H_\gamma | \psi_E \rangle =$$

$$\int dx\, \alpha^*_g(x) H_\gamma (x) \alpha_E(x) + g^2 \int dx\, \alpha_g(0)\, G_\beta(x)\, H_\gamma (x)\, G_\beta^{(+)}(x)\, \alpha_E(0). \qquad (13)$$

For a sufficiently narrow $G_\beta(x)$ one can write Eq.(13) as

$$T_\gamma = \int dx\, \alpha^*_g(x) (H_\gamma (x) + g^2\, G_\beta(x)\, H_\gamma (x)\, G_\beta^{(+)}(x)) \alpha_E(x) =$$

$$= \int dx\, \alpha^*_g(x) H_\gamma (x) (1+F(x))\alpha_E(x). \qquad (14)$$

We can clearly see that the transition operator $H_\gamma(x)$ is now "dressed" by the function 1+F(x), i.e., it has become an effective and, as we shall see immediately, non-Hermitian operator. The function F(x), namely, can be approximately related to the absorptive potential V_{opt} of the optical model which generates the wave function $\alpha_E(x)$:

$$F(x) \approx -i\, (g^2/2k_\beta)\, \delta(x)/\kappa_\beta^2 = V_{opt}/\kappa_\beta^2 \qquad (15)$$

In more realistic circumstances when one uses optical model wave functions, such as in the direct-semi-direct model, there is no clue on how to arrive at the functions $\beta_E(x)$ and $\beta_g(x)$. The correct transition matrix element should therefore be derived from the functions $\alpha_g(x)$ and $\alpha_E(x)$ and the corresponding potentials which generate them. We have recently proposed a

new method on how to properly "dress" the operator H_γ (x). The function F(x) is determined so that the Siegert's theorem holds for the matrix element given in Eq. (14).
The approximation which led us to the function F(x) in Eq. (14) can, namely, be understood as an attempt to recover the continuity equation, which is violated by using optical model wave functions in the transition matrix element without altering the transition operator. By recovering charge conservation in the direct-semi-direct capture model one can substantially improve its predictive power, as shown in numerous analyses of experimental data for a wide range of nuclei, from very light to heavy ones [9]. In the treatment of direct reactions, however, the effective non-Hermitian operators are seldom used [10]. The reason lies in difficulties related to the determination the strength, form factor and energy dependence of such interactions from the first principles [4]. Up to now, even in shell model calculations the effective operators have always been introduced in a phenomenological manner by fitting the experimental data. What we propose is a generalization of the principle we successfully used in the direct-semi-direct model to other direct reactions and it is our intention to re-analyze available experimental data and test this approach on a wide basis.

Conclusion

We have presented a simple model of a direct reaction in order to illustrate the importance of using effective transition operators when dealing with optical model wave functions as initial states of the particle-plus-target-nucleus system. Recovery of continuity equation is the bear minimum of what one should do to properly treat the coupling to complicated states of the evolving system. Importance of non-Hermitian effective operators increases when one treats not just pure direct processes, but also the ones for which the excitation of intermediate states strongly affects the reaction cross section.

References

[1] V. Weisskopf and E. Wigner, Z. Phys. 65, 18 (1930).
[2] U. Fano, Phys. Rev. 124, 1866 (1961).
[3] H. Feshbach, Ann. Phys. (N.Y.) 19, 287 (1962).
[4] A. Volya, V. Zelevinsky, Phys. Rev. C6, 054322 (2003).
[5] V. Sokolov, V. Zelevinsky, Phys. Lett. B202, 10 (1988), Nucl. Phys. A504, 562 (1989).
[6] M. Lipoglavsek, A. Likar, M. Vencelj, T. Vidmar, R. A. Bark, A. E. Gueorguieva, F. S. Komati, J. J. Lawrie, S. M. Maliage, S. M. Mullins, S. H. T. Murray, T. M. Ramashidza, Nucl. Instrum. Meth. in Phys. Res., A 55, 523 (2006).
[7] M. Lipoglavsek, A. Likar, M. Vencelj, T. Vidmar, R. A. Bark, A. E. Gueorguieva, F. S. Komati, J. J. Lawrie, S. M. Maliage, S. M. Mullins, S. H. T. Murray, T. M. Ramashidza, Phys. Rev. C73, 044609 (2006).
[8] A. Likar, T. Vidmar, Nucl. Phys. A591, 458 (1995), A593, 69 (1995).
[9] A. Likar, T. Vidmar, Nucl. Phys. A635, 43 (1998), A619, 57 (1997).
[10] Norman K. Glendenning, Direct nuclear reactions, World Scientific, 2004.

NEPTUNE – the new isomer spectrometer at IRMM

S. Oberstedt[1)], M. Gawrys[2)], G. Lövestam[1)], A. Oberstedt[3)], A. Plompen[1)], V. Semkova[1)]

1) EC-JRC Institute for Reference Materials and Measurements, Retieseweg 111, B-2440 Geel
2) Chalmers University of Technology, S-41296 Göteborg
3) Örebro University, Dept. of Natural Science, S-70182 Örebro
Stephan.oberstedt@ec.europa.eu

Abstract: A new spectrometer has been built at the EC-JRC IRMM to investigate isomer decay in the millisecond range and activation cross-sections of isotopes, where isomeric states exist and are populated. The spectrometer uses high-resolution γ-ray detectors and an ionisation chamber for the measurement of charged particles, e. g. fission fragments. NEPTUNE provides pulsed quasi mono-energetic neutrons at pulse repetition frequencies up to 5 kHz and tuneable neutron pulse widths. For this purpose a beam chopper based on a parallel-plate condenser has been integrated into the accelerator beam-line in order to deflect the charged-particle beam onto a tantalum beam dump.
An instrument status report is given together with results from first experiments dedicated to the search for shape isomers in ^{235,239}U performed with the NEPTUNE isomer spectrometer.

Introduction

The picture of a double-humped barrier in the nuclear energy landscape is able to successfully explain a number of phenomena revealed in nuclear reactions on actinide nuclei, see e. g. Refs. [1-3]. The observed intermediate structure in sub-threshold fission as well as meta-stable fission isomers may be described within this model. Decay mode and half-life of these so-called shape isomers directly probe the fission barrier height and penetrability, which both are important input parameters for the modelling of nuclear reactions.
Since the early 1960s many fission isomers have been discovered in nuclei ranging from ^{234}U to ^{245}Bk [4]. One of the persisting problems associated with fission isomers is the interesting question of competing decay modes as for example decay by γ-ray emission, which has been studied thoroughly in the 1980s and 1990s in ^{240}Pu [5], ^{238}U [6] and ^{236}U [7]. Even more intriguing today is the lack of any shape-isomer half-life data for odd-N uranium and neptunium isotopes. Only for ^{239}U the population of the super-deformed (SD) ground state in a neutron-induced capture experiment was observed [8, 9]. Since for these isotopes fission half-lives are expected to be in the order of several hundreds of μs or even longer, the detection with commonly used pulsed particle beams is very difficult. It is even more difficult in neutron-induced reactions, where the environmental background created from sub-sequent pulses is extremely disadvantageous. Together with the extremely low production cross-section for shape isomers, typically of the order of a few μb, as well as half-life predictions ranging in some cases over five orders of magnitude leaves the measurement of shape-isomer decay data to a challenging venture for the experimentalist.
Here, we report about the construction of a dedicated isomer spectrometer and present results from first experiments, performed during the first two years of operation.

The isomer spectrometer NEPTUNE

In the frame of the exploratory research exercise 2004 of the EC-JRC, the design and construction of the NEPTUNE isomer spectrometer had been started [10]. For this purpose a new pulsing device was integrated into one of the Van de Graaff (VdG) accelerator beam lines. The purpose was to produce pulsed neutron beams with variable duty cycles and pulse lengths for investigations of activation products with half-lives below 1 s and short-lived super-deformed, meta-stable states in fission-fragments and actinide nuclei. NEPTUNE provides pulsed quasi mono-energetic neutron beams with repetition rates between less than 1 Hz and

5 kHz with a pulse width tuneable between 10 μs and the maximum length between two successive neutron pulses.
The principle is based on the deflection of the charged-particle beam before hitting the neutron production target. The deflection system consists of a pair of parallel steering plates to which a high voltage is applied. The high voltage, powered by a high voltage pulse generator [11], is adjusted according to the particle energy to deflect the beam onto a tantalum beam dump at about 3 m distance from the deflection device and is driven by a precision pulse generator with tunable pulse repetition frequency and pulse length. Tantalum is chosen as beam dump material because of its high melting point of higher than 3300 K, a value only exceeded by tungsten and rhenium, and its very low (p, xn) cross-section at proton energies below 4.5 MeV, $\sigma_{pn} \leq 1.1 \times 10^{-4}$ b [12]. Furthermore, the module provides a trigger signal to give full control on the timing between the start of a neutron pulse and a registered detector event.
In Fig. 1 a photograph of the accelerator beam line with the pair of electric steering plates is shown together with spectra, characterising the neutron environment after switching the charged particle beam away from the neutron production target onto the tantalum beam dump. In the fission fragment pulse height spectrum (upper right part of Fig. 1) the achieved late-to-prompt fission for a static deflection of the beam was about $(5 \pm 3)\ 10^{-5}$. During an experiment the dynamic neutron background due to prompt neutrons, moderated to thermal energies typically within some tens of μs, is monitored with a sample of fissile material, here about 2.4 mg of ^{235}U.
The NEPTUNE spectrometer may be equipped with different detector systems according to the requirements of a particular experiment. Ionisation chambers are used to investigate shape-isomeric fission and to monitor residual low-energy neutron background. High-resolution γ-ray detectors behind appropriate radiation shielding are used to investigate de-excitation of (shape-) isomers through γ-ray emission. A NE213 scintillation detector, capable to discriminate between neutrons and γ-rays, is used at 0° relative to the neutron beam-axis to monitor the quality of neutron suppression and the time structure of the pulsed neutron beam.

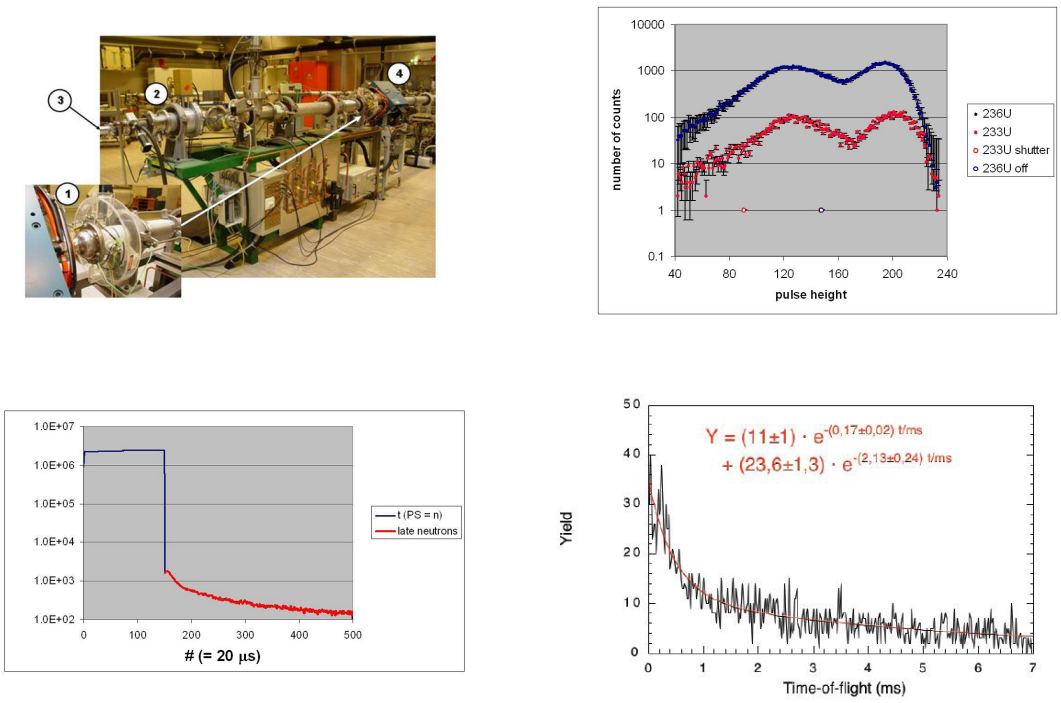

Figure 1. *NEPTUNE isomer spectrometer: (1) pair of electrostatic steering plates, (2) Ta beam dump, (3) neutron source, (4) focussing magnet (upper left). Some results from the investigation of the neutron background for different conditions as explained in the text: fission-fragment pulse height spectrum (upper right), neutron time distribution during a full pulse period (lower left); "late" fission from ^{235}U (n, f) used as low-energy neutron background monitor (lower right).*

First experimental results

The first experiments were dedicated to investigate the decay of the SD ground state, called shape isomer, in odd-A uranium isotopes. In ^{239}U the possible population of the shape isomer has been observed and the corresponding ground state energy, E_{II}, was determined previously [8, 9]. However, no subsequent decay by either fission or γ-decay back to the normal ground state was found, yet. If the half-lives range from several tens of μs to several ms as predicted, this decay should be found with NEPTUNE. Next, the fission decay mode of a possible shape isomer in ^{235}U has been searched for, whose half-life is estimated to lie between 1 and 10 ms [13-15]. Then, the range of applications of the NEPTUNE spectrometer has been extended by a feasibility study of spin-isomer population and subsequent de-excitation by γ-ray emission in ^{206}Pb. This particular delayed reaction process is important to determine correct cross-section data for inelastic neutron scattering reactions, which are relevant for lead-cooled reactors and sub-critical reactor assemblies.

Investigation of the γ-decay of the super-deformed ground state in ^{239}U

The experiment was performed with NEPTUNE settings of 1 and 5 kHz with neutron pulse lengths of 300 μs and 60 μs, respectively. The sample consisted of 157 g depleted uranium, contained in a brass can with thin (0.3 mm) aluminium windows. The sample diameter was 115 mm. The can was centred in an aluminium frame at the same height as the neutron producing target. The distances between the neutron source and the uranium sample or the radiation detector were 45 cm and 50 cm, respectively. For γ-ray measurements a high-purity germanium detector with 45% efficiency relative to NaI was used. The germanium crystal was n-doped to reduce the effect of fast neutron-induced radiation damage.
Between the detector and the neutron source a copper cone was mounted as shielding for the detector crystal against fast neutrons. The optimum position of the shielding was controlled by using a NE213 liquid scintillation detector. Pulse-shape discrimination was employed for an efficient n/γ discrimination. Residual neutrons still reaching the detector were monitored by inspecting the well-known γ-ray line from inelastic scattering of neutrons in ^{72}Ge with E_γ = 693.4 keV during the experiment.
The incident neutron energy, $E_{n,}$ was about 1 MeV. For the time being only data taken with 5 kHz repetition frequency have been analysed. The analysis of the beam-*OFF* spectra was done in three steps,

1) correction for the sample activity
2) search for γ-ray lines, which fulfil the following conditions: they appear only in the *OFF*-spectra, are well below E_{II} and fit into the decay scheme above the normal ground state
3) comparison of line intensities A_1 and A_2 for two different time bins for a possible half-life determination according to $T_{1/2} \sim \ln (A_2/A_1)$.

Details about the experimental set-up and the data analysis may be found in Refs. [10, 16].
In the left part of Fig. 2 a part of the level scheme in ^{239}U is shown. At least two γ-ray lines have been found de-populating the SD ground state and feeding well-known states above the

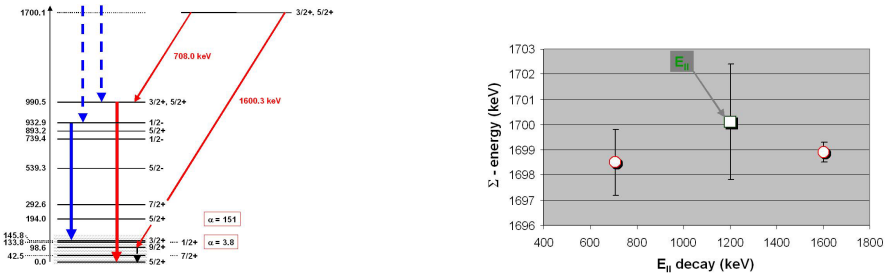

Figure 2. *Part of the level scheme above the normal ground state in ^{239}U for level energies $\varepsilon_i < E_{II}$ = 1700.1 keV. Full lines indicate presumable γ-decay of the shape isomeric ground state in ^{239}U, whereas the dashed lines indicate decay above the normal ground state due to prompt neutron capture (see text). Both decay chains have the same total decay energy and correspond to the previously determined isomeric ground-state energy E_{II} = 1.7 MeV [8-10].*

normal ground state. In one case the sub-sequent γ-decay to the ground state has been observed. The right part of Fig. 2 shows the sum-energy of both decay chains, both nicely corresponding to the observed SD ground state energy E_{II}. The effect of residual low-energy neutron background visible through γ-rays de-populating levels above E_{II} (dashed lines in the level scheme in Fig. 2). From the presently analysed data a half-life according to step 3) could not be determined, yet.

The fission isomer in ^{235}U

For the compound nucleus ^{235}U no fission isomer has been reported to date. Existing fission half-life estimations range between 1 and 10 ms. Therefore, ^{235}U is one of the most favourable candidates to perform a shape-isomer search.
The fission fragments were detected with a twin Frisch-grid ionisation chamber (IC) with common anode. A 1.364 mg sample of ^{234}U was placed in the centre of the cathode closest to the neutron source. The contamination from ^{235}U was smaller than 9×10^{-4}. A sample with 2.38 mg of ^{235}U served as monitor for room-scattered neutrons down to thermal energies and was mounted on the second cathode of the IC. Measurements were performed at E_n = 0.95 and 1.27 MeV at pulse frequencies ν = 100 Hz and 50,100 and 150 Hz, respectively.
Fission fragment pulse-heights were measured and corrected for angular-dependent energy loss. The quality of the corrections may be depicted from the prompt ^{234}U (n, f) fission fragment pulse-height spectrum shown in the right part of Fig. 3. From the time distribution of delayed fission events (see left part of Fig. 3) a tentative decay half-life $T_{1/2}$ = (4.5 $\pm$ 3.0) ms has been determined. Possible background due to thermal fission of the parasitic ^{235}U has been determined analysing spectra from the ^{235}U monitor sample (see lower right part of Fig. 1) and subtracted. Comparing the fission yield obtained during beam-*ON* and beam-*OFF* results in a population probability of the SD ground state in a neutron-induced reaction P_{iso} = (7.5 $\pm$ 6.0) 10^{-6}, which corresponds to a cross-section well below 10 μb.

Spin-isomer population cross-sections in lead isotopes

This experiment has been performed in the context of a measurement series based on the (n, xnγ) technique at the GELINA facility. In the course of this work it became clear, that for two important lead isotopes spin isomer population plays an important role. These isomers cannot be tackled by the technique employed at GELINA.
One relevant isomer is the 11th excited state of ^{206}Pb (E = 2200 keV, $J^{\pi} = 13/2^{+}$, $T_{1/2}$ = 125 μs). This isomer carries an important fraction of the inelastic cross-section and, therefore, is of importance to verify model predictions with experimental data.
The purpose of this experiment was to demonstrate NEPTUNE's ability to clearly identify γ-rays from this decay and to determine its contribution to the cross-section due to the de-population of the isomer state. Experiments were performed with a repetition frequency ν = $(750\mu s)^{-1}$ and a neutron pulse width of 250 μs. The incident neutron energies were E_n = 5.1, 6.2 and 7 MeV. As shown in Fig. 4, the relevant γ-ray line at E_γ = 803 keV has clearly been identified. The calculated decay curve describes well the time spectrum constructed for E_γ = 803 keV (right part of Fig. 4, lower full line) and demonstrates the feasibility to obtain correct data on spin-isomer population with NEPTUNE.

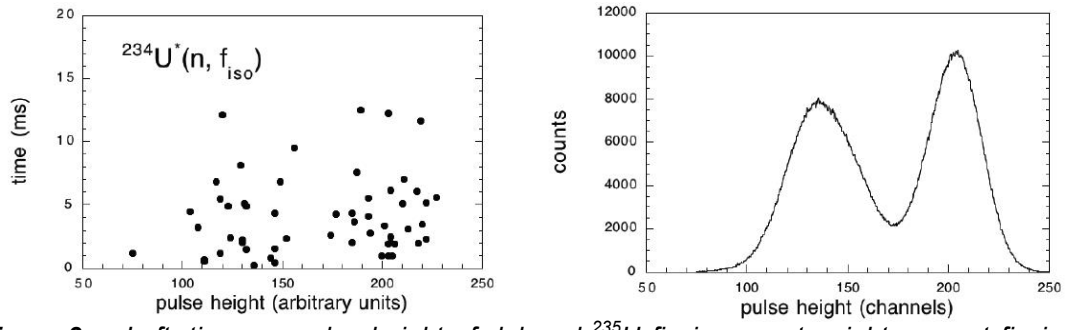

Figure 3. *Left: time vs. pulse height of delayed ^{235}U fission events; right: prompt fission pulse height spectrum from ^{234}U (n, f).*

Summary and outlook

The isomer spectrometer NEPTUNE is operational and first experiments have been performed. They were dedicated to the investigation of super-deformed shape isomers in odd-A uranium isotopes. In the case of ^{239}U, γ-rays possibly de-exciting the shape isomer towards the normal ground state were observed. The determination of a decay time is still pending. For ^{235}U a fission shape-isomer was found. Combining data for two different incident neutron energies and different NEPTUNE settings allowed the determination of a tentative decay half-life $T_{1/2}$ = (4.5 $\pm$ 3.0) ms. The population probability of the super-deformed isomer in a neutron-induced reaction, P_{iso} = (7.5 $\pm$ 6.0) 10^{-6}, corresponds to a cross-section well below 10 μb. This is in agreement with cross-section values obtained in neighbouring isotopes.
The population of the 11th excited spin-isomer state in ^{206}Pb with a half-life $T_{1/2}$ = 125 μs was successfully investigated by a (n, xnγ) reaction at E_n = 5.1, 6.2 and 7.0 MeV, demonstrating the possibilities provided by NEPTUNE. However, for deuteron-induced neutron production some improvements to both beam collimation and beam dump have to be considered, since deuterium deposition in the accelerator beam line gives rise to a measurable neutron background.

Acknowledgements
Two of the authors (A.O. and M.G.) are indebted to the European Commission for funding expenses for performing an experiment at IRMM within the NUDAME programme.

References

[1] V. M. Strutinsky, Nucl. Phys. A81 (1966) 1.
[2] H. Weigmann, Zeit. Phys. 214 (1968) 7.
[3] S. Björnholm, J. E. Lynn, Rev. Mod. Physics, Vol. 52 (1980) 725.
[4] B. Singh, R. Zywina and R. B. Firestone, Nuclear Data Sheets 97 (2002) 241.
[5] D. Pansegrau et al., Phys. Lett. B484 (2000) 1.
[6] J. Kantele et al., Phys. Rev. Lett. 51 (1983) 91 and J. Kantele et al., Phys. Rev. C29 (1984) 1693.
[7] U. Goerlach et al., Phys. Rev. Lett. 48 (1982) 1160.
[8] S. Oberstedt, F. Gunsing, Nucl. Phys. A589 (1995) 435.
[9] S. Oberstedt, F. Gunsing, Nucl. Phys. A636 (1998) 129.
[10] "Exploratory Research at IRMM 2004", Final report, comp. by the IRMM scientific Committee, Internal Report GE/SCIRMM/ER/2005 (2005).
[11] GBS-Elektronik GmbH, http://www.gbs-elektronik.de/
[12] EXFOR experimental data library, JANIS version 2.1 (2004).
[13] H. Weigmann and J. P. Theobald, Nucl. Phys. A187 (1971) 305.
[14] V. Metag (1974) cited in ref. [3].
[15] Zhongzhou R. and Chang Xu, Nucl. Phys. A759 (2005) 64.
[16] S. Oberstedt et al., to be published.

Calculation of fission product yield with selective channel scission model

M. Ohta

Japan Atomic Energy Agency, 2-4 Shirane, Shirakata, Tokai-mura, Naka-gun, Ibaraki, 319-1195, Japan
ohta.masayuki@jaea.go.jp

Abstract: The mass-distributions of fission yield were obtained for the thermal neutron-induced fissions of U-235 and Pu-241 by the selective channel scission model. The results were consistent with the experimental data except for fragment mass-regions of A = 140–150 (and A = 85–95). And the shape elongation factor of nucleus at the saddle point was also obtained. It was shown that the symmetric and asymmetric fissions exist in the fission process by the correlation between the elongation factor and fission modes.

Introduction

More than 60 years have passed since the discovery of the fission phenomenon by Hahn and Strassmann in 1938 [1]. The first theories, which were presented by Meitner and Erisch [2] and Bohr and Wheeler [3] in 1939, explained the break-up into two lighter fragments of roughly equal size. Then, in 1947, Frankel and Metropolis explored the saddle-point shapes of fissioning nuclei and the thresholds (fission barriers) using ENIAC, which is the first large-scale, electronic and digital computer at the University of Pennsylvania [4]. These studies lead to a recent excellent work by Möller *et al*. [5] in 2001 that showed the existence of symmetric and asymmetric fissions with a calculation of five-dimensional potential-energy landscapes. In spite of many years of research, the mechanism of fission is not completely established yet. The present standard model is the multimodal random-neck rupture model, which is also called BGM model, by Brosa *et al*. [6] The BGM model achieved a great success, especially with the explanation of mass and energy distributions of the fission fragments that has been one of the main aspects of fission physics, although the BGM model is phenomenological one. However, the BGM model has disadvantages for a prediction of fission product yields from nuclei whose fission results are unknown. And the fission yield is analyzed with the BGM model by the superposition of Gaussian distributions based on a few fission modes, which are related to symmetric and asymmetric fissions. It is difficult to predict fission products and to get information from the products beyond the Gaussian probability functions on the BGM model.
We have proposed the “selective channel scission (SCS) model [7]” to predict fission product yields of any fissionable nuclei deterministically, including W and Au whose fission product yield are not usually discussed. On the SCS model, all fission channels are considered, instead of a few fission modes. The “channel-dependent” fission potentials or barriers are calculated to obtain the fission product yield from the penetrability of the barriers for an excitation energy. This paper gives the results of fission yields for thermal neutron-induced fissions of U-235 and Pu-241 obtained by SCS model with simple assumptions concerning the channel-dependent fission barrier and discussions about correlations between a shape elongation factor of nucleus obtained in this analysis and the existence of symmetric and asymmetric fissions.

Model Assumptions and Calculations

Figure 1 shows fission process and the potential. The excited nucleus is deformed and induces tandem (dumbbell) oscillation collectively. It starts scission to form two fission fragments (FP1 and FP2). We consider a fission-potential for each fission channel. The potential is assumed as one-humped shape for simplicity. The barrier height E_f for a fission channel, which is called “channel-dependent” fission barrier, is estimated from the difference between the Coulomb potential $E_c^{'}$ between two fission fragments of the channel and the Q-value.

$$E_f = E_c^{'} - Q. \qquad (1)$$

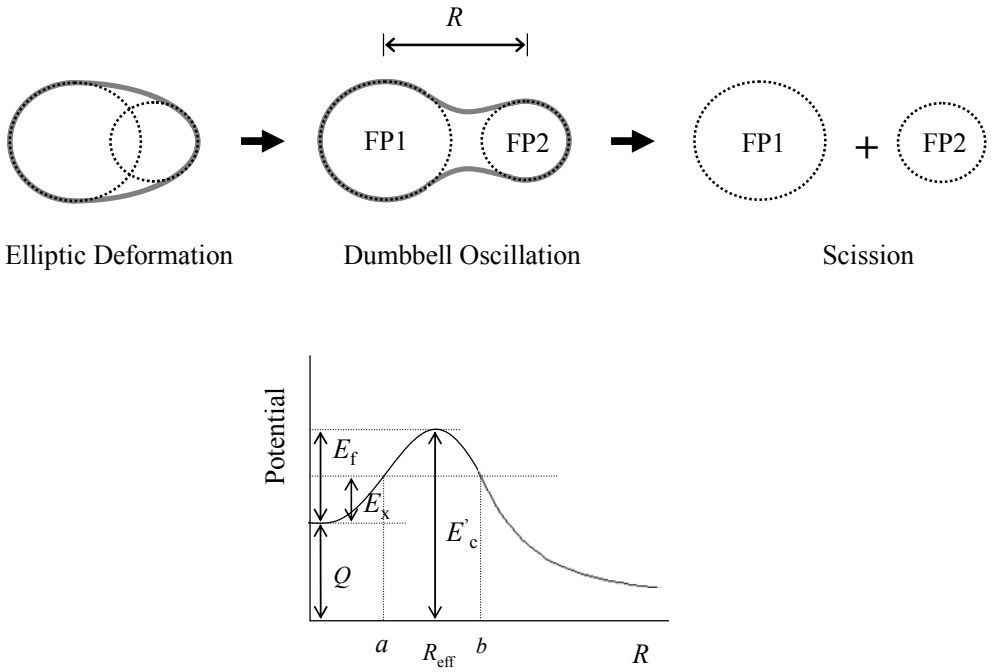

Figure 1. *Fission process and potential*

The "effective scission distance" R_{eff}, which gives the E_c', is defined as the sum of half the length of the major axis of two fragments at the grand state (R_1' and R_2') and the length of the nuclear interaction ($\Delta \approx 2$ fm) in this analysis.

$$R_{\text{eff}} = R_1' + R_2' + \Delta. \tag{2}$$

The R_{eff} approximately corresponds to the interaction distance of the nuclear reaction. The data of KTUY mass formula [8] was used for the deformation of nuclei. Almost same results can be deduced from the data of Möller *et al* [9].

The Coulomb barrier E_c' is given by Eq. (3),

$$E_c' = \frac{1.44\, Z_1 Z_2}{R_{\text{eff}}}, \tag{3}$$

in MeV and fm units, where Z_1 and Z_2 are atomic numbers of the two fragments FP1 and FP2, respectively. The E_c' is nearly equal to the Coulomb barrier of fusion as the reversal process of fission.

The fission probability for the *i*-th channel is given by the tunnel probability P_i of the channel-dependent fission barrier from point *a* to *b* for the excitation energy E_x in Fig. 1. The potential-shape near the saddle point is approximated by an inverted parabola and the curvatures α is assumed as a constant for all channels ($\alpha = 0.6$) for simplicity. Then, the P_i is reduced as

$$P_i \approx \frac{1}{1+\exp\left[0.218\,\alpha\sqrt{\mu}\;\Delta E\right]}, \tag{4}$$

in MeV and fm units, μ is the reduced mass $\mu = A_1 A_2/(A_1+A_2)$, $\Delta E = E_f - E_x$ and A_1 and A_2 are mass numbers of FP1 and FP2, respectively [10]. The mass-distribution of fission yield is obtained by summing up the probabilities for the same mass number of the product.

Also, the shape elongation factor η was calculated to discuss how much the deformation of nucleus deviates from the spherical shape. The η is defined by

$$\eta = \frac{R_{\text{eff}}}{R_1 + R_2}, \tag{5}$$

where R_1 and R_2 are radii of FP1 and FP2, respectively.

The R_1 and R_2 are defined as following equation,

$$R_{1\text{ or }2} = r_0\, A_{1\text{ or }2}^{1/3}, \tag{6}$$

where $r_0 = 1.2$ fm.

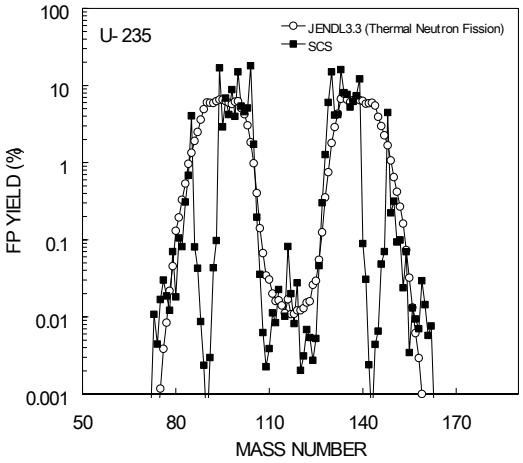

Figure 2-a. *Fission product yield of n+^{235}U*

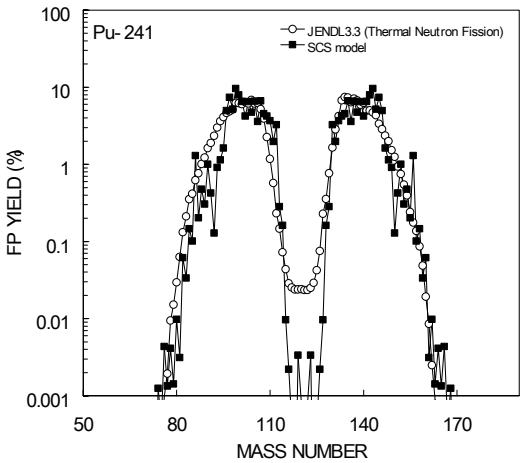

Figure 3-a. *Fission product yield of n+^{241}Pu*

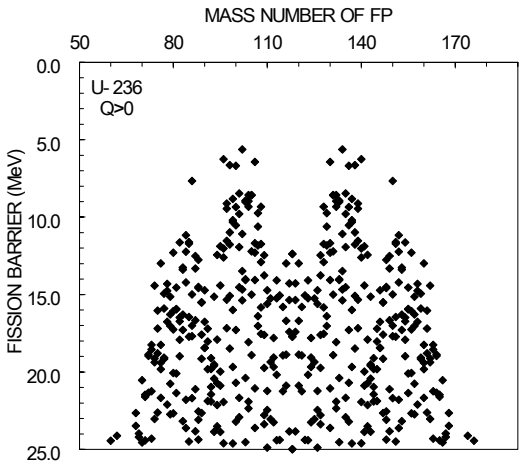

Figure 2-b. *Fission barriers of ^{236}U*

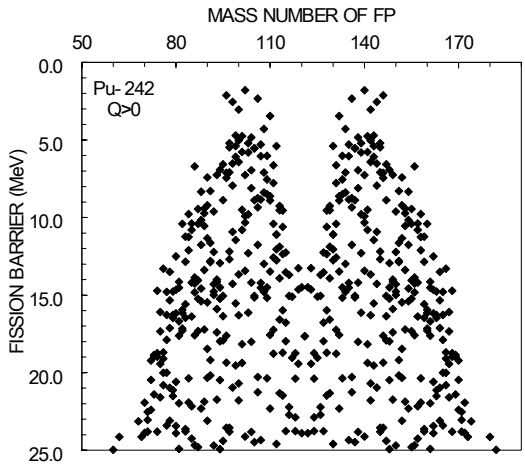

Figure 3-b. *Fission barriers of ^{242}Pu*

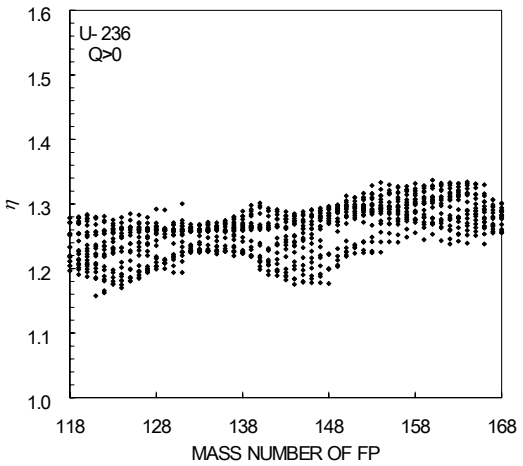

Figure 2-c. *η of ^{236}U*

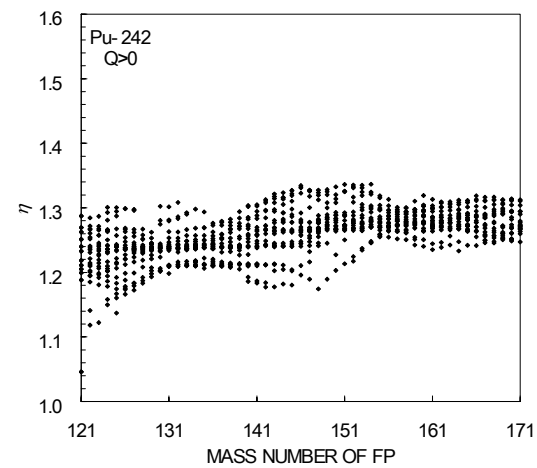

Figure 3-c. *η of ^{242}Pu*

Results and Discussion

Figures 2-a and 3-a are the calculated fission yields for the thermal neutron-induced fissions of ^{235}U and ^{241}Pu shown as squares, respectively. Prompt neutron emission was considered only for the result of ^{235}U. These results were compared with the data of JENDL-3.3 shown as circles [11], which are the data after the prompt neutron emission. The fission yields coincided with the data of JENDL-3.3 [11] except for the dips in the mass region of A = 140–150 (and A = 85–95). The discrepancies of the fission yields may depend on differences between the real distance at the saddle point and the assumption of R_{eff}. The shell effect would be overestimated in the mass region, because the data of the fission fragments after scission were used to calculate the R_{eff} where the nucleus does not break up yet. The channel-dependent fission barriers E_{f} for ^{236}U and ^{242}Pu were shown in Figs. 2-b and 3-b, respectively. And figures 2-c and 3-c shows the shape elongation factors η for ^{236}U and ^{242}Pu, respectively. The upper part of the η increases around A = 130–140 with the mass number of fragments. Zhao *et al*. showed the existence of symmetric and asymmetric fissions by using the shape elongation factor β at the scission configuration [12]. The β is obtained from the experimental total kinetic energy (TKE) data. The β changed the trend at fragment mass of A = 130–135. The present result of η also shows the existence of symmetric and asymmetric fissions in the SCS analysis.

Conclusions

The channel-dependent fission barriers were calculated for the neutron-induced fissions of ^{235}U and ^{241}Pu by the SCS model with simple assumptions about the effective scission distance. And the mass-distributions of fission yield were obtained. These mass-distributions showed good agreements with the data of JENDL-3.3 [11] except for discrepancies at mass regions of A = 140–150 (and A = 85–95). Also, the existence of the symmetric and asymmetric fissions was shown by the shape elongation factor of nucleus.

References

[1] O. Hahn and F. Strassmann: Naturwiss, 27, 11 (1939).
[2 L. Meitner and O.R. Frisch: Nature, 143, 239 (1939) 239.
[3] N. Bohr and J.A. Wheeler: Phys. Rev., 56, 436 (1939).
[4] S. Frankel and N. Metropolis: Phys. Rev., 72, 914 (1947).
[5] P. Möller, D.G. Madland, A.J. Sierk and A. Iwamoto: Nature, 409, 785 (2001).
[6] U. Brosa, S. Grossmann and A. Müller: Phys. Rep., 197, 167 (1990).
[7] A. Takahashi, M. Ohta and T. Mizuno: Jpn. J. Appl. Phys., 40, 7031 (2001).
[8] H. Koura, T. Tachibana, M. Uno and M. Yamada: RIKEN Accel. Prog. Rep., 36, 9 (2003).
[9] P. Möller, J.R. Nix, W.D. Myers, and W.J. Swiatecki: Atomic Data Nucl. Data Tables, 59, 185 (1995).
[10] M. Ohta and S. Nakamura: Jpn. J. Appl. Phys., 45, 6431 (2006).
[11] K. Shibata, T. Kawano, T. Nakagawa, O. Iwamoto, J. Katakura, T. Fukahori, S. Chiba, A. Hasegawa, T. Murata, H. Matsunobu, T. Ohsawa, Y. Nakajima, T. Yoshida, A. Zukeran, M. Kawai, M. Baba, M. Ishikawa, T. Asami, T. Watanabe, Y. Watanabe, M. Igashira, N. Yamamuro, H. Kitazawa, N. Yamano and H. Takano: J. Nucl. Sci. and Technol., 39, 1125 (2002).
[12] Y.L. Zhao, I. Nishinaka, Y. Nagame, M. Tanikawa, K. Tsukada, S. Ichikawa, K. Sueki, Y. Oura, H. Ikezoe, S. Mitsuoka, H. Kudo, T. Ohtsuki and H. Nakahara: Phys. Rev. Lett., 82, 3408 (1999).

Application of INAA to identify lead white pigment in icons from the 15th-18th centuries from South-Eastern Poland

E. Pańczyk[1)], J. Giemza[2)], L. Waliś[1)]

1) Institute of Nuclear Chemistry and Technology, Dorodna 16, 03-195 Warsaw, Poland
2) Castle Museum in Lancut, Zamkowa 1, 37-100 Łańcut, Poland
epanczyk@ichtj.waw.pl

Abstract: The purpose of the work was to analyse lead white from icons of 15th-18th centuries, collected at the Orthodox Art Department at the Castle Museum in Łańcut, using the neutron activation analysis method. These tests allowed to identify concentration of trace elements in collected samples. The achieved results provided a basis for the conclusion that lead white from analysed icons demonstrates specific common characteristic features and differs from lead white from panel paintings from the Małopolska and Silesia regions. Identifying similarities and differences in the applied lead white would allow to create a "map" of its common features and in the future would support the territory identification of the pigment, as well as the age, origin and authenticity of an object under examination.

Lead white identification

The chemical analysis of pigments and the structure of painting layers allow to identify the time of creating the painting and isolate subsequent repaintings. The chemical composition as well as pigment production methods changed with time. However, results of these analyses are not always explicit. Many pigments were used over long periods and thus, any analysis of their chemical composition would not provide sufficient information to precisely identify the date of a painting creation. Consequently, it was concluded that much more information can be obtained from analysing impurities included in pigments.
Lead white is a pigment the most frequently used for determining trace elements. This is due to its features; having been varnished, lead white is resistant to degradation and additionally, it is one of the most frequently used pigments for the last twenty centuries. Also, in the case of icon painting, lead white is the only known white pigment used until the 19th Century [1, 2, 3]. The lead production process changed over time and the analysis of impurities in the pigment can be used to identify approximate date of its production.
There are three potential methods for physical and chemical classification of lead white:

- test of changes in the level of impurities by analysing concentration of elements;
- test of changes in $^{206}Pb/^{204}Pb$ isotope ratio;
- analysis of crystal structure modification.

The crystal structure and the level of main impurities are typical for the production method, while the isotope ratio and trace impurities are related to the origin of the mineral. Consequently, the analysis of trace elements allows to determine the time of the painting creation and its origin. Additionally, it is possible to identify repainting and conservation activities, which is of key importance to historians of art. In 1960s, Houtman and Turkstra [4] carried out tests of trace elements in lead white, using the neutron activation analysis. They tested lead white collected from recognised works by Dutch and Flemish masters, created from 1500 to 1909. Additionally, they analysed the pigment manufactured in the 19th and 20th Century. Their works allowed to identify a very important sequence of some impurities related to the lead production process. They noticed that in mid-seventeenth century, the content of chromium significantly decreased and identified a similar drop in the content of silver, copper and mercury in the half of the 19th century. At the same time, high content of zinc and antimony was identified in the pigment from the 20th century. This sequence of impurities can be used for detecting contemporary forgeries of old masters' paintings. Lux and Braustein in the co-operation with Kuhn [5] used the same analysis procedure to compare lead white isolated from paintings of Dutch and Venetian masters, from the late-Renaissance period. The analysed content of trace elements turned out to be different for both regions and differences referred mainly to the content of antimony, silver, copper and manganese. Based

on to date quantitative analysis of trace elements in lead white collected from paintings from the 15th-19th century, it can be concluded that lead white from regions south to Alps, found inter alia in Venetian paintings, shows higher content of copper and manganese and lower content of silver and antimony than lead white from regions north to Alps, applied in Northern Europe [4, 5, 8]. It is nonetheless interesting to obtain an answer to the question whether the distribution of trace elements in lead white and the ground is distinctive and unique for a particular object or rather repeats the distribution identified in materials used in another important European school, which could have had an impact on the author of a particular painting. To reliably confirm authenticity of a tested object it is necessary to have an access to a large database of tested paintings, the authenticity of which is certain.

Analysis

Neutron activation analysis is one of the methods that are widely used in art work analysis. Due to its high sensitivity and repeatability as well as the possibility to determine the content of a few dozens elements in one sample with a mass on the level of 1 mg, this method remains important within the group of other analytical methods of similar sensitivity. This method has been used at the Institute of Nuclear Chemistry and Technology for testing art works and archaeological objects for many years [6 – 11].
The analysis included selected icons dated from the 15th-18th century from the Orthodox Art Department at the Castle Museum in Łańcut. Eighteen icons were selected for the analysis, from which samples of lead white were collected. Table 1 includes the description of the collected samples.

Table1. *Description of the analysed samples*

Sample number	Catalogue number	Author	Icon	Dating
I	S.12011	n/n	Mandylion Owczary	XV-th century
II	D.990 MŁ	n/n	St. Paraskevi Tyrnowska Korytniki	End of XV-th century
III	S.12296 MŁ	n/n	Pantocrator, Świątkowa Wielka	XV/XVI -th century
IV	MZŁ-SZR-1026	n/n	Archangel Michael and St. George Wola Wielka	XV/XVI – th century
V	MZŁ-SZR-819	n/n	Hodigitria Świątkowa Wielka	about 1550
VI	WS-2193	n/n	Tsar's Gate Krościenko	XVI - th century
VII	MZŁ-SZR-821	n/n	Pantocrator Świątkowa Wielka	about 1550
VIII	MZŁ-SZR-987	n/n	The Christ Baptism Korytniki	XVI-th century
IX	MZŁ-SZR-979	n/n	The Last Judgment Korytniki	XVI-th century
X	MZŁ-SZR-849	n/n	St.Nicolas Łodyna	XVI-th century
XI	S.12191 MŁ	n/n	Archangel Michael Brzeżawa	XVI-th century
XII	MZŁ-SZR-813	n/n	Pantocrator Tyniowice	XVII – th century
XIII	MZŁ-SZR-1551	Jacenty Rybotycki	St. Cosmas and Damian Kotań	1691
X IV	MZŁ-SZR-1570	Jacenty Rybotycki	Pantocrator/ Tsar's Gate Kotań	1689
XV	MZŁ-SZR-1567	Tymotej Rybotycki	Deesis (The Apostles) Kotań	1673
XVI	MZŁ-SZR-908	Ioan malarz Hyrowski	Deakon's Gate Pielgrzymka	1660
XVII	S.12061 MŁ	n/n	St. Paraskevi Piatnica Surochów(?)	XVII-XVIII-th century (?)
XVIII	MZŁ-SZR-2185	n/n	Deesis (The Apostles) Smolnik	

Collecting a sample including pure lead white in the case of paintings such as icons is very difficult due to the lavish gilding. 1-3 samples from each object, with a mass from 0.1 to 1 mg were collected after removing the varnish, from the top lights, in order to ensure that they include pure lead white without other pigment additives. The analysis of lead white samples was carried out using the INAA method without chemical separation, using standards of analysed elements. Additionally, Sc and Au standards were attached to every sample series, to act as the monitor of thermal neutron flux. Samples were irradiated in MARIA reactor in Świerk, in the channel with $8*10^{13}$n/cm^{2}s thermal neutron flux. Samples were irradiated for 24 hours and cooled for 8 hours. Irradiated samples after taking out from the package were washed in HCl 1:1 solution and then in alcohol to remove surface contaminations. Measurements of radioactivity of samples and standards were carried out using HP germanium detector with active volume of 80 cm^3 and energy resolution of 1.95 keV for 1333 keV - ^{60}Co energy. The detector co-operates with S100 Canberra analyser, controlled by IBM/PS-2. The analysis of complex gamma radiation spectra was carried out using micro-SAMPO programme. 40 elements were identified and determined in analysed samples.

Results

Contents of the elements in analysed lead white samples are very different. Various methods of statistical analysis were used to evaluate whether these differences are related to using different input materials or result from errors during the analysis (non-representative sample collected). Additionally, only distributions of the elements that are important in lead white identification were analysed [6, 9]. Out of 40 determined elements, only the elements identified in all tested samples were selected for further analysis. Elements such as cadmium, gal, holmium, lutetium, molybdenum, nickel, rubidium, selenium, terbium, tantalum and zirconium, the content of which in a majority of analysed samples, was below the method detection threshold, were disregarded. Collecting a sample free from other pigments is very important in lead white identification. Sometimes, it is very difficult or even infeasible. All tested icons had been previously subject to conservation and different disinfection methods, but despite these inconveniences only some samples included admixtures of other pigments or elements from disinfecting substances (mainly bromine). Ultimately, 28 elements were selected for multi-parameter statistical analysis aimed at identifying the degree of similarity of analysed icons.
The clustering analysis using STATISTICA (StatSoft) programme [6-11] was carried out to identify the similarity degree of analysed objects. Similarity between analysed samples can be determined based on the distribution of points in multidimensional space. Hierarchical object clustering methods are used most frequently. This allows to obtain a structure arranged in a hierarchy, with increasing distance corresponding to decreasing similarity. The result is presented in form of a dendrogram (clustering tree). The clustering analysis was carried out for standardised variables.

Summary

The clustering analysis for all tested 18 icons was carried out. Results of this analysis are presented in Figure 1, which clearly shows division into groups closely related to chronology of tested icons. Icons from the 15th and 16th centuries are much more alike than icons from the 17th and 18th centuries. Probably, the applied lead white was obtained from different sources that had changed over time. Icons from the workshop of Jacenty and Tymotej Rybotyccy (St. Cosmas and Damian – marked as XIII on the diagram, Pantocrator – marked as XIV and Deesis – marked as XV) are much the same, which indicates that they used lead white from the same source. The analysis results of Polish paintings from the so-called Małopolska and Silesian schools were evaluated to compare the type of lead white used in icon paintings in South- Eastern Poland. Figure 2 presents results of this analysis. The analysed icons constitute a separate group with the distribution of determined trace elements different than in the case of Małopolska and Silesian schools. The aforementioned comparisons indicate that lead white used in analysed icon paintings, constituting a unified, very typical group that had underwent changes with time, came from sources different than lead white used in Małopolska and Silesian paintings. Further qualification will be feasible after obtaining the database from lead white analysis of icons from other centres, such as the Ukraine or Slovakia. As a result, it would allow to compare characteristic features of lead white used in important regions of icon paintings.

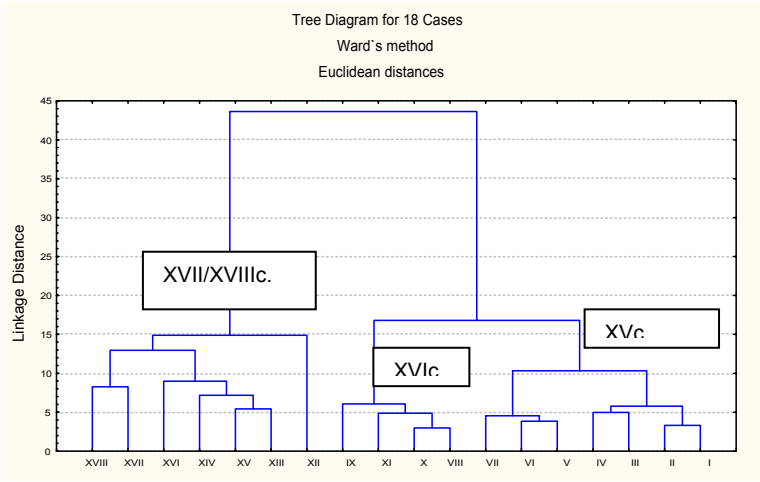

Figure 1. *Cluster analysis of 18 analysed icons described 28 features (features number = determinated elements number); standardised variables*

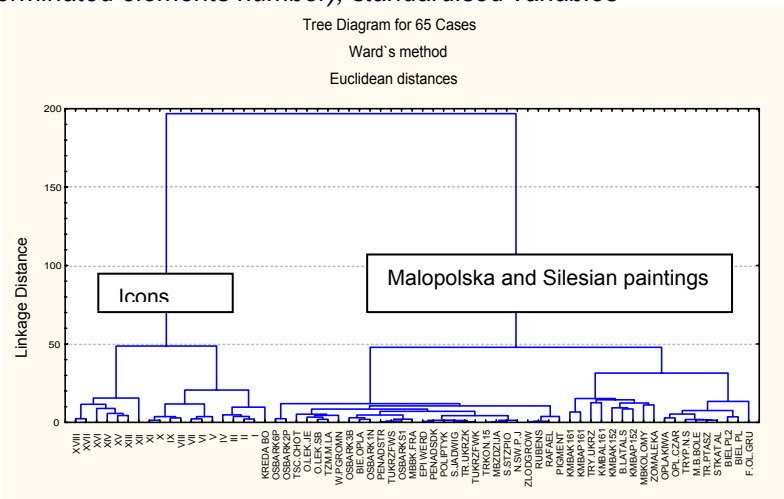

Figure 2. *Cluster analysis icons, Malopolska and Silesian paintings (XV- XVIIc.)*

References

[1] I. Perlman, F. Asaro, H.V. Michel, Nuclear applications in art and archaeology, Annu.Rev.Nucl.Sci.

[2] E.V. Sayre, Activation analysis applications in art and archaeology, Advan.Activ.Anal.2 (1972).

[3] S.J. Fleming, Authenticity in Art., London (1975).

[4] J.P.W. Houtman, J. Turkstra, Neutron activation analysis and its possible application for age determination of paintings, Radiochemical Methods of Analysis, Conf. Proc. Salzburg 1964, vol.1, IAEA, Wien (1965).

[5] F. Lux, L. Braunstein, Aktivierungsanalytische Gemaldeuntersuchungen, Zeitschrift fur Analytische Chemie, 221 (1966).

[6] E. Pańczyk, M. Ligęza, L. Waliś , Nukleonika 37 (1992) 29.

[7] M. Ligęza, E. Pańczyk, L. Waliś, in Proceedings of the 4-th Conf. Non-Destructive Testing of Works of Art, Berlin, 3-8 October (1994) 561.

[8] E. Pańczyk, M. Ligęza, L. Waliś, Czech J.Phys. 49(1999), 401.

[9] E. Pańczyk, M. Ligęza, L. Waliś, Journal of Radioanal. & Nucl. Chemistry, 244, (2000),543.

[10] E. Pańczyk, L. Waliś, J. Flik, J. Olszewska-Świetlik, The examination of lead white in selected paintings of the Silesian School from the second half of the 15-th century by means of INAA, Acta Universitatis Nicolai Copernici, XXXII, 2002, 30-50.

[11] J. Olszewska-Świetlik, E. Pańczyk, The Research on Concentration of Trace Elements of Lead white by Neutron Activation analysis of the Jerusalem Triptych ca.1500, Ars Longa Vita Brevis- Tradycyjne i nowoczesne metody badania dzieł sztuki, pod redakcją Józefa Flika, Uniwersytet Mikołaja Kopernika, Toruń 2003, 51-68.

Production of delayed neutrons with 1 GeV protons interacting with thick Pb and Bi targets

A. Prévost[1)], V. Blideanu[1)], J.-C. David[1)], D. Doré[1)], D. Ridikas[1)], X. Ledoux[2)], A. Barzakh[3)], D. Fedorov[3)], F. Moroz[3)], V. Panteleev[3)], O. Shcherbakov[3)], A.Vorobyev[3)], R. Plukiene[4)], A. Plukis[4)]

1) CEA Saclay, DSM/DAPNIA, 91191 Gif-Sur-Yvette, France
2) CEA/DAM Ile-de-France, DPTA/SPN, 91680 Bruyères-le-Châtel, France
3) Petersburg Nuclear Physics Institute, 188350 Gatchina, Leningrad district, Russia
4) Institute of Physics, Savanoriu pr. 231, 02300, Vilnius, Lithuania
danas.ridikas@cea.fr

Abstract: In this paper we present the first experimental results on measured delayed neutron (DN) yields and time spectra from high energy protons interacting with ^{nat}Pb and ^{209}Bi targets. The 1 GeV protons from the accelerator impinged on targets of different thicknesses producing a huge number of spallation-fission products, which in some cases can be DN precursors. After the beam is switched off, the DNs were detected with optimized He-3 detector. Interesting observations concerning the obtained DN yields will be outlined. Some of our findings should help to constrain the physics models within the simulations codes, in particular, for the production cross sections of light DN precursors as ^{17}N and "usual" fission products as ^{87}Br and ^{88}Br.

Introduction

The next generation spallation neutron sources, neutrino factories or RIB production facilities currently being designed and constructed around the world will increase the average proton beam power on target by a few orders of magnitude. Increased proton beam power requires the use of liquid metal targets such as Hg, Pb, or Pb-Bi. Radioactive nuclides produced in such targets are transported into hot cells, into pumps with radiation sensitive components and electronics, etc. Due to a short transit time a significant amount of the DN precursor activity can be accumulated in the target fluid contributing significantly to the activation and dose rate. This phenomenon was discussed in detail in the earlier work [1] including the estimation of the DN flux and corresponding time spectra in the case of the MegaPie spallation target at PSI (Switzerland). In Ref. [1] we also demonstrated that the final estimates of DNs were very much model-dependent within the MCNPX code [2].
The goal of our experiments was to measure for the first time the DN yields from high energy fission-spallation reactions on the Pb and Bi targets of variable thicknesses. These measurements were realized in December 2005 and April 2006 at PNPI Gatchina (Russia). Here we present some preliminary results from the analysis of the DN yields and time spectra from 1 GeV protons interacting with thick ^{nat}Pb and ^{209}Bi targets. Corresponding calculations with MCNPX [2] and PHITS [3] codes were also performed leading to some recommendations related to the use of these tools.

Experimental set-up and measurement procedure

A schematic view of the experiment is shown in Fig. 1a. 1 GeV protons from accelerator impinged on the ^{nat}Pb and Bi targets of different thicknesses (0.5, 5, 10, 20, 40 and 55 cm). The emitted DNs were detected with the optimized He-3 detector following specific irradiation periods after the beam is switched off. Long (300 s), intermediate (20 s) and short irradiation (350μs – a single pulse) times were used to optimize the extraction of different time parameters of DN groups. The He-3 tube was surrounded by a 5 cm thick polyethylene (CH_2) and coated by 1 mm ^{nat}Cd foils (see Fig 1a.) in order to increase the neutron detection efficiency in terms of neutron moderation and to avoid the background due to the thermal neutrons correspondingly. The detector optimization was performed using Monte Carlo simulations with MCNPX [2]. Finally, the detector was calibrated with a standard ^{252}Cf neutron source, and its efficiency was reproduced within 9 % by MCNPX.

The proton beam intensity was monitored with relative errors around 12 % by activation of ^{27}Al foils and the γ-spectroscopy off line from the ^{7}Be, ^{22}Na and ^{24}Na activity. Fig. 1b explains the experimental procedure used in our work and represents the case of a long irradiation and long decay campaign (300s–300s). Each individual irradiation-decay cycle was recorded on line and summed off line afterwards to accumulate the statistics.

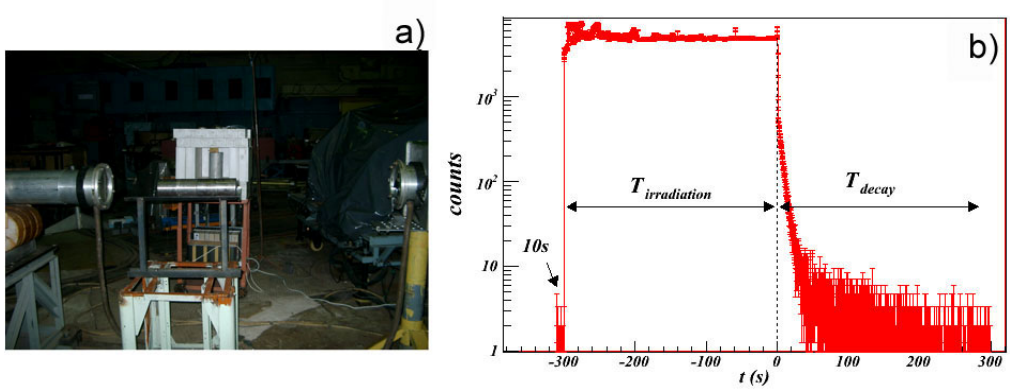

Figure 1. *a) A photo of the experimental setup to measure DNs with the proton beam line (coming from the right), the Bi target (in the centre) and He-3 counter (in the background).*
b) The data accumulation procedure during the DN experiment: $T_{irradiation}$ and T_{decay} regions are shown in detail.

Using the same technique, some measurements without target and with iron or brick targets were also performed to characterize the active background contribution due to the environment of the experimental area. During these test measurements without any target and with non-fissile targets we observed only two dominating decay periods of $T_{1/2}$ ~ 4.2 s and 0.17 s, which we attributed to the reaction products ^{17}N and ^{9}Li with $T_{1/2}$ = 4.173 s and $T_{1/2}$ = 0.178 s respectively. Indeed, these two DN precursors can be produced in the reactions from 1 GeV protons on different targets as Al, Cu, Fe or any other materials present in the experimental hall or accelerator structures [4]. It is important to note that no longer half-lives were observed during these test irradiations [5]. Once the irradiations with ^{nat}Pb or Bi targets started, we noticed that the DN decay curves also extended to the longer half-lives than ~4 s [5], which are characteristic for neutron-rich fission products only.

Results

Analysis of the DN decay curves for all ^{nat}Pb and Bi target thicknesses and with identical irradiation-decay periods of 300 s – 300 s were performed by fitting data with exponential sums using the TMinuit class implemented in the ROOT toolkit [6]. The following expression was used to obtain the $\{a_i, \lambda_i\}$ values:

$$DN(t) = \sum_i a_i \exp(-\lambda_i t)(1 - \exp(-\lambda_i T_{irr})) + C, \qquad \text{(Eq. 1)}$$

with $T^i_{1/2} = \ln 2 / \lambda_i$, C - a constant representing the background, and the irradiation time T_{irr} = 300 s. Note that during the fitting procedure the expression $a_i = \exp(a_i')$ was used giving more stable solution. Systematic errors due to the estimation of the C values have been taken into account.

Contrary to the conventional 6-group approach to reproduce the DN decay curves from neutron induced fission on actinides, only 4 terms of the above expression were sufficient in our case. Half-lives for these 4 terms correspond to the previously identified spallation products, namely ^{9}Li and ^{17}N, in addition to two fission products ^{87}Br and ^{88}Br (with $T_{1/2}$ = 55.6 s and $T_{1/2}$ = 16.29 s respectively).

The accumulated data for the ^{nat}Pb target (55 cm thick),are presented together with the fits of exponential sums in Fig. 2. Similar quality fits using the same 4 terms in the exponential sum, i.e. with four half-lives fixed to those of ^{9}Li, ^{17}N, ^{87}Br and ^{88}Br, were obtained for all target thicknesses and both ^{nat}Pb and ^{209}Bi targets.

Discussion

Some conclusions can already be drawn just looking at the fitted DN decay curves for the ^{nat}Pb and Bi targets for all thicknesses. First, the DN contribution from light mass products as ^{9}Li and ^{17}N is clearly more important than the contribution from fission products. In addition, this "unusual" DN emission dominates the DN decay curve for Pb and Bi targets up to the cooling time of 10 – 20 s (see Fig. 2). For longer decay times, say 50 -100 s, the long lived DN precursors, being "usual" fission products as ^{88}Br and ^{87}Br, remain the only contributors to the DN activity. Note that this finding is very important in the case of high power liquid metal targets, where the liquid metal makes the "round trip" typically in the period of 10-30 s (e.g., the MegaPie loop makes a turn in ~20 s [1]).

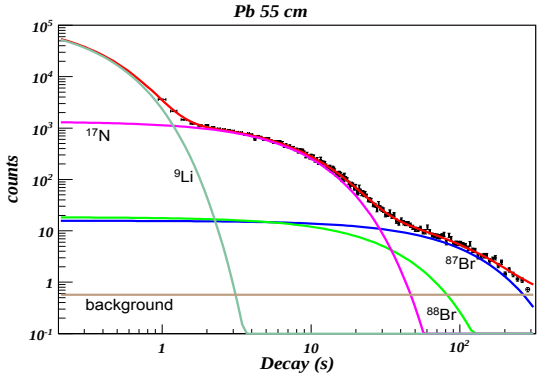

Figure 2. *The accumulated DN decay curves from p(1GeV)+Pb(55cm).*

Thanks to the efficiency determination of the He-3 counter and to the proton beam intensity monitoring, it was possible to extract the DN yields in absolute values. In brief, once the DN(t) is determined during the fitting procedure (see Fig. 2 and Eq. 1), i.e. $DN(t=0)=\sum_i a_i + C$, one can use the following expression to calculate the individual DN yields given by $P_n^i Y^i = a_i/(\varepsilon_{He-3} I_p \Delta t_{ch} N_{cycles})$, where P^i_n is the DN emission probability, Y^i – the DN precursor yield (atoms per incident proton), ε_{He-3} – the total efficiency of the He-3 counter (events per emitted source neutron), I_p – proton beam intensity (protons per second), Δt_{ch} – the channel width (seconds), N_{cycles} – a number of accumulated irradiation-decay cycles.
Fig. 3 represents the DN precursor productions yields Y^i for i = ^{17}N, ^{87}Br and ^{88}Br as a function of target thickness. Both for Pb (a) and Bi (b) targets the DN precursor production is very similar in shapes and in absolute values. In both cases the yields are increasing with thickness and the saturation is observed with targets thicker than 20-30 cm. Indeed, most of the reactions take place in the 1st half of the stopping target. Note that the extraction of ^{9}Li yields was impossible due to its short half life, which is comparable with the channel width being 200 ms.

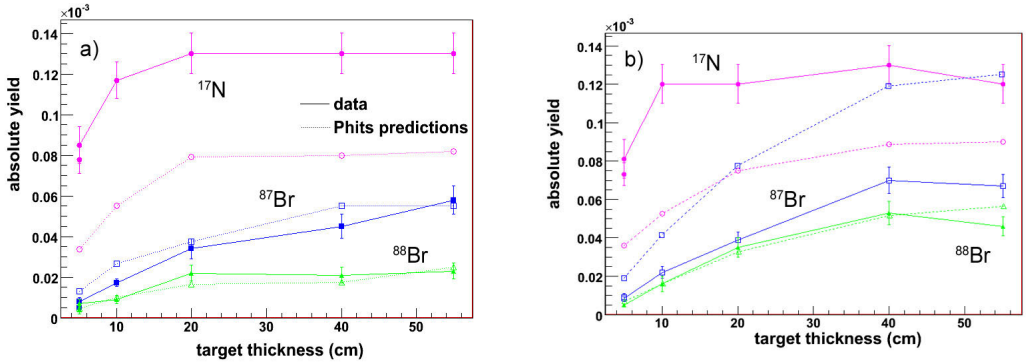

Figure 3. *The DN precursor yields Y^i (atoms per proton) as a function of target thickness for the a) Pb and b) Bi targets. The experimental data are in filled symbols with error bars, while PHITS predictions are in open symbols without error bars. The lines are only to guide the eye.*

Some comparisons of the data have also been made with PHITS code predictions (NMTC+JAM+GEM) [3] and prove that this code can reproduce rather accurately the formation of DN precursors in high energy spallation-fission reactions (see the same Fig. 3) - in most of the cases within a factor 2 or better.
Using the data taken with thin targets (5 mm and 5 cm), production cross sections of ^{87}Br, ^{88}Br and ^{17}N have been extracted and preliminary results are shown in Table 1 for different target combinations. In the same Table 1 comparisons are made with PHITS [3] and MCNPX (INCL4+ABLA) [2] code predictions including some older data or extrapolations from Ref. [4] for ^{17}N and from Ref. [7] for ^{87,88}Br. As it was mentioned earlier in the case of thick targets, PHITS [3] gives reasonable results both for ^{17}N and ^{87,88}Br, while MCNPX can be trusted only for ^{87,88}Br (see Fig. 4). In other words, MCNPX does not calculate the production of light spallation fragments as ^{17}N at all. It is worth mentioning that ^{17}N and ^{88}Br cross sections reported here have been measured for the first time both for the ^{nat}Pb and Bi targets.

Table 1. *Production cross sections of some of the DN precursors from 1 GeV protons interacting with ^{nat}Pb and ^{209}Bi. The experimental data marked by "*" are extrapolated values.*

σ (μb)	This work	Old data	PHITS (NMTC-JAM+GEM)	MCNPX (INCL4+ABLA)
^{17}N from Pb	510	~600* [4]	249 ± 17	-
from Bi	560	~600* [4]	298 ± 14	-
^{87}Br from Pb	40	33±20 [7]	52 ± 8	65±8
from Bi	61	-	95 ± 10	74±9
^{88}Br from Pb	33	~20* [7]	8 ± 3	18±4
from Bi	37	-	25 ±5	14±3

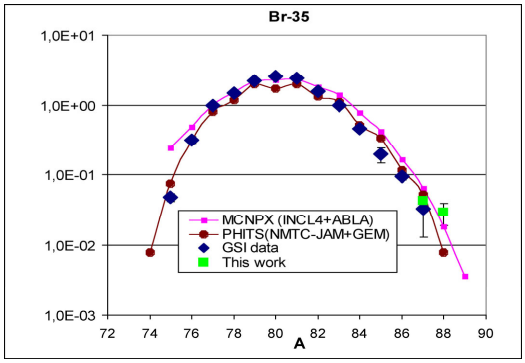

Figure 4. *Comparison of experimental and predicted production cross sections of the Br isotopes from 1 GeV protons interacting with ^{nat}Pb. See the legend for details.*

Conclusions

In this work we present for the 1st time the experimental data on measured DN yields and time spectra from 1 GeV protons interacting with thick ^{nat}Pb and Bi targets. In brief, the emission of DNs in both cases is dominated by light reaction products as ^{9}Li and ^{17}N during the decay time from 0 to ~20-30 s, while after the decay time >30 s the fission fragments as ^{88}Br and ^{87}Br are the major contributors. The DN yield production per incident proton is increasing with the target thickness: the majority of the DNs from 1 GeV protons are produced in the 1st half of the stopping target.
In addition to the DN yields, the production cross sections of the DN precursors have been extracted for ^{17}N, ^{87}Br and ^{88}Br.
The above experimental observations are confirmed with the PHITS transport code, which is able to predict the production of the DN precursors within a factor of 2 or better.
These new data are of great importance for the new generation high power spallation targets based on liquid metal technology as well as for further development of high energy fission-spallation-fragmentation models.

References

[1] D. Ridikas et al., Proc. of the 3rd International Workshop Fission2005, 11-14 May 2005, CEA Cadarache, France; published in AIP Conf. Proc. 798 (2005) 277.
[2] J. Hendricks et al., LA-UR-05-2675, LANL, USA, April 2005.
[3] H. Iwase et al., Nucl. Instr. &. Meth. B 183 (2001) 374.
[4] I. Dostrovsky et al., Phys. Rev. 139 (1965) 1513.
[5] D. Ridikas et al., Proc. of the American Nuclear Society Topical Meeting PHYSOR2006, 10-14 September 2006, Vancouver, British Columbia, Canada.
[6] R. Brun, F. Rademaker, Nucl. Instr. & Meth. A 389 (1997) 81.
[7] T. Engvist et al., Nucl. Phys. A 686 (2001) 481.

Neutron actinides evaluations with the TALYS code

P. Romain[1)], B. Morillon[1)], A.J. Koning[2)]

1) Commissariat à l'Énergie Atomique, DAM/DIF/DPTA, Boîte Postale 12, 91680 Bruyères-le-Châtel, France
2) Nuclear Research and Consultancy Group NRG, P. O. Box 25, NL-1755 ZG Petten, The Netherlands

pascal.romain@cea.fr

Abstract: In order to build neutron actinides evaluations based only on nuclear reaction models, we have to use robust computational nuclear reaction codes. The aim of this paper is to prove that the new developed TALYS code belongs to this class, by comparing it to the GNASH (Los Alamos) code written long time ago and used all around the world.

Introduction

Over the last five years, new neutron evaluations of plutonium and uranium have been performed at Bruyères-le-Châtel in the 1 keV - 30 MeV energy range. Only nuclear reactions models have been used to build these evaluations. Total, shape elastic and direct inelastic cross sections are obtained from a coupled channel model using a dispersive optical potential devoted to actinides. All the other cross sections are calculated owing to the Hauser-Feshbach theory taking into account pre-equilibrium emission processes. We take particular care of the fission channel. For uranium isotopes, a triple humped barrier is required in order to reproduce accurately the variations of the experimental fission cross sections. With increasing neutron incident energy, a lot of residual nuclei produced by nucleon emission lead also to fission. All available experimental data assigned to the various fission mechanisms of the same nucleus are used to define its fission barrier parameters.
In a first time all these calculations were done with a modified version of the Los Alamos nuclear reaction code GNASH [1, 2], and now redone with the TALYS code [3]. TALYS is a nuclear reaction program created at NRG Petten, the Netherlands and CEA Bruyères-le-Châtel, France. Our aim is to show that TALYS represents a robust computational approach that covers the whole path from fundamental nuclear reaction models to the creation of complete data libraries for nuclear applications. On the basis of a large suite of implemented nuclear reaction models, this code is able to produce a complete set of cross sections, yields, energy spectra and angular distributions.

The TALYS code

TALYS [3] is a computer code system for the prediction and analysis of nuclear reactions. TALYS simulates reactions that involve neutrons, gamma-rays, protons, deuterons, tritons, helions and alpha-particles, in the 1 keV - 200 MeV energy range and for target nuclides of mass 12 and heavier. This is achieved by implementing a suite of nuclear reaction models into a single code system. It enables to evaluate nuclear reactions from the unresolved resonance region up to intermediate energies. The calculations described in this paper are based on a theoretical analysis that uses the optical model, compound nucleus statistical theory, direct reactions and pre-equilibrium processes, in combination with databases and models for nuclear structure.

Neutron optical model

Our model calculations are based on the recently constructed optical model potentials (OMP) [4, 5]. These potentials give the optimal description of the basic scattering observables (total, shape elastic cross sections, elastic differential cross section, …) over a large part of the periodic table. However, actinides nuclei are of rotational nature (deformed nuclei in their ground state), so that the spherical OMP is not appropriate, and has to be replaced by a coupled-channels one in order to describe inelastic scattering to the first few levels of the rotational band built on the ground state. However, the level scheme consists not only of this ground state rotational band, but also of the lowest octupolar vibrational band, because for

many actinides these states are also easily excited (direct interaction). Indeed, this kind of coupling was introduced for the first time by Maslov et al. [6], in order to reproduce all the existing structures (signature of direct interaction mechanism) in the experimental neutron emission spectra of ^{238}U. Furthermore, a dispersive approach (based on causality principle) seems more suitable as proved previously [7], including also a local energy approximation as in [5, 7].

Comparisons between GNASH and TALYS

In this paragraph some comparisons between the GNASH code [1] and the TALYS code [3] will be presented. In fact in these calculations we used a modified version of the GNASH code [1,2]. More precisely it incorporates the calculation of the widths fluctuation factors [8] and can also consider triple humped fission barriers nuclei [2]. Therefore, it includes of course the treatment of the Class II (resp. III) states in the fission process [2] in order to reproduce the resonant phenomena.
In the past, with this modified version of the GNASH code, we performed a neutron-induced cross section evaluation of ^{238}U from 1 keV up to 200 MeV. In this evaluation ^{239}U (first chance fission), ^{238}U (second chance fission), ^{237}U (third chance fission), were considered as triple humped fission barrier nuclei. So, we attempted to run these calculations again, using the TALYS code, with the same sets of parameters, in order to show that the calculations done with GNASH can be reproduced using TALYS. This means that the same barrier parameters (and triple humped fission barriers), the same levels density parameters, the same optical model parameters, and so on, were kept.

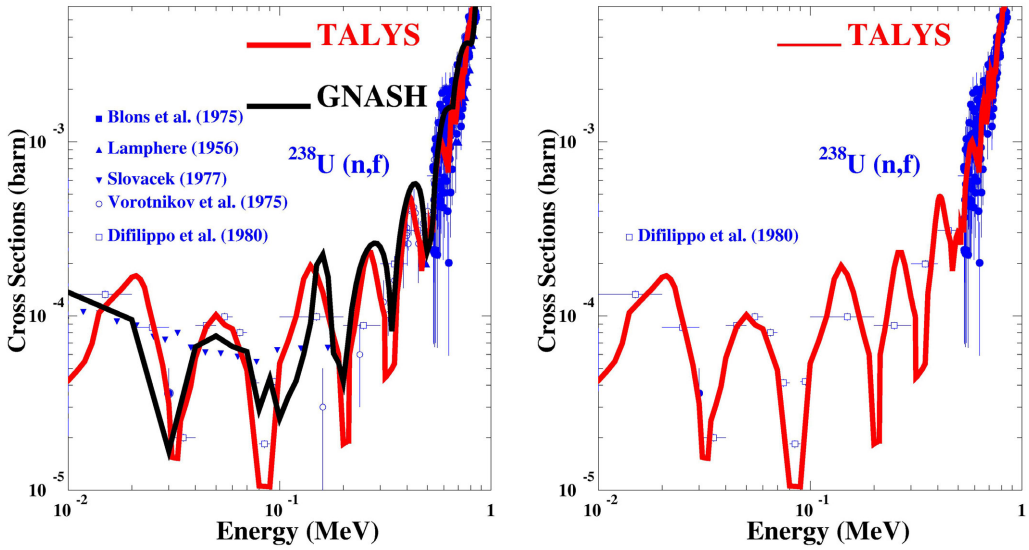

Figure 1. *^{238}U neutron-induced fission cross section between 10 keV and 1 MeV incident energy. Comparison between GNASH and TALYS code calculations. The figure on the right shows the accuracy of the Talys code to reproduce the Difilippo et al. experimental data.*

As easily shown on Figures 1 and 2, TALYS is able to reproduce the neutron induced fission cross section of ^{238}U, with the same accuracy as GNASH. If we look more precisely at Figure 1 (right side), it can even be said, that the TALYS code reproduces the Diffilipo et al. data more accurately. The same conclusion may be done with respect to the data of Blons et al., if we look at Figure 2 (on the left) corresponding to zoom on neutron incident energy range of Figure 1. Note here, that due to all the fine structures in the fission cross section, Blons [9] was the first assuming 239U a triple humped fission barrier nucleus.
As usual, in this kind of calculations all the opened channels are treated simultaneously. So we are able to compare Figure 2 (on the right) what these two codes give for the neutron capture cross section of 238U.

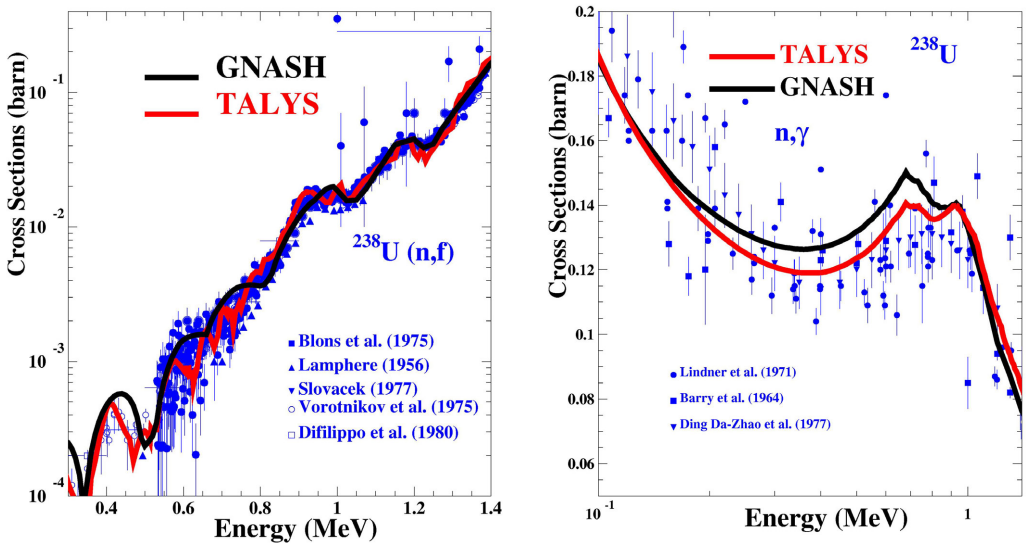

Figure 2. *^{238}U neutron-induced fission cross section between 0.35 and 1.40 MeV incident energy (on the side) and ^{238}U neutron capture cross section between 0.10 and 2.00 MeV incident energy. Comparison between GNASH and TALYS code calculations.*

It may be also interesting to view how predictive is TALYS compared to GNASH, for photo-nuclear reactions studies. As shown on Figure 3 (fission on the left and neutron emission on the right), TALYS seems again in better agreement with the experimental data.

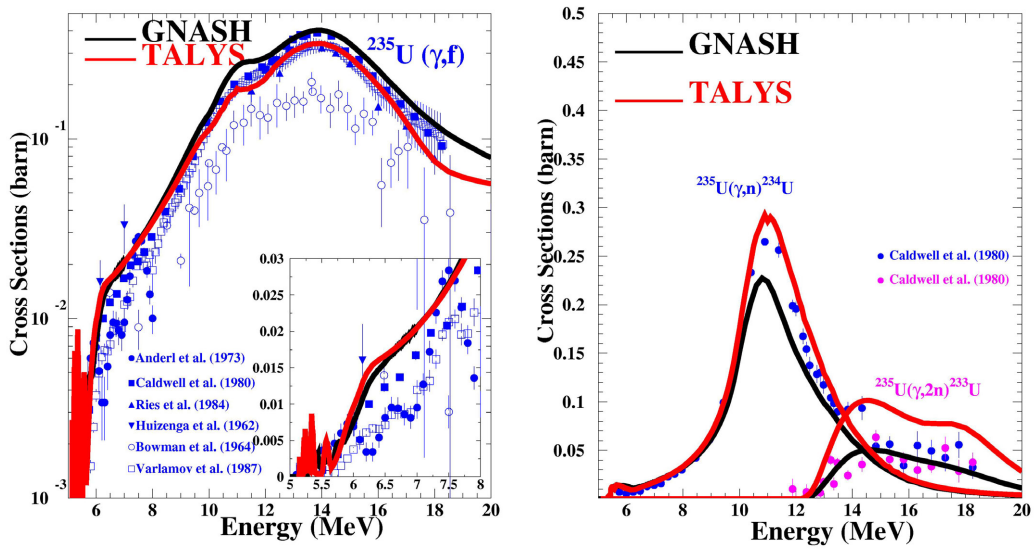

Figure 3. *^{235}U photon-induced fission cross section between 5.0 and 20.0 MeV incident energy (on the left), and ^{235}U photon-induced reaction. (γ,n) and (γ,2n) cross sections between 5.0 and 20.0 MeV incident energy (on the right). Comparison between GNASH and TALYS code calculations.*

At last, neutron induced fission cross section was calculated for the ^{230}Th with the TALYS code. This study is another crucial test of TALYS (triple humped fission barrier model), because the ^{231}Th compound nucleus formed here is commonly considered a triple humped fission nucleus. On Figure 4 we can easily be convinced that TALYS is predictive !

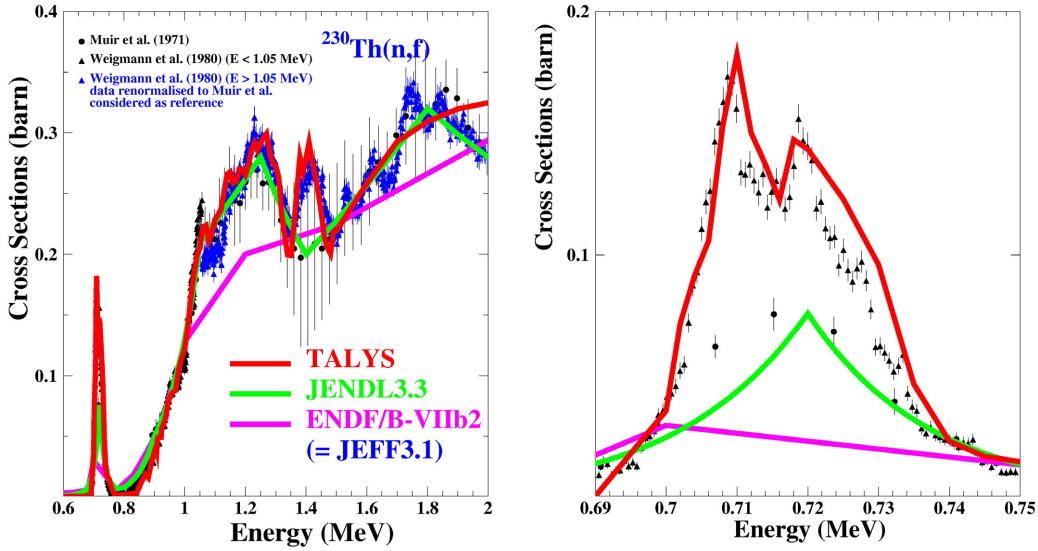

Figure 4. *Evaluated neutron induced fission cross section for the system n + ^{230}Th, with the TALYS code (red curve) compared to JENDL3.3 (green) and ENDF/B-VII (magenta) and experiments black and blue points on the left, the right side corresponds to a zoom on the peak located between 690 and 750 keV neutron incident energy.*

Conclusion

Among all these comparisons, TALYS has been demonstrated to be a robust and predictive computational nuclear reaction code. This means also that we are now able to provide consistent evaluations for a large series of target isotopes with the TALYS code.

References

[1] P.G. Young, E.D. Arthur, M.B. Chadwick, 1996. “Comprehensive nuclear model calculations : Introduction to the theory and use of the GNASH code”, Workshop on Nuclear reaction data and nuclear reactors, April 15 - May 17 1996, Trieste, Italy.
[2] M.J. López Jiménez, B. Morillon and P. Romain, Ann. Nuc. Ener.. 32, 195 (2005).
[3] A.J. Koning, S. Hilaire and M.C. Duijvestijn, “TALYS: Comprehensive nuclear reaction modelling”, Proceedings of the International Conference on Nuclear Data for Science and Technology - ND2004, AIP vol. 769, eds. R.C. Haight, M.B. Chadwick, T. Kawano, and P. Talou, Sep. 26 - Oct. 1, 2004, Santa Fe, USA, p. 1154 (2005).
[4] A.J. Koning and J.P. Delaroche, Nucl. Phys. A713, 231 (2003).
[5] B. Morillon and P. Romain, Phys. Rev. C 70, 014601 (2004).
[6] V. Maslov, “Neutron Scattering on 238U and 232Th”, Proceedings of the international Conference on Nuclear Data for Science and Technology - ND2001}, oct. 7-12, 2001 Tsukuba, Ibaraki, Japan, p.148 (2001).
[7] P. Romain and J.-P. Delaroche, “A dispersive coupledchannels analysis of nucleon scattering from 181Ta and 182,184,186W up to 200 MeV” Proceedings of the NEA Specialists' Meeting on the Nucleon-Nucleus Optical Model up to 200 MeV, Bruyères-le-Châtel (1996) (OECD, Paris, 1997), (http//db.nea.fr/html/science/om200/), p.167.
[8] S. Hilaire, Ch. Lagrange, and A.J. Koning, Ann. Phys. 306, 209 (2003).
[9] J. Blons, PhD. Thesis, Orsay, France, p.162 (1982).

Neutron-induced activation cross sections of different isotopes of Zr, W and Ta from the threshold to 20 MeV

V. Semkova[1,2], R. Jaime Tornin[1], A. Moens[1], A.J.M. Plompen[1]

1) European Commission, Joint Research Centre, Institute for Reference Materials and Measurements, Retieseweg 111, B-2440 Geel, Belgium
2) Institute for Nuclear Research and Nuclear Energy, 1784 Sofia, Bulgaria
arjan.plompen@ec.europa.eu

Abstract: New measured results were obtained for the $^{50}Cr(n,x)^{48}V$ $^{58}Ni(n,p\alpha)^{54}Mn$, $^{63}Cu(n,p\alpha)^{59}Fe$, $^{181}Ta(n,2n)^{180g}Ta$, $^{181}Ta(n,p)^{181}Hf$, $^{181}Ta(n,x)^{180}Hf$, $^{181}Ta(n,\alpha)^{178m}Lu$, $^{181}Ta(n,\alpha)^{178g}Lu$, $^{184}W(n,\alpha)^{181}Hf$, $^{186}W(n,\alpha)^{183}Hf$, $^{184}W(n,p)^{184}Ta$, and $^{90}Zr(n,x)^{89m}Y$ reaction cross sections. Measurements were carried out at the 7 MV Van de Graaff accelerator at IRMM, Geel. Use was made of the activation technique in combination with high-resolution γ-ray spectrometry. A pneumatic transport system was used for the reaction $^{90}Zr(n,x)^{89m}Y$ on account of the short half life of ^{89m}Y. The present results are compared with other measurements, evaluated data and model calculations.

Introduction

Neutron-induced cross section data for Zr, Ta and W are of importance both for nuclear technologies research and development and for basic studies. The neutron-induced reaction cross sections on W isotopes and Ta has been experimentally studied around 14 MeV however due to the high threshold for most of the reactions measurements at higher incident neutron energies are needed to guide evaluations and model calculations. Precise experimental cross section data for fast neutron-induced reactions are of considerable interest for testing nuclear model calculations. Several reaction channels are energetically allowed in the investigated energy range and different reaction mechanisms play roll. A precise and complete experimental data base for a given mass region allows systematic development of nuclear model parameterization.

Experimental procedure

Measured cross sections were determined by the activation technique in combination with high-resolution γ-spectrometry. A detailed description of the measurement procedure has been given earlier[1]. The emphasis here will be on the specifics for the present study.

Samples and irradiation procedure

High purity metallic chromium, nickel, copper, zirconium, tantalum and tungsten samples with natural abundances supplied by Goodfellow Metals, Cambridge, UK were employed in these measurements. Except for $^{90}Zr(n,x)^{89m}Y$, all reactions are free from interference with reactions on other isotopes of the element leading to the same radioactive product. Information about the sample masses and dimensions is given in Table 1.
The irradiations were carried out at the 7 MV Van de Graaff accelerator at IRMM, Geel. Quasi mono-energetic neutrons with energies between 14.8 and 20.5 MeV were produced via the $^{3}H(d,n)^{4}He$ reaction (Q = 17.59 MeV) employing a solid-state Ti/T target (2 mg/cm^2 thick) on a silver backing (0.4mm thick) at incident deuteron energies of 1, 2, 3 and 4 MeV. The samples, each sandwiched between monitor foils, were placed at angles between 0° and 75° relative to the incident deuteron beam and at a distance between 4 and 7 cm from the centre of the target depending on the size of the sample.
A long-counter operated in multichannel-scaling acquisition mode was used to record the time profile of the neutron flux during the irradiation in order to correct for fluctuation of the flux.

Neutron energy and flux determination

The neutron energy and yield distributions as a function of deuteron energy and emission angle were determine by the program code EnergySet that is based on the cross sections of DROSG-2000 of IAEA, version 2.1 and the stopping powers of Ziegler.

The neutron fluence rate was determined by the $^{27}Al(n,\alpha)^{24}Na$ ENDF/B-VI.6 standard cross section.
To account for the contribution of the low energy neutrons the neutron flux density distributions were determined by the spectral index method that involves the $^{115}In(n,n')^{115m}In$, $^{58}Ni(n,p)^{58}Co$, $^{27}Al(n,p)^{27}Mg$, $^{27}Al(n,\alpha)^{24}Na$, $^{56}Fe(n,p)^{56}Mn$, and $^{93}Nb(n,2n)^{92m}Nb$ dosimetry reactions with distinct energy thresholds combined with time-of-flight spectrum measurements.

Table 1. *Decay constants of the reaction products, samples weight and dimensions.*

Reaction	*Decay constant NuDat 2.1*			*Size (mm)*	*Nominal weight (mg)*
	$T_{1/2}$	E_γ (keV)	I_γ (%)		
$^{50}Cr(n,x)^{48}V$	15.9735 d	983.35	100	Ø 30 x 5	25500
$^{58}Ni(n,p\alpha)^{54}Mn$	312.05(4) d	834.848(3)	99.976	Ø 14 x 5	5000
$^{63}Cu(n,p\alpha)^{59}Fe$	44.495(9) d	1099.245(3)	56.5(18)	Ø 20 x 5	14000
		1291.590(6)	43.2(14)		
$^{181}Ta(n,2n)^{180g}Ta$	8.154(6) h	93.4(2)	4.51	Ø 13 x 0.1	222
$^{181}Ta(n,p)^{181}Hf$	42.39(6) d	482.18(9)	80.5(4)		
$^{181}Ta(n,x)^{180}Hf$	5.47(4) h	332.275(11)	94.1(12)		
$^{181}Ta(n,\alpha)^{178m}Lu$	23.1 (2) m	426.36(5)	97.0(18)	Ø 15 x 1	2900
$^{181}Ta(n,\alpha)^{178g}Lu$	28.4(2) m	1340.8 (2)	3.42(16)		
$^{184}W(n,\alpha)^{181}Hf$	42.39(6) d	482.18(9)	80.5(4)	Ø 13 x 0.25	640
$^{186}W(n,\alpha)^{183}Hf$	8.7(1) h	252.85(4)	43(3)		
$^{184}W(n,p)^{184}Ta$	1.067(17) h	783.753(21)	66(9)		
$^{186}W(n,x)^{185}Ta$	49.4(15) m	177.59(10)	25.7(10)		
$^{90}Zr(n,x)^{89m}Y$	15.663(5) s	908.960(25)	99.16(3)	Ø 13 x 0.125	115
$^{90}Zr(n,2n)^{89}Zr$	78.41(12) h	909.15(15)	99.04(3)		

Measurements of radioactivity
The radioactivity of the samples was measured by γ-ray spectrometry. A HPGe detector with 100 % relative efficiency was used. The data acquisition was controlled by S100 Software supplied by Canbera and the γ-ray spectra were analysed by Genie-2000 Spectrometry Software. Standard point sources were used for detector efficiency calibration. A fitting of experimental values with empirical functions provides accuracy of 2.5 to 5% for conventionally used sample geometry. However in order to enhance counting statistics samples with more mass and respectively larger dimensions were needed. To achieve higher geometry flexibility and better accuracy for extended samples. Monte Carlo simulations of the full-energy peak and total efficiencies of the detector in the energy range 60-1500 keV were performed with the MCNP code (Briesmeister, 1997). The absolute detector efficiency was measured by standard point sources at various source-to-detector positions. The geometry parameters of the detector model have been optimized until the agreement within the uncertainty limits between calculated and measured values was reached. Photo-peak and total efficiency for standard size W samples were determine by MCNP calculations as well, to account for the high γ-ray attenuation coefficient of Tungsten.
A correction for coincidence summing effects was applied for the radionuclides with complex decay scheme.

Data analysis
The cross sections were determined by the well known activation formula. The measured γ-ray count rates were corrected for γ-ray abundance, γ-ray self-absorption, efficiency of the detector, coincidence summing effects, irradiation and measurement geometry, neutron flux fluctuation during the irradiations, and secondary neutrons.
For the $^{90}Zr(n,x)^{89m}Y$ reaction cross section measurement a pneumatic transport system was used due to the short half-life of ^{89m}Y. The irradiation time was set to approximately five half-lives of ^{89m}Y and the measurement time to approximately three half-lives, so the contribution of the activity induced in the i^{-th} irradiation cycle to the measured spectrum in the $i+1^{-st}$ cycle is negligible. However ^{89g}Zr from $^{90}Zr(n,2n)^{89}Zr$ reaction decays by EC to ^{89m}Y. Although the half-lives are considerably different and the irradiation time is very short in comparison with the

^{89g}Zr half-life, the ^{90}Zr(n,2n)^{89}Zr reaction cross section can not be neglected especially if several cycles of irradiations and spectrum measurements are repeated and the sum of the measured spectra is taken for the cross section analysis. However the ^{89}Zr activity induced during the irradiations can be measured separately after complete decay of the ^{98m}Y and subtracted from the total activity. The contribution of the ^{89g}Zr to the total 909 keV γ-activity was estimated to be 10 to 15 % for about 15 cycles.

Results and discussion

The experimental results of this work are shown graphically in Figs. 1 and 2.

The ^{50}Cr(n,x)^{48}V, ^{58}Ni(n,pα)^{54}Mn, ^{63}Cu(n,pα)^{59}Fe, and ^{90}Zr(n,x)^{89m}Y reaction cross sections (Fig. 1). Due to the generally low cross sections for (n,t) or multiple charge particle emission cross sections in the investigated energy range care was taken for possible interference with reactions that occur on impurities in the sample provided by the supplier. The threshold of the reactions which contribute to the ^{48}V production from ^{50}Cr are 12.9 MeV for (n,t), 19.3 MeV for (n,nd) and 21.6 MeV for (n,2np) reactions respectively. So we can consider ^{50}Cr(n,x)^{48}V as a pure (n,t) reaction in the investigated energy range. Our results for ^{50}Cr(n,x)^{48}V are in a very good agreement with EAF-2005 and TALYS calculations. The new results for ^{58}Ni(n,pα)^{54}Mn agree with the data of Fessler et al. and the EAF-2005 evaluation.

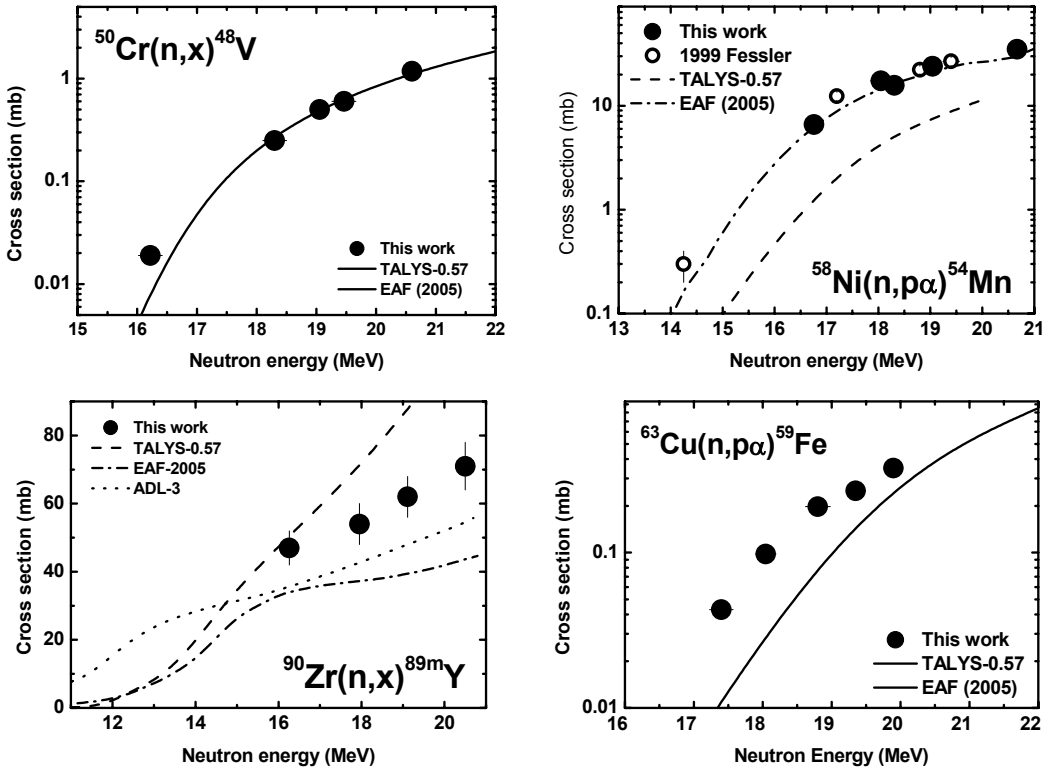

Figure 1. *Comparison of experimental cross sections for the indicated reactions with evaluated data and TALYS-0.57 calculations.*

The neutron-induced reaction cross sections on W and Ta isotopes (Fig. 2). Unique data above 14 MeV were produced for the ^{181}Ta(n,x)^{180}Hf, ^{181}Ta(n,α)^{178m}Lu, ^{181}Ta(n,α)^{178g}Lu, ^{184}W(n,α)^{181}Hf, ^{186}W(n,α)^{183}Hf, and ^{184}W(n,p)^{184}Ta reactions. Our results are in agreement with most of the data from other authors at 14 MeV for ^{184}W(n,α)^{181}Hf, ^{186}W(n,α)^{183}Hf, and ^{184}W(n,p)^{184}Ta reactions. Measurements using both enriched and natural W are on-going at the IRMM Van de Graaf laboratory. Concerning the ^{181}Ta(n,α) reaction cross sections both to the ground and isomeric states and the ^{181}Ta(n,x)^{180m}Hf reaction the results from this work agree with the EAF-2005 evaluation and the shape of the excitation curves agree with the data around 14 MeV. The new data tend to agree better with the data of Lu Hanlin et al. (1989) both for the ^{181}Ta(n,2n)^{180g}Ta and ^{181}Ta(n,p)^{181}Hf reaction cross sections.

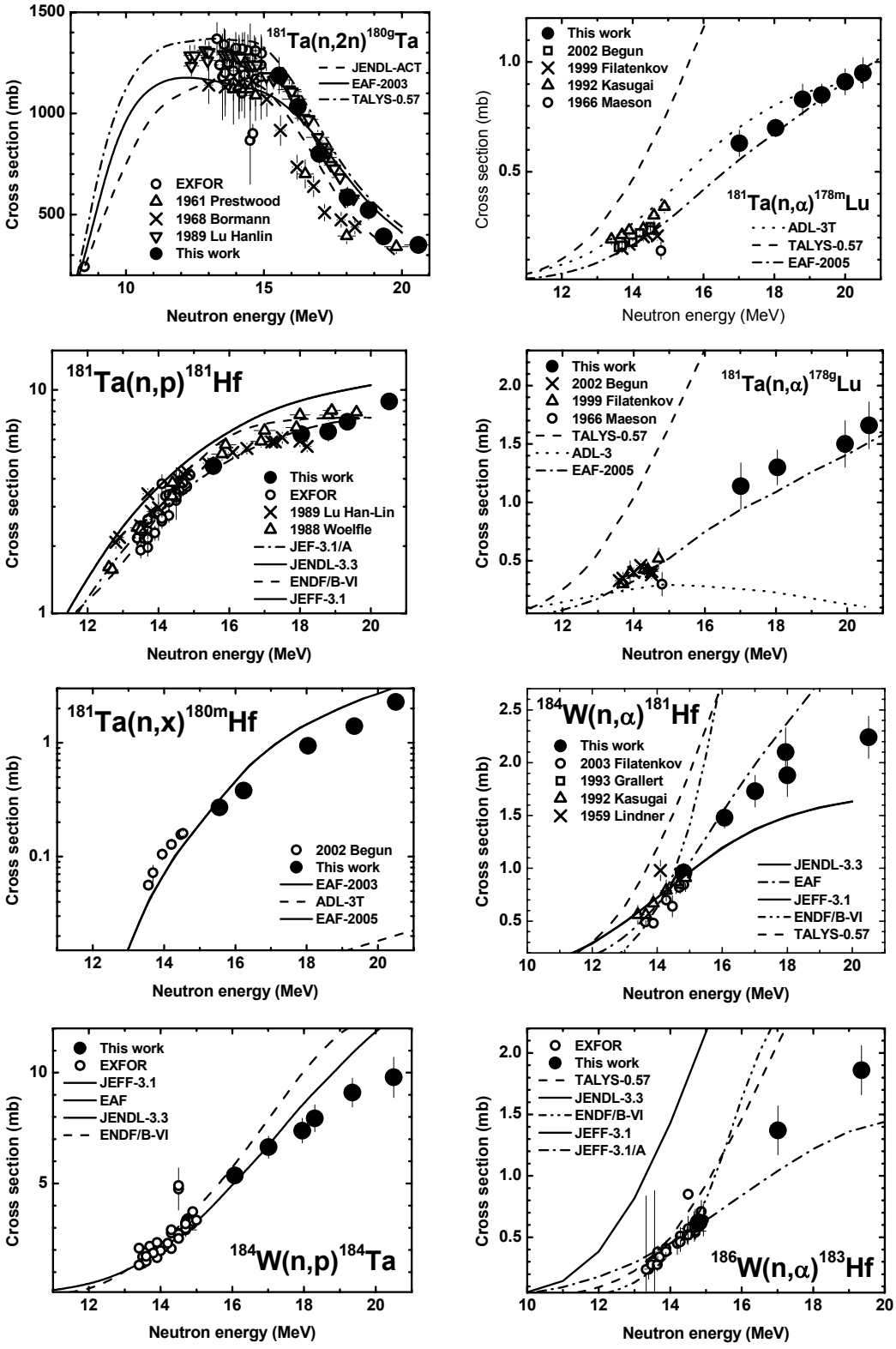

***Figure 2**. Comparison of experimental cross sections for the indicated reactions with evaluated data and TALYS-0.57 calculations*

Acknowledgements
The authors are grateful to the IRMM Van de Graaff Laboratory personnel for providing us with the best possible experimental conditions.

References

[1] A. Fessler, A.J.M. Plompen, D.L. Smith, J.W. Meadows, Y. Ikeda, Nucl. Sci. Eng. 134 (2000) 171-200.

Integral cross section measurements for the validation of excitation functions of (n,p) reactions relevant to the production of the therapeutic radionuclides ^{32}P, ^{64}Cu, ^{67}Cu, ^{89}Sr, ^{90}Y and ^{153}Sm

I. Spahn[1)], M. Al-Abyad[1)], S. Sudár[2)], S.M. Qaim[1)], H. H. Coenen[1)]

1) Forschungszentrum Jülich GmbH, Institut für Nuklearchemie, D-52425 Jülich, Germany
2) Institute of Experimental Physics, University of Debrecen, H-4010 Debrecen, Hungary

i.spahn@fz-juelich.de

Abstract: Nuclear data for production of the therapeutic radionuclides ^{32}P ($T_{½}$ = 14.26 d), ^{64}Cu ($T_{½}$ = 12.7 h), ^{67}Cu ($T_{½}$ = 61.83 h), ^{89}Sr ($T_{½}$ = 50.53 d), ^{90}Y ($T_{½}$ = 64.10 h) and ^{153}Sm ($T_{½}$ = 46.75 h) via (n,p) reactions on ^{32}S, ^{64}Zn, ^{67}Zn, ^{89}Y, ^{90}Zr and ^{153}Eu, respectively, are discussed. The available information on each excitation function was analysed. From the recommended data set for each reaction the average integrated cross section for a standard 14 MeV d(Be) neutron field was deduced. The spectrum-averaged cross section was also measured experimentally. A comparison of the integrated value with the integral measurement served to validate the excitation function within about 15 %. A fast neutron source appears to be much more effective than a fission reactor for production of the above mentioned radionuclides in no-carrier-added form via the (n,p) process. In particular, the possibility of production of high specific activity ^{153}Sm is discussed. An alternative reaction, namely ^{150}Nd(α,n)^{153}Sm, was also investigated. The resulting possible yield is much lower than via the conventional (n,γ) method, but the product is in no-carrier-added form.

Introduction

For cancer treatment internal radiotherapy is gaining increasing significance. For this application, radionuclides with highly ionising, short-range radiation (β^-- and α-particles, Auger and conversion electrons) are of high importance [1, 2]. Most of those nuclides are produced at nuclear reactors [1, 3], although in recent years the use of cyclotrons has also been enhancing [2, 4, 5]. In a reactor, utilisation of the (n,γ) process leads to the highest production yields. However, the obtained radionuclides are generally of low specific activity, unless the activated product decays to a daughter radionuclide that can be separated chemically. Another important source of therapeutic nuclides is the fission process, which, however, may demand rather complex separation procedures. In case of the radionuclides ^{32}P, ^{64}Cu, ^{67}Cu and ^{89}Sr the (n,p) reaction is utilised for production. This route leads to high specific activities, but the reaction cross sections with fission neutrons are low. Nowadays the production of ^{64}Cu and ^{67}Cu has shifted over mainly to cyclotrons [cf 5]. Another therapeutic radionuclide ^{90}Y is presently available via the fission-produced ^{90}Sr/^{90}Y generator system. And yet another radionuclide, ^{153}Sm is commonly produced via the ^{152}Sm(n,γ) reaction. In a recent publication Spahn et al. [6] described cross section measurements on the reactions ^{64}Zn(n,p)^{64}Cu, ^{67}Zn(n,p)^{67}Cu and ^{89}Y(n,p)^{89}Sr with 14 MeV d(Be) break-up neutrons. The values were found to be 3 - 5 times higher than with fission neutrons, suggesting that the yield of the therapeutic radionuclide with fast neutrons (e.g. from a spallation source) would be appreciably higher than that from the present day fission reactors. In the present work the nuclear data relevant to the production of the above mentioned six therapeutic radionuclides via the (n,p) reaction were considered in some detail. An evaluation of all the available cross section data was done and for each reaction a fitted excitation function was obtained. A comparison of the integrated cross section deduced from the evaluated excitation function and the spectral distribution of a 14 MeV d(Be) neutron source with the integral cross section measured using the same neutron source should then establish the reliability of the database for the production of each of the above mentioned therapeutic radionuclides.

Evaluation of excitation functions

For the six (n,p) reactions under consideration the experimental cross section data given in EXFOR [7] were plotted as a function of the neutron energy. The resulting experimental excitation functions were scrutinised regarding the consistency of data and some very discrepant values were ignored.

The nuclear model calculations were done using the code STAPRE, which is a combination of the Hauser-Feshbach and precompound model, and the code EMPIRE 2.19, which is also based on the Hauser-Feshbach formalism and considers direct contribution as well. The detailed results have already been reported [8].

Here we discuss three cases in three mass regions, viz. the (n,p) reactions leading to the formation of ^{32}P, ^{89}Sr and ^{153}Sm (Figs. 1 to 3). Data points found to be discrepant are encircled and were neglected.

In the light mass region (Fig. 1) theory cannot reproduce the experimental results. In the medium mass region (Fig. 2) the model calculations can successfully reproduce the data up to about 14 MeV, with STAPRE giving somewhat better results. As far as the heavier mass region is concerned (Fig. 3) the available experimental (n,p) cross section data are limited only to the 14 MeV energy region. Here the theory plays a much more important role in the construction of the excitation function.

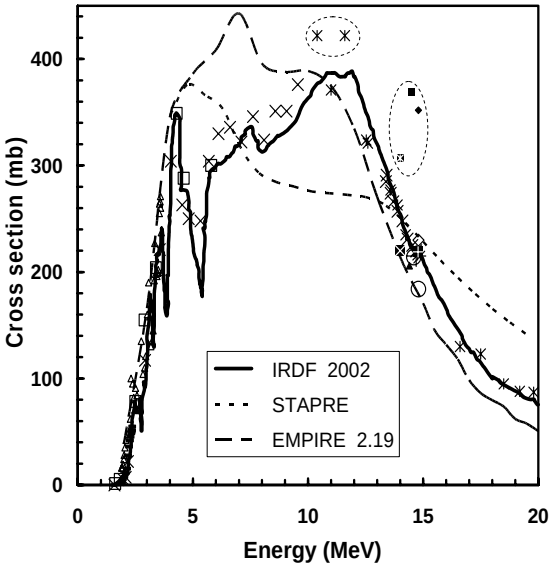

Figure 1. *Excitation function for the ^{32}S(n,p)^{32}P reaction. For references to experimental data, see [7,8]. The IRDF-2002 curve is recommended.*

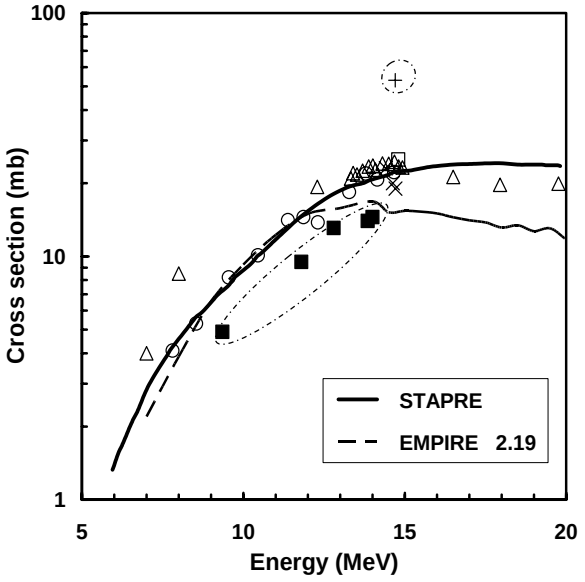

Figure 2. *Excitation function of the ^{89}Y(n,p)^{89}Sr reaction. For references to experimental data, see [7,8]. The STAPRE curve is recommended.*

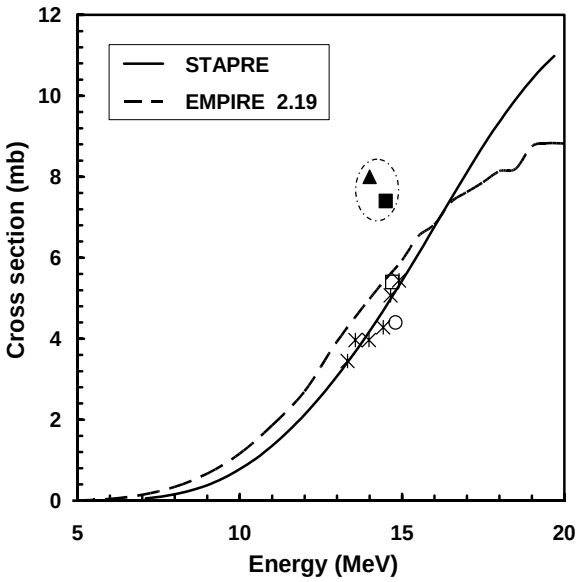

Figure 3. *Excitation function of the ^{153}Eu(n,p)^{153}Sm reaction. For references to experimental data, see [7,8]. The STAPRE curve is recommended.*

Measurement of integral cross section

The spectrum averaged cross sections of the investigated (n,p) reactions were measured integrally via the activation technique. The results on the $^{64}Zn(n,p)^{64}Cu$, $^{67}Zn(n,p)^{67}Cu$ and $^{89}Y(n,p)^{89}Sr$ reactions have already been reported and discussed in terms of radionuclide production [6]. Details on the characterisation of the 14 MeV d(Be) neutron field are described in [8]. In the following, the cross section measurements on the $^{32}S(n,p)^{32}P$, $^{90}Zr(n,p)^{90}Y$ and $^{153}Eu(n,p)^{153}Sm$ reactions are described.

Pellets of high-purity materials were prepared using ^{nat}S, $^{nat}ZrO_2$ and $^{nat}Eu_2O_3$. The diameter of each pellet was 1.3 to 2.0 cm and the thickness ranged between 0.5 and 3 mm.

All neutron irradiations were done at the compact cyclotron CV28 of the Forschungszentrum Jülich, utilising the breakup reaction of 14 MeV deuterons on a thick Be target. The neutron yields and energy spectra from the d(Be) source have been studied by several groups [cf. 8, and references cited therein]. The beryllium target installed in Jülich consists of a metallic Be disk (19.7 mm diam, 1.9 mm thick) which is embedded into a water-cooled copper holder of 2 mm thickness.

The monitoring of the neutron flux densities was done with Al and Fe monitor foils on both sides of a sample using the $^{27}Al(n,\alpha)^{24}Na$ and $^{56}Fe(n,p)^{56}Mn$ reactions. The respective excitation functions were taken from the International Reactor Dosimetry File [9].

The radionuclides ^{32}P and ^{90}Y are pure β^- emitters with relatively high end-point energies of 1.7 MeV and 2.3 MeV respectively. These nuclides were characterised via β^- counting in a gas-flow proportional counter and decay curve analyses. In case of ^{153}Sm, the activity was determined via high resolution HPGe detector γ-ray spectrometry using the 103.18 keV γ-ray (28.3 %).

Results and discussion

The results of all the measurements are given in Table 1 together with the values calculated from the differential data. We estimated the uncertainties in cross section values as about 17 % [6]. By checking the analysed data with our experimentally obtained cross section data, the results could be validated within an overall uncertainty of about 15 %. This uncertainty is based partly un the uncertainty of the spectral distribution of the 14 MeV d(Be) neutrons, which is estimated to be about 8 % and the inherent uncertainties of the recommended excitation functions, which amount to 4 to 8 %, depending on the quality of the available differential data.

Table 1. *Experimental integral data and their comparison with integrated data*[*]

Nuclear reaction	(n,p) reaction cross section [mb]		Ratio
	Integral (σ_{Exp})	Integrated (σ_{Calc})	$\sigma_{Exp}/\sigma_{Calc}$
$^{32}S(n,p)^{32}P$	152 ± 27	167	0.91 ± 0.16
$^{64}Zn(n,p)^{64}Cu$	132 ± 25	140	0.94 ± 0.18
$^{67}Zn(n,p)^{67}Cu$	5.13 ± 0.87	5.0	1.03 ± 0.17
$^{89}Y(n,p)^{89}Sr$	0.91 ± 0.20	1.05	0.87 ± 0.19
$^{90}Zr(n,p)^{90}Y$	2.7 ± 0.50	3.20	0.85 ± 0.15
$^{153}Eu(n,p)^{153}Sm$	0.26 ± 0.04	0.30	0.87 ± 0.13

[*] deduced from the recommended excitation function and the 14 MeV d(Be) breakup neutron field

Applications of data

Besides data development in general, it is interesting to consider the significance of the measured integral cross sections in the actual production of the above mentioned therapeutic radionuclides with high specific activity. The four most important radionuclides are ^{32}P, ^{64}Cu, ^{67}Cu and ^{89}Sr. As mentioned above, in the case of ^{64}Cu and ^{67}Cu the emphasis has shifted over to cyclotron production. For the other two radionuclides, the only way of achieving high specific activity is presently the production via the (n,p) reaction. Our earlier study [6] showed that the $^{89}Y(n,p)^{89}Sr$ reaction with 14 MeV d(Be) neutrons has three times higher cross

section than with fission neutrons. The present work gives approximately the same result for the reaction $^{32}S(n,p)^{32}P$ as well. Thus the production of both ^{32}P and ^{89}Sr can be done more effectively with high-intensity fast neutron spectral sources (e.g. a fusion or a spallation source) than with the present day research reactors.
As far as the production of ^{90}Y is concerned, the $^{90}Zr(n,p)^{90}Y$ reaction does not have high enough cross section to be able to compete with the commonly used $^{90}Sr/^{90}Y$ generator system.
^{153}Sm is presently produced via the $^{152}Sm(n,\gamma)$-process in large quantities but with low specific activity. The increasing importance of this radionuclide in radiotherapy demands a search for alternative production routes which could lead to higher specific activity ^{153}Sm. In this regard, the $^{153}Eu(n,p)^{153}Sm$ reaction investigated in this work may be worth considering. The estimated cross section of this reaction with fission neutrons is only 0.015 mb [cf. 10], and thus too low for production purposes. The measured value with 14 MeV d(Be) neutrons is considerably higher (0.26 ± 0.06 mb). Use of an enriched ^{153}Eu target would increase the yield but the total ^{153}Sm activity would still be rather low for practical applications. Newer concepts of spallation neutron sources may be sufficient and more suitable for production of therapeutic radionuclides via the (n,p) process.
Another possibility of enhancing the specific activity of ^{153}Sm is to use the $^{150}Nd(\alpha,n)^{153}Sm$ reaction. The excitation function of this reaction was measured via the stacked-foil technique and the results have been reported elsewhere [11]. From those results it is concluded that this process could give no-carrier-added ^{153}Sm in quantities sufficient for medical applications, provided a highly enriched ^{150}Nd target capable of withstanding high intensity α-particle beams is developed.

Acknowledgments
This work was done under an Egyptian–German bilateral research cooperation and partly under a DAAD exchange programme. Part of the motivation came through the IAEA-CRP on standardisation of data for production of therapeutic radionuclides. We are grateful to all the authorities concerned. We thank the crew of the compact cyclotron CV 28 at Jülich for performing the irradiations.

References
[1] G. Stöcklin, S.M. Qaim and F. Rösch, Radiochim. Acta 70/71, 249 (1995).
[2] S.M. Qaim, Radiochim. Acta 89, 297 (2001).
[3] IAEA-TECDOC-1340, 2003. Manual of reactor produced radioisotopes, Vienna, Austria
[4] S.M. Qaim, J. Nucl. Sci. Technology, Supplement 2, 1272 (2002).
[5] S.M. Qaim, Cyclotron production of medical radionuclides, in Handbook of Nuclear Chemistry (Vértes, A., Nagy, S., Klencsár, Z., Editors), p. 47, Kluwer, Dordrecht, The Netherlands 2003.
[6] I. Spahn, H.H. Coenen, S.M. Qaim, Radiochim. Acta 92, 183 (2004).
[7] EXFOR, 2003. Nuclear reaction data, EXFOR is accessed on line at http://www.nndc.bnl.gov/exfor/exfor00.htm.
[8] M. Al-Abyad, I. Spahn, S. Sudár, M. Morsy, M.N.H. Comsan, J. Csikai, S.M. Qaim, H.H. Coenen, *Appl. Rad.* Isot. 64: 717 (2006).
[9] International Reactor Dosimetry File: IRDF-2002, available online at http://www-nds.iaea.org/irdf2002/
[10] A. Calamand, Cross sections for fission neutron spectrum induced reactions. In: Handbook of Nuclear Activation Cross Sections, Technical Report No. 156, p.273, IAEA, Vienna, Austria 1974.
[11] S.M. Qaim, I. Spahn, S.A. Kandil, K. Hilgers, H.H. Coenen, Radiochim. Acta, in press.

Formation of high spin mercury isomers in neutron and charged particle induced reactions

S. Sudár [1,2], M. Al Abyad [2], S.M. Qaim [2]

1) Institute of Experimental Physics, University of Debrecen, Bem tér 18/a, 4026 Debrecen, Hungary
2) Institut für Nuklearchemie, Forschungszentrum Jülich GmbH, D-52425 Jülich, Germany

sudarsa@delfin.unideb.hu

Abstract: Formation of the isomeric pairs $^{195}Hg^{m,g}$, $^{197}Hg^{m,g}$ was studied in the reactions $^{196}Hg(n,2n)^{195}Hg^{m,g}$, $^{198}Hg(n,2n)^{197}Hg^{m,g}$, $^{nat}Pt(^{3}He,xn)^{195}Hg^{m,g}$, $^{nat}Pt(^{3}He,xn)^{197}Hg^{m,g}$, and $^{nat}Pt(alpha,xn)^{197}Hg^{m,g}$ over the energy range of 7.6 - 12.5 MeV for neutrons, 18–35 MeV for ^{3}He particles and 17–26 MeV for alpha particles. The reactions $^{197}Au(p,n)^{197}Hg^{m,g}$ were also investigated over the proton energy range of 6–20 MeV. The four projectiles were produced at the Jülich variable-energy compact cyclotron (CV 28); for neutron production the $^{2}H(d,n)^{3}He$ reaction was used. The cross sections were determined by the activation technique in combination with conventional high-resolution as well as low-energy HPGe-detector gamma-ray spectroscopy. From the experimental data, isomeric cross-section ratios were obtained. Nuclear model calculations using the code STAPRE were undertaken to describe the formation of both the isomeric and the ground states of the products. The calculations were compared with the results of the EMPIRE-II code. The total reaction cross section of a particular channel is reproduced fairly well by the model calculations, with STAPRE giving slightly better results. Regarding the isomeric cross sections, the agreement between the experiment and theory is only in approximate terms. A description of the isomeric cross-section ratio by the model was possible only with a very low value of η, i.e. the $\Theta_{eff}/\Theta_{rig}$ ratio. A mass dependence of η is proposed.

Introduction

Studies of excitation functions of nuclear reactions are of considerable importance for testing nuclear models as well as for practical applications. Furthermore, isomeric cross-section ratios are of fundamental significance. Two isomeric pairs, namely $^{195}Hg^{m,g}$, and $^{197}Hg^{m,g}$ appeared to be very interesting: in both cases the ground state has a low spin ($1/2^-$) and the metastable state a higher spin ($13/2^+$). In addition to commonly used projectiles, neutrons and protons, we also investigated reactions induced by ^{3}He- and alpha particles. The higher angular momentum brought by those projectiles might shed some more light on the effect of spin distribution of the level density on the isomeric cross-section ratio.

A common assumption in the global parameterization of the nuclear level density within the framework of the Fermi gas model is that the spin distribution is described by the formula

$$\frac{\rho_J}{\rho} = \frac{2J+1}{2\sqrt{2\pi\sigma^3}} e^{-\frac{J(J+1)}{2\sigma^2}}$$

where ρ is the total level density, while ρ_J is the density of spin-J levels without the 2J+1 degeneracy factor. The parameter σ is known as spin-cutoff parameter. The ρ, ρ_J and σ are all functions of the excitation energy.

In the empirical parameterization, the σ is determined using the rigid body moment of inertia (Θ_{rig})

$$\Theta_{rig} = \frac{2}{5} mA\left(r_0 A^{1/3}\right)^2$$

where r_0 is the nuclear radius parameter, A the mass number and m is the nucleon mass. Introducing the $\eta=\Theta_{eff}/\Theta_{rig}$ the square of the spin-cutoff parameter can be expressed as

$$\sigma^2 = \eta\Theta_{rig}\frac{T}{\eta^2}$$

where T is temperature in thermal ensembles.

Since Bethe's pioneering work [1] the nuclear level density problem has remained an active area of both theoretical and experimental studies. The spin distribution of the levels can be studied experimentally by investigating the rotational band of the nuclei [2] or by comparing the measured and calculated isomeric cross-section ratios [3-7].

Experiment

Cross sections were measured by the activation method which is almost ideal for studying closely spaced low-lying isomeric states, provided their lifetimes are not too short. In work on charged particle induced reactions, high purity thin platinum and gold foils were stacked together. In a given stack about 4 or 5 such foils were placed together with the monitor foils, which also served to degrade the projectile energy as well as to determine the incident particle energy and the beam intensity. Each stack was irradiated for 30-60 minutes at the Compact Cyclotron CV 28 at the Forschungszentrum (FZ) Jülich. The primary energies used were 27.7 MeV for α-, 36.9 MeV for ^{3}He-particles and 20 MeV for protons. The average particle energy effective at each foil was calculated using the standard formalism and corrected by the method described in [8]. The energy degradation along the stack and the beam current were checked by the reactions induced in the inserted monitor foils. In work with neutrons, pellets of $HgCl_2$ with monitor foils were irradiated using dd neutrons at the cyclotron.
A HPGe and a low energy HPGe detector were used to measure the activities of the irradiated monitor foils and the activities of $^{195}Hg^{m,g}$ and $^{197}Hg^{m,g}$ in the irradiated samples. Peak area analyses were done using the PC version of the GAMANAL spectrum analyser programme.The detector efficiency was determined experimentally using a selected set of γ-ray standard sources. The true coincidence corrections for the gamma lines were calculated by the TrueCoinc code [9]. The details have already been reported [10,11].
The count rates at the end of bombardment (EOB) were converted to decay rates A_g, A_m by introducing corrections for emission probabilities of γ-rays, detector efficiency, self-absorption, coincidence loss, dead time, and random pile up. Cross sections were calculated using the activation equation. The isomer ratio was obtained from the ratio of σ_m to σ_g.
The individual uncertainties of the cross sections and cross section ratios were combined in quadrature, taking into account the correlation of the data, to obtain an overall uncertainty of 9-31% and 9-50%.for the cross sections and for the cross section ratios, respectively.

Nuclear model calculations

Cross sections were calculated using the statistical model taking into account the preequlibrium effects. In general, two codes, namely STAPRE and EMPIRE, were used.

STAPRE calculations

The details of the calculation are given elsewhere [10]. In the present work the emphasis was on the isomeric cross sections. Since such calculations are strongly dependent on the input level scheme of the product nucleus [4,5], we chose those parameters carefully. The energies, spins, parities and branching ratios of discrete levels were extracted by using the NNDC On-Line Data Service from the ENSDF database. In the continuum region the level density was calculated by the back-shifted formula with adjusted level density parameter. We characterized the spin distribution of the level density by the parameter η (see above) and the calculations were performed for different η values to find the best value getting agreement with the experimental data.

EMPIRE calculations

In most of the STAPRE calculations done in this work an η value of about 0.25 was found to be most suitable as compared to about 0.5 normally used. In order to check the credibility of those calculations we also used the EMPIRE-II (version 2.19) code [12]. In this case the standard library of input parameters was used. For the proton induced reaction the direct contribution was determined via the Coupled Channel calculation using the built in ECIS03 code. The particle transmission coefficients were generated via the spherical optical model using the computer code (ECIS03) and the default set of global parameters. In the calculation the Multi Step Direct, Multi Step Compound, Hauser-Feshbach model with width fluctuation correction (HRTW), the DEGAS and PCROSS codes were used. For the level densities, the dynamic approach of the EMPIRE-II and HF-BCS microscopic level densities were used.

Results and discussion

Experimental and theoretical studies showed that the excitation functions of ^{3}He-, α-particle, proton and neutron induced reactions leading to the formation of the isomeric pairs $^{195}Hg^{m,g}$ and $^{197}Hg^{m,g}$ are described to varying degree of success by the statistical theory incorporating pre-compound effects. Despite the relatively high spins of the metastable states, the isomeric cross-section ratios are relatively high for the pairs two even at low excitation energies; they increase with the increasing projectile energy. The results for the pair $^{197}Hg^{m,g}$ in four reactions are shown in Figs. 1 to 4. The isomeric cross-section ratio for each of the two pairs appears to be reproduced by the STAPRE calculation only when an η value of 0.15 – 0.25 or less is used. The ratios cannot be described by a nuclear reaction model code using the conventional level density formalism with the usual η value. The agreement between the STAPRE calculation with η =0.25 and EMPIRE with HF-BCS microscopic treatment implies that the low η values originate from the microscopic structure of these nuclei.

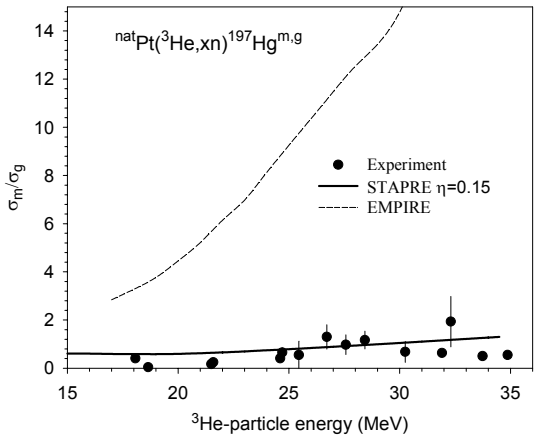

***Figure 1**. Isomer ratio in the $^{nat}Pt(^{3}He,xn)^{197}Hg^{m,g}$ process.*

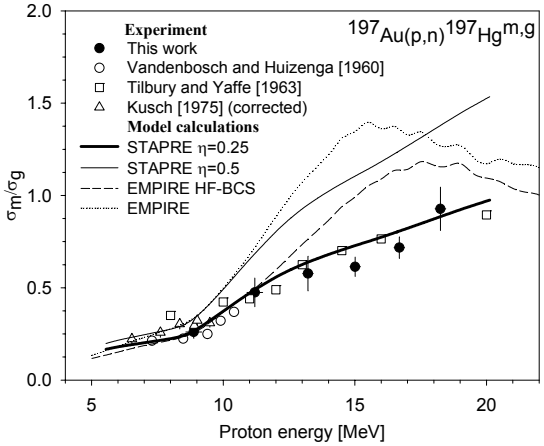

***Figure 2.** Isomer ratio in the $^{197}Au(p,xn)^{197}Hg^{m,g}$ process*

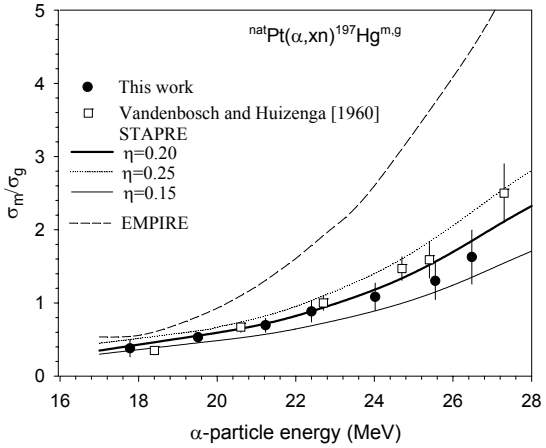

***Figure 3**. Isomer ratio in the $^{nat}Pt(\alpha,xn)^{197}Hg^{m,g}$ process.*

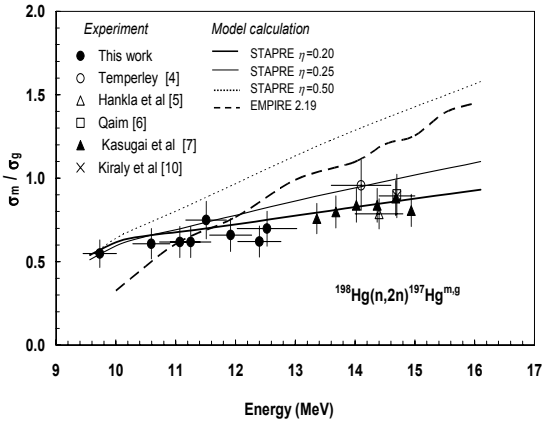

***Figure 4.** Isomer ratio in the $^{198}Hg(n,2n)^{197}Hg^{m,g}$ process*

The advantage of using the alpha and helium-3 induced reactions for studying the isomeric cross-section ratio is that the compound system gets larger angular momentum transferred than in nucleon induced reactions. As a result the isomeric cross-section ratio becomes more sensitive to the spin distribution. The energy dependence of the isomeric cross-section ratio is described well by the model calculations. This implies that the contribution of two proton stripping direct process is negligible. It also indicates that to a first approximation η is independent of energy and the energy dependence of the spin-cutoff factor is adequate. Similar results were obtained from measurements on neutron and proton induced reactions. Analyses of those measurements confirmed the low value of η.

The characteristics of the discrete levels as well as their branching ratios play an important role in the calculation of isomeric cross-section ratios. The constancy in the η value in describing

(within the uncertainty of the experimental data) the different particle induced reactions (α, ^{3}He, p, n) shows that there cannot be any serious error in the decay scheme of the discrete levels. Since the population of the discrete levels by particle emission and gamma cascade from the continuum will be different for different types of reactions, the error in the level scheme would lead to a large deviation between the needed η values to fit the calculated and measured isomeric cross-section ratios. For example the maximum of the spin distribution for the ^{198}Hg compound nucleus is at 5 ħ in the ^{197}Au(p,n)^{197}Hg^{m,g} reaction but it is at 16 ħ in the ^{194}Pt(α,n)^{197}Hg^{m,g} reaction at about the same excitation energy of the ^{198}Hg.

It can thus be stated that the spin-cutoff factor and the ratio of the effective moment of inertia Θ_{eff} to the rigid-body moment of inertia Θ_{rig} ($\eta = \Theta_{eff}/\Theta_{rig}$ show anomaly for the isotopes ^{195}Hg and ^{197}Hg.

In a recent work [13] the spin cutoff factor (σ) has been evaluated at low excitation energy in the mass range of 20≤A≤110. It was concluded, that using the formula.

$$\sigma = const\left(U-\Delta\right)^{0.25} A^{5/6} / a^{1/4} \quad (1)$$

for the energy(U), energy shift (Δ), mass number (A) and level density parameter (a) dependence of σ the fitted "const" in the formula shows a mass number dependence: const=0.10578-0.000202A.

This "const" is directly connected to the parameter η used in this paper

$$\eta^{1/2} = \frac{const}{const_{rigid}} = 0.878152 - 0.001677A \quad (2)$$

If we accept the mass dependence given above the extrapolated value for the η(197)=0.30, which is quite near to our value of 0.25 from the isomeric cross-section measurement. It can also be seen from the evaluation of [13], that the individual values strongly scattered around the value in equation above. The recent analysis of Ref. [14] suggesting η=0.75 for ^{51}V, a lot of successful model calculations with η =0.5 in the medium mass region, and our conclusion of η=0.25 for heavy nuclei, all agree quite well with the data calculated from Eq. 2 (η(51)=0.63, η(100)=0.50, η(197)=0.30,). Since energy dependence for η has not been observed, the results of the low energy analysis can be extended to higher excitation energies and we can postulate that η has a mass dependence even up to mass number 197.These empirical results should be confirmed for the higher mass number region with new experiments, and an explanation of mass dependence needs further theoretical work.

Acknowledgements

We thank Prof. H. H. Coenen and Prof. J. Csikai for their kind support of this project, Mr. S. Spellerberg for some technical assistance.

References

[1] H. Bethe, Phys. Rev. 50, 332 (1936).
[2] W. F. Mueller, W. Reviol, M. P. Carpenter, et al., Phys. Rev. C 69, 064315 (2004).
[3] P. A. DeYoung, B. Atallah, B. Hughey, et al., Phys. Rev. C 62, 047601 (2000).
[4] S. M. Qaim, A. Mushtaq, and M. Uhl, Phys. Rev. C 38, 645(1988).
[5] S. Sudár and S. M. Qaim, Phys. Rev. C 53, 2885 (1996).
[6] B. Strohmaier, M. Fassbender, and S. M. Qaim, Phys. Rev. C 56, 2654 (1997).
[7] S. Sudár, A. Hohn, and S. M. Qaim, Appl. Radiat. Isot. 52, 937(2000).
[8] S. Sudár and S. M. Qaim, Phys. Rev. C 50, 2408 (1994).
[9] S. Sudár, TrueCoinc, a Software Utility for Calculation of the True Coincidence Correction, Specialized Software Utilities for Gamma Spectrometry, IAEA-TECDOC-1275 (International Atomic Energy Agency, Vienna, 2002), p. 37.
[10] S. Sudár and S. M. Qaim, Phys. Rev. C 73, 034613 (2006).
[11] M. Al-Abyad, S. Sudár, M.N.H. Comsan and S. M. Qaim, Phys. Rev. C 73, 064608 (2006).
[12] M. Herman, R. Capote, B. Carlson, P. Oblozinsky, M. Sin, A. Trakov, and V. Zerkin, EMPIRE-II, Nuclear reaction model code, version 2.19 (International Atomic Energy Agency, Vienna, 2005).
[13] S. I. Al-Quraishi, S. M. Grimes, T. N. Massey, and D. A. Resler, Phys. Rev. C 67, 015803 (2003).
[14] P. Reimer, V. Avrigeanu, A. J. M. Plompen, and S. M. Qaim, Phys. Rev C, 65, 014604 (2001).

Neutrons as a multifunctional tool for geophysicists

U. Woźnicka[1)], T. Zorski[2)]

1) Henryk Niewodniczanski Institute of Nuclear Physics, PAN, Radzikowskiego 152 PL-31-342 Kraków, Poland
2) AGH University of Science and Technology, Faculty of Geology, Geophysics and Environmental Protection, Mickiewicza 30, PL-30-059 Kraków, Poland
urszula.woznicka@ifj.edu.pl

Abstract: Neutrons offer worth instrument for geophysical applications especially for direct borehole measurements. Neutron source creates a neutron field in a whole space which encompasses a borehole and surrounded geological layers. The field is variable in space, energy, and time, and can produce gamma ray in nuclear reactions with elements. Another gamma ray can be produced in a rock formation because of a presence of natural radioactive elements (K, U, Th). Neutrons (and gammas) which reach the system of detectors bring complex information of rock. Thermal and epithermal neutron detectors measure suitable neutron fluxes and the thermal neutron absorption cross section of a geological formation. These quantities permit to calculate one of the most important petrophysical parameter of the formation, i.e. the porosity, and in consequence, resources of a hydrocarbon deposit. Scintillation detectors measure gamma rays created by the thermal neutron capture and inelastic scattering of fast neutrons. Depending on the energy range of the spectrometer, a content of Si, Ca, Fe Al and K, U, Th can be directly determined. Polish scientists offer an idea of the Complex Nuclear Tool (CxNT) which combines all possibilities of measurements which are induced by a neutron field. The new tool consists of Am-Be source and two sets of detectors: four thermal/epithermal neutron detectors and three scintillation gamma detectors. Qualitative and quantitative information obtained from the CxNT tool depends both of the types and the configuration of the detectors. A complex interpretation procedure of measured data enables the precise determination of the mineral composition in the analyzed geological formation.

Introduction

Measurements of various physical quantities in a borehole by means of geophysical well logging tools are designed for the determination of different categories describing underground geological formations. Measurements of nuclear radiation are indispensable components of the well logging in geophysical prospecting. Raw data (logs) are engaged in the comprehensive interpretation to get values of geological parameters. The comprehensive interpretation of well logs is aimed to calculate mineral volumes (i.e. lithology), porosity and water saturation of reservoir rocks. The following logs are frequently employed for lithology-porosity solution: intensity of natural radioactivity, neutron porosity, bulk density and equivalent atomic number determined by gamma rays emitted from ^{137}Cs source and scattered in rocks acoustic wave parameters, electric parameters (e.g. resistivity log). The comprehensive interpretation of a set of well logs is a mathematical task consisting a solution of a set of equations. The number of equations is determined by the number of the measured logs and additional conditions determining boundary and geological requirements. The main set of equation circumscribes the rock model, i.e. shows dependences between the signal, TM_i, generated by physical phenomena (e.g. electric current, acoustic wave, gamma ray or neutron fields), and geological parameters of the rock:

$$TM_i = \sum_{j=1}^{n} \left(a_{ij} V_j \right) \quad i = 1,..., m \tag{1}$$

where V_j is the volume fraction of the *j*-th component of the rock (such mineral components as clay, cl, sandstone, $sand$, limestone, lim, porosity, ϕ, and saturation, S_w of the formation fluid, w) and a_{ij} is the *i*-th matrix parameter of the *j*-th component.

Gamma Ray Log

The decay of radioactive isotopes is the key to the creation of the Gamma Ray log. The gamma ray log functions to discriminate the shales from "clean" formations and to estimate the relative shale proportions in reservoir units. The higher levels of radiation in shale are caused by absorption of thorium and uranium by clay minerals and by higher potassium content in crystal lattices of some clays. In contrast, sandstones, limestones and dolomites have usually low levels of radioactivity.

For example, the total natural gamma signal, γ, measured in the formation is described by the equation:

$$\gamma = \phi S_w \gamma_w + V_{cl}\gamma_{cl} + V_{sand}\gamma_{sand} + V_{lim}\gamma_{lim} + \sum_k V_{min\,(k\,)}\gamma_{min\,(k\,)} \quad (2)$$

where $\gamma_{w,\ cl,\ sand,\ lim,\ min}$ is the gamma ray intensity characteristic for the given medium.

The Spectrometric Gamma-Ray log (SGR) is displayed as three curves from all sources of thorium, uranium and potassium. The spectral gamma ray log can be used, in specific cases, to estimate volumes and types of clay minerals.

Spectral Neutron-Gamma Log (SNG)

Another spectrometric measurement makes a base of the spectrometric Neutron-Gamma Well Logging tool (SNG) equipped with an efficient scintillation detector and an isotopic neutron source [1, 2]. The log offers possibility of identifying and quantifying the rock elements: Si, Ca and Fe by a detection of the characteristic gamma rays generated in the neutron interactions. The Si, Ca, Fe concentrations are determined using the multiple linear regression of the form:

$$C_n = a_{n0} + a_{n1}\, I_H + a_{n2}\, I_{Si} + a_{n3}\, I_{Ca} + a_{n4}\, I_{Fe} \quad (3)$$

where C_n are the elemental concentrations of the *n*-th element of interest (in wt. %), I_H, I_{Si}, I_{Ca}, I_{Fe} are the gross gamma counts of the gamma-ray spectra taken from the spectral “windows” ΔE_γ around the prominent γ lines from the radiative capture in Si, Ca, Fe and H (3.54 MeV and 4.93 MeV for Si, 6.42 MeV for Ca, 7.631 MeV and 7.645 MeV doublet for Fe and 2.22 MeV for H). Coefficients a_{n0} ,..., a_{n4} are obtained from the calibration procedure. A detailed description of the quantitative analysis is presented in [3].

Neutron Log

The tool [4] contains a continuously emitting neutron source (generally AmBe) and either a neutron (He-3) or a gamma-ray detector. High energy neutrons from the source are slowed down by collisions with atomic nuclei. The hydrogen atoms are the most effective in the slowing down process. Thus, the distribution of the neutrons at the time of detection is primarily determined by the hydrogen concentration. Depending on the tool type, the detection is performed by either thermal neutrons or gamma rays, generated when thermal neutrons are captured by absorbers in the formation (primarily chlorine) or epithermal neutrons. The tool response is mainly related to hydrogen concentration but is also affected by mineralogy and borehole effects. The neutron log does not distinguish between the hydrogen in the pore fluids (water, oil, gas), in water of crystallization, or in water bound to solid surfaces. In clean oil-filled or water-filled formations the apparent porosity reading of the neutron log reflects the amount of the liquid-filled pore volume. When the hydrogen concentration of the zone surrounding the well bore is large, most of the neutrons are slowed down and captured close to the well bore. This results in a low count rate and is interpreted as an indication of high porosity. If the zone which surrounds the well bore has a small concentration of hydrogen, neutrons must travel farther from the source before being captured. This results in a high count rate and is interpreted as an indication of low porosity. Hard, dense dolomites and limestones usually have high count rates, while porous zones usually have lower count rates.

A dual-spacing formation density log. The compensated formation density logging device employs two detectors spaced at different distances from the source. The detector at the

shorter spacing is particularly sensitive to the density of material immediately adjacent to the face of the pad. The contribution of this material which includes mud cake and drilling mud filling minor borehole wall irregularities, affects the response of each detector to a different degree. The measurements from both detectors provide a means for making a correction for the influence of drilling mud and mud cake on the measurements.

The Neutron Lifetime Log

The Neutron Lifetime logging technique employs a pulsed neutron source which is periodically actuated to produce short bursts of neutrons. During an interval between the bursts, the neutrons die away. Their average lifetime can be measured by measuring the length of time required for the neutron population at a particular instant to die away to half value. The radiation intensity is measured in each of two preselected intervals and, by intercomparing these measurements, determines the rate of the neutron die-away. This measured rate has been shown both by theory and experiment to be a measure of the thermal neutron capture cross section Σ of the medium in which the neutrons are captured. Thermal neutrons are captured mainly by the chlorine present. Hence, the tool responds to the amount of salt in formation waters. Hydrocarbons result in longer lifetimes than salt water. Measurements with this tool are porosity-dependent and sensitive to clay content. The tool response (1) is scaled in neutron capture cross section units:

$$\Sigma_{\log} = (1 - \phi)\, \Sigma_{\mathrm{m}} + \phi\, \Sigma_{\mathrm{h}}\, (1 - S_w) + \phi\, \Sigma_{\mathrm{w}}\, S_w \qquad (4)$$

where $\Sigma_{\mathrm{m,\ h,\ w}}$ is the thermal neutron capture cross section of the rock matrix, hydrocarbons and formation fluid, respectively.

Complex Nuclear Tool CxNT

The idea is to joint all of the nuclear method mentioned above in one complex nuclear logging tool (fig. 1). The Spectral Gamma-Ray log (SGR) and the Spectral Neutron-Gamma log (SNG) is considered in its typical conventional application to measure K-U-Th content, and Si, Ca and Fe content. The additional activation measurement can be added to measure the Al content. It requires only one additional scintillation detector of gamma ray for the activation analysis. The one neutron source forms the neutron field for all measurement methods used.
The Neutron log applied in the Complex Tool is extended [5] and consists of four even five thermal and epithermal neutron detectors (NNTE Tool). The proposed combination of the neutron log allows to realize the compensated logging and to calculate the thermal neutron capture cross section $\Sigma_{\log}$. It is a unique solution with the application of the steady state isotopic source. The pulse neutron source (as for the Neutron Lifetime logging) is unnecessary. The NNTE tool gives information on the porosity of the formation and on the neutron capture cross section.
The Complex Nuclear Tool delivers eight even nine geological parameters to the comprehensive interpretation of the well logs. Present requirements for the geophysical measurements are directed to the quantitative lithology and porosity solutions. The results obtained by the geophysical measurement should be geologicaly calibrated. The aim of the geological calibration is transformation of the data available in log measurements to the basic reservoir parameters as porosity, clay typing and permeability estimation. The geological calibration of the tool is dependent on specific, regional geological formations. The calibration of the CxNT tool is focused on thin – bedded shaly – sand Miocene gas formation in Carpathian Foredeep, Poland [6].

Acknowledgements
The project has been realized in the year 2006 in the frame of the Scientific Network: "Nuclear Methods for Geophysics" sponsored by the Ministry of Science and Higher Education, Poland.

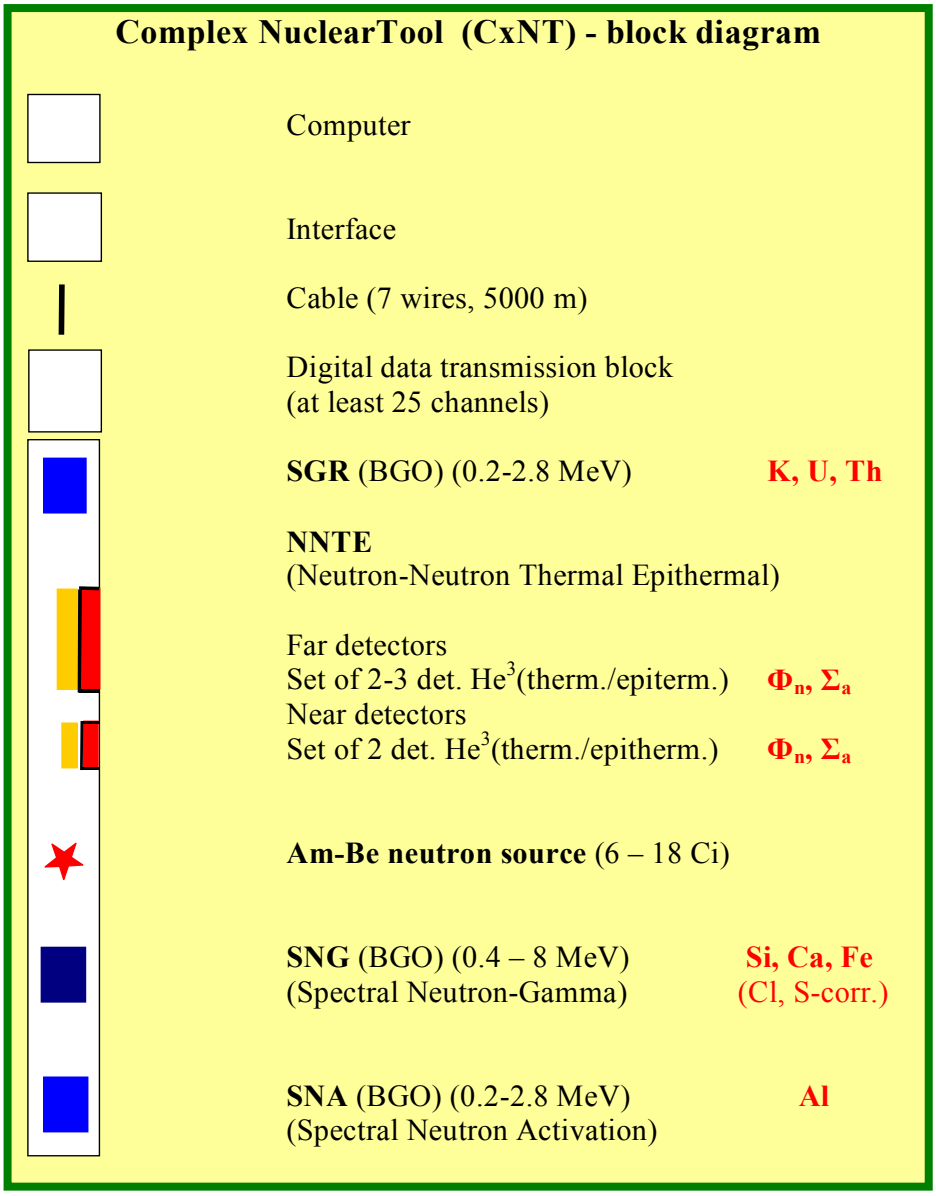

Figure 1. *Block diagram of the Complex Nuclear Tool.*

References

[1] Schweitzer J. S., Ellis D. V., Grau J. A., Hertzog R. C.: Elemental Concentration from Gamma-ray Spectroscopy Logs, Nucl. Geophys. 2 (3), 175-181, (1988).

[2] Herron S. L., Herron M. M.: Quantitative Lithology: an Application for Open Cased Hole Spectroscopy, Transactions of SPWLA, Thirty-seventh Annual Logging Symposium, New Orleans, LA, June 16-19 1996, Paper E, (1996).

[3] Cywicka-Jakiel T., Zorski T.: Monte Carlo Simulation of the Upgraded, Neutron-gamma Logging Tool, SO-5-90-SN Type. Comparison of the Simulations and Measurements. IFJ Report No 1965/AP, Institute of Nuclear Physics PAN, Kraków, (2005) http://www.ifj.edu.pl/reports/2005/1965.pdf.

[4] http://www.spwla.org/library_info/glossary/

[5] Drabina A., Zorski T.: Geophysical neutron logging-tool NNTE for measurements of porosity and rock matrix Sigmaa - numerical simulations. Neutron Measurements, Evaluations and Applications -2, NEMEA-2 Workshop, 20-23 October 2004, Bucharest, Romania, ISBN 92-894-8618-X, @European Communities, 81-84, (2005).

[6] Zorski T.: Methodology of well log interpretation in thin-bedded gas bearing formations in the Carpathian Foredeep. AGH University of Science and Technology Editions, Quarterly AGH: Geologia 30/5. (in Polish – extended summary and figures in English), (2004).

Evaluations of the excitation functions for ^{27}Al(n,p)^{27}Mg and ^{28}Si(n,p)^{28}Al reactions

K. I. Zolotarev[1)], P. K. Zolotarev[2)], J. Csikai[3,4)]

1) Institute of Physics and Power Engeneering, Obninsk, Russia
2) Scientific and Engineering Center for Nuclear and Radiation Safety of the Federal Nuclear Safety Authority of Russia, Moscow
3) Institute of Experimental Physics, Debrecen University, Debrecen-10, Pf. 105, Hungary
4) Institute of Nuclear Research of the Hungarian Academy of Sciences, 4001-Debrecen, Pf. 51, Hungary

csikai@delfin.unideb.hu

Abstract: Cross sections and related uncertainties were evaluated for the ^{27}Al(n,p)^{27}Mg and ^{28}Si(n,p)^{28}Al reactions from the threshold to 23 MeV and 21 MeV incident neutron energies, respectively. Evaluations were carried out by means of PADE-2 code on the basis of analyzed experimental data published up to November 2004 for Al and May 2006 for Si. New evaluation of cross sections for ^{27}Al(n,p)^{27}Mg reaction in comparison with data from IRDF-90 ver.2 and JENDL/D-99 dosimetry files agrees well with the microscopic and integral experimental data. The same holds for ^{28}Si(n,p)^{28}Al reaction in comparison with data taken from the ENDF/B-VI rel.8 and JENDL-3.3 libraries. Analytical expressions are given for the $\sigma(E_n)$ functions for (n,p) reactions on Al and Si in order to complete the neutron energy and fluence monitors in the 13-15 MeV and 14-21 MeV intervals, respectively.

Introduction

The ^{27}Al(n,p)^{27}Mg reaction is commonly used in the reactor dosimetry and neutron metrology mainly for neutron spectrum determination in the critical assemblies and power reactors, in addition for the bulk media assay. In the neutron spectrum unfolding procedure based on the ^{27}Al(n,p)^{27}Mg reaction rate provides information about flux component above 1.9 MeV. The ^{27}Al(n,p)^{27}Mg reaction is very often used in experimental nuclear physics as a cross section standard in the neutron energy interval between 13 – 15 MeV.
The construction of ITER requires special structural materials resistant to high heat flux and nuclear radiations. Sintered silicon carbide, SiC, can be considered as an advanced structural material in fusion reactors, mainly due to its low decay heat and activation properties. Therefore, integral activation, transmission, shielding capability, shutdown dose rate measurements and model calculations are in progress on the SiC assembly in addition to clearing up its behaviour as an important element in the V3Ti1Si-alloy and in the Li_4SiO_4 breeder material. Silicon plays an important role in many other fields, e.g. in the development of neutron based humanitarian de-mining methods that requires the knowledge of the different interaction of neutrons with the soil (SiO_2) environment similarly to the evaluation of the results of neutron well-logging experiments. Presence of silicon in metals and alloys has a strong effect in their physical and chemical properties. The ^{28}Si(n,p)^{28}Al reaction is used also in unfolding the neutron fields connected to the bulk media assay as well as a cross section standard in the 14 − 21 MeV range.
This work was undertaken with the aim to describe new evaluations of cross sections and related covariance matrices of uncertainties for the ^{27}Al(n,p)^{27}Mg and ^{28}Si(n,p)^{28}Al reactions.

Experimental data for the ^{27}Al(n,p)^{27}Mg and ^{28}Si(n,p)^{28}Al excitation functions

In the process of evaluations of cross sections and their uncertainties for the ^{27}Al(n,p)^{27}Mg and ^{28}Si(n,p)^{28}Al reactions two sources of information were used, namely the available differential and integral experimental data [1,2]. These data were taken mainly from EXFOR Library (Versions November 2004 for Al, February 2006 for Si) which were completed with the information taken from the original publications. The excitation function of the ^{27}Al(n,p)^{27}Mg reaction was analysed for the incident neutron energies from the threshold (E_{th}=1.89 MeV) to 23 MeV. During this analysis about 76 papers published in the period from 1952 to 2000 were

reviewed. Database for the evaluation of the excitation function of $^{27}Al(n,p)^{27}Mg$ reaction from the threshold to 23.0 MeV was formed from microscopic experimental data [1]. The excitation function of the $^{28}Si(n,p)^{28}Al$ reaction has been analysed for the incident neutron energies from the threshold (E_{th} = 3.999 MeV) to 21 MeV. During this analysis 42 works published in the period from 1953 to 2006 were reviewed. Microscopic experimental data were used for the evaluation of the excitation function of $^{28}Si(n,p)^{28}Al$ reaction [2]. Details of the evaluation procedures have been described elsewhere [1,2]. The excitation function for the $^{29}Si(n,x)^{28}Al$ reaction from threshold to 21 MeV and related uncertainties were evaluated also in this work on the basis of experimental data corrected to the new standards given in our recent paper [2].

Evaluated excitation function for the reaction $^{29}Si(n,x)^{28}Al$ from threshold to 21 MeV in comparison with experimental data is shown in Fig.1. All experimental data obtained by using the activation method and samples of natural isotopic composition were corrected above 12 MeV for the contribution from the $^{29}Si(n,x)^{28}Al$ reaction where x = (n+p) + (p+n) + d, i.e. the sum of the outgoing particles. Integral experiments for the $^{27}Al(n,p)^{27}Mg$ and $^{28}Si(n,p)^{28}Al$ reactions were carried out in the neutron fields produced by ^{241}Am-Be source, $^{9}Be(d,n)$ reaction, ^{235}U thermal fission and ^{252}Cf spontaneous fission neutron spectra.

The main characteristics of the evaluated $^{27}Al(n,p)^{27}Mg$ and $^{28}Si(n,p)^{28}Al$ excitation functions

Statistical analysis of prepared experimental database carried out by means of PADE-2 code permits to evaluate the excitation functions of $^{27}Al(n,p)^{27}Mg$ and $^{28}Si(n,p)^{28}Al$ reactions for the incident neutron energies from threshold (E_{th} = 1.89637 MeV) to 23 MeV and (E_{th} = 3.9924MeV) to 21 MeV, respectively.

The evaluated excitation function of $^{27}Al(n,p)^{27}Mg$ reaction satisfactorily reproduce the resonance structure in the excitation function observed in the high-resolution measurements of Smith and Meadows [3]. The energy dependence of cross section in the interval 13 – 15 MeV could be correctly reproduced only in the present evaluation (see Fig. 2).

Evaluated excitation function for the $^{28}Si(n,p)^{28}Al$ reaction in the energy range from threshold to 21 MeV in comparison with ENDF/B-VI rel.8, JENDL-3.3, EFF-3 cross sections and experimental data is given in Fig. 3. As shown in Fig. 4 the new evaluation well reproduces the resonance structure in $^{28}Si(n,p)^{28}Al$ excitation function observed in the high-resolution measurements. The $^{27}Al(n,p)^{27}Mg$ and $^{28}Si(n,p)^{28}Al$ reactions can be recommended as reference cross sections and incident energy monitors for the activation measurements with short-lived residual nuclei.

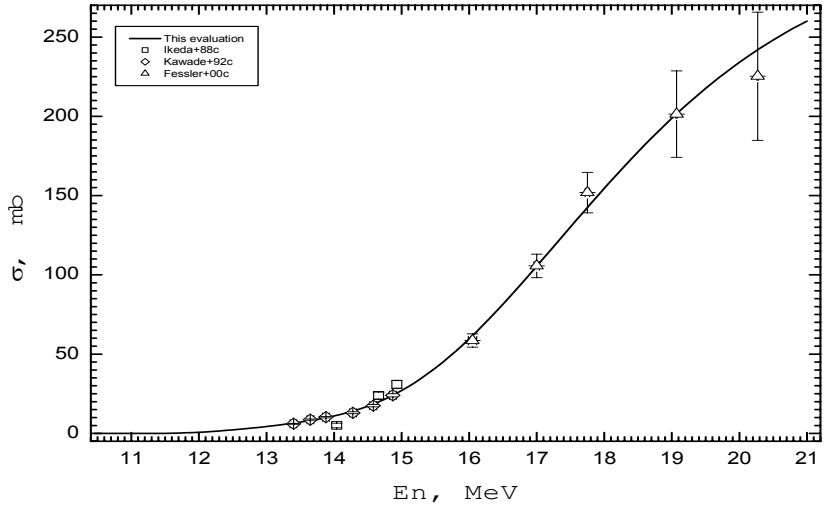

Figure 1. *Evaluated excitation function for the reaction $^{29}Si(n,np+pn+d)^{28}Al$ from threshold to 21 MeV in comparison with experimental data.*

The following analytical expressions describe the energy dependence of the cross sections in the 13 – 15 MeV for Al and 14 − 21 MeV for Si intervals: $\sigma(E_n) = (– 12.654E_n + 254.117)$mb; $\sigma(E_n) = (-3215.18 + 676.316E_n - 42.093E_n^2 + 0.826E_n^3)$. In this case the $^{90}Zr(n,2n)^{89}Zr$ and the $^{52}Cr(n,2n)^{51}Cr$ energy monitors can be completed with the ^{27}Mg and ^{28}Al short-lived products.

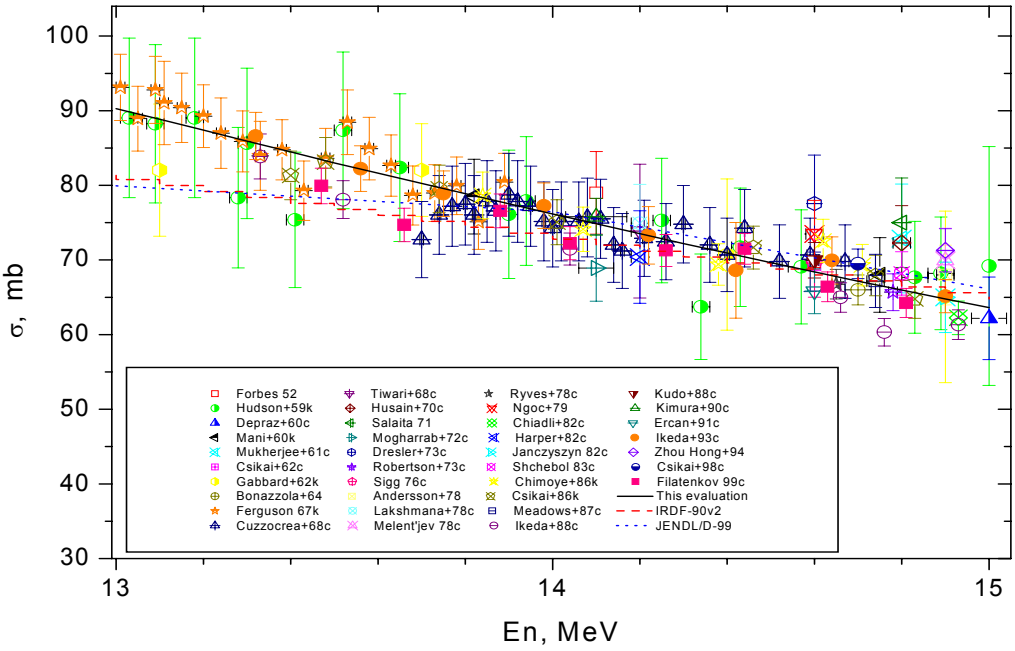

Figure 2. *Evaluated excitation function for $^{27}Al(n,p)^{27}Mg$ reaction in the energy range 13-15 MeV in a comparison with IRDF-90v.2, JENDL/D-99 and experimental data.*

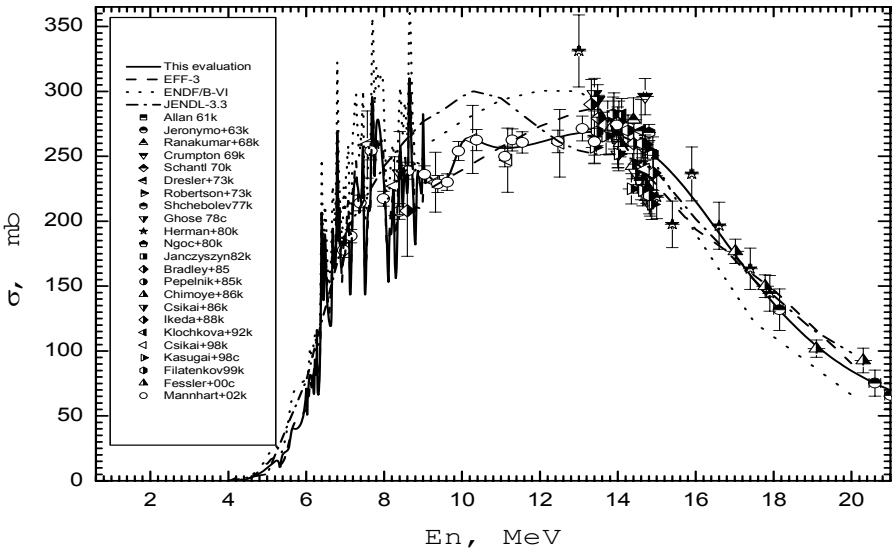

Figure 3. *Evaluated excitation function for the reaction $^{28}Si(n,p)^{28}Al$ in the energy region 4 – 21 MeV in comparison with EFF-3, END/B-6, JENDL-3.3 and experimental data.*

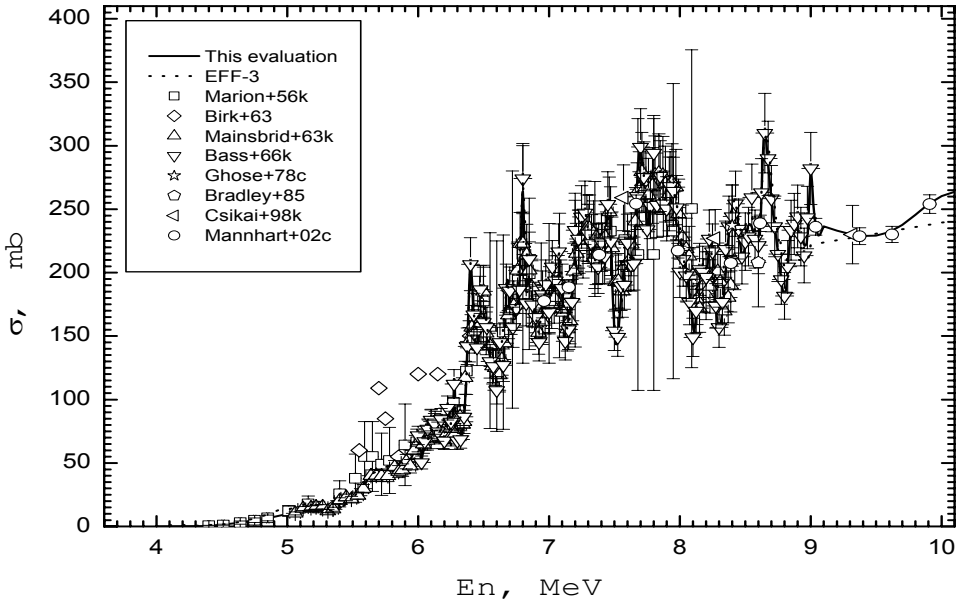

Figure 4. *Evaluated excitation function for the reaction $^{28}Si(n,p)^{28}Al$ from threshold to 10 MeV in comparison with EFF-3 and experimental data.*

Conclusions

The $^{27}Al(n,p)^{27}Mg$ reaction cross sections for the neutron energies between 13 – 15 MeV determined with an accuracy of (1.45 – 1.95) % agree better with microscopic and integral experimental data than with those obtained from the IRDF-90v.2 and JENDL/D-99 libraries. The ENDF-6 formatted data file for $^{27}Al(n,p)^{27}Mg$ reaction was adopted for the new International Reactor Dosimetry File, IRDF-2002 [4].

A new evaluation was performed for the excitation functions of $^{28}Si(n,p)^{28}Al$ and $^{29}Si(n,x)^{28}Al$ reactions from threshold to 21 MeV. Results of benchmark calculations carried out on the basis of the integral data for two standard neutron spectra (^{235}U, ^{252}Cf) show that the microscopic cross sections for $^{28}Si(n,p)^{28}Al$ reaction both from this work and EFF-3 library are evaluated rather correctly in the energy range 5.3 – 10.8 MeV but EFF-3 have higher discrepancies with integral experimental data than the present evaluation. The results of test show also that the ENDF/B-VI rel.8 and JENDL-3.3 overestimate significantly the cross sections in the energy range from threshold to 13 MeV. The obtained uncertainties of (1.97 – 3.55) % in the evaluated $^{28}Si(n,p)^{28}Al$ excitation function in the energy range 9 – 16 MeV permit to use these data in fusion reactor design calculations.

Acknowledgements

This work was supported in part by the Hungarian Research Fund (OTKA T037190), the EC JRC IRMM, Geel (Contract No. IRMM/ST/2001-248 CCR 478519) and the International Atomic Energy Agency, Vienna (Contract No. 7687/R0).

References

[1] K. I. Zolotarev, A. B. Pashchenko, J. Csikai, Acta Phys. Debrecina 38-39(2005) 381.
[2] K. I. Zolotarev, P. K. Zolotarev, J. Csikai, Acta Phys. Debrecina 40(2006)137.
[3] D. L. Smith, J. W. Meadows, Nucl. Sci. Eng. 58(1975)314.
[4] O. Bersillon, L. R. Greenwood, P. J. Griffin, et al., International Reactor Dosimetry File-2002 (IRDF-2002), Report IAEA, Vienna, 2004.

Development of the EURITRACK Tagged Neutron Inspection System: from simulation to experiment

S. Bernard[1)], B. Perot[1)], C. Carasco[1)], A. Mariani[1)], A. Donzella[2)], A. Zenoni[2)], I. Bodini[3)], A. Fontana[4)], V. Valkovic[5)], D. Sudac[5)]

1) Commissariat à l'Energie Atomique, 13108 St Paul-lez-Durance Cedex, France
2) INFN and Università di Brescia, 38 Via Branze 25123 Brescia, Italy
3) Università di Brescia, 38 Via Branze 25123 Brescia, Italy
4) INFN and Università di Pavia, 6 Via Bassi 27100 Pavia, Italy
5) Institute Ruder Boskovic, 54 Bijenicka c. 10000 Zagreb, Croatia
bertrand.perot@cea.fr

Abstract: The EURopean Illicit TRAfficing Countermeasures Kit project is part of the 6th EU Framework program and aims at developing a neutron inspection system for detecting threat materials in see-going cargo containers. Neutron interactions in the container produce specific gamma-rays used to determine the chemical composition of the inspected material. The use of D-T tagged neutrons allows the inspection of a suspect voxel identified by previous X-ray scan. The EURITRACK Tagged Neutron Inspection System (TNIS) elements have been recently integrated in the Neutron Laboratory of the Institute Ruder Boskovic (Zagreb, Croatia). The tested system mainly consists of a transportable sealed tube neutron generator, including a position sensitive YAP:Ce alpha detector, fast gamma-ray detectors, a front-end electronics to process alpha-gamma coincidence time and gamma-ray energy, and an integrated software to read-out and sort the data. The TNIS was extensively tested with several container fillings and hidden materials. The experimental data will be used to validate the Monte Carlo model used to design the TNIS, which is based on the MCNP computer code, in view to confirm the predicted performances. The comparison between experiment and simulation will be presented and discussed.

Introduction

The terrorist use of cargo containers has become, in recent years, a serious threat for civil populations. In complement to control systems based on X-ray or γ-ray radiography, which cannot provide information on the chemical composition of the inspected items, the EURITRACK project aims at developing an innovative Tagged Neutron Inspection System (TNIS) [1-2]. The container is irradiated with fan beams of 14-MeV neutrons produced by the $^{3}H(^{2}H,n)^{4}He$ fusion reaction in a transportable sealed tube neutron generator [3]. The beam is tagged by detecting the associated alpha particle produced in the reaction with a 8×8 matrix of YAP:Ce alpha crystals coupled to a multi-anode photomultiplier. The position of the alpha particle defines the neutron emission angle because they are emitted almost back-to-back. Neutrons undergo inelastic scattering on chemical elements of the cargo with emission of gamma-rays. The time delay between the hit in the alpha tracker and the detection of the produced gamma-rays determines the depth of the neutron collision. The analysis of the relative amounts of carbon, oxygen and nitrogen in the gamma-ray spectrum, produced in high-efficiency 5"×5" and 5"×5"×10" NaI(Tl) detectors located around the cargo container, makes possible to characterize the chemical composition of the inspected volume.
The general design and performances of the TNIS EURITRACK system were previously determined [4] using the MCNP Monte Carlo program [5]. A prototype of the TNIS has been assembled and tested at the Ruder Boskovic Institute (IRB) of Zagreb, Croatia. The numerical model and main calculation options have already been tested [7] and qualitatively validated [8] using experimental data collected with an early version of the TNIS where the tagged neutron beam was produced by the IRB line equipped with a reduced version of the alpha detector (4×4 YAP:Ce matrix instead of 8×8). Performance tests have been carried out recently with different container fillings and targets, using the full prototype including the transportable neutron generator [6]. The aim of the present work is to quantitatively validate the simulation method using the new experimental data.

Geometrical model of the experimental setup

The IRB experimental set-up and the associated MCNP geometry are shown in fig.1. A reference test has been carried out with a mixed target composed of a liquid nitrogen aluminium-dewar, two water bottles and six graphite blocks, simulating a 100-Kg TNT target hidden in the centre of 2-m long section of a container with full-scale 2.4×2.4-m² transversal cross-section. The latter is entirely loaded with a 0.2-g/cm^3 average density iron matrix, made of iron boxes filled with iron wire balls, surrounding the target elements.
Sixteen 5"×5"×10" NaI(Tl) top detectors are located in two rows above the container. Two 5"×5" NaI(Tl) reflection detectors are placed above the portable neutron generator. A small lead block is located just above the generator to protect the top detectors from direct neutron irradiation. On the other side of the container, two 5"×5"×10" NaI(Tl) transmission detectors are located on top of a composite iron-lead shield used during previous experiments.
Walls, soil, ceiling, paraffin and water tanks of the experimental room are also modelled in view to calculate the random background, as discussed in a next section.

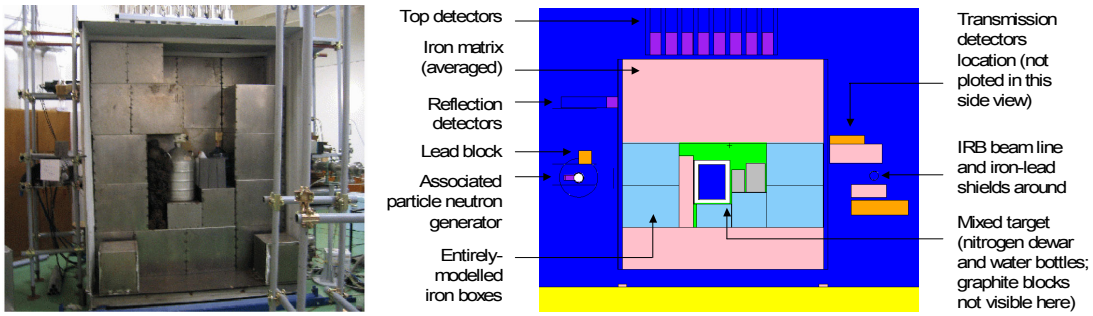

Figure 1. *Experimental setup (left) and associated MCNP model (right).*

Calculation vs. experiment comparison

Fig. 2 shows the alpha-gamma coincidence time of the top detectors with a 2-MeV low-energy threshold, and the energy spectra of the events within the [22-40 ns] target time window. Error bars of the experimental time spectrum are smaller than the marks. Error bars of calculation are discussed hereafter.

Coincidence time spectrum

The flat signal at negative time is due to random coincidences. The second peak at about 7-8 ns is related to the first walls of both the cargo container and the iron box located in front of the target along the beam axis. Then the signal of the wire balls filling can be observed, up to a small peak near 19-20 ns due to the second wall of the box. The main peak centred around 25 ns corresponds to the liquid nitrogen dewar and the smaller one at 34 ns comes from graphite and water. It is followed by another small bump after 40 ns related to the iron box located after the target. The last peak near 53 ns marks the second walls of this box and of the cargo container, and the large iron-lead shield located behind the container.
To obtain the MCNP spectrum, the probability to have a primary photon interaction in the gamma detectors, i.e. the photon flux (MCNP type-4 tally) has been calculated and multiplied by the Compton scattering and pair production cross-sections [7-8]. Alpha-neutron coincidence measurements were performed with an organic scintillator to determine the size of the tagged beam, which was then modelled with MCNP. The intrinsic time resolution of the TNIS is taken into account by broadening the calculated spectrum with a 2.8-ns FWHM Gaussian smearing function. A scaling factor is used to normalize the MCNP result to experiment, which includes the total number of alpha hits (i.e. of tagged neutrons) and takes account of the number of events filtered out by the data reduction software. A total of 2.17 10^9 alpha events were recorded during this long measurement (more than 12-hours). The filtering keeps 60% of the incoming events. Finally, to ease comparison with the experimental spectra, we added to the calculated data the mean random-background level observed at negative time in the experiment, which calculation is presented in the last section.

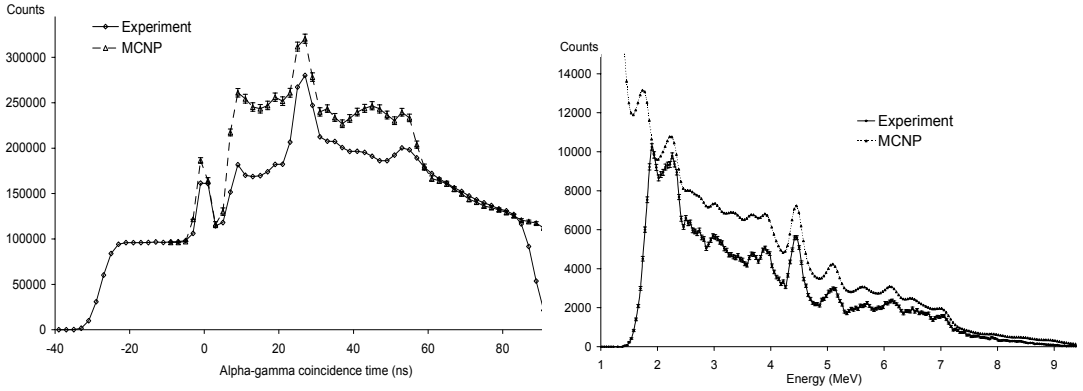

Figure 2. *Experimental and calculated coincidence time spectra of the top detectors (left) and energy spectra in the [22-40 ns] time window corresponding to the target hidden in the metallic matrix (right). The random background estimated in the negative time region has been subtracted from the experimental energy spectrum.*

The calculated coincidence spectrum correctly reproduces experiment, the main difference being an overestimation of the signal due to the iron boxes. The density of the wire balls inside the boxes has been averaged but does not consider local voids (air gaps) which may be present inside the boxes. To investigate this point, we computed the net area of the main 4.44-MeV peak of the energy spectrum (see fig.2 and next section) without and with iron matrix. The obtained ratio of 2.6 provides an estimation of the signal attenuation due to the matrix. The experimental value is about 1.9, which confirms the overestimation of the iron density in the model.
The small error bars of the calculated spectrum refer to Monte Carlo statistics, but the main source of uncertainty comes from the modelling precision. Geometry, density and chemical composition of the setup components are indeed of major importance, as well as the spatial distribution of the tagged beam. Other important uncertainties come from physical approximations in the simulation method and from the scaling factor, which depends on count losses in electronics and data processing. Though it is difficult to provide a justified uncertainty including all these aspects, calculation quite correctly reproduces the shape and order of magnitude of the time spectrum. The overestimation of the iron matrix signal could be reduced by refining the model of the iron boxes.

Energy spectrum
The energy spectra of the events selected in the [22-40 ns] time window show the characteristic peaks of the target elements: nitrogen (2.3- 3.7- 4.4- 5.1-, 7.0-MeV), carbon (4.4-MeV), oxygen (2.7- 3.7- 6.1-, 7.1-MeV), aluminium (2.2- and 3.0-MeV). Connected escape peaks also contribute significantly. Events below 2 MeV are cut by the electronic threshold.
The MCNP spectrum is obtained in a two-steps simulation. The photon flux generated by the tagged neutron beam in the location of the NaI(Tl) detectors is first calculated using the MCNP point detector tally (type-5 tally [5]). In the second step, this flux is used as a photon source to calculate the energy deposition in the NaI(Tl) crystals using the MCNP pulse-height tally (type-8 tally). In order to avoid modelling multiple photon incoming angles, only eight top detectors located above the target were selected to form the energy spectra of fig. 2. The photon direction is assumed to be perpendicular to the entrance surface. The energy resolution of the detectors is also taken into account in the calculated spectrum. For instance, a 5% FWHM broadening is considered for the 4.44-MeV full-energy peak. The factor used to scale calculation to experiment is the same as previously: $2.17\ 10^9 \times 0.6 = 1.3\ 10^9$.
Calculation error bars associated to Monte Carlo statistics are unpractical to compute in such a two-steps simulation. Anyhow, the observation of the statistics in each step show that they would be less than 10%, which is lower than the real uncertainty. Again, the latter is mainly related to the modelling precision and knowledge of the experimental scaling factor. We have not estimated this total uncertainty but the peaks and Compton continuum of the experimental spectrum are reproduced by calculation within a rough 30% discrepancy.

Total count rate and random background

The random background observed in negative time on fig. 2 can be deduced from the total count rate of the gamma-ray detectors, which has been calculated with two different methods. First, the photon flux multiplied by the Compton scattering and pair production cross-sections (type-4 tally) is computed for each detector. The integral on all energy bins, excluding the low energy region below 2 MeV, cut by the electronic threshold, is calculated and multiplied by the total neutron intensity of 7 10^6 n/s. A total count rate of 4.23 10^4 c/s is obtained, to be compared to the experimental value of about 4.77 10^4 c/s.

On the other hand, a calculation with a pulse-height tally (type-8 tally) for photons gives a value of 2.91 10^4 c/s, i.e. a factor 0.7 smaller than the first calculation, like in [8]. Type-4 tally is here closer to the measured total count rate, whereas type-8 tally provided a better agreement in [8]. It is therefore difficult to determine which method is more reliable. The neutron source was not the same here and in the previous study (transportable generator vs. IRB beam) and it was placed in a different environment (opposite sides of the container), as well as the reflection and transmission detectors. Neutron interactions in the environment (walls, ground, ceiling, other equipments) being an important fraction of the total count rate, the setup model should be as precise as possible. However, the complex geometry and lack of precise data about material densities and compositions are severe limitations. On the other hand, type-4 and type-8 tallies are intrinsically very different. Type-8 tally provides a representative description of the energy deposition in the detectors, which is not the case of the type-4 tally, but may produce unreliable results in neutron-photon transport problems due to the intrinsic non-analog nature of neutron transport in MCNP [5]. Its use for such neutron-photon transport and detection in NaI(Tl) detectors has required a specific validation [8].

In conclusion, both methods provide a good order of magnitude of the total count rate of the gamma-ray detectors and we keep the average result. Multiplying by the 1.3 10^9 scaling factor and the 2-ns channel width leads to a random background level of 8.47 10^4 counts per channel, to be compared to the experimental value of 9.63 10^4 counts per channel. The agreement is correct considering the limitations mentioned above about the model precision.

Conclusion

This calculation vs. experiment comparison confirms that MCNP simulation correctly reproduces the shape and magnitude of the time and energy spectra produced by the EURITRACK Tagged Neutron Inspection System (TNIS), as well as the random-coincidence and Compton backgrounds. This conclusion validates the predictive performances calculated during the design studies for reference inspection cases. The simulation tool could also be used to test and optimise the decision making algorithm [9], calibration procedures and extrapolate the TNIS performances to various other threat materials.

Acknowledgements

This work is supported by the European Union through the EURITRACK project (FP6-2003-IST-2 Proposal/Contract 511471).

References

[1] G. Viesti et al., "Projects for cargo inspection by using nuclear techniques in Europe", in CAARI-2006 International Conference on the Application of Accelerators in research and Industry, Fort Worth (USA), 20-25 August, 2006.
[2] B. Perot et al., "The EURITRACK project: development of a tagged neutron inspection system for cargo containers", in SPIE's International Symposium on Defense and Security, Orlando (USA), 17-21 April, 2006.
[3] S. Pesente et al., "Progress in tagged neutron beams for cargo inspection", same proceedings as [1].
[4] G. Perret et al., Journal of Physics: Conference Series 41 (2006) 375.
[5] J. F. Briesmeister, Editor, MCNP – A General Monte Carlo N-Particle Transport Code(Version 4C), LA-13079-M, Los Alamos National Laboratory, March 2000.
[6] C. Carasco et al., "The EURITRACK project: experimental tests of a Tagged Neutron Inspection System for cargo containers", this conference.
[7] A. Donzella et al., Journal of Physics: Conference Series 41 (2006) 233.
[8] A. Donzella et al., "Experimental validation of the calculated performances of the EURITRACK Tagged Neutron Inspection System", same proceedings as [1].
[9] P. Peerani et al., "The EURITRACK concept for cargo inspection with tagged neutrons", this conference.

A comparison of the neutron slowing down and reflection methods used for bulk hydrogen analysis

R. Dóczi [1,2], J. Csikai [1,2]

1) Institute of Experimental Physics, University of Debrecen, 4010 Debrecen-10, Pf. 105, Hungary
2) Institute of Nuclear Research of the Hungarian Academy of Sciences, 4001 Debrecen, Pf. 51, Hungary

drita@falcon.phys.klte.hu

Abstract: The advantages and limitations of two methods, namely the slowing down of epithermal neutrons in hydrogenous samples and the thermal neutron reflection have been compared for bulk hydrogen analysis. Therefore, in both cases the same sample dimension was used, i.e. 10 cm diam. and 8 cm height. It was found that the sensitivity of the slowing down method is higher by a factor of ~20 in average than that obtained by the neutron reflection technique.

Experimental procedure

The importance of the bulk hydrogen analysis and the related techniques and methods have been described in detail elsewhere [1,2]. The principle of the neutron slowing down and the neutron reflection techniques can be found in several references [3-6]. In the present experiment neutrons thermalized by the hydrogenous samples have been detected by the foil activation method using the $^{164}Dy(n,\gamma)^{165}Dy$ reaction, while for the reflection technique a small BF_3 counter was applied. The two measuring arrangements are shown in Fig. 1. As shown in Fig. 1 the PuBe neutron sources of different intensities were placed in hydrogenous moderator along the central line below the sample. The samples were placed in Cd holders of 10.2 cm diameter and 8 cm height assuring the analysis of a sample dimension of about 1 litre. For the reflection arrangement the Cd box was opened at the BF_3 detector side in order to cross the interface between the moderator and the reflector by the thermal neutrons. In both cases a 30 cm diam. and 40 cm height ε-caprolactam moderator and shielding was applied.

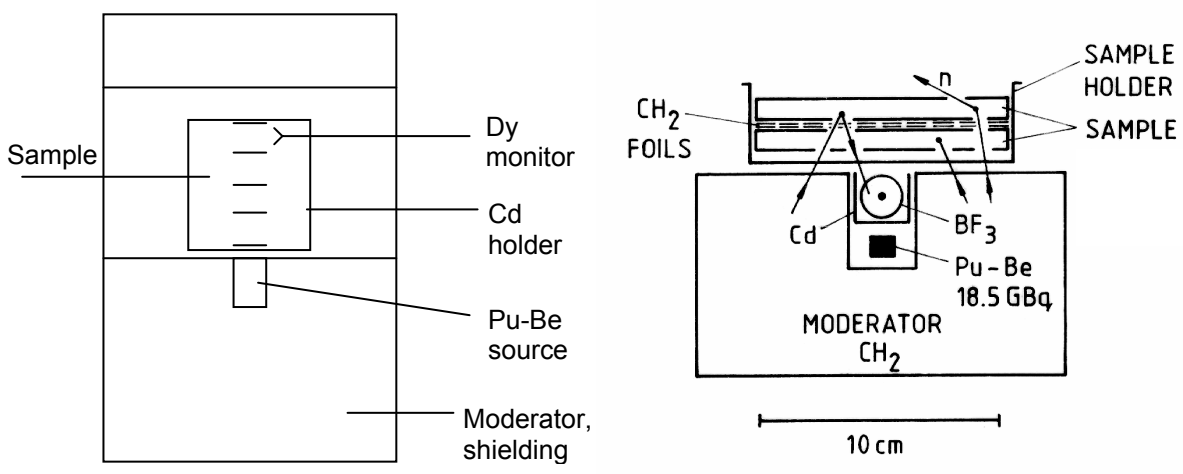

Figure 1. *Irradiation arrangements for bulk hydrogen analysis using the slowing down of epithermal neutrons (left) and the thermal neutron reflection methods (right).*

Results and discussion

The present measuring arrangement based on the slowing down of epithermal neutrons in hydrogenous samples as shown in Fig.1 has been improved to that applied in our previous experiments [4,5]. It was found that the flux distribution of thermalized neutrons in a sample dimension of ~ kg and liters can be determined by the simple foil activation technique. The axial flux distributions measured along the central line of the samples by Dy foils have been approximated by a second order polynomial. The flux values averaged over the sample, <F> were determined by the usual way [3]. The relative excess flux values, $R=(<F>-<F_0>)/<F_0>$ are based on the experiments performed with <F> and without $<F_0>$ a sample.
A strong correlation was found between the relative excess flux and the hydrogen content of the given sample. The calibration curve of the system was measured using different types of hydrogen standards, such as polyethylene (CH_2), polystyrene (C_8H_8), ε-caprolactam ($C_6H_{11}ON$), plexi glass ($C_5H_8O_2$), paraffin (CH_2), water (H_2O), ammonium-nitrat (NH_4NO_3), etil-alcohol (C_2H_5OH). The calibration curve shown in Fig. 2 rendered the determination of hydrogen concentration for example in oils and coals of different origins possible.

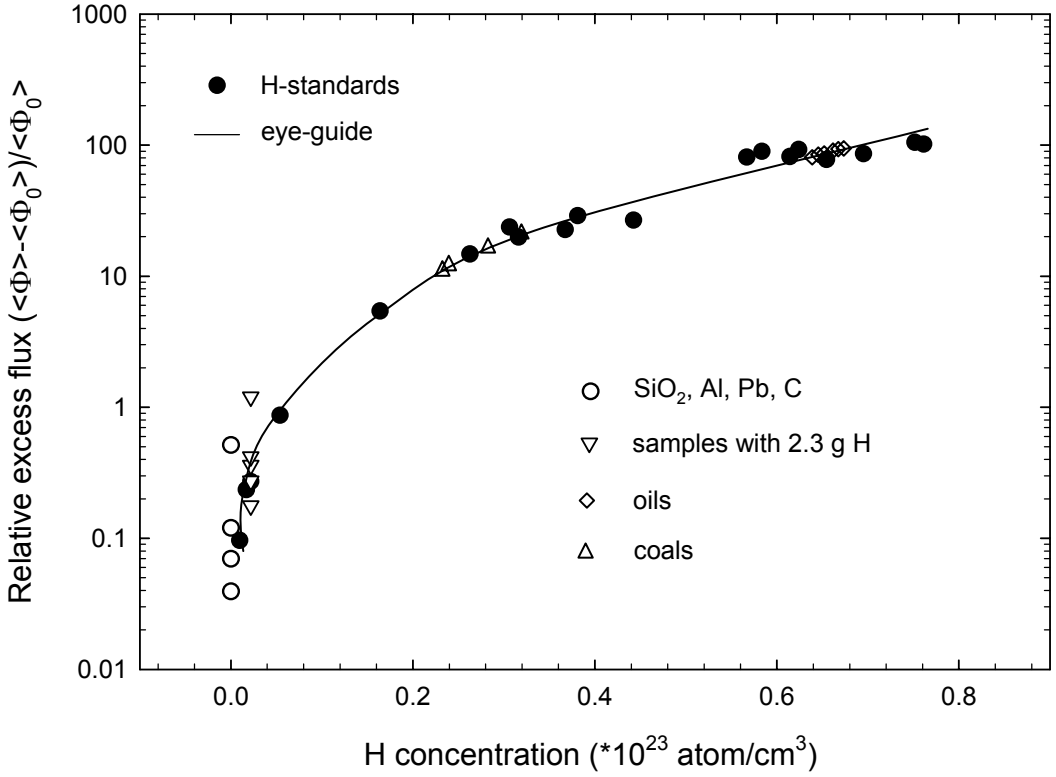

Figure 2. *Average excess neutron flux, R vs. hydrogen concentration, C_H measured by Dy foils using a Cd box.*

The sensitivity of this improved method is higher by a factor of ~20 in average as compared to the reflection method. The results of the comparison of the neutron slowing down and reflection methods are demonstrated in Fig. 3. It should be noted that not only the sensitivity for hydrogen is higher for the slowing down technique as compared to the reflection method but also in this case the matrix effect can be neglected. This clearly indicates in Fig. 2 at zero hydrogen content for different matrices.

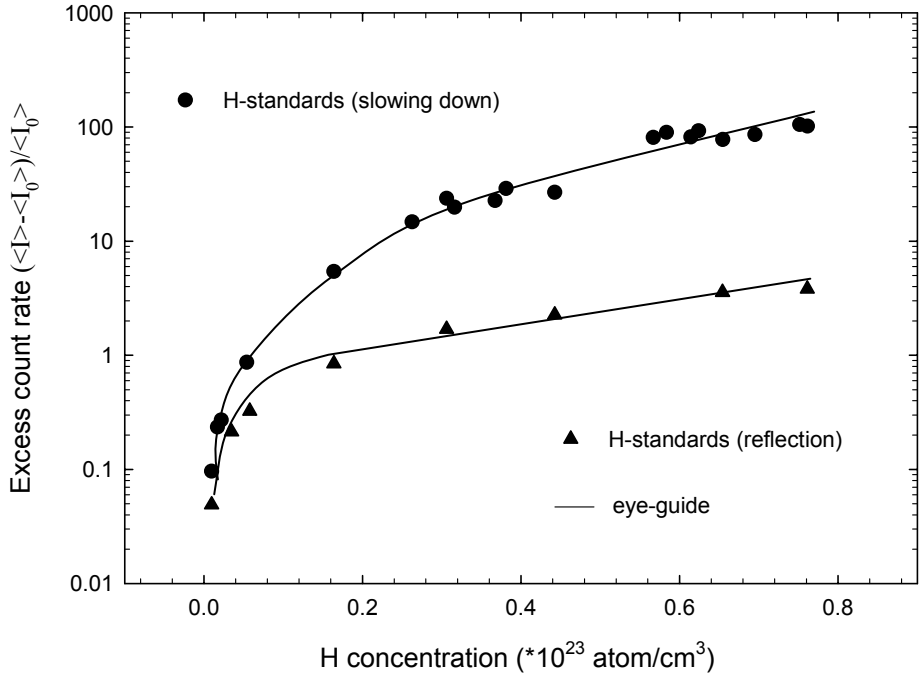

Figure 3. *Comparison of the sensitivity of the neutron slowing down and reflection methods.*

Furthermore, the simple second order polynomial obtained for the description of thermal neutron flux distributions inside the samples requires the knowledge of the flux values only in three points, i.e. for example at the two edges and the centre of the sample. Therefore, replacing the activation foils with prompt neutron counters (e.g. BF_3) can assure a routine application of this method for bulk hydrogen analysis needed in science and technology.

References

[1] Bulk Hydrogen Analysis Using Neutrons, Final report of the First Co-ordinating Meeting, IAEA/PS/RCM97-1, Vienna, Austria, 1997.
[2] Bulk Hydrogen Analysis Using Neutrons, Report of the Third Research Co-ordinating Meeting 23-26 October 2000, F1-RC-655.3, IAEA, Vienna, Austria, 2001.
[3] B. Király, T. Sanami, J. Csikai, Advantages and limitations od thermal and epithermal neutron activation analysis in bulk samples. Appl. Radiat. Isot. 58. (2003) 691.
[4] J. Csikai, R. Dóczi, B. Király, Investigations on landmine detection by neutron-based techniques. Appl. Radiat. Isot. 61. (2004) 11.
[5] R. Dóczi, M. A. Ali, M. Fayez-Hassan, J. Csikai, Determination of hydrogen content in bulk samples using the neutron activation method, Applied Radiation and Isotopes 63 (2005) 137-140.
[6] R. Dóczi, J. Csikai, T. Sanami, M. Fayez-Hassan, Bulk Hydrogen Analysis Using Epithermal Neutrons, Journal of Radioanalytical and Nuclear Chemistry, Vol. 266, No 1 (2005) 11-17.

Contribution of NAA to the certification of reference materials for inorganic trace analysis

R.S. Dybczyński

Department of Analytical Chemistry, Institute of Nuclear Chemistry and Technology, 03-195 Warszawa, Dorodna 16, Poland
rdybczyn@ichtj.waw.pl

Abstract: Certified reference materials (CRMs) play nowadays an important role in quality assurance for analytical chemistry and contribute significantly to the global harmonization of chemical measurements. Neutron activation analysis (NAA) owing to its generally good accuracy, freedom from blank and multielement capability have always significantly contributed to the process of certification of reference materials for inorganic trace analysis. Examples of such contributions in earlier and recent interlaboratory intercomparisons aimed at certification of the candidate reference materials are presented and discussed. Definitive methods based on the special radiochemical version of radiochemical NAA devised in this Department are characterized by high accuracy and deserve to be recognized as primary methods of measurement and can be considered as an option or alternative to ID-MS methods. Examples of using definitive methods by RNAA to confirm the validity of certified values established in the course of interlaboratory comparisons are given. NAA has been also frequently employed as a suitable technique for checking homogeneity of the candidate reference materials.

According to the latest ISO definition: Certified reference material (CRM) – is an RM characterized by a metrologically valid procedure for one or more specified properties, accompanied by a certificate that states the value of the specified property, its associated uncertainty, and a statement of metrological traceability [1].
CRMs are an indispensable element of quality assurance in analytical chemistry as a whole and in trace analysis in particular.
Neutron activation analysis (NAA) has always played an important role in the certification of RMs in which “recommended” (certified) and “information” values were established on the basis of worldwide interlaboratory comparisons [2-4]. This is illustrated in Fig.1. As can be seen, the share of results provided by NAA in the case of solid samples invariably exceeded

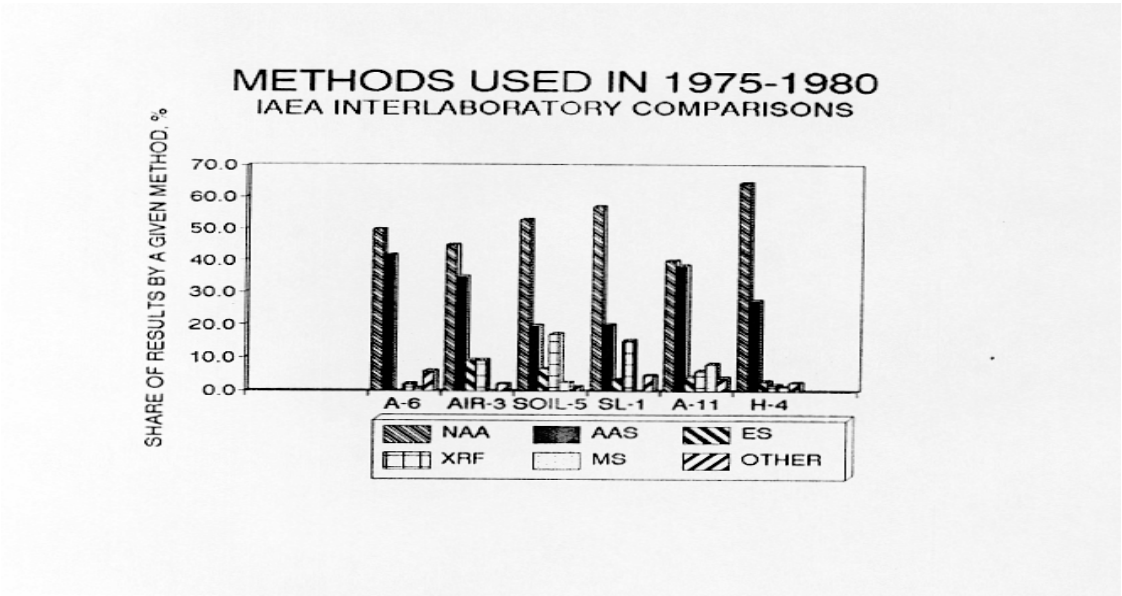

Figure 1. *Percent contribution of various analytical techniques in several earlier intercomparisons organized by International Atomic Energy Agency (IAEA)*
A-6 –Fish solubles; Air-3 – Simulated Air Filters; Soil-5 – Peruvian Soil;
Sl-1 – Lake sediment; A-11 – Milk powder; H-4 – Animal muscle

40% and in some cases was even over 60%. The second most frequently employed technique was Atomic absorption spectrometry (AAS), usually followed by X-ray fluorescence (XRF), Emission spectroscopy (ES) and mass spectrometry (MS) and an array of less frequently used techniques as e.g. electrochemical, chromatographic etc. methods (Other).
As can be inferred, among others, from the intercomparisons organized by the Institute of Nuclear Chemistry and Technology (INCT), similar situation lasted till the beginning of the nineties of the last century [3]. In the last decade this trend was slightly reversed because of emerging and rapid development of new techniques like ICP-OES and ICP-MS on one hand and significant diminishing of research establishments which use and develop NAA method. Even then the total share of NAA amounted to *ca.* 30% which gave it second place among the various methods after AAS [4,5].
Fig.2 shows how the share of various methods for Zn (which was never the most convenient element for NAA) changed with time when analyzing the same material i.e. CTA-OTL-1 Oriental Tobacco Leaves , first as a intercomparison sample (1991) and then as a reference material (the identity of which was unknown to the participants : 2000 and 2004) [6].
The increase of significance of ICP-OES and ICP-MS is apparent while NAA still manages to keep the prominent position.

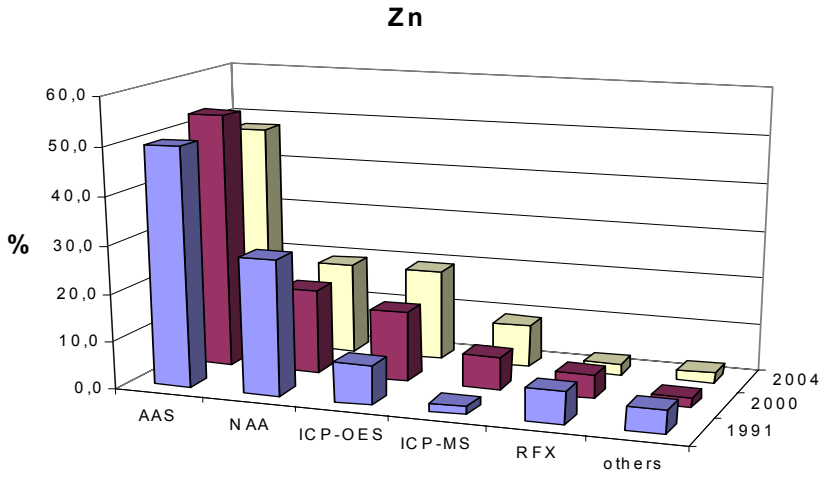

Figure 2. C*hanges of frequency of use of different techniques for the determination of zinc in interlaboratory comparisons in the same material over the period of 13 years*

It is worth noting that also in the practice of leading CRM producers as NBS/NIST, which rely in the certification process exclusively or mostly on their own analytical results, NAA have always played a prominent role [7,8].
The reason that NAA provided much greater share of analytical results in international intercomparisons than it could be expected on the basis of a real portion of results obtained by NAA in routine applications, even at the time of its greatest popularity, are unique merits of this method [5,7], Most important among them is the freedom from blank and good accuracy, i.e. substantial freedom from systematic errors, multielement capability, possibility of non-destructive analysis of solid samples, good selectivity and good detection limits for many elements as well as easy calibration with elemental standards.
Another contribution of NAA to the certification of RMs are the methods of “guaranteed accuracy” based on a special version of radiochemical neutron activation analysis (RNAA).
Such “definitive” methods, which as was shown in a recent publication [9] are equivalent to “Primary methods of Measurement) (PMMs) and can constitute an option or alternative to ID-MS methods, are constructed by combining neutron activation with highly selective and quantitative isolation of an indicator radionuclide by column chromatography followed by γ-ray spectrometric measurement.
The analytical scheme for the definitive method for the determination of cobalt in biological materials is shown in Fig.3.

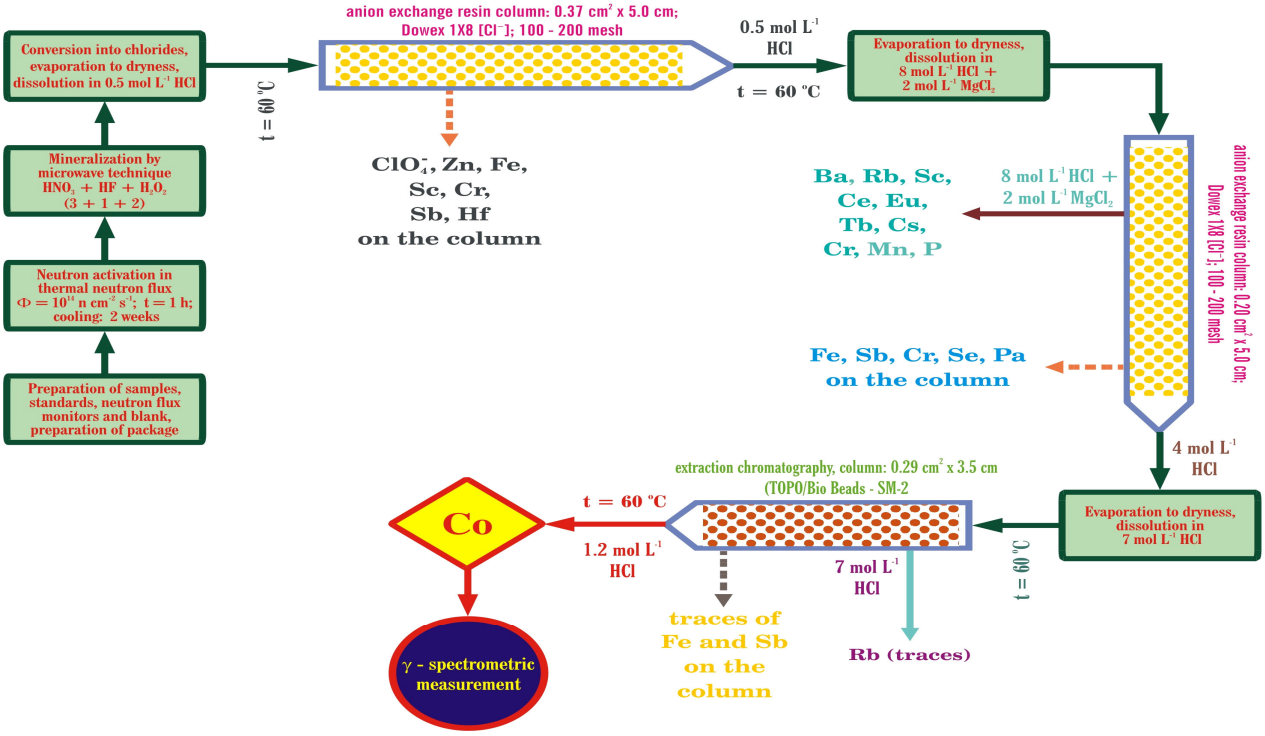

***Figure 3**. Definitive method for Co by RNAA*

The example how the definitive method is used for the verification of the correctness of certification is shown in Fig.4.

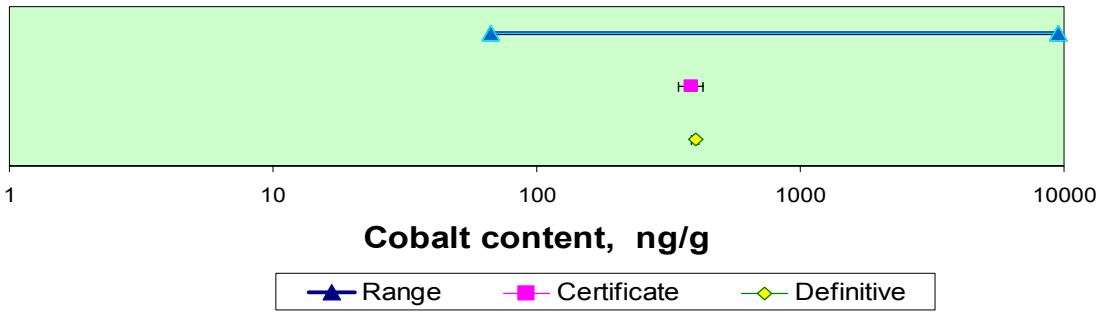

***Figure 4.** Comparison of the certified value for Co in INCT-TL-1 (Tea Leaves) CRM with the result by definitive method and original range of results supplied by laboratories in the interlaboratory comparison*

NAA is also a convenient tool to study homogeneity of the candidate RMs.
One of the ways of numerical expressing homogeneity is Ingamells' sampling constant, K_s , [10, 11] defined as:

$$K_s = R_s^2 \bullet m$$

where: R_s^2 is sampling variance and m is sample mass.
Sampling variance can be calculated by subtracting analytical variance from the overall variance. If the measurements aimed at estimation of sampling variance are done by INAA all components of analytical variance can be conveniently evaluated. The details of the procedure can be found in references [10] and [11].

References

[1] ISO/REMCO April 2005.
[2] R. Dybczyński, J. Radioanal.Chem., 60, 45 (1980).
[3] R. Dybczyński, Fresenius J. Anal. Chem., 352, 120 (1995).
[4] R. Dybczyński, B. Danko, K. Kulisa, E. Maleszewska, H. Polkowska-Motrenko, Z. Samczyński, Z. Szopa, Czech.J.Phys., 53 (Suppl.A) A171 (2003).
[5] R. Dybczyński, The position of NAA among the methods of inorganic trace analysis in the past and now, in: NEMEA-2, Proceedings of the enlargement workshop on Neutron Measurements, Evaluations and Applications, 20-24 Oct., 2004, Bucharest, Romania, A.J.M.Plompen Ed., Report EUR 22136 EN, European Communities, Luxembourg, 2005.
[6] H. Polkowska-Motrenko, R. Dybczyński, J. Radioanal. Nucl. Chem., 269, 339 (2006).
[7] R.M. Lindstrom, Nuclear Analytical Methods in Standards Certification, in: Comparison of Nuclear Analytical Methods with Competitive Methods, IAEA-TECDOC-435, IAEA, Vienna, 1987.
[8] R. Zeisler, E.A. Mackey, G.P. Lamaze, T.E. Stover, R. Oflaz Spatz, R.R. Greenberg, J. Radioanal. Nucl. Chem. 269, 291 (2006).
[9] R. Dybczyński, B. Danko, H. Polkowska-Motrenko, Z. Samczyński, RNAA In Metrology: A Highly Accurate (Definitive) Method, Talanta 2006 (in press).
[10] R. Dybczyński, B. Danko, H. Polkowska-Motrenko, J. Radioanal. Nucl. Chem. 245, 97 (2000).
[11] R. Dybczyński, B. Danko, H. Polkowska-Motrenko, Fresenius J. Anal. Chem., 370, 1126 (2001).

The cross sections for (n,x) nuclear reactions on zirconium and germanium isotopes

N. Dzysiuk[1)], S. Begun[1)], I. Kadenko[1)], V. Maidanyuk[1)], G. Primenko[1)]

1) National Taras Shevchenko University of Kyiv, Department of Nuclear Physics, Kyiv, Ukraine
dzysyuk@univ.kiev.ua

Abstract: Investigation of neutron reaction cross section at the energy range about 14 MeV is important for development of fusion reactor technology from the point of view of activation, radiation-damage and mechanical stability of construction materials as well as radiation protection etc. Furthermore, measurements of nuclear reaction cross sections in this energy region are of great value for testing nuclear reaction models. All measurements have been carried out with neutron activation method. The samples in a shape of foils of natural zirconium have been irradiated by DT- neutrons. Instrumental gamma-spectra of activation products have been measured using spectrometer with HPGe detector. The following factors are taken into account: instability of neutron flux in time, real geometry of experiment, the effect of true coincident summing of gamma-quantum during activation products spectrum measurements and the effect of self-absorption of gamma-quantum in a sample. The average neutron energy has been determined experimentally with Zr/Nb method. The cross sections of nuclear reactions ^{92}Zr (n, p) ^{92Y} and ^{94}Zr (n, p)^{94}Y were measured in the neutron energy range 13.56÷14.53 MeV. The discrepancies between existing results from different experimental groups in the selected energy range for the specified nuclear reactions are within 20÷60 %. The results obtained could be useful to avoid ambiguity in values of cross sections for nuclear reactions specified and to indicate the necessity of additional experiments to reduce the cross sections' determination uncertainty. In order to address a gap of EXFOR data base information regarding ^{72}Ge(n,2n)^{71}Ge reaction cross sections of specified nuclear reaction have been measured. Such information for the first time can be introduced into the modern data bases.

Introduction

Nowadays precise determination of cross sections has taken prevalent place in modern nuclear spectroscopy. Zirconium is the constructive material which is widely used in construction of present and future nuclear reactors. That is why extensive knowledge of cross sections's values of different nuclear reactions on these isotopes in wide energy range is very important for safe operation of nuclear power plants. In one's turn germanium is the element which widely used in construction of detectors. Regardless of the fact that there are many investigations performed which are devoted to neutrons interactions with zirconium and germanium isotopes, there is still essential discrepancy observed between obtained results. The discrepancy in ^{92}Zr(n, p)^{92}Y and ^{94}Zr(n, p)^{94}Y cross-sections is within 20÷60 % in the investigated energy range. Moreover, these results do not match at all in the 13.3÷14.3 MeV energy range. There is a need to emphasize that for reactions ^{70}Ge(n,p)^{70}Ga and ^{72}Ge(n,p)^{72}Ga there only several papers available with poor results contingency. Also the determination of precise value of cross-sections for germanium isotopes demands for Monte Carlo simulation of absolute effectiveness of HPGe detector [1]. The choice of ^{72}Ge(n,2n)^{71}Ge nuclear reaction for investigation is considered due to lack of such information in nuclear experimental data base. Moreover such a discrepancy between results leads to errors during interpolation of experimental data and influences on the quality of estimated data. Thus, these nuclear reactions are subjected in the present paper.

Experimental method

Determination of all cross sections was performed using neutron-activation method. Samples in the foil shape of natural germanium and zirconium isotopes have been irradiated by DT neutrons. The neutron generator NG-300/15, which built at the Department of Nuclear Physics, University of Kyiv, has been used as a source of fast neutrons. It is an electrostatic accelerator of charged particles (deuterons). It has been made two series of experimental

measurements. First measurements of excitation function for zirconium isotopes were performed and second - cross sections for reaction ^{72}Ge(n,2n)^{71}Ge, ^{70}Ge(n,p)^{70}Ga and ^{72}Ge(n,p)^{72}Ga only for 14.53 MeV neutron energy were measured. All instrumental spectrums of nuclear products have been measured with HPGe spectrometer. The maximum current of ions beam is 10 mA. Neutrons with energy ~ 14 MeV are generated in T(d, n)^{4}He reaction. For this purpose a molecular component of deuteron beam D_2^+ has been used. A diaphragm, which gave an opportunity of getting beam diameter 10 mm, has been used to decrease disperse of neutron energy in ion-pipe that allows to use different parts of sample after every irradiated series. Location of deuteron beam axis has been defined from distribution of neutron flux density on the target by method of foil activation. The average neutron energy have been determined experimentally using Zr/Nb ratio [2]. Contribution of scattered neutrons wasn't taken into account, because threshold of specified nuclear reaction is higher then 2.8MeV. Zirconium samples were irradiated under 0, 30, 120 and 150 degrees angles relative to deuteron flux direction on 75 mm distance from Ti-T target. The average neutron flax density was ~ $1.3 \cdot 10^7$ neutrons/cm^2. Magnitude of neutron flax density was kept constant with accuracy ≤ 5 %. Time of irradiation has been chosen in range of 10-80 min. All instrumental spectrums have been measured by HPGe detector with sensitive volume of ~110 cm^3 and single-board analyzer SBS-30. Detector was placed in 50 mm thick lead shielding. Energy resolution was determined as 2.1 KeV γ1332 KeV ^{60}Co and 1.2 KeV for γ122 KeV ^{152}Eu. During calibration procedure the coincident summing effect has been considered using early developed methodology [3]. Cross sections have been determined by relative method and reactions ^{90}Zr(n, 2n)$^{89(g+0.9377m)}$Zr and ^{70}Ge(n,2n)^{69}Ge have been selected as monitor ones. Usage of such a monitor gives essential advantage because inner monitors lead to decrease errors caused by incomplete knowledge of irradiation geometry, geometry of spectrums measurements and assumption of uniform volume distribution of activity. Because of thickness of germanium samples (2 mm) it was very important to take into account self-absorption effect, which is calculated by method [4]. Identification of activation products has been implemented varying the irradiations conditions and measuring conditions. The information about decay of nuclear activity has been taken from data bases [5].

Results of measurements

In the Table 1. the determined values of cross sections of ^{92}Zr(n, p)^{92}Y, ^{94}Zr(n, p)^{94}Y ^{70}Ge(n,p)^{70}Ga, ^{72}Ge(n,p)^{72}Ga, ^{74}Ge(n,a)^{71m}Zn are presented. The comparison of results with resent experiments showed on Figure 1 and Figure 2. Overestimation of results of Japanese group (Ikeda, 1988; Katoh, 1989 [Exfor]) in the case of ^{92}Zr(n, p)^{92}Y reaction can be explained by missing the existence of niobium impurity in zirconium samples. Underestimation of results in the case of ^{94}Zr(n, p)^{94}Y can be explained by not enough good energy resolution of gamma-spectrometer.

Table 1. *Measured cross sections*

Nuclear reaction	*Neutron energy, MeV*	*Cross section, mb*
^{92}Zr(n,p)^{92}Y	13.56	14.3(23)
	14.53	19.8(22)
^{94}Zr(n,p)^{94}Y	13.56	8.3(18)
	13.69	8.7(15)
	14.53	8.8(6)
^{70}Ge(n,p)^{70}Ga	*14.53*	*169(16)*
^{74}Ge(n,a)^{71m}Zn	*14.53*	*6.9(3)*
^{72}Ge(n,p)^{72}Ga	*14.53*	*55.5(15)*

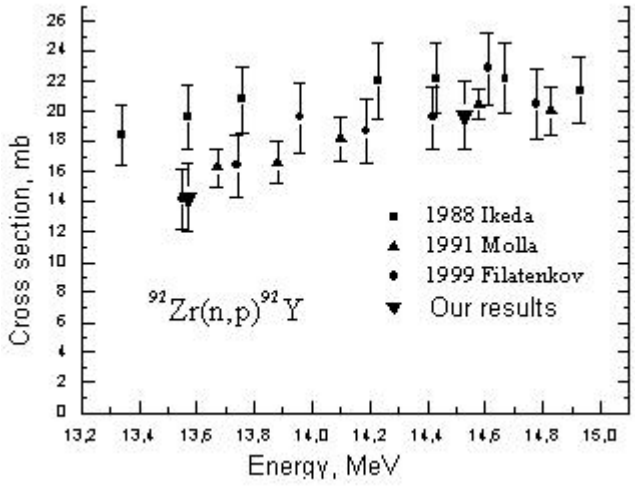

Figure 1. *Results of cross section's for $^{92}Zr(n,p)^{92}Y$*

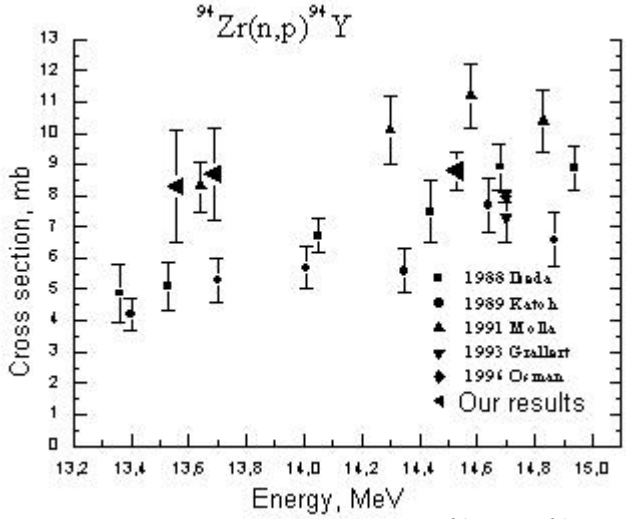

Figure 2*. Results of cross section's for $^{94}Zr(n,p)^{94}Y$*

Determination of cross section of nuclear reaction $^{72}Ge(n,2n)Ge^{71}$

The essential part of the present work is the investigation of $^{72}Ge(n,2n)Ge^{71}$ nuclear reaction. This task is quite complicated, because the product of reaction is a nucleus Ge^{71} which do not emit prompt gamma-quantum at excited state but decays only by electron capture channel. The decay scheme of ^{71}Ge is presented on Figure 3. The half-life of Ge^{71} is 11.4 days. The cross section has been determined by detection of gallium X-ray with energy 9.252 KeV. Germanium sample with 10 mm diameter have been irradiated by neutron flux on neutron generator close to Ti-T target. The time of irradiation was 80 min, with further cooling time of 23 days. During this cooling time the activities of others reaction products with half-time life less then 10 days, entirely decayed. Time of germanium foil measurement was determined as 19 hour. A niobium foil has been irradiated simultaneously and measured under the same conditions for simplification of geometrical factor calculation. Spectrum has been measured with Si(Li) detector. Before entering sensitive volume a gamma-quantum passed through a collimator with 4 mm diameter and 4.5 mm length. The collimator located at 30 degree angle to vertical direction. This detector is very sensitive in X-Ray range, and it's energy resolution gives a possibility to distinguish X-Rays of neighbor nuclei.

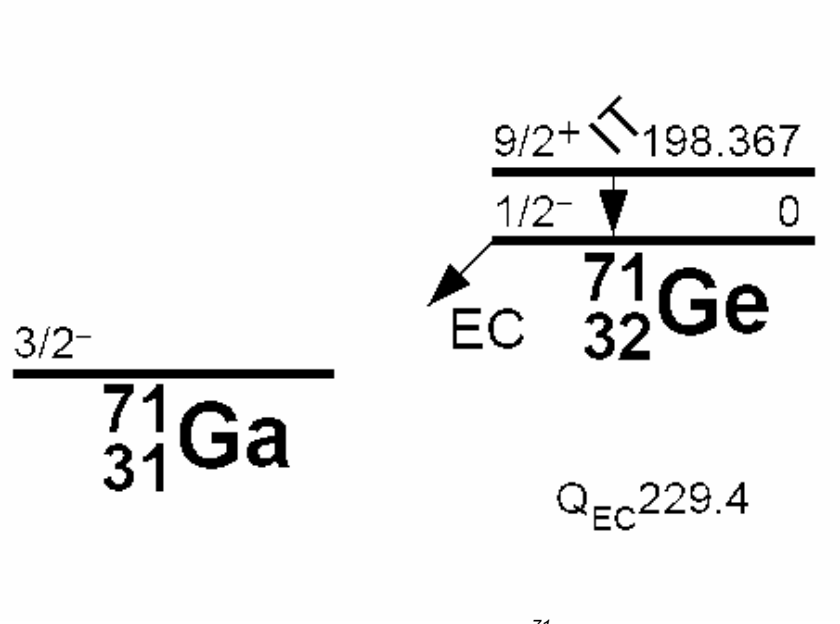

Figure 3. *Decay scheme of the ^{71}Ge nucleus*

The absolute efficiency of this detector for 5-20KeV energy range is ~ 100%. Full energy peak was acquired with 696±34 events. But for correct peak area determination, self-absorption effect must be taken into account [4]. This correction has been performed considering real geometry, effective working sample part and solid angle dΩ between collimator and sample. The energy of used X-Rays is not high and absorption in the sample with 700 microns thickness is essential, that is why this correction has strong influence on the final results of calculations. The assumption of uniform activity distribution has been made. The value of this reaction cross section has been roughly estimated ~ 952 ±252 mb.

Conclusions

The series of measurements confirm the effectiveness and selectivity of neutron-activation method. The results of measurement of cross sections of nuclear reactions ^{92}Zr(n, p)^{92}Y and Zr(n, p)^{94}Y in range of 13.5÷14.6 MeV neutron energy is present in this work. Obtained results can be considered as important aspect in the process of estimated data calculation and provide more correct determination of cross section values for these reactions. The preliminary result regarding ^{72}Ge(n,2n)Ge^{71} reaction has pointed out the possibility of correct cross section evaluation by presented method. In order to obtain final results it is necessary to evaluate the contribution of scattered neutrons for consideration of interfering (n,γ) reaction on Ge^{70}, which also leads to Ge^{71} generation. The optimization of further experiments is planned by research group.

References

[1] R.G. Helmer, J.C. Hardy, V.E. Iacob The use of Monte Carlo calculations in the determination of a Ge detector efficiency curve. Nuclear Instr. and Methods in Physics Research A 511(2003) 360-381.

[2] H. M. Agrawal and R. Pepelnik. Determination of the mean neutron energy using the Zr/Nb and the Ni method, Nuclear Instrum. and Methods in Physics Research. A – 1995. – Vol. 366, Pages 349-353.

[3] Sima O., Arnold D. Accurate computation of coincidence summing corrections in low level gamma-ray spectrometry, Applied Radiation and Isotopes. – 2000. – Vol. 53. – p. 51–56.

[4] Norman H. Cutsall, Ingvar L. Larsen. Direct analysis of ^{210}Pb in sediment samples: self-absorption corrections Nuclear Instrum. and Methods in Physics Research 206(1983) 309-312.

[5] 349–353Cross section information storage and retrieval system (EXFOR), National Nuclear Data Center (NNDC), Brookhaven National Laboratory, USA. – http://www.nndc.bnl.gov/index.jsp, (online).

Neutron cross-section measurements on ^{103}Rh and ^{133}Cs for improved nuclear criticality safety

L.C. Mihailescu[1)], A. Borella[3)], R. Capote[4)], K. H. Guber[2)], I. Ivanov[1)], S. Kopecky[1)], L. C. Leal [2)], P. Schillebeeckx[1)], P. Siegler[1)], I. Sirakov[1,6)], R. Wynants[1)]

1) European Commission, Joint Research Centre, Institute for Reference Materials and Measurements, Retieseweg 111, 2440 Geel, Belgium
2) Oak Ridge National Laboratory, P.O. Box 2008, Oak Ridge, TN 37831-6356, USA
3) CEA DAPNIA/SPhN F-91911 Gif-sur-Yvette Cedex, France
4) IAEA Nuclear Data Section, Wagramer Strasse 5, A-1400 Vienna, Austria
6) Institute for Nuclear Research and Nuclear Energy, 1784 Sofia, Bulgaria

Liviu.Mihailescu@ec.europa.eu

Abstract: New transmission and capture cross-section measurements were performed at GELINA for ^{103}Rh and ^{133}Cs. These experiments are part of a series of measurements that are planned to improve the evaluations of the nuclear data for the present nuclear power plants and for criticality safety of spent fuel storage and transport. The detection system was based on C_6D_6 detectors for the neutron capture experiment and on ^{6}Li-glass detectors for the neutron transmission experiment. Samples with different thicknesses were used. The useful energy range for this experiment was from 20 eV to about 150 keV. In the Resolved Resonance Region (RRR) a resonance shape analysis was done with the code REFIT [1], while in the Unresolved Resonance Region (URR) the data was interpreted in terms of average resonance parameters.

Introduction

Improved capture and total cross sections for several fission products (i.e. ^{103}Rh, ^{133}Cs, ^{143}Nd, ^{149}Sm, ^{151}Sm, ^{155}Gd and ^{131}Xe) are on the NEA High Priority Nuclear Data Request List [2]. They are motivated by the objective to extend and optimize the operation of present nuclear power plants and for criticality safety studies of spent fuel storages. Collaboration has been started between the IRMM Geel (B) and the ORNL (USA), with initial measurements at GELINA for ^{103}Rh and ^{133}Cs. To improve the above-mentioned data, the capture cross-section was measured at the 28.8 m flight path length and the total cross-section was measured at 50~m flight path length. The pulsed white neutron spectrum from GELINA (Geel Linear Accelerator) was used. GELINA delivers neutron burst with a full width at half maximum of less than 1 ns, which, in combination with fast detectors allow a very good neutron energy resolution.

Experimental setup

Capture measurements: The capture experiments were performed at 28.8 m flight path length and 800 Hz repetition rate of GELINA. The shape of the neutron spectrum was measured with a double Frisch-gridded ionization chamber loaded with ^{10}B. Two C_6D_6-based liquid scintillators (NE230 with 10 cm diameter and 7.5 cm height), placed at 125^{o} with respect to the direction of the neutron beam, were used to detect the neutron capture gamma rays. A pulse height weighting function was used to make the detection efficiency for a neutron capture event proportional to the total energy released in the capture event. The weighting function was determined using a Monte Carlo simulation [3]. The capture cross-sections was measured for two metallic samples of ^{103}Rh with thicknesses of $3.36\cdot10^{-3}$ at/b and $1.86\cdot10^{-3}$ at/b and one powder sample of Cs_2CO_3+S. The effective thickness of the ^{133}Cs was $2.34\cdot10^{-4}$ at/b. The background for the C_6D_6 detectors was determined by additional measurements without the sample in position or with a dummy sample in the case of ^{133}Cs. The dead time of the detection chain was monitored by registering the time-interval distribution between different events. The time dependence of the background for the flux measurements was derived using "black" resonances.

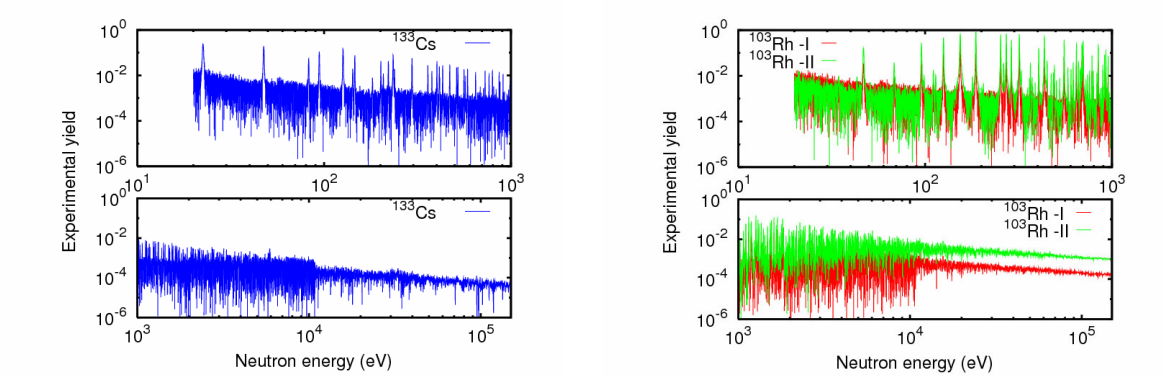

Figure 1. *Experimental capture yield. Left: ^{133}Cs sample with thickness of $2.34 \cdot 10^{-4}$ at/b. Right: ^{103}Rh-I samples had a thickness of $3.36 \cdot 10^{-3}$ at/b and ^{103}Rh-II had a thickness of $1.86 \cdot 10^{-3}$ at/b.*

Transmission measurements: The transmission experiments were carried out at a 50 m flight path with the accelerator operating at a 400 Hz operation frequency. The ^{103}Rh sample was placed in an automatic sample changer at a distance of 25 m from the neutron producing target. The neutrons were detected by a 6 mm thick NE912 Li-glass scintillator. The sample was a disc of metallic rhodium, with a thickness of $4.58 \cdot 10^{-2}$ at/b. A Cd filter was used to eliminate the slow neutrons of previous bursts. The background was measured at the "black" resonances of filters of Cd, Au, Co and Na.

Data reduction and results

The data reduction for both capture and transmission measurements was done with the AGS (Analysis of Generic t.o.f Spectra) code [4]. The code manipulates time of flight spectra and propagates the uncertainties from different spectra operation. The AGS code creates the covariance matrix for the output spectrum.

Capture measurements: For the capture cross-section the experimental yield is calculated from the dead time corrected response of the C_6D_6 detectors in the measurement with the sample and in the background measurement. The experimental yield is shown in Figure 1 for the 103Rh and 133Cs samples. The useful energy range for this measurement was from about 20 eV up to 150 keV. The quality of the new experimental data is shown in Figure 3. The new experimental yield for ^{103}Rh was compared with the calculation with REFIT [1] using the latest ENDF parameters. Two different resolution functions were used: an analytical one, used as default in REFIT [1] and a simulated resolution function obtained with MCNP [5]. The simulation contains a detailed description of the GELINA target and of the moderator around. A slight systematic difference was observed between the results obtained with the two resolution functions, but the difference was within the uncertainties of the data. No adjustment of the resonance parameters was done yet at this stage.

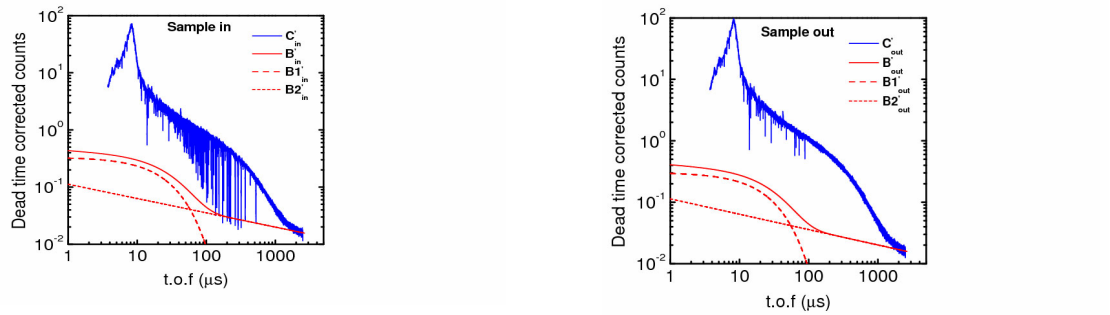

Figure 2. *The response of the Li-glass detector after the dead time correction in the two configurations: Left: sample in and Right: sample out. The two components of the background, B'_{in} and B'_{out}, are shown explicitly.*

Transmission measurements: The response of the Li-glass detector is given in Figure 2 for the two measurement configuration, sample in the beam and sample out of the beam. The transmission factor was determined from the dead time corrected response of the Li-glass detector in the configurations sample-in and sample-out. In the Unresolved Resonance Region (URR), the experimental transmission factor was averaged and compared with other experimental data and with evaluations (Figure 3). A Dispersive Coupled-Channel Optical Model Potential (DCCOMP) has been fitted to all available nucleon scattering data on ^{103}Rh, including the present measurements, following a well established methodology [6]. A derived DCCOMP was used to get information about the energy dependence of the potential scattering radius and neutron strength functions, allowing for a smooth transition of the cross section from the URR to the fast neutron region.

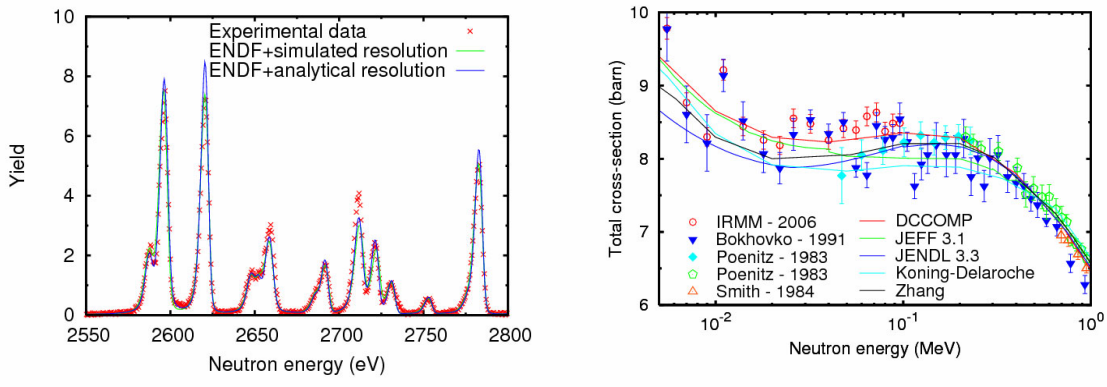

Figure 3. *Left: The present experimental capture yield was compared with the yield calculated using the latest ENDF resonance parameters with two different resolutions functions (see the text below). Right: ^{103}Rh total cross-section in the URR: Experimental data vs OMP calculations.*

Conclusions

New experimental data were obtained at GELINA for the capture and total cross-sections for two stable fission products (^{103}Rh and ^{133}Cs). Preliminary results from a RSA with REFIT are shown. All the experimental data will be interpreted in terms of resonance parameters, both in the RRR and URR. The new measurements will improve the evaluated databases due to a better statistics, better neutron energy resolution and larger number of samples with different thickness that are analyzed simultaneously. As a consequence of better neutron energy resolution the RRR will be extended to higher energies.

References

[1] M.C. Moxon and J.B. Brisland, Technical Report Harwell Laboratory, CBNM/ST/90-131/1 (1990).
[2] F. Storrer, Ph. Bioux, D. Biron, D. Hittner, J.M. Palau, B. Roque, J.M Ruggieri, A. Santamarina, H. Toubon, C. Traka and G. Willermoz, ND2001, J. Nucl. Sci. & Tech., Supplement 2, 1357 (2002).
[3] A. Borella, G. Aerts, F. Gunsing, A. Moens, R. Wynants and P.Schillebeeckx, Proceedings of ND2004, AIP Vol.769, 26 September - 10 October 2004, Santa Fe, USA, 2005.
[4] C. Bastian, A. Borella, F. Gunsing, J. Heyse, S. Kopecky, G. Noguere, P. Siegler and P.Schillebeeckx, Proceedings of PHYSOR-2006, 10-14 September 2006 , Vancouver, Canada.
[5] J. F. Briesmeister, MCNP^{TM} - A General Monte Carlo N-Particle Transport Code, Report LA-13709-M, LANL, USA (2000).
[6] E. S. Soukhovitskii, R. Capote, J. M. Quesada, S. Chiba, Phys.Rev. C72, 024604 (2005).

Upgrade of the setup for neutron inelastic scattering measurements at GELINA

A. Negret[1)], C. Borcea[1,2)], A.J.M. Plompen[1)]

1) European Commission, Joint Research Centre, Institute for Reference Materials and Measurements, Retieseweg 111, 2440 Geel, Belgium
2) IFIN "Horia Hulubei", P.O. Box MG-6, Bucharest-Magurele, Romania
alexandru-liviu.negret@ec.europa.eu

Abstract: The neutron inelastic scattering measurements program running at the GELINA facility produced high-quality results during the last years. However, it is possible to improve the present setup to decrease the measurement time of the experiments by increasing the detection efficiency.
Our latest efforts were pointed in the direction of increasing of the number of HPGe detectors. This is further facilitated by the migration towards digitised acquisition systems that provide a substantial simplification of the necessary electronic scheme together with an increase of the detection efficiency. In order to physically support more detectors around the target an aluminium frame was designed, produced and mounted at the 200 m flight path. It provides support for up to four detectors at each of the scattering angles of 110°, 125° and 150°. The new setup will allow reduced measurement times for the inelastic scattering experiments and could represent also a powerful spectroscopic device.

Introduction

The inelastic interaction of the neutron with the nucleus produces gamma radiation and reduces the energy of the incident particle. The phenomenon accounts for a significant part of the total interaction cross section and therefore the knowledge of the cross sections associated to it is important for numerous applications. We refer to the total inelastic cross section but also to the gamma and level production cross sections which are of importance e.g. for shielding calculations. Additionally, the X(n,2nγ) and occasionally the X(n,3nγ) channels are investigated.
During the last years a neutron inelastic scattering measurement program running at the GELINA time-of-flight facility of IRMM produced very precise high resolution nuclear data on ^{52}Cr, ^{58}Ni, $^{206, 207, 208}$Pb and ^{209}Bi. The typical uncertainty of the main cross sections was of the order of 5%.
The normal duration of a data-taking campaign was of the order of two months. Taking into account the success of the previous measurements and the need for new improved data, we decided to increase the detection efficiency by upgrading the setup. Two major possibilities exist: the increase of the number of detectors and the upgrade of the acquisition system. We addressed both these approaches.

Detection setup and main experimental problems

The measurements take place in the cabin situated on Flight path 3 of GELINA at a distance of 200 m from the neutron source. The neutron bursts have a frequency of 800 Hz and an energy range from 10 meV to about 20 MeV. HPGe detectors are used to detect the gamma radiation emitted by the investigated sample. The energy and the timing of the detected gammas are both recorded and time-of-flight – γ energy matrices are built and analysed in order to extract the differential gamma production cross section for each energy of the neutrons. Setting the angular position of the detectors to 110° and 150° allows optimal accounting of the angular distribution of the emitted gammas and therefore a simple angular integration procedure. Further, the level cross sections and the total inelastic cross section are deduced based on the known level structure of the sample.
An essential limitation of the conventional acquisition system is related to the gamma flash that is produced by the incident electron beam in the neutron source via bremsstrahlung. This very intense gamma radiation precedes the neutron burst and, if detected, it induces a dead time in the detection system equal to almost the entire neutron burst.

The solution applied in the past was to block all signals whose timing corresponds to the arrival of the gamma flash at 200 m. If a detector senses a gamma flash, the corresponding beam burst is completely disregarded by that detector. The timing of the conventional detection system is shown in Figure 1.

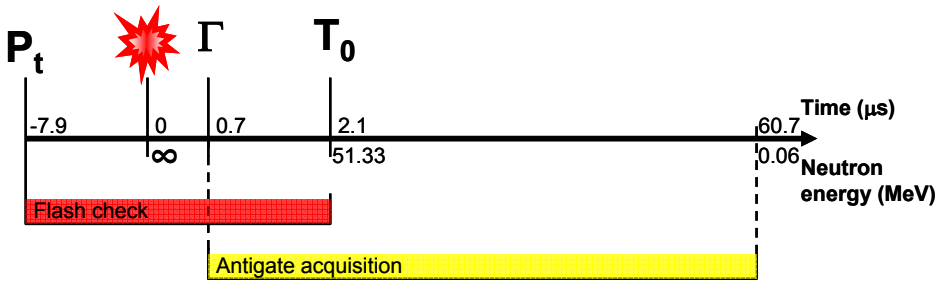

Figure 1. *Timing of detection system at 200 m for the conventional acquisition.*

However, this procedure induces a decrease of the detection efficiency of the order of 15%.

Upgrade of the detection setup

As already mentioned, two approaches were taken into account in order to increase the detection efficiency: the increase of the number of detectors and the migration towards a digitised system that would allow us to overcome the gamma-flash limitation.

Increase of detector number

During the last years, the experiments used two, three or four HPGe detectors, placed in a horizontal plane at 110° and 150° scattering angle with respect to the incoming beam. Backward angles are preferred in order to reduce the gamma flash detection probability.
In order to further increase the number of detectors, an aluminium frame that can hold up to 12 detectors was designed. It is shown in Figure 2.

Figure 2. *The aluminium frame*

Out of the 12 positions, 8 cover the 110° and 150° angles in the horizontal and vertical planes. The 4 remaining positions correspond to scattering angles of 125° and are of interest only for studies of the angular distribution of the gamma rays.
Presently, the number of detectors was extended from four to six and a further upgrade is foreseen to eight for early next year. The acquisition electronics can now accommodate eight detectors.

The digitised acquisition system
An effort was made during the last years for the migration towards a digitised acquisition system. We currently use four digitiser cards Acquiris DC440, capable to record $420 \cdot 10^6$ samples of 4 Mbytes per second. Each digitiser card has two data inputs.
The timing scheme of the digitised acquisition is shown in Figure 3. We typically record a trace of 10^5 samples of 2.38 ns each directly from the preamplifier of the detector. Each card is triggered only when a signal is present in the time region of interest. Then the trace is transferred to a PC where a dedicated software performs the analysis.

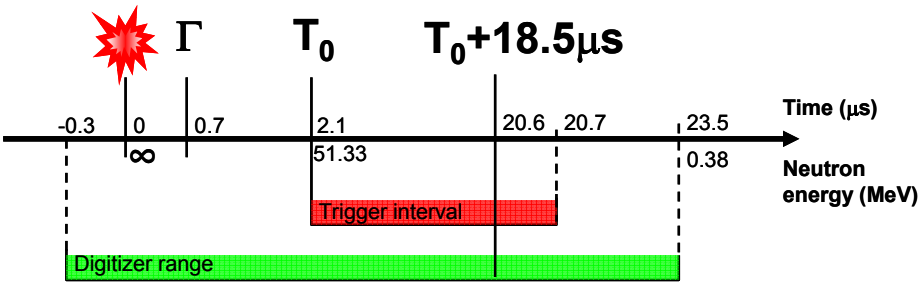

Figure 3. *Timing of detection system at 200 m for the digitised acquisition.*

Choosing the trigger and the digitiser intervals as shown in Figure 3, the digitiser is triggered only when a signal is present in the region of interest and avoids triggering on the (very intense) gamma flash. Following this procedure we do not have to eliminate from the analysis the traces containing a coincidence between a neutron-induced event and a gamma flash. This increases the efficiency of the digitised acquisition by about 15%, while the electronics used for the trigger signal remain very simple compared to those used for the conventional acquisition. An increased reliability is expected to arise from a reduced number of used electronic modules.

Conclusions

The setup for neutron inelastic scattering measurement at GELINA undergoes major upgrades. The number of detectors will be extended from four to eight, six being already in place. The acquisition system migrates towards digitisation, providing a better handling of the gamma flash together with much simplified electronics. As soon as the reliability and compatibility tests of the digitised acquisition will be concluded, we will eliminate completely the conventional one.
The higher efficiency will have impact on the duration of the experiments and consequently on the stability of the system during one experiment. This setup will provide highly reliable results and will become a “data factory” for the present and future applications and could also be used as a powerful spectroscopic tool for improving the knowledge of the structure of the studied nuclei.
Once the commissioning period is finished, the setup will be available also as a user facility for external collaborators.

The EURITRACK concept for cargo inspection with tagged neutrons

P. Peerani[1)], M. Salvato[1)], V. Sequeira[1)], B. Perot[2)], C. Carasco[2)], S. Bernard[2)], A. Mariani[2)], M. Lunardon[3)], S. Moretto[3)], G. Viesti[3)], J. Battais[4)], JS Lacroix[4)], M. Lhuissier[4)], P. Le Tourneur[4)]

1) European Commission – JRC/IPSC – Ispra (I)
2) Commissariat à l'Energie Atomique – St Paul-lez-Durance (F)
3) INFN and Dipartimento di Fisica – Università di Padova – Padova (I)
4) EADS Sodern – Limeil-Brevannes (F)
paolo.peerani@jrc.it

Abstract: The EURITRACK project aims to design and field test the prototype of a non-intrusive inspection system for the detection of explosives and other illegal materials in cargo containers using tagged neutrons. In this paper we will give a short introduction to the general physical concept of the EURITRACK system, the layout and functionalities of the information system with details of the data treatment and of the inspection strategy and finally an analysis of the first experimental results. The results demonstrate the detection capabilities of the EURITRACK inspection system.

Principle

The EURITRACK project aims at developing a non-intrusive Tagged Neutron Inspection System (TNIS) based on the Associated Particle Technique (APT) [1]. A sealed-tube generator produces 14-MeV neutrons and alpha particles from the D(T,α)n reaction. Alpha particles and neutrons are emitted nearly back-to-back, simultaneously and isotropically. A portion of the alpha particles are detected by a 8×8 matrix of YAP:Ce crystals enabling to tag a portion of the neutrons in terms of direction and time, which is used to interrogate a defined volume inside the container. Interaction of fast neutrons with the container structure and transported goods will induce the emission of prompt photons (mainly by inelastic scattering reactions), whose energy is characteristic of the element. For instance the 4439- and 6130-keV gamma ray lines are respectively used for carbon and oxygen determination whereas the 2313- and 5100 keV gamma-ray lines are the most useful for nitrogen determination. In the EURITRACK portal, gamma-rays are detected using two "reflection" 5"×5" NaI(Tl), four "transmission" 5"×5"×10" NaI(Tl) and sixteen "top" 5"×5"×10" NaI(Tl) detectors. Suitable front-end electronics allow measuring coincidence between alpha particles and gamma-rays with nanosecond resolution. The general layout of the TNIS is shown in figure 1. The specific hardware features of the tagged neutron system and the dedicated Monte Carlo studies for design optimisation are described in two other papers presented in this conference [2,3].

Functional specifications of the EURITRACK system

Nowadays cargo containers are typically inspected with X-rays. In the EURITRACK concept, all containers will be inspected first with X-rays, whereas the TNIS inspection will be launched only when the radiography identify a suspect item where the tagged beam will be focused.
The detection capabilities of the EURITRACK system is strongly dependent on the characteristics of the goods transported in the inspected container. Due to the moderation of neutrons by hydrogenated material, intensity and energy spectrum of the neutron beam can vary significantly when penetrating through the container. As a main consequence, the analysis of measured data must be performed in a different way according to the nature of the material. Basically we can simplify the process by classifying containers according to two main categories: "organic" and "metallic" matrices.
All explosives contain C, O, H and N. Neutrons do not produce prompt gamma rays on hydrogen, so this element cannot be analysed by the TNIS. Therefore we rely only on the detection of C, O and N.
Metallic and inert matrices do not contain substantial quantities of C. Consequently, the detection of C reveals presence of unexpected organic and can be considered as an indication of non-conformity. The elemental ratios (C/N and C/O) could eventually be used to

identify the illicit material. On the contrary, the absence of the carbon line inside a metal matrix can already exclude the presence of a sizeable quantity of explosives or other illicit materials. So the analysis of metallic matrices is relatively straightforward.
Analysis of organic matrices is more complex, because we need first to identify heterogeneities inside the organic composition and then to be able to discriminate between the composition of the matrix and that of the suspect object. In this case we need to determine with a good precision the elemental ratios, which is difficult due to the changing properties of the neutron beam penetrating a moderating material.

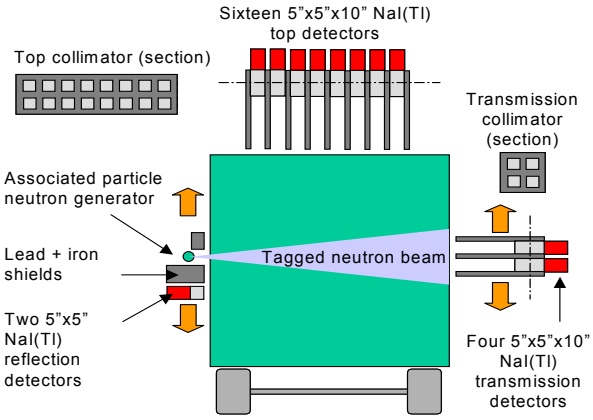

Figure 1. *TNIS set-up*

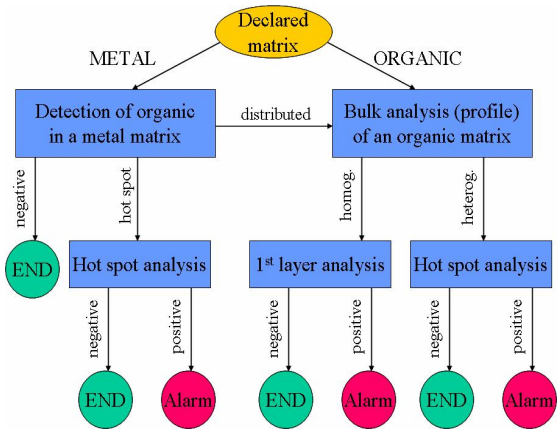

Figure 2. *Architecture of the Decision Making Algorithm (DMA)*

Architecture of the decision making process

The data analysis and decision making procedure follows the scheme described in figure 2. A short outline of the different steps is given in the following.

STEP 1 – Confirm absence or detect presence of organic material in a metallic matrix
The first questions that the expert system will have to answer when analysing a metallic matrix are the following: is this really a pure metallic matrix or is there some organic materials inside? And in such a case, where is it and what is it?
The most straightforward way to determine the presence of a significant quantity of organic is to construct the energy spectrum due to the entire inspected volume for each detector array (reflection, transmission and top) and search for the 4.44 MeV peak of C. If the latter is detected, there must be a significant quantity of organic material inside, then the container will be processed as an organic matrix (GO TO STEP 3).
If there is no significant quantity of organic matter distributed in the inspected volume, still there is the possibility of a concentrated organic presence in a "hot spot". To reveal the presence of an hot spot, an alpha-gamma time-of-flight spectrum (TOF) can be used, which reveals the neutron depth of interaction along the beam axis, In addition, a cut on the gamma energy around the 4.44 MeV line allows enhancing the carbon signal. If the TOF spectrum is flat, there is no evidence of organic presence (STOP with green light). If there is a bump, this will indicate the presence of an hot spot. The system can locate the position (corresponding to a time window) and GO TO STEP 2

STEP 2 – Analysis of an organic hot spot in a metallic matrix
This step should allow detecting explosives hidden in metallic matrices. The analysis procedure starts with the identification of the hot spot location and the associated time window from the time-of-flight spectrum. A time window is selected in order to get the spectra corresponding to the random background, which is subtracted to the active spectrum.
The elemental ratios can be obtained at this step by using a spectrum unfolding technique. The unfolding algorithm is based on the use of a library of experimental pure element gamma-ray spectra taken with the EURITRACK inspection system. Then the measured spectrum having an unknown composition is compared with a combination of the elemental spectra in order to find the combination of the relative intensities of each element that best reproduces the composite spectrum. The relative intensities of the pure element spectra are related to the

chemical proportions of these elements in the inspected materials using appropriate scaling factors.

STEP 3 – Profile of an organic matrix
The system will access this step either directly when the matrix is declared “organic” or when in a metallic matrix (step 1) we detect the presence of a significant quantity of organic material. The first questions that the expert system will have to answer when analysing an organic matrix are the following: is the content an homogeneous organic material or is there evidence of the presence of several different compositions?
The basic principle is that when a single homogenous material fills the container, the profile along the beam axis (corresponding to the TOF spectrum) of all spectral parameters (e.g. C, O and N relative counts) should be regular. In principle it should be constant, but, due to the interaction of the neutron beam with the material, the beam properties (intensity and energy) change along the beam path. Consequently we can expect a variation of the spectral parameters as a function of depth. Nevertheless if the material is homogeneous this variation should be smooth, regular and monotonic. Therefore the expert system will divide the inspected volume in a number of voxels by slicing it longitudinally. The behaviour of the elemental ratios as a function of depth is analysed. If the trend is regular and monotonic, there is no evidence of heterogeneity (GO TO STEP 4), otherwise GO TO STEP 5.

STEP 4 – Analysis of an homogeneous organic material
If the organic material is supposed to be homogeneous, we can derive its composition from the analysis of any slice (i.e. any time window). Since the beam properties change when the beam penetrates the organic, the optimal position for obtaining the “true” elemental ratios from the unperturbed beam is at the front surface of the container. Therefore, the matrix composition will be determined by analysing the first slice thus deriving the elemental ratios using the spectrum unfolding procedure.

STEP 5 – Analysis of a heterogeneous organic material
This could be the most difficult task for the EURITRACK inspection system. At the current status of the project, it is still questionable whether elemental ratios can be determined with sufficient accuracy deep inside an organic cargo for a voxel where significant neutron moderation has already taken place. We are investigating the possibility to compare the computed spectral parameters with the values expected in a homogeneous matrix or using correction factors obtained by Monte Carlo simulations.

Analysis of the first experimental campaigns

During the first half of 2006 two experimental campaigns of laboratory measurements with the TNIS prototype have been completed at the IRB in Zagreb. The first one in March focussed on a metallic matrix and was performed by using the IRB neutron generator with a smaller 4x4 associated alpha particle detector. In May the EURITRACK neutron generator with the full 8x8 detector matrix was delivered, so the second campaign in June was performed using the final EURITRACK hardware components. The second campaign focussed on organic and heterogeneous matrices and on the EURITRACK success case (detection of explosive in a metallic matrix). These are extensively shown in another paper presented at this conference [2].
The experimental setup of the first campaign consisted in a portion of container with full-scale transversal dimensions, filled with metal wires inside iron boxes (average density 0.2 g/cm^3) with a block of organic material hidden in the middle (approximately 90 kg of paper). Left picture of figure 3 shows the container section filled with metal boxes, the IRB neutron generator being visible at the left and the top array of photon detectors above the container. The picture on the right shows the paper block hidden in the middle.
Several measurements were completed with different neutron intensity and acquisition time. In all cases the time-of-flight spectrum showed a behaviour similar to that reported in figure 4. The peak structure in the middle of the time spectrum indicates the presence of extraneous organic material inside the metallic matrix and the time delay of the peak is used to localise the object in the middle of the container.

Figure 3. *Setup of the experiments with metallic matrix*

Once localised the suspect item, a spectral analysis is performed: the events corresponding to the correct time window are extracted, random background is subtracted and the spectrum unfolded. The characteristic peaks of C at 4.44 MeV and O at 6.13 MeV are clearly evident in the energy spectrum (figure 5). The results from the unfolding algorithm are quite consistent and reproducible: the ratio of C/O events from the analysis of 16 spectra from the TOP-array detectors gave an average value of 0.62 with a standard deviation of 0.08. This gives an idea of the reproducibility of the measurement and a preliminary indication of the accuracy that we can expect.

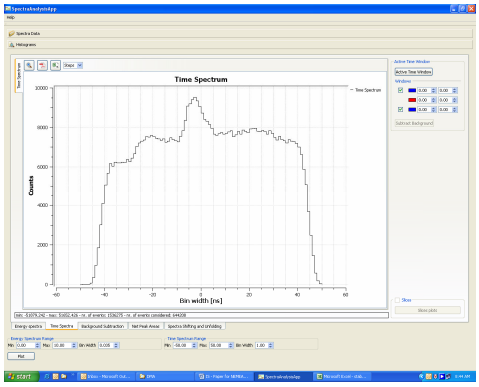

Figure 4. *Peak in the time spectrum indicating presence of an organic hot-spot*

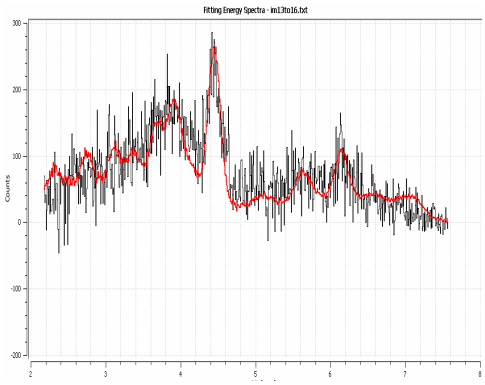

Figure 5. *Unfolding of the background subtracted spectrum (paper inside a metal matrix)*

Conclusions

The results of the first experimental campaigns with the EURITRACK inspection system clearly demonstrate the capability to detect (and possibly identify) explosives inside a cargo container filled with a metallic matrix. This confirms the success of the project whose target was the detection of 100 kg TNT in a metallic matrix within a 10-minutes measurement.
In the case of organic or heterogeneous matrices, the system can help in detecting presence of anomalies and heterogeneities, whereas it is not yet demonstrated that a clear identification of an explosive material can be obtained when the tagged neutron beam is strongly scattered and attenuated inside the organic material. This point is being explored to define a detailed user manual for the tagged neutron portal.

References

[1] B. Perot et al.: “The EURITRACK project: development of a Tagged Neutron Inspection System for cargo containers”, SPIE International Symposium on Defence and Security, Orlando (FL), 17-21 April 2006.
[2] C. Carasco et al.: “The EURITRACK project: experimental tests of a Tagged Neutron Inspection System for cargo containers”, this conference.
[3] S. Bernard et al.: “Development of the EURITRACK Tagged Neutron Inspection System: from simulation to experiment”, this conference.

MCNP calculation of neutron shielding for RBMK-1500 spent nuclear fuel containers safety

R. Plukienė[1)], A. Plukis[1)], V. Remeikis[1)] and D. Ridikas[2)]

1) Institute of Physics, Savanorių 231, LT-02300 Vilnius, Lithuania,
2) C.E.A. Saclay, DSM/DAPNIA/SPhN, F-91191 Gif-sur-Yvette Cedex, France
rita@ar.fi.lt

Abstract: The RBMK-1500 spent nuclear fuel (SNF) composition determine the radiation characteristics of the CONSTOR and CASTOR containers, where SNF from Ignalina NPP (Lithuania) is temporarily stored now. The extension of containers storage time depends on the knowledge of the characteristics of SNF and resulting dose rates. The fuel containers safety assessment can be performed using powerful modelling tools. Modelling of nuclide composition and it axial distribution along the fuel channel is done using the Monteburns code systems. MCNP5 code was used for the evaluation of radiation shielding and the surface dose rate of the CASTOR cask taking into account the heterogeneity of the different burnup of SNF assemblies' distribution. The simulation results confirm what neutron flux distribution is extremely sensitive to the fuel burnup and influence the neutron dose rate calculation results. The modelling results are compared with existing experimental data of the representative container leading to satisfactory agreement. This result proves the validation of calculation methodology for the radiation shielding safety assessment of CASTOR and similar containers used for the storage of RBMK-1500 SNF.

Introduction

Part of Ignalina Nuclear Power Plant (INPP) SNF is stored in the CASTOR and CONSTOR containers [1]. The metallic CASTOR cask is designed for transportation and long term storage purposes, while heavy concrete based CONSTOR cask is usually used for the long term immobile storage. Both of these containers are designed for 50 years with possible extension up to 100 year depending on their safety condition. To assess the radiation doses outside the containers and to evaluate their reliability after expire time the composition of SNF must be known and the transport of resulting source neutrons and γ quanta modeled properly. One has to note that the extension of storage time using these containers depends on the knowledge of the characteristics of SNF and resulting dose rates. Unfortunately, there are a few published data on RBMK SNF characteristics. Even the information on neutron fluxes in the fuel elements is not known precisely. Therefore, experimental measurements of dose rates outside the representative storage containers are indispensable despite of powerful modeling tools available today for radiation transport estimates.
In this work we consider a typical CASTOR cask dedicated for RBMK-1500 SNF storage, for which radiation dose rates are calculated and compared with experimental results.

Modeling procedure of the RBMK-1500 SNF storage cask CASTOR

A 3D model of the RBMK-1500 spent nuclear fuel storage container CASTOR has been created using the 3D MCNP5 geometry set-up (see Fig. 1 for details). The geometrical parameters, material properties and spent nuclear fuel filling history of the container were taken from the data of representative CASTOR container No.0067-14. The 2.08 m of diameter, 4.4 m of height and 30 cm of wall thickness cylindrical metallic container CASTOR is produced from cast iron. The container is filled with "32M" stainless steel basket where SNF assemblies are placed. This "32M" basket contains 51 fuel assemblies, each of them being divided into two parts (341 cm long each). The burnup of 2 % ^{235}U enrichment spent nuclear fuel in the container varies from 13 MWd/kg to 22 MWd/kg. In order to simplify our approach only 6 types of different fuel burnup assemblies were modeled as presented in Table 1. 102 different half-assemblies were located in the specified places using MCNP5 hexagonal lattice option filled with appropriate assemblies (see Fig. 1) as reported in the CASTOR container.
To perform the calculations several computational codes had to be combined. Modeling of SNF nuclide composition was done using Monteburns code [2]. Afterwards, the gamma and neutron source spectra were calculated with the ORIGEN-ARP code from the SCALE 5 codes

package. Finally, MCNP5 was used for neutron and gamma transport and evaluation of radiation dose rates at the surface of CASTOR cask. For the input data MCNP5 requires detailed 3D geometry and particle source description, material composition, their densities and specific nuclear data. In this case, ENDF/B-VI data library was used for the fuel and structure materials, while JENDL-3.2 data files were employed for fission products.

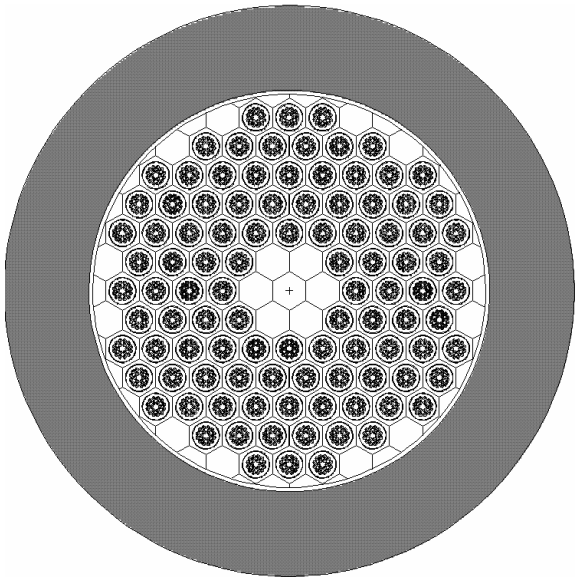

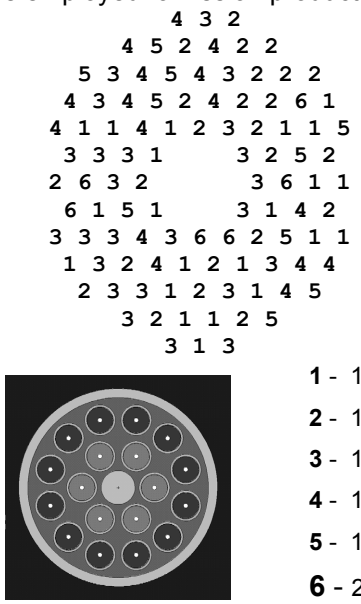

Figure 1. *Left: cross-section of the SNF container CASTOR modeled with MCNP5; Right: the arrangement of the different burnup fuel assemblies (from 13MWd/kg (label **1**) to 22MWd/kg (label **6**)) (on the right) and cross-section of RBMK fuel assembly (lower part).*

This particular container No.0067-14 was also examined experimentally with standard thermo-luminescence (TLD) and "Series 1000 MIN-RAD" dosimeters. The dose in the TLD attached at 8 points around the CASTOR container was accumulated during the period of 167 hours, the total measurement uncertainty of ±5-10%. In addition, γ dose rates were also measured with MIN-RAD at 4 points at the CASTOR cask surface. The precision of MIN-RAD was somewhat worse compared to TLD, i.e. about ±10-15%.

Results

Gamma source, resulting from ORIGEN-ARP calculations, for different burnup of RBMK-1500 SNF is presented in Fig. 2 (left). The energy distribution of γ rays is very similar for every fuel burnup considered, but on the other hand, the γ rays intensity is changing moderately with fuel burnup. The difference of total γ source intensity between 13 MWd/kg and 22 MWd/kg fuel is about 50 %.

The neutron spectra are also similar for different cases of fuel burnup as shown in Fig. 2 (right). The difference between 13 MWd/kg and 22 MWd/kg fuel burnup results in the increase in the neutron source intensity nearly by one order of magnitude (~8 times).

The total γ source intensity in the cask is about $1.76 \cdot 10^{16}$ γ/s, and the total neutron source intensity is ~$7.62 \cdot 10^{7}$ n/s. These values were used in our further calculations for normalization of gamma and neutron doses calculated with MCNP5. The average intensity of the γ source from one fuel assembly is about $3.45 \cdot 10^{14}$ γ/s, which corresponds to 16 MWd/kg fuel burnup. The averaged intensity of the neutron source from one fuel assembly is $1.49 \cdot 10^{6}$ n/s corresponding to the fuel burnup between 16 MWd/kg and 17 MWd/kg.

The dose rate calculations were performed with MCNP5 using ring detector option for two different particle source descriptions: homogeneous gamma and neutron source distribution of 16 MWd/kg SNF in all 102 half-assemblies and heterogeneous distribution taking into account different burnup SNF assemblies from 13 MWd/kg to 22 MWd/kg according to the existing irradiation history.

Due to γ rays attenuation in CASTOR wall the photon flux decreases about by 10 orders of magnitude at the surface. In order to obtain a statistically significant result in a reasonable

computing time specific variance reduction techniques was applied to increase the statistics of Monte Carlo calculations: the photon tracking transport importance in MCNP5 was gradually increased from 1 to 10^6 starting from the initial to the outside wall of the cask.

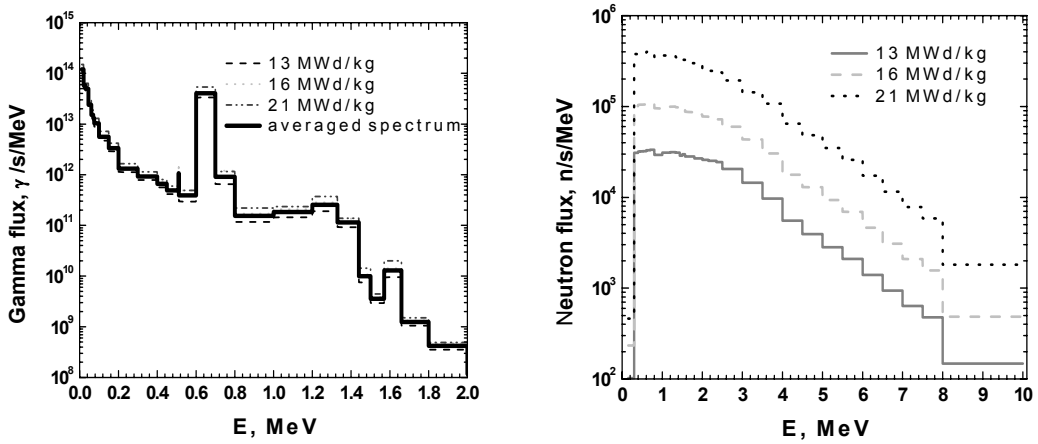

Figure 2. *Energy spectra for different burnup SNF modeled with ORIGEN-ARP. Left: γ source case; Right: neutron source case.*

The results of γ dose rates at the surface of CASTOR cask are presented in Fig. 3. The experimental data measured with TLD and MIN-RAD dosimeters are presented in circles and triangles, respectively. The MCNP5 modeling results are also compared to SCALE 4.3 predictions from Ref. [1]. We note that γ dose rates obtained from Monte Carlo simulations even taking into account the neighboring containers (we assumed the γ dose rate from the similar container surface at 1 m distance (11.8 μSv/h) and added to the calculated surface dose rate (26.8 μSv/h)) give a somewhat smaller average value of 38.6±0.4 μSv/h compared with measurements. All experimental γ dose points are ~1.6 times above the MCNP5 calculated average, especially for MIN-RAD measurement at 180º angle, where difference is almost 2.5 times. In our opinion, this result is rather good taking into account other uncertainties of our model (spent nuclear fuel composition, irradiation and cooling history, Co contents in the fuel cladding, etc.). In addition, this difference might also be due to the CASTOR container surface contamination with fission products from the cooling pool. In addition, the TLD are sensitive to the thermal neutron flux, which also might explain the increase in the measured γ dose.

On the other hand, the Monte Carlo calculations agree quite well with independent calculations performed with SCALE 4.3, which resulted in the 52 μSv/h dose rate after 10 years of cooling time [1]. The difference in the γ dose after ~13 years (our work) and 10 years [1] is determined mainly by ^{106}Rh (daughter of ^{106}Ru) high energy gammas, which have great influence on the γ dose due to the higher penetration through the cask walls, and by the ^{60}Co with its relatively short half-life ($T_{1/2}$ = 5.27 years).

Neutron dose rate at the surface of the CASTOR cask calculated with MCNP5 is presented in Fig. 4. The two cases were considered: a) the case of a homogeneously distributed neutron source of 16 MWd/kg fuel burnup, and b) the case of a heterogeneously distributed neutron source taking into account fuel assemblies of higher burnup. The average neutron dose rate is about 75 μSv/h, and for the homogeneously distributed neutron source of 16 MWd/kg fuel burnup the neutron dose rate values vary within the range from 68 μSv/h to 85 μSv/h. In addition, one sees that for the neutron source even a few assemblies with high burnup can cause observable anisotropy of neutron dose rates. This can be explained by lower neutron attenuation rates compared to gammas both in the absolute value and changes in energy spectra. For the heterogeneously distributed neutron source the average neutron dose rate is about 85 μSv/h, and the neutron dose rate values vary within the range from 76 μSv/h to 104 μSv/h. The local superposition of half-assemblies of higher burnup (16 MWd/kg - 22 MWd/kg) at the angles of 270º and 220º resulted in about 28 μSv/h increase in the neutron dose rate. This result confirms what neutron flux distribution is extremely sensitive to the fuel burnup and influences the neutron dose rate calculation results. In conclusion we would like to emphasize that neutron dose rate calculation should be performed with real SNF neutron source distribution in the container, because averaged burnup fuel (in our case 16 MWd/kg)

causes incorrect results. The measurements of neutron dose rates would be very useful to validate our predictions.

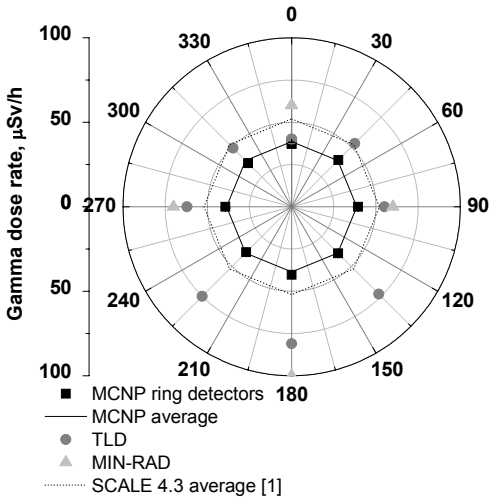

Figure 3. Angular gamma dose rates on the surface of CASTOR cask calculated with MCNP5 against SCALE 4.3 predictions from Ref. [1] and experimental data measured with TLD and MIN-RAD dosimeters (see the legend for details).

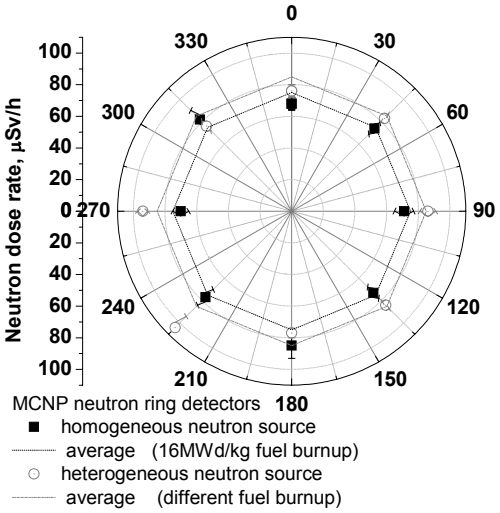

Figure 4. Angular neutron dose rates on the surface of CASTOR cask calculated with MCNP5 in case of homogeneously distributed neutron source and in the case of heterogeneously distributed neutron source (see the legend for details).

Conclusions

The neutron and gamma ray sources in the SNF storage cask CASTOR have been estimated using different radiation transport and material evolution code packages as ORIGEN-ARP, MCNP5 and Monteburns. The neutron dose rate from the surface of the cask varies within the range between 76 μSv/h and 104 μSv/h. The anisotropy of dose rates is observed for neutrons and is explained by heterogeneous distribution of different burnup fuel assemblies inside the container. The averaged gamma dose rate is the 38.6±0.4 μSv/h, and is determined mainly by ^{137}Cs and ^{60}Co. This result underestimates the corresponding measurements performed with TLD and MIN-RAD dosimeters by ~50 %. The obtained discrepancies might be due to possible surface contamination, the partial gamma dosimeters sensitivity to neutron flux from the container, etc. Some additional investigations on this subject will be performed in the near future, although in general the agreement between our predictions and measurements is satisfactory. This work validates the methodology of the radiation shielding and dose rate calculations for RBMK SNF storage facilities. However, more experimental data are needed (in particular for other types of storage containers) in order to provide more precise uncertainties of the predicted values.

Acknowledgements

This research was supported in part by a Lithuanian State Science and Studies Foundation in the frame of the project No.C-19/2006 and by Lithuanian and French cooperation program “Gilibert” (No. 09395TB).

References

[1] A. Šmaižys, P. Poškas, D. Lukauskas, V. Remeikis, Experimental determination of radiation safety of spent nuclear fuel dry storage casks CASTOR and CONSTOR, Lithuanian Journal of Physics, 41(4-6), 547-550 (2001).

[2] R. Plukienė, A. Plukis, V. Remeikis and D. Ridikas, Benchmark calculations of RBMK spent nuclear fuel isotopic composition using MCNP and ORIGEN codes, Lithuanian Journal of Physics, 45(4), 281-287(2005).

Activation experiment on Ta and W constituents of the Eurofer-97 steel in the NPI p-D_2O neutron field

E. Šimečková[1)], P. Bém[1)], V. Burjan[1)], U. Fischer[2)], M.Götz[1)], M. Honusek[1)], V. Kroha[1)], J. Novák[1)], S.P. Simakov[2)]

1) Nuclear Physics Institute, CZ-250 68 Řež, Czech Republic
2) Forschungszentrum Karlsruhe, D-76021 Karlsruhe, Germany
simeckova@ujf.cas.cz

Abstract: Activation experiments on the Eurofer-97 low activation steel and on some of important activity contributors W and Ta in particular were performed to provide the database for validating activation cross-section data in the energy range relevant for the International Fusion Material Irradiation Facility (IFMIF). An IFMIF-like white neutron fields extending up to energy of 32 MeV was produced at the NPI isochronous cyclotron U-120M by bombarding a flowing heavy water target with a 37 MeV proton beam. The induced gamma-radioactivity for 6 radionuclide products dedicated to the reactions on W and Ta constituents was determined by gamma-ray spectrometry at different cooling time intervals using calibrated HPGe detectors. In parallel, the pure-element foils W and Ta were investigated as well. Up to 12 and 10 activation products have been determined from the irradiation of W and Ta samples, respectively.
Measured activities of pure W and Ta foils are compared with the data of the same isotopes from activation experiment on Eurofer-97. The overall agreement is indicated for most of nuclides. Further details of experiments are discussed and the comparison of measured data with ALARA/EAF-2001 and EASY-2005 calculations is outlined.

Introduction

The reduced-activation ferritic-martensitic steel Eurofer-97 is a potential structural material for fusion power plants. The objective of present activation experiment is to provide the experimental data base for validation of activation cross-section data in the energy range relevant for the International Fusion Material Irradiation Facility (IFMIF). Continuing the investigation of Eurofer-97[1], the samples of W and Ta (main constituents of Eu-97, see Tab. 1) were activated in the neutron field provided of NPI p-D_2O source.

Table 1. *Composition of Eurofer-97 sample (main constituents).*

Main constituens	Fe	Cr	W	Mn	V	Ta
Weight %	88.5	9.21	1.148	0.502	0.204	0.145
+/-		0.12	0.028	0.012		0.005

Experimental procedure

The samples were irradiated in the neutron spectrum running up to 32 MeV (mean energy of 14 MeV) produced by the neutron source from bombarding the flowing heavy water target by 37 MeV proton beam. The spectral flux at the position of irradiated samples (see Fig.1) was determined by multi-foil-activation (MFA). In this procedure, the spectral yield measured in the point-like geometry by scintilation detector technique (NE-spectrum) was used as the guess spectrum. The neutron flux density at usual position of irradiated samples (3 mm from the target) was of about 1.2×10^{11} $cm^{-2}s^{-1}$.
The investigated samples were surrounded by aluminum and gold foils for a supplementary monitoring of the neutron flux. The time profile of the neutron source was monitored by proton beam current, recorded by calibrated current-to-frequency converter and scaled on PC.

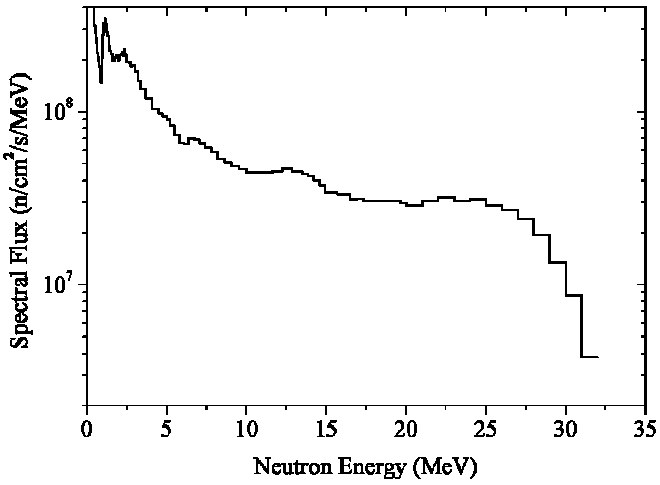

Figure 1. *Neutron spectra from the $D_2O(p,xn)$ source reaction for E_p= 37 MeV, I_p = 12 μA at the target-to-sample distance of 156 mm.*

Sample disks of 10 mm diameter were fabricated from Eurofer-97 sheet of 1.6 mm thickness. Natural elements W and Ta were Goodfelow products. Natural tungsten consists of five stable isotopes – ^{186}W (28.6 %), ^{184}W (30.7 %), ^{183}W (14.3 %), ^{182}W (26.3 %) and ^{180}W (0.1 %), tantalum consists almost of one isotope - ^{181}Ta: 99.988 %,^{180}Ta (0.012 %).
To test the internal consistency of experiment, the irradiation was performed at different runs and different source-to-sample distance.
The activated samples were investigated by two calibrated HpGe detectors of 23 and 50% efficiency and of FWHM 1.8 keV at 1.3 MeV, respectively. Gamma spectra were measured repeatedly, after different cooling time intervals up to 150 days. Evaluation of spectra was performed utilizing the NPI code DEIMOS .

Experimental results and analysis

Activated isotopes were identified on the basis of $T_{1/2}$, γ-ray energies and intensities. By analyzing the spectra, the 12 resulting specific activities A_{sp} in Becquerels per kilogram to the end of irradiation were obtained for W (see Tab. 2) and 10 for Ta elements (see Tab.3). The uncertainty includes statistical errors and the uncertainty of the detector-efficiency calibration (including the geometry factor).

Table 2. *Specific activities A_{sp} of isotopes identified from the W foils irradiated in the NPI p(37MeV)+D_2O neutron field.*

Product	$T_{½}$	W14 Asp [Bq/kg]	W4 Asp [Bq/kg]	W7 Asp [Bq/kg]
187 W	23.72 h	1.118 E8 (3)	1.720 E8 (3)	8.777 E8 (4)
185 W	75.1 d			2.238 E8 (6)
181 W	121.2 d			1.828 E8 (6)
185 Ta	49.4 m	1.870 E8 (4)	2.026 E8 (3)	2.918 E8 (20)
184 Ta	8.7 h	3.865 E7 (3)	4.020 E7 (3)	1.631 E8 (4)
183 Ta	5.1 d	5.967 E6 (4)	6.337 E6 (5)	3.378 E7 (4)
182 Ta	114.43 d	2.467 E5 (4)	2.614 E5 (12)	1.539 E6 (4)
183 Hf	1.067 h	2.188 E7 (7)	2.542 E7 (5)	
182m Hf	61.5 m	3.183 E6 (15)	2.751 E6 (15)	
181 Hf	42.39 d	6.989 E4 (4)	7.225 E4 (8)	4.109 E5 (4)
180m Hf	5.5 h	1.395 E6 (5)	1.498 E6 (7)	5.951 E6 (7)
179n Hf	25.05 d	5.886 E3 (15)		3.558 E4 (11)

Table 3. *Specific activities A_{sp} of isotopes identified from the Ta foils irradiated in the NPI p(37MeV)+D_2O neutron field.*

Product	$T_{½}$	Production Reaction	Treshold [MeV]	Q [MeV]	A_{sp}(Ta 4) [Bg/kg]	A_{sp}(Ta 1) [Bq/kg]
182 Ta	114.43 d	^{181}Ta(n,γ)	0.000	6.063	3.575 E7 (3)	4.256 E5 (9)
182m Ta	15.84 min	^{181}Ta(n,γ)	0.000	6.063		1.243 E7 (3)
180 Ta	8.152 h	^{181}Ta(n,2n)	7.619	-7.577	7.337 E10 (5)	1.037 E9 (3)
178 Ta	9.31 min	^{181}Ta(n,4n)	22.245	-22.122		1.124 E9 (3)
178m Ta	2.36 h	^{181}Ta(n,4n)	22.245	-22.122	4.319 E9 (3)	1.445 E8 (2)
181 Hf	42.39 d	^{181}Ta(n,p)	0.246	-0.245	4.962 E6 (3)	
180m Hf	5.5 h	^{181}Ta(n,d)	3.737	-3.716	1.667E8 (4)	3.327 E6(2)
179n Hf	25.05 d	^{181}Ta(n,t)	4.874	-4.847	2.194 E5 (8)	
177 Lu	6.734 d	^{181}Ta(n,nα)	0.000	1.526	7.480 E6 (4)	
177m Lu	160.4 d	^{181}Ta(n,nα)	0.000	1.526	2.259 E4 (10)	

To test the internal consistency of experiment, the reaction rates (specific activity in Bq/kg/μC corrected for decay during the irradiation) were calculated and compared for samples irradiated in different conditions. All but ^{187}W data agree with unity within 2σ. It indicates the consistency of irradiation experiments and of the results from gamma-spectrometry analysis.

Table 4. *Comparison RR from activation experiments on W, Ta and Eurofer-9. The RR data for W and Ta are normalized to the concentration of these nuclides in Eurofer-97.*

Isotop	RR(Eu97)(Er%)	RR(W7)(Err%)	RR(Ta4)(Err%)	RR(W+Ta)(Err%)
187W	99.48 E1 (2)	31.52 (4)		31.52 (4)
184Ta	6.156 (4)	7.710 (4)		7.710 (4)
183Ta	0.855 (5)	1.059 (4)		1.059 (4)
182Ta	0.725 (5)	0.0471 (4)	0.088 (3)	0.115 (5)
180Ta	291.9 (5)		282.3 (5)	282.3 (5)
180mHf	3.092 (30)	0.351 (7)	0.775 (4)	1.126 (9)

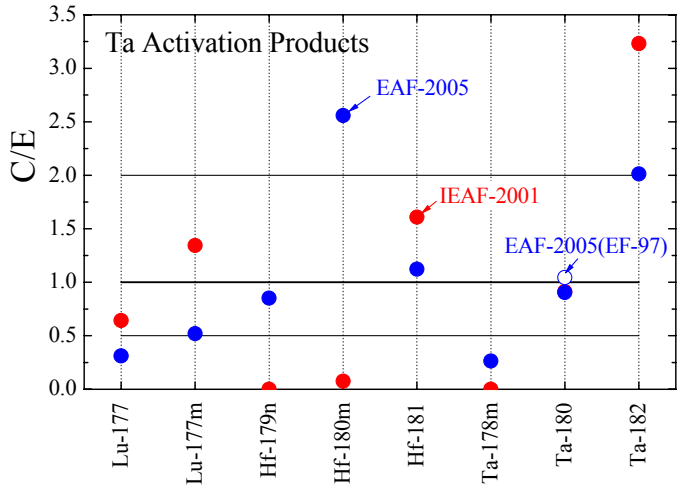

Figure 2. *The C/E data for Ta (sample No 4) with ALARA/EAF-2001 (red solid sircles) and EASY-2005 (blue solid circles); C/E for EF-97 (open blue circle) are given for comparison.*

By analyzing measured γ-ray spectra from irradiated Eu-97, the 22 resulting specific activities A_{sp} in Bequerels per kilogram to the end of irradiation were obtained (6 of them were dedicated to the decay of W or Ta elements).
The comparison of the results of the activation experiments on Eu-97, W and Ta in terms of reaction rates are given in Tab. 4.

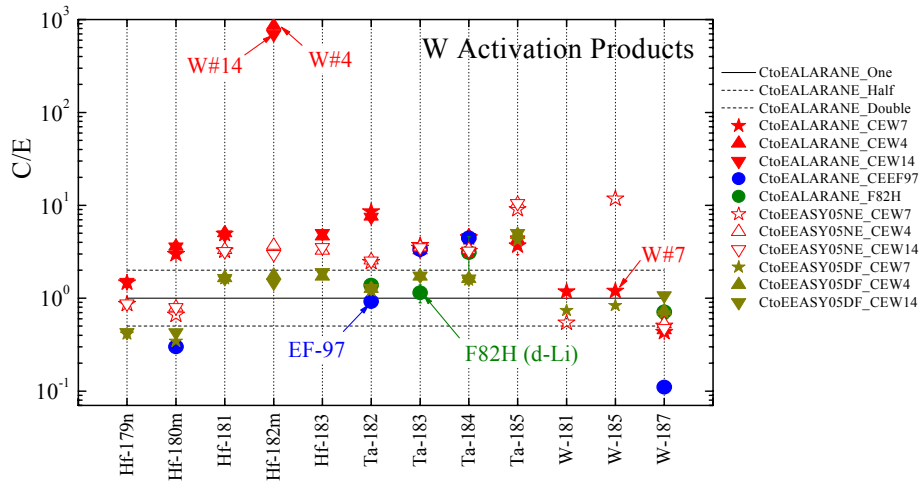

Figure 3. *The C/E data for W (samples No 4, 14 and 7) using two neutron spectra: measured by NE detector (NE): red solid symbols – ALARA/EAF-2001, red open symbols – EASY-2005; (2) measured by dosimetry foils (DF): yellow solid symbols – EASY-2005.*

The results were compared with calculation carried out at FZK using the European Activation System (EASY). The Calculation-to-Experiment ratios for Ta are in Fig. 2. The Calculation-to-Experiment ratios for W (samples No 4, 14 and 7) using two neutron spectra: (1) measured by NE detector (NE) and (2) measured by dosimetry foils (DF) are shown in Fig. 3.

Conclusion

Eurofer-97, W and Ta foils were irradiated at IFMIF-like neutron field, 12 activation products have been determined from the irradiation of W sample, 10 activation products have been determined from the irradiation of Ta sample. The internal consistency of results was proved. The activation data of W and Ta were compared with the data of the same isotopes from activation experiment on Eurofer-97. The overall agreement is indicated for most of nuclides but the case neutron-capture reactions ^{181}Ta(n,γ) and ^{186}W(n,γ). The reason is not well understood yet due to undetermined thermal part of the NPI-DF spectrum.
Measured activities were analyzed in terms of the Calculation-to-Experiment ratios using the ALARA inventory code with the EAF-2001 and EAF-2005 libraries. The present validation indicates the need to update the relevant tantalum and tungsten activation cross sections in the both libraries.

Acknowledgements
This work was performed with partial support of EFDA Technology Program, the Ministry of Education and the Ministry of Trade and Industry of CR

References

[1] P. Bém, V. Burjan, M. Götz, M. Honusek, U. Fischer, V. Kroha, J. Novák, S.P. Simakov and E. Šimečková, Fus. Eng. and Design, v. 75-79 (2005) p. 829-833.

Status of Pb resonance neutron data for ADS design

M.Todorov

INRNE-BAS, Tzarigradsko Shaussee Blvd, №72, 1784 Sofia, Bulgaria
todoroff@inrne.bas.bg. www.todoroff.tk

Abstract: Accelerator-driven systems for transmutation of nuclear waste have been suggested as solution to the problem of nuclear spent fuel that in reality is serious radiological hazard. Lead and bismuth are important constructive materials for coolant and spallation target in these systems. We present an overview of the existing lead and bismuth nuclear data in the available nuclear libraries for developing innovative nuclear energy systems. The qualities of necessary data, neutron cross-sections, resonance parameters and especially the accuracy of the neutron cross-section over a wide energy range have been examined in comparison with the requirements of ADS design. Discrepancies between different evaluated data files are discussed, as well as the newly obtained experimental data. The statistical methods of data analysis in the unresolved resonance region developed in INRNE were used for estimation the quality of the evaluated files. Recommendations for improvement of Pb data status pertinent to ADS are prepared.

Introduction

In the recent decades construction of subcritical ADS involves suggestion of new materials such as lead and bismuth for spallation target as well as coolant and moderator of the experimental reactor. Designing of a spallation target is a matter of developing special technology of molten lead or lead-bismuth eutectic. Those studies implicate reliable nuclear data for lead and bismuth isotopes especially evaluated in nuclear databases. At present, the accuracy of nuclear data seems to be enough to design ordinary fission reactors, but for innovative ADS more accurate data are needed for special nuclides, which have not yet played important roles in ordinary reactors. The new measurements on MA, Pb, and Bi cross-sections are foreseen [1]. The required accuracies of Argonne National Laboratory sensitivity study (Aliberti et al) accomplished: $^{204\text{-}208}$Pb: 8-10%, ^{208}Pb: 10-15%. Fast neutron ^{206,207}Pb (n,n') measurements still needed. Capture in ^{208}Pb presents a large discrepancy between ENDF and JEFF in the neutron balance. Discrepancies in the nuclear data for ^{207}Pb have an important effect on the neutron multiplication of the ADS subcritical system, which should not be neglected [2].

Calculation of resonance parameters for ^{208,207,206}Pb

Arithmetic averaging for some resonance parameters was performed. Several nuclei and libraries (Table 1) are compared to give more detailed picture of nuclear data status.

Table 1. *Inventory of nuclear data's for several lead isotopes [3].*

Isotope	Library	RRR E-range	Formalism	Authors
206Pb	ENDF/B-VI	up to 900keV	Reich-Moore	M.B. Chadwick
	JENDL-3.3	up to 500keV	Reich-Moore	M.Mizumoto
	JEFF	up to 900keV	Reich-Moore	A.J. Koning
	BROND-2	up to 900keV	MLBW	A.I.Blokhin
207Pb	ENDF/B-VI	up to 475keV	Reich-Moore	M.B. Chadwick
	JENDL-3.3	up to 475keV	Reich-Moore	M.Mizumoto
	JEFF	up to 475keV	Reich-Moore	A.J. Koning
	BROND-2	up to 500keV	MLBW	A.I.Blokhin
208Pb	ENDF/B-VI	up to 1MeV	Reich-Moore	M.B. Chadwick
	JENDL-3.3	up to 1MeV	Reich-Moore	M.Mizumoto
	JEFF	up to 1MeV	Reich-Moore	A.J. Koning
	BROND-2	up to 1.6MeV	MLBW	A.I.Blokhin

Calculation of <D> (average level spacing of S – resonances) is performed by simple averaging of observed resonances positions:

$$< D(N) >= \frac{1}{N-1}\sum_{i=1}^{N} D_i = \frac{E_N - E_1}{N-1}, \quad (1)$$

where $D_i=E_{i+1}-E_i$; N is number of resonances, E_1 and E_N are respectively the first and the last resonance in the energy interval. The same procedure is performed for Γ_γ and Γ_n. Strength function - S_n^l is reckoned by:

$$S_n^l = \frac{< \Gamma_n^{0l} > / \sqrt{E}\,\mathrm{P}_l}{< D_l >} = \frac{< \Gamma_n >}{< D_l >} \quad (2)$$

Γ_n^{0l} - is reduced neutron width; P_l is penetrability coefficient. The result of calculation for every nuclide is shown on Table 2-4 with the number of levels in the list shown on Table 5.

Table 2. *The average resonance parameters of ^{206}Pb for the RRR calculated from data of the libraries.*

LIBRARY	R'[fm]	D_l[KeV]			$Sn^0(x10^{-4})$			Γ_γ[eV]		
		s	p	d	s	p	d	s	p	d
ENDF/B-VI	9,5	24,9	6,15	4,43	1,08	0,49	2,06	4,58	0,34	1,19
JENDL-3.3	8,0	28	6,7	6,26	1,53	0,71	3,76	1,46	0,25	0,64
BROND-2	9,5	24,9	6,42	4,43	1,08	0,54	2,71	2,24	0,51	0,72

Table 3. *The average resonance parameters of ^{207}Pb for the RRR calculated from data of libraries.*

LIBRARY	R'[fm]	D_l[KeV]			$Sn^0(x10^{-4})$			Γ_γ[eV]		
		s	p	d	S	P	d	s	p	d
ENDF/B-VI	9,5	46,8	4,73	17,1	1,62	1,53	3,83	12,17	0,49	1,42
JENDL-3.3	9,5	46,9	4,91	18,2	1,86	1,51	4,12	2,01	0,26	0,51
BROND-2	9,4	37,5	4,59	24,3	2,09	2,33	2,91	7,83	0,53	0,5

Table 4. *The average resonance parameters of ^{208}Pb for the RRR calculated from data of libraries.*

LIBRARY	R'[fm]	D_l[KeV]			$Sn^0(x10^{-4})$			Γ_γ[eV]		
		s	p	d	s	p	d	s	p	d
ENDF/B-VI	9,7	246*	38	64,5	1,15	0.55	1,46	0.37	0,28	1,01
JENDL-3.3	9,7	246*	38	64,5	1,15	0,53	1,46	0,24	0,26	0,59
BROND-2	8,6	-	72	91,9	-	0,81	1,77	-	0,31	1,54

*There are only three levels in the library (see Table 5).

Table 5. *Number of resonances included in calculation.*

LIBRARY	Pb 206			Pb 207			Pb 208		
	s	p	d	s	p	d	s	p	d
ENDF/B-VI	36	146	189	10	99	18	3	25	15
JENDL-3.3	18	75	67	10	95	17	3	25	15
BROND-2	36	140	190	13	102	13	1	21	17

Comparison between lead cross-sections

Resonance parameters from nuclear data llibraries were used to estimate potential, resonance and total cross-section by (3),(4),(5),(6) formulae and perform averaging by medium energy intervals.

$$\sigma(E) = \sigma_{pot} + \sigma_{res} \tag{3}$$

$$\sigma_{res}^{J} = 2\pi^2 k^{-2} \frac{1}{\Delta E} \sum_{l} \Gamma_n^l g(J) \tag{4}$$

$$\sigma_{pot} = 4\pi k^{-2} \sum_{l} (2l+1) \sin^2 \varphi_l \tag{5}$$

$$k = 2.196771 = \frac{AWRI}{AWRI+1} 10^{-3} \sqrt{E} \tag{6}$$

Table 6. *Dependence of phase(φ) from ρ for different* l .

l	φ_l	$\rho = kR$
0	ρ	
1	$\rho - \arctan\rho$	$g = \frac{2J+1}{2(2I+1)}$
2	$\rho - \arctan\frac{3\rho}{3-\rho^2}$	

J is compound nucleus spin (spin of the resonance); ***AWRI*** is ratio of the mass of the particular isotope to that of the neutron; l is value of the *l*-state (neutron angular momentum); ***R*** is scattering (channel) radius; ***I*** is nuclear spin of the target nucleus (positive number); $\boldsymbol{\varphi_l}$ are the phase; $\boldsymbol{\Gamma_n}$ are the neutron width evaluated at the resonance energy.
In addition comparison between calculated and energy averaged (7) total cross-section from point wise data file were done. Result is shown on the Figure 1 – 6.
$\langle\sigma(E)\rangle$ is averaged by energy intervals total cross-section

$$\langle\sigma(E)\rangle = \sum_{i} (\Delta E)_i \frac{\sigma(E_i) + \sigma(E_{i+1})}{2} \tag{7}$$

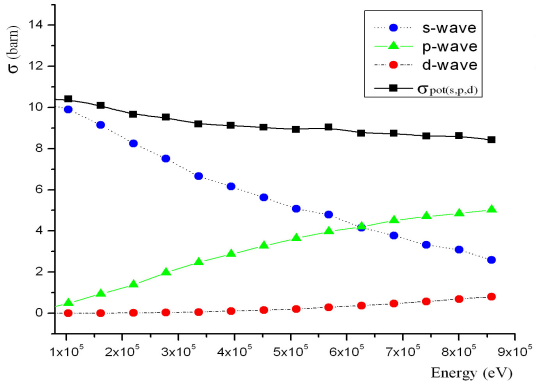

Figure 1. *s,p,d waves and* σ_{pot} *calculated from* ENDF resonance parameters for ^{206}Pb.

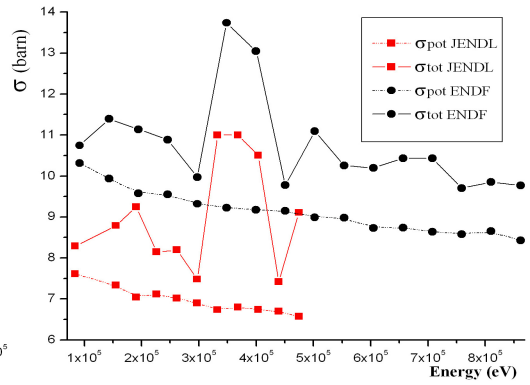

Figure 2. *Comparison between estimated* σ_{pot} and σ_{tot} from ENDF and respectively JENDL resonance parameters for ^{206}Pb.

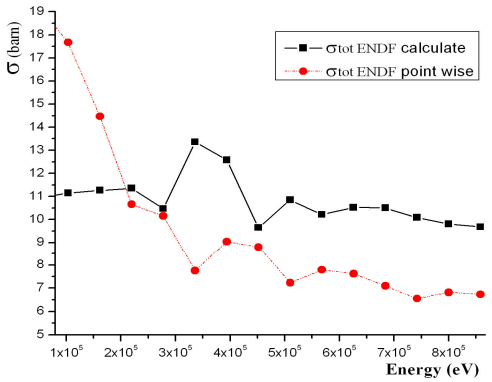

Figure 3. Comparison between σ_{tot} calculated from ENDF res. par. and σ_{tot} point wise data for ^{206}Pb.

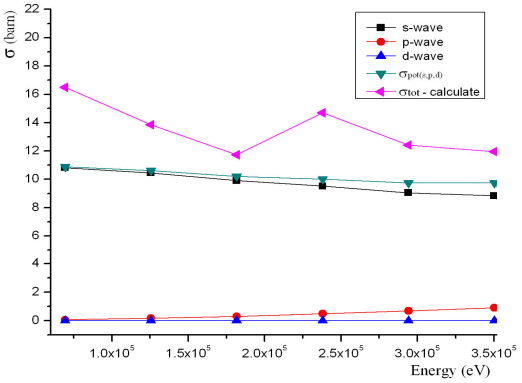

Figure 4. s,p,d waves,σ_{pot} and σ_{tot} for ^{207}Pb from BROND res. parameters.

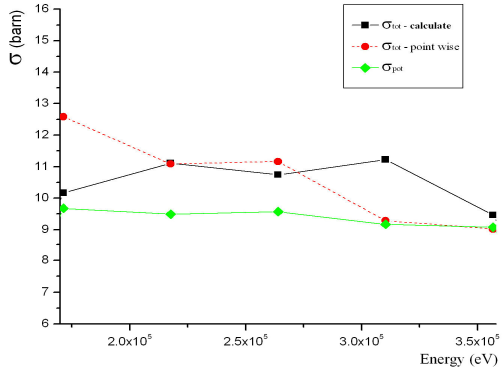

Figure 5. σ_{pot} and σ_{tot} calculated from ENDF res. par.compared with σ_{tot} point wise data for ^{207}Pb.

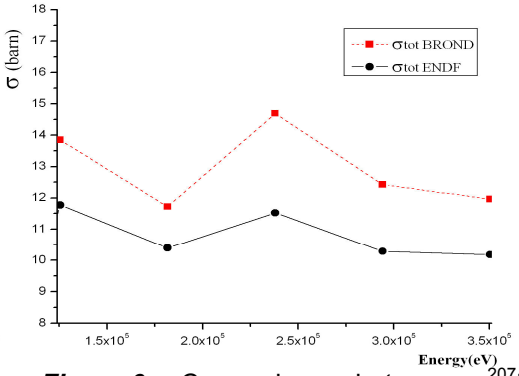

Figure 6. Comparison between ^{207}Pb-σ_{tot} from ENDF and respectively BROND res. par.

Summary

Review of evaluated nuclear data files for several Lead and Bismuth nuclei was done. In addition basic information is given for status of data. Energy averaging of resonance parameters was performed which gives an idea for quality of the data and discrepancy between different libraries. In particular the points that make impression of major differences are:
There is two-three or more times difference in Γ_γ for all Pb isotopes. Strength function for ^{206}Pb in JENDL is 50% higher than ENDF/B; for ^{207}Pb in BROND is more than 10% higher than others. The accurate measurement of these cross sections is important to improve the accuracy of the evaluated data. New resonance analysis is necessary in low energy region on the base of existing new measurements in CERN n-TOF and Gelina Belgium from 2004.
New investigations were performed on consistency of resonance parameters of Pb isotopes from evaluated data files. The preliminary analysis of resonance averaged cross-sections via resonance parameters and point wise data files shows some inconsistency between them and stress on the necessity of new experimental data and analysis of resonance cross section structure.

References

[1] Sixth framework programme Euratom integrated project Annex 1- 03.02.2005: “European Research Programme for the Transmutation of High Level Nuclear Waste in an Accelerator Driven System”.
[2] New nuclear data libraries for Pb and Bi. Arjan Koning, Marieke Duijvestijn, Steven van der Marck, Robin Klein Meulekamp, Alfred Hogenbirk.
[3] Nuclear data for ADS. Mihail Todorov – Proceeding from XVI International school on nuclear physics, neutron physics and nuclear energy, Varna, Bulgaria, October 2005.
[4] Evaluated nuclear data files from Nuclear Data Centers.

Optical fiber detector (SOF) in pulsed thermal neutron experiments

U. Woźnicka, A. Igielski, A. Kurowski

The Henryk Niewodniczański Institute of Nuclear Physics Polish Academy of Sciences, ul. Radzikowskiego 152, 31-342 Kraków, Poland.
Urszula.Woznicka@ifj.edu.pl

Abstract: The scintillator with optical fiber detector (SOF) consists of a small amount of the ZnS(Ag) scintillator mixed with a transparent adhesive material and a thermal neutron converter (^{6}Li, in this case). It is tightly connected to the tip of an optical fiber. The other tip is optically coupled with a small photomultiplier. A preliminary test has been done to compare the SOF detector and the ^{3}He proportional counter which has been used for a long time in the pulsed neutron experiments. It was found that the SOF detector may be used successfully instead of the ^{3}He proportional detector. Small dimensions of the detector (diameter is about 2 mm) allow to obtain accurate information on the spatial distribution of the thermal neutron flux inside a small investigated system.

The SOF detector

The scintillator with optical fiber detector (SOF) consists of a small amount of scintillator tightly connected to the tip of an optical fiber and the other tip is optically coupled with a small photomultiplier. It was originally developed by Mori et al. [1, 2]. The scintillator on the tip of the fiber was ZnS(Ag) mixed with LiF enriched with ^{6}Li up to 99.9% and transparent adhesive material. The other type of the scintillator like the plastic one may be used as well as the other type of the thermal neutron converter, e.g. boron. The scintillator and the fiber are covered with a lightproof screen. The idea of the SOF detector is presented in Fig. 1. We use the thermal neutron SOF detector based on a plastic fiber with diameter 2 mm and the lenght 2.1 m. The scintillator is ZnS(Ag) mixed with LiF enriched with ^{6}Li up to 99.9% and adhesive material with the volume ratio of 1:1:1. The thickness of the scintillator is about 1.5 mm. The reactions between ^{6}Li nuclei and thermal neutrons emit alpha particles and tritons which produce scintillations as a result of interacting with ZnS(Ag). The emission spectrum of ZnS(Ag) has a maximum at 450 nm [3] and well matches Hamamatsu type R1635 photomultiplier with the bialkali photocatode which diameter is 8 mm. We use a bunch of three SOF detectors connected to one photomultiplier (Fig. 2).

Pulsed neutron experiment

In the pulsed neutron experiment the investigated sample is irradiated with a pulsed beam of fast neutrons. The neutrons are slowed down in the sample and the die-away rate of escaping thermal neutrons is measured with a thermal neutron detector [4, 5]. The thermal neutron flux is very intense during the neutron burst and decays to the background value before the next burst. Therefore the thermal neutron detector should have a good dynamic range of linearity. A preliminary test has been done to compare the SOF detector and the ^{3}He proportional counter used till now in pulsed neutron experiments. A simplified diagram of the measuring system is shown in Fig. 3. A 10 cm paraffin cuboid – covered by a cadmium layer with a hole for the SOF detector on the top and with an opening on the bottom for a ^{3}He detector – has been irradiated by 14 MeV fast neutron bursts. The duration of neutron burst has been equal to 100 μs and the repetition time has been 1.3 ms. After each neutron burst the neutrons thermalized in the sample have diffused up to the final absorption or have been scattered outside. The SOF and ^{3}He detectors counted thermal neutrons. Both die-away curves of thermal neutrons have been registered in two multiscalers which have had the dwell time equal 2 μs. An example of the die-away curves is presented in Fig. 4. The decay constant of the fundamental exponential mode of the thermal neutron flux derived from the recorded curves has been 14 724 ± 334 [s^{-1}] for the SOF detector and 14 876 ± 56 [s^{-1}] for the ^{3}He one. This means that they do not differ. The standard deviation of the decay constant from the SOF detector is higher because its active volume is much smaller than of the ^{3}He detector and the counting statistics is poorer.

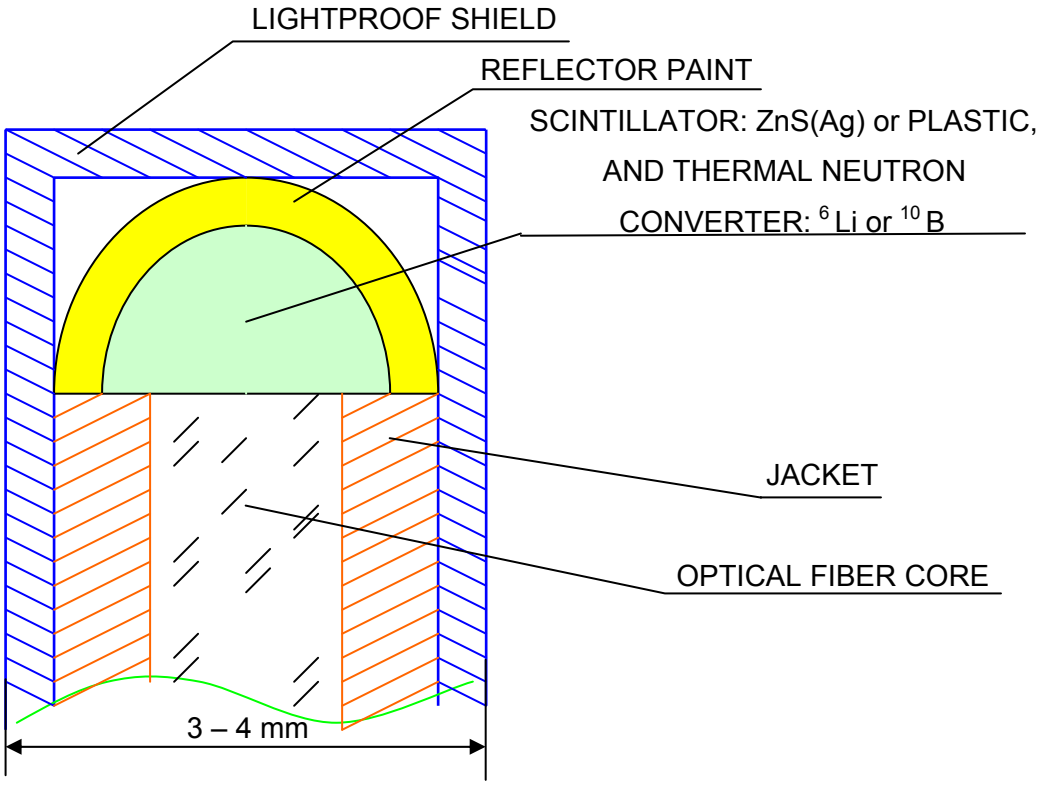

Figure 1. *Schematic diagram of the SOF detector.*

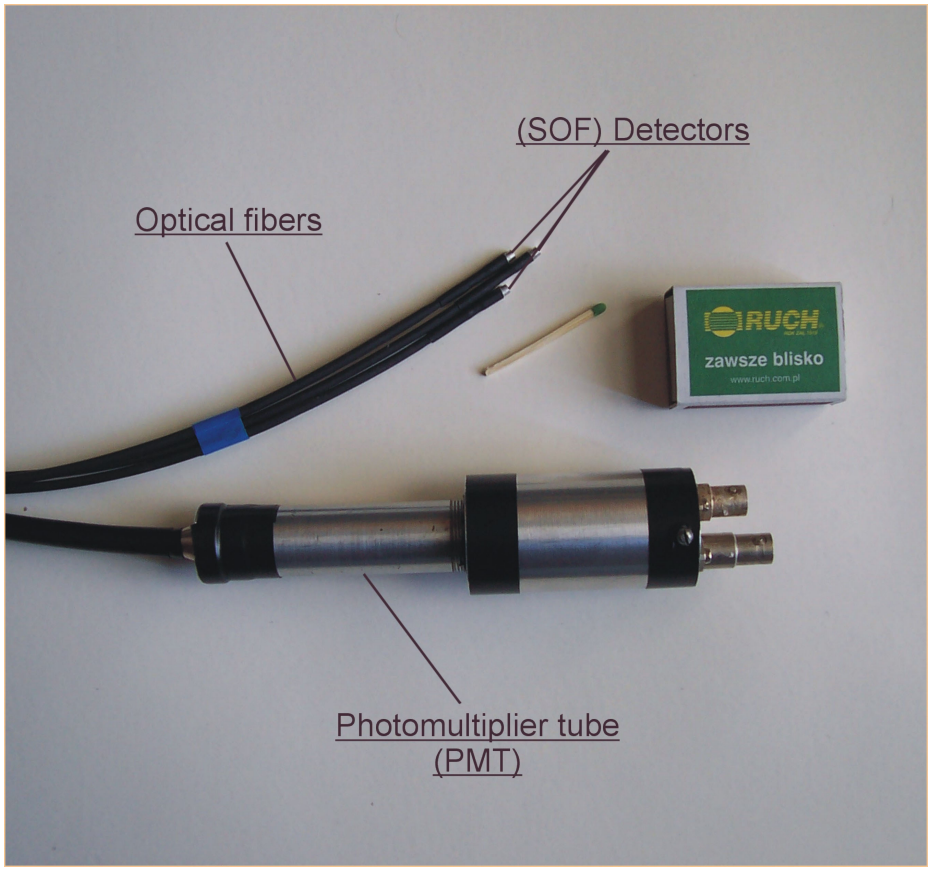

Figure 2. *The SOF detector.*

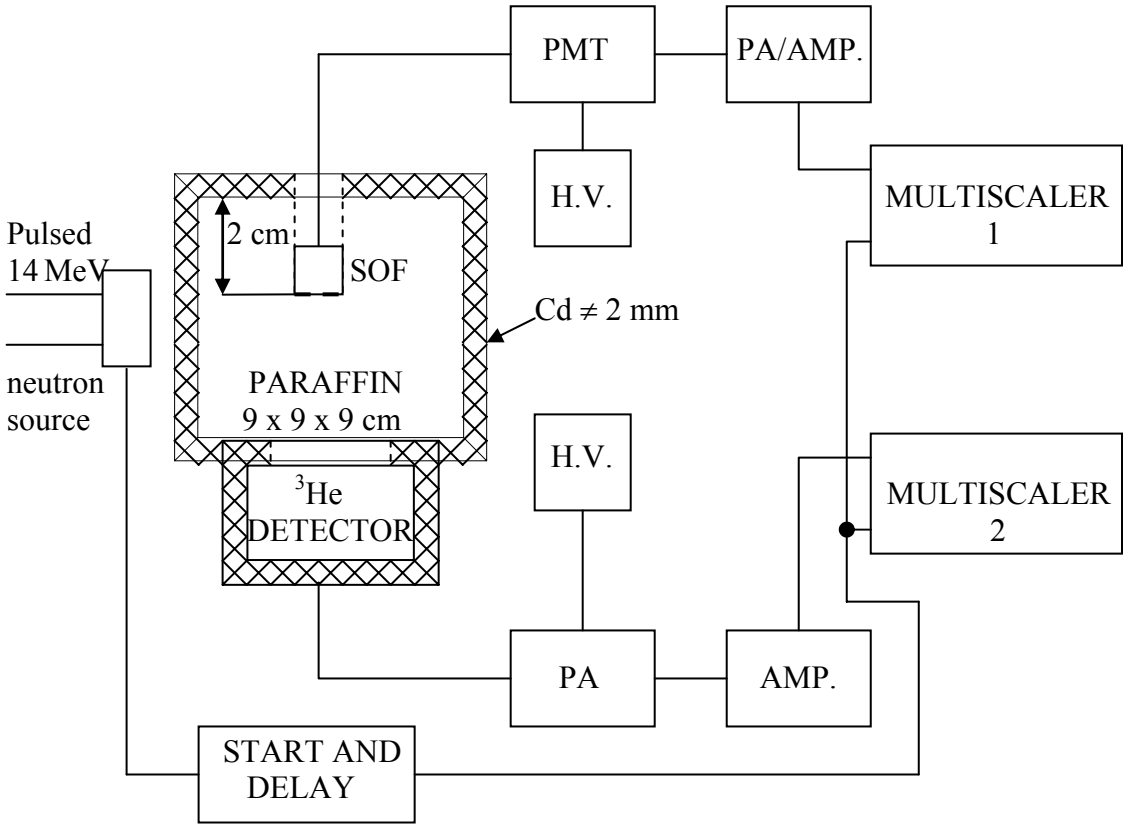

Figure 3. *Measuring system.*

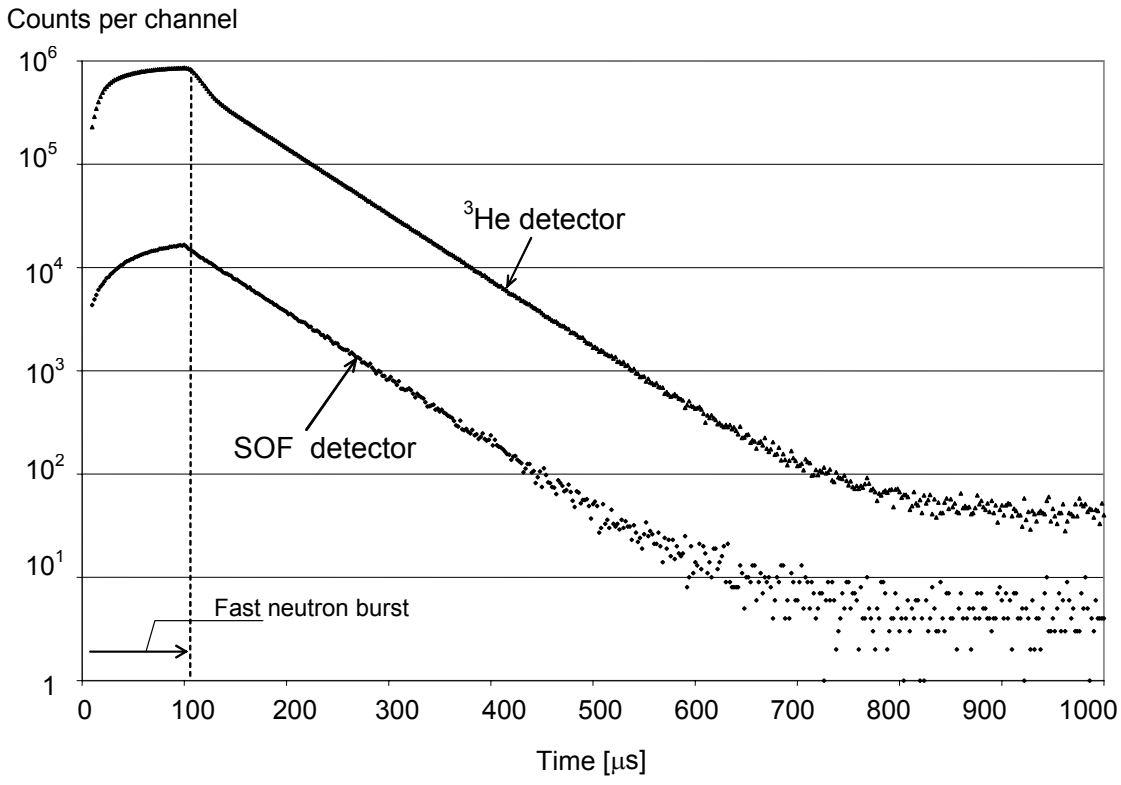

Figure 4. *Thermal neutron die-away curves measured by the SOF and ^{3}He detectors.*

Conclusions

Small dimensions of the SOF detector allow to use it as a quasi-point detector. Thus, a measurement of the spatial distribution of the thermal neutron flux in a small medium is possible without disturbing the neutron field. The fiber optic connection between the scintillator and photomultiplier makes the SOF detector resistant for a harsh electromagnetic environment. The sensitivity to gamma rays of the scintillator makes difficult to measure only a pure signal from thermal neutrons. The problem is solved by a pulse height discrimination or by using a pair of SOF detectors, one with a thermal neutron converter and the other without [6]. The scintillation decay time equal 200 ns for the ZnS(Ag) scintillator ensures a wide dynamic range of measurements. It may be improved be using the plastic scintillator with the decay time on the order of a few nanoseconds. The SOF detector is a very convenient replacement of the ^{3}He or BF_3 proportional detectors used in the pulsed thermal neutron experiments.

References

[1] C. Mori et al., J. Nucl. Sci. Technol. 31, 248 (1994).
[2] C. Mori et al., Nucl. Instr. Meth. A 422, 129 (1999).
[3] G.F. Knoll, Radiation Detection and Measurement, Wiley, New York, 2000.
[4] E. Krynicka et al., J. Phys. D: Appl. Phys. 38, 2967 (2005).
[5] E. Krynicka et al., Nucl. Instr. Meth. B 251, 19 (2006).
[6] M. Ishikawa et al., Nucl. Instr. Meth. A 551, 448 (2005).

Author index

European Commission

EUR 22794 EN – DG Joint Research Centre, Institute for Reference Materials and Measurements – NEMEA-3, Neutron Measurements, Evaluations and Applications, proceedings of the enlargement workshop, 25-28 October, Borovets, Bulgaria

Editor: A.J.M. Plompen

Luxembourg: Office for Official Publications of the European Communities

2007 – 196 pp. – 21.0 x 29.7 cm

EUR - Scientific and Technical Research series; ISSN 1018-5593

ISBN 978-92-79-06158-5

Abstract

The enlargement workshop NEMEA-3, Neutron Measurements, Evaluations and Applications was held from 25 to 28 October 2006 in Borovets, Bulgaria. These proceedings collect the full papers summarising oral and poster contributions to this workshop.

EUROPEAN COMMISSION
DIRECTORATE-GENERAL
Joint Research Centre

The mission of the Joint Research Centre is to provide customer-driven scientific and technical support for the conception, development, implementation and monitoring of European Union policies. As a service of the European Commission, the JRC functions as a reference centre of science and technology for the Community. Close to the policy-making process, it serves the common interest of the Member States, while being independent of special interests, whether private or national.

LA-NA-22794-EN-C

ISBN 978-92-79-06158-5

Publications Office
Publications.eu.int

9 789279 061585